Microstructural Control For High Strain Rate Superplasticity And Deformation Characteristics

Mamoru MABUCHI

MICROSTRUCTURAL CONTROL FOR HIGH STRAIN RATE SUPERPLASTICITY AND DEFORMATION CHARACTERISTICS

MAMORU MABUCHI

CONTENTS

ACKNOWLEDGEMENTS

The author would like to express his sincere gratitude to Professor Natsuo Hatta of Kyoto University for his valuable advice and kindly guidance throughout preparation of the present thesis.

He is also deeply grateful to Professor Susumu Shima and Professor Tadashi Maki of Kyoto University for their beneficial suggestion leading to this thesis.

The author would like to acknowledge Professor K. Kubo of Setsunan University and Dr. T. Imai of National Industrial Research Institute of Nagoya for their consideration towards this study. He wishes to thank many people in National Industrial Research Institute of Nagoya for support and all their assistance.

He is indebted to Associate Professor H. Iwasaki of Himeji Institute of Technology for helpful discussion and suggestion. His special thank is also due to Associate Professor K. Higashi of Osaka Prefecture University for his constant encouragement and valuable discussion throughout this work.

CHAPTER 1

INTRODUCTION

1.1 Progress in research on superplasticity

Superplasticity is the ability of a polycrystalline material to exhibit, in a generally isotropic manner, very high tensile elongations prior to failure. Elongations of ~ 500% are common in superplastic metals. In an aluminum-bronze alloy, an extremely large elongation of more than 8000 % is recorded (Fig. 1.1 [1]). The detailed study on superplasticity was originally conducted in the Pb-Sn and Bi-Sn eutectic alloys by Pearson in 1934 [2]. He showed a tensile elongation of 1950 % without failure. To data, research on superplasticity has advanced, and superplasticity has been utilized in industrial applications because complex shaped components can be produced readily by superplastic forming.

Recently, it has been demonstrated that superplasticity is attained for materials exhibiting poor workability such as ceramics [3], intermetallics [4] and metal matrix composites with discontinuous reinforcements [5]. In addition, it has been demonstrated that very fine-grained materials exhibit superplastic behavior at extremely high strain rates (> 1 s^{-1}) for metals [6-8]. Overview of superplastic behavior as a function of strain rate for aluminum based materials is shown in Fig. 1.2 [9]. Superplastic behavior is attained at strain rates of ~ 10^{-3} s^{-1} for a superplastic 7475 Al alloy, which is a typical superplastic aluminum alloy. On the other hand, IN 9021 & 90211 Al alloys show superplasticity at extremely high strain rates ≥ 1 s^{-1}. High strain rate

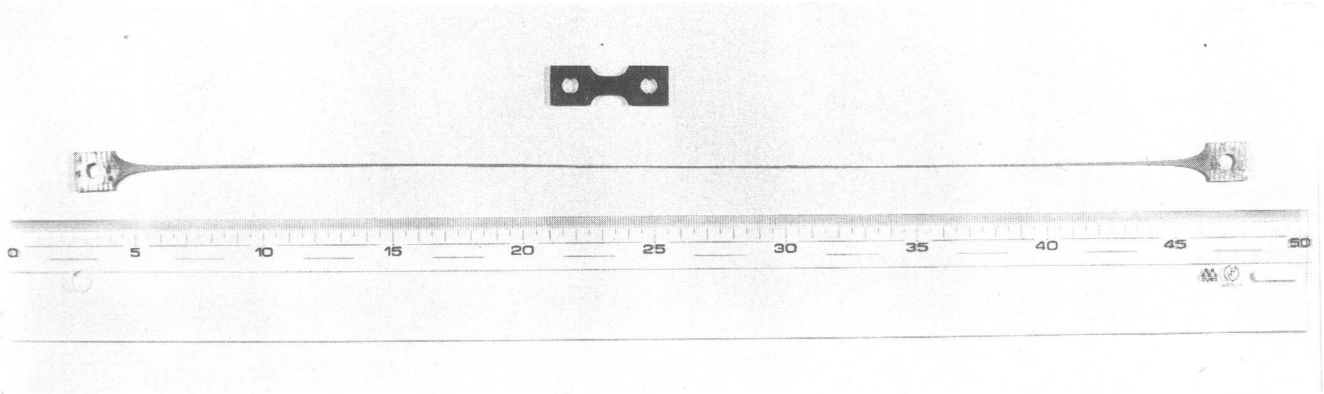

Fig. 1.1 Extremely large elongation of more than 8000 % for an aluminum-bronze alloy [1].

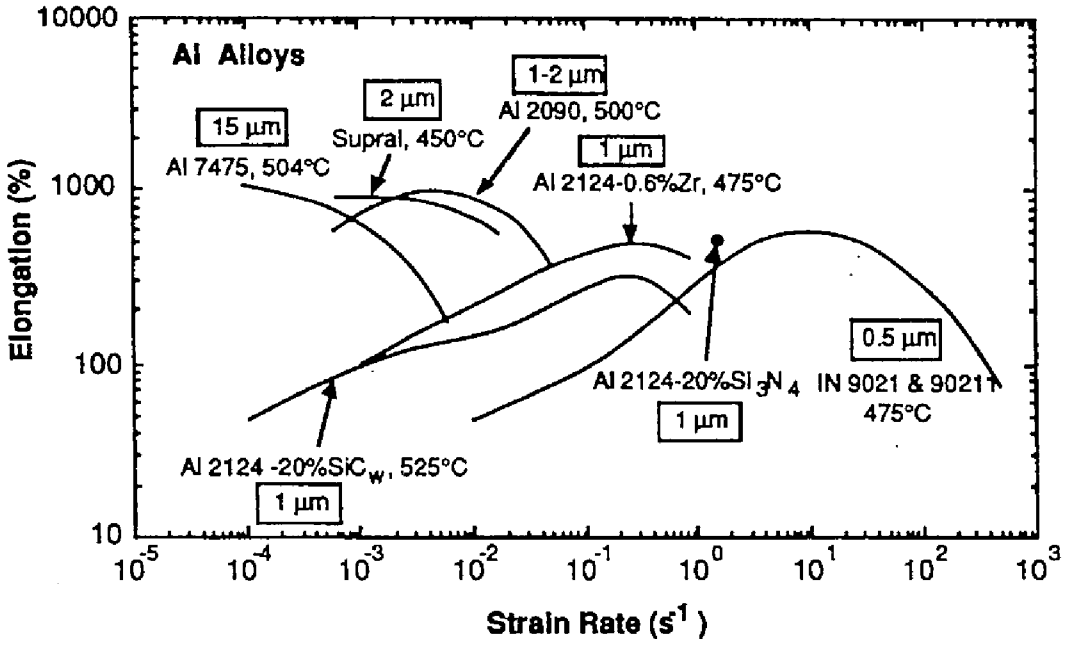

Fig. 1.2 Overview of superplastic behavior as a function of strain rate for aluminum based materials [9].

superplasticity is very attractive for commercial applications because one of the current drawbacks in superplastic forming technology is a slow forming rate, which is typically ~ 10^{-3} s^{-1}. However, the origin of high strain rate superplasticity is the subject in some debate. It is important to investigate microstructural control for high strain rate superplasticity and understand the deformation characteristics and mechanisms not only for scientific aspects, but also for industrial applications.

1.2 Review of superplasticity

1.2.1 Types of superplasticity

There are two types of superplasticity: internal stress superplasticity and structural (fine-grain) superplasticity. Internal stress superplasticity is attained when a low stress is externally applied in some materials in which internal stress can be developed, for example, during thermal cycling [10-12]. A high strain rate sensitivity $\cong$ 1 is obtained and the dominant deformation process is a slip deformation mechanism for internal stress superplasticity.

Structural superplasticity is attained when the requirements of the testing conditions (for example, $T \geq 0.5\ T_m$) and the microstructures of a material (for example, $d \leq 10$ μm for metals) are satisfied [13], where T is a testing temperature, T_m is the melting point and d is the grain size. A high strain rate sensitivity > 0.3 is obtained and the dominant deformation process is grain boundary sliding for structural superplasticity. The materials used in the present investigation belong to structural superplasticity.

1.2.2 Grain refinement

It is recognized that a small and stable grain size is microstructural requirement for structural superplasticity. In general, a small grain size, (but not necessarily) less than 10 μm is required to attain superplasticity for

metallic materials. Therefore grain refinement is important for the development of superplastic materials. Several methods are available for grain refinement: phase transformation, phase separation in duplex alloys and mechanical working/thermo-mechanical treatment with recrystallization in duplex alloys and pseudo single phase alloys [14,15]. The mechanical working/thermo-mechanical treatment is an important grain refinement method for materials showing no phase transformation and no phase separation. Schematic illustration of grain refinement due to mechanical working with recrystallization is shown in Fig. 1.3 for duplex alloys [14] and in Fig. 1.4 for pseudo single phase alloys [14]. For duplex alloys, working would fragment the harder phase and the softer phase would infiltrate and separate the harder phase, and then fine equiaxed grain structure can be developed by recrystallization.

For pseudo single phase alloys, particles play a vital role in grain refinement. Namely, large particles (> about 1 μm) cause high dislocation density by mechanical working, resulting in acceleration of nucleation for recrystallization, and fine particles (< approximately 0.1 μm) restrict grain growth during recrystallization. Finally, large particles are required to dissolve because large particles hamper grain boundary sliding which is the dominant deformation process of superplasticity. Many superplastic materials have been developed by the mechanical working/thermo-mechanical treatment for pseudo single phase alloys [16-23]. For example, Wert *et al.* [16] developed a grain refinement method for a commercial Al-Zn-Mg-Cu (7075) alloy, which is a pseudo single phase alloy, by thermo-mechanical treatment including solution treatment, over age, hot rolling and static recrystallization treatment. A small grain size of about 10 μm was attained by the thermo-mechanical treatment and the fine-grained aluminum alloy showed superplastic behavior at ~ 10^{-4} s^{-1}. Thus, grain size control for materials exhibiting

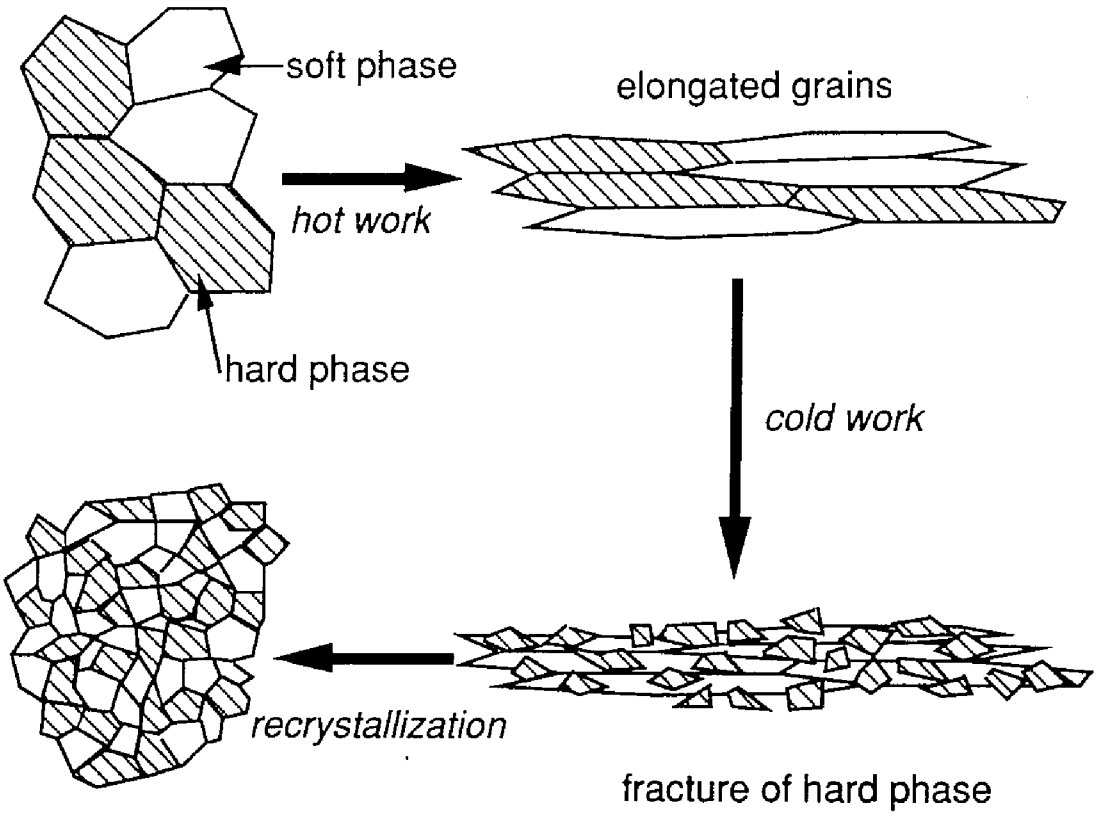

Fig. 1.3 Schematic illustration of grain refinement due to mechanical working for duplex alloys [14].

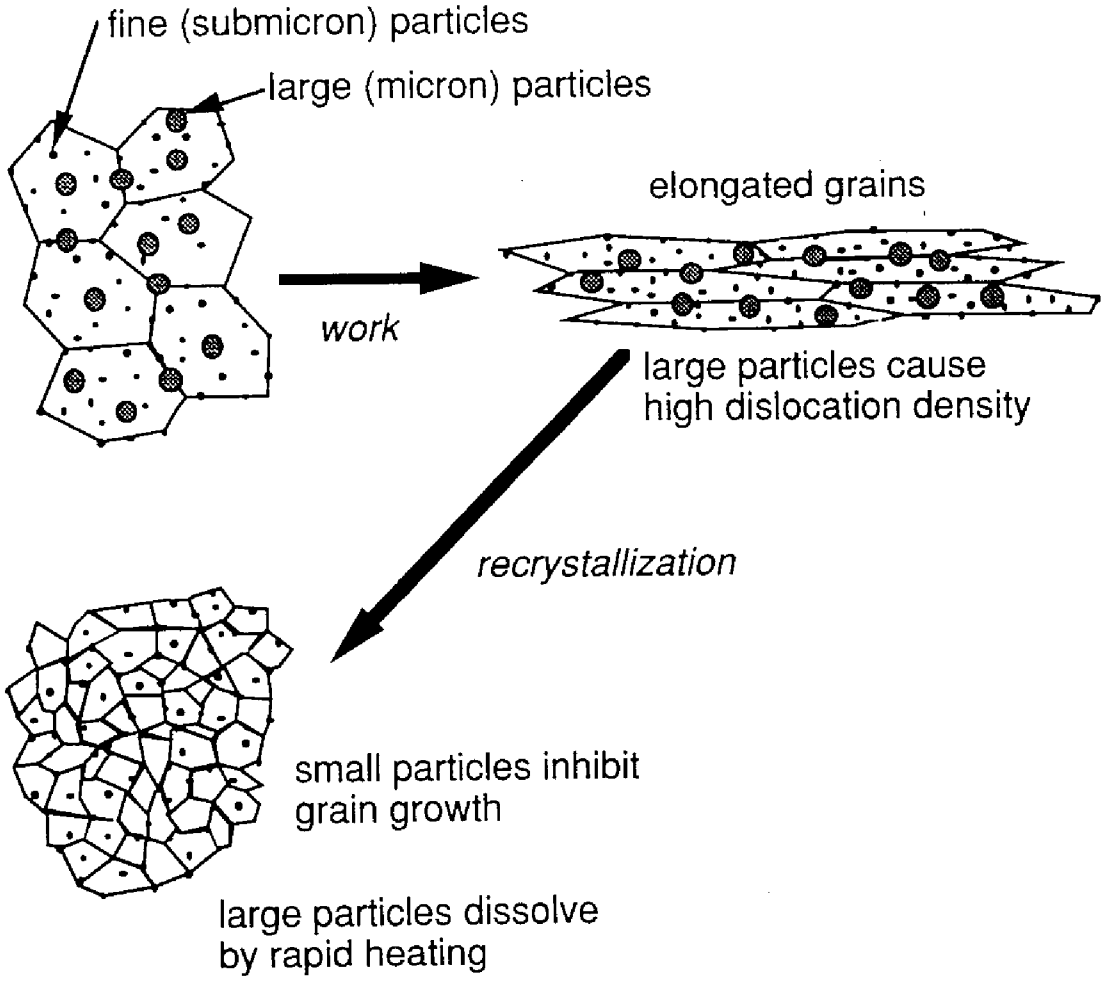

Fig. 1.4 Schematic illustration of grain refinement due to mechanical working for pseudo single phase alloys [14].

superplasticity at ~ 10^{-4} s^{-1} has been advanced. However, microstructural control for high strain rate superplastic materials is not sufficiently understood.

1.2.3 Deformation characteristics of superplastic materials

The relationship between the flow stress σ and the strain rate $\dot{\varepsilon}$ at elevated temperatures in crystalline materials can be given by

$$\sigma = K\dot{\varepsilon}^m \tag{1.1}$$

where K is a constant incorporating structure and temperature dependencies and m is the strain rate sensitivity of flow stress. It is recognized that for superplastic metals, there is a sigmoidal relationship between the logarithmic flow stress and the logarithmic strain rate, dividing the behavior into three regions. Schematic illustration of the strain rate dependence of flow stress in a superplastic material is shown in Fig. 1.5, where the strain rate sensitivity m is a slope of the curve. The high strain rate sensitivity of $m \simeq 0.5$ is found in an intermediate strain rate range (Region II), which is the superplastic region. In this region, the elongations to failure are large. Both the high (Region III) and low (Region I) strain rate ranges exhibit values of $m < 0.3$ and there are decreases in the elongation to failure in these regions. The high strain rate sensitivity is an important characteristic for superplastic deformation [24]. Since the high strain rate sensitivity gives rise to a large change in the flow stress with a slight change in the strain rate, the strain rate hardening is enhanced and the development of necking is limited [25]. Therefore, a superplastic material with the high strain rate sensitivity exhibits a uniform elongation with little necking, resulting in a large elongation.

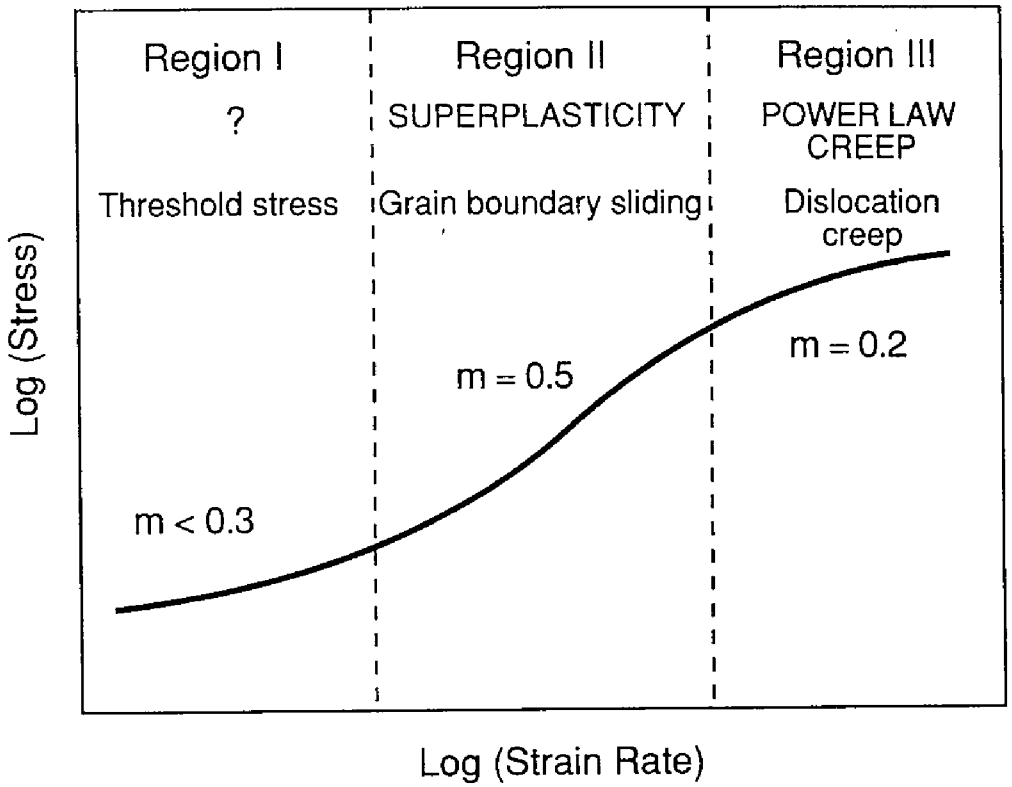

Fig. 1.5 Schematic illustration of the strain rate dependence of flow stress in a superplastic material.

Table 1.1 Contribution of grain boundary sliding to the total axial strain [27].

Material (wt.%)	$\gamma_{GBS} = \varepsilon^{a)}_{GBS} / \varepsilon^{b)}_{Total}$ Region I	Region II	Region III
Zn-22Al	30	60	30
Zn-22Al	30	60	30
Zn-0.4Al	40	50	30
Sn-38Pb	21±5	56±12	20±4
Mg-1.5Mn-0.3Ce	33±4	49±6	30±4
Al-11Zn-1Mg	60	80	50
Al-9Zn-1Mg	42	63	26
Cu-2.6Al-1.8Si-0.4Co	28±12	44±10	20±5
Al-6.3Mg-0.5Mn	44±5	55±7	27±4

a) the strain due to grain boundary sliding
b) the total strain

The dominant deformation process at high strain rates, Region III, is power law creep, that is, diffusion-controlled dislocation creep, and a value of m is predicted to be 0.2 for pure metals and Class II alloys and 0.33 for Class I alloys. The dominant deformation process at an intermediate strain rate range, Region II, is believed to be grain boundary sliding [26-29]. Contribution of grain boundary sliding to the total axial strain is listed in Table 1.1 [27]. It is found that contribution of grain boundary sliding to the total axial strain is 50 ~ 80 %. The high strain rate sensitivity is associated with the deformation mechanisms based on grain boundary sliding. The dominant deformation process at a low strain rate range, Region I, is not clear. The strain rate sensitivity is low (< 0.3) in this region. This is probably because of the presence of threshold stress [30,31].

1.2.4 Deformation mechanisms of superplasticity

It is accepted that the dominant deformation process of superplastic flow is grain boundary sliding. Schematic illustration of grain boundary sliding is shown in Fig. 1.6. In this figure, the accommodation of grain boundary sliding is not taken into consideration. The grain boundary sliding mechanism can explain the phenomenological fact that the grains are not elongated in spite of large elongation of a specimen. However, if grain boundary sliding occurs in a complete rigid system, as shown in Fig. 1.6, cavitation will be excessively caused. In such a case, a large elongation is not attained. Therefore the accommodation process is required to attain superplasticity. When the rate of the accommodation process is slower than the rate of grain boundary sliding, the rate-controlling process for superplastic flow is not grain boundary sliding, but the accommodation process. Therefore, many models on superplastic flow [32-39] have been proposed from the viewpoint of the

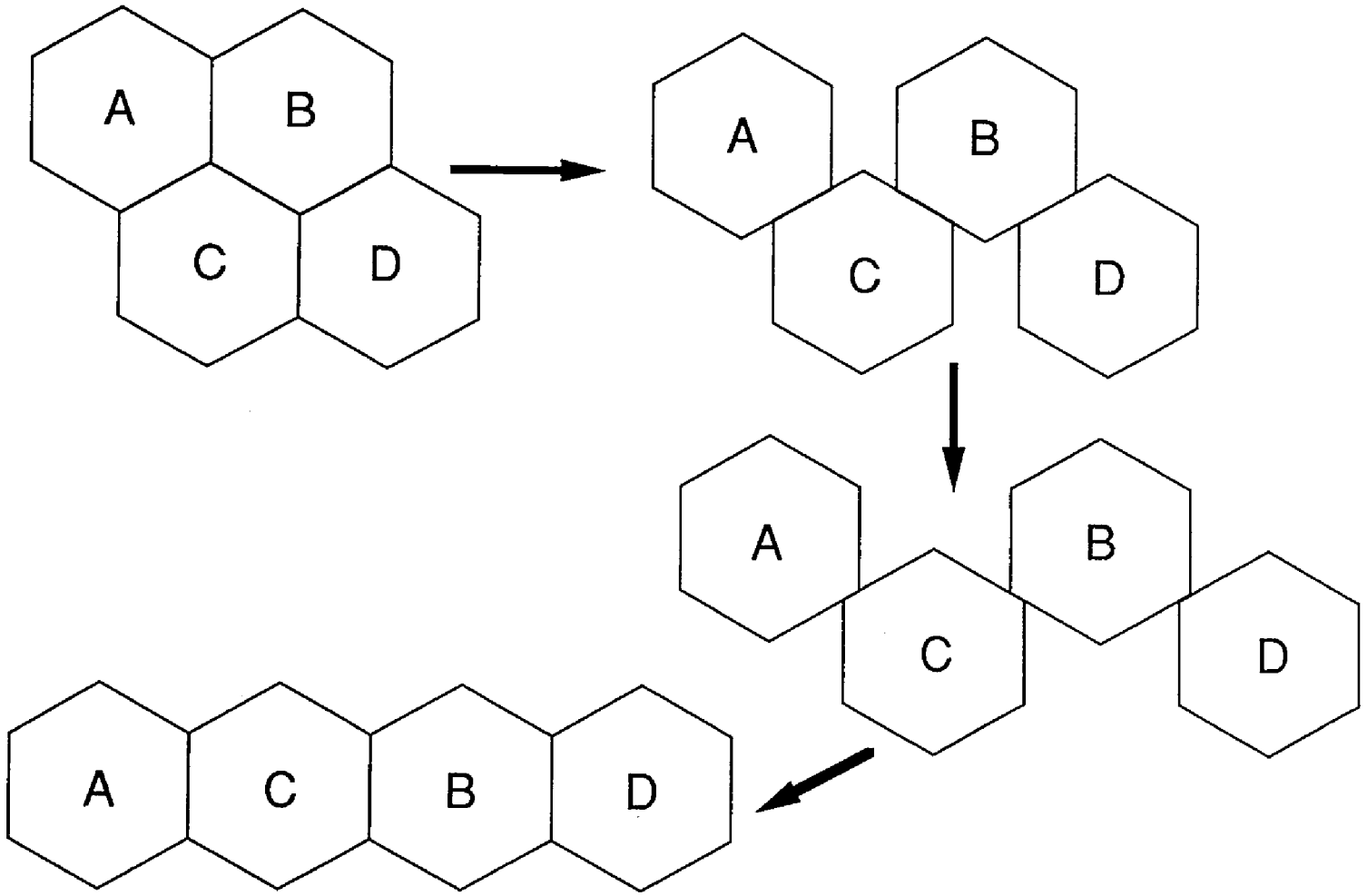

Fig. 1.6 Schematic illustration of grain boundary sliding.

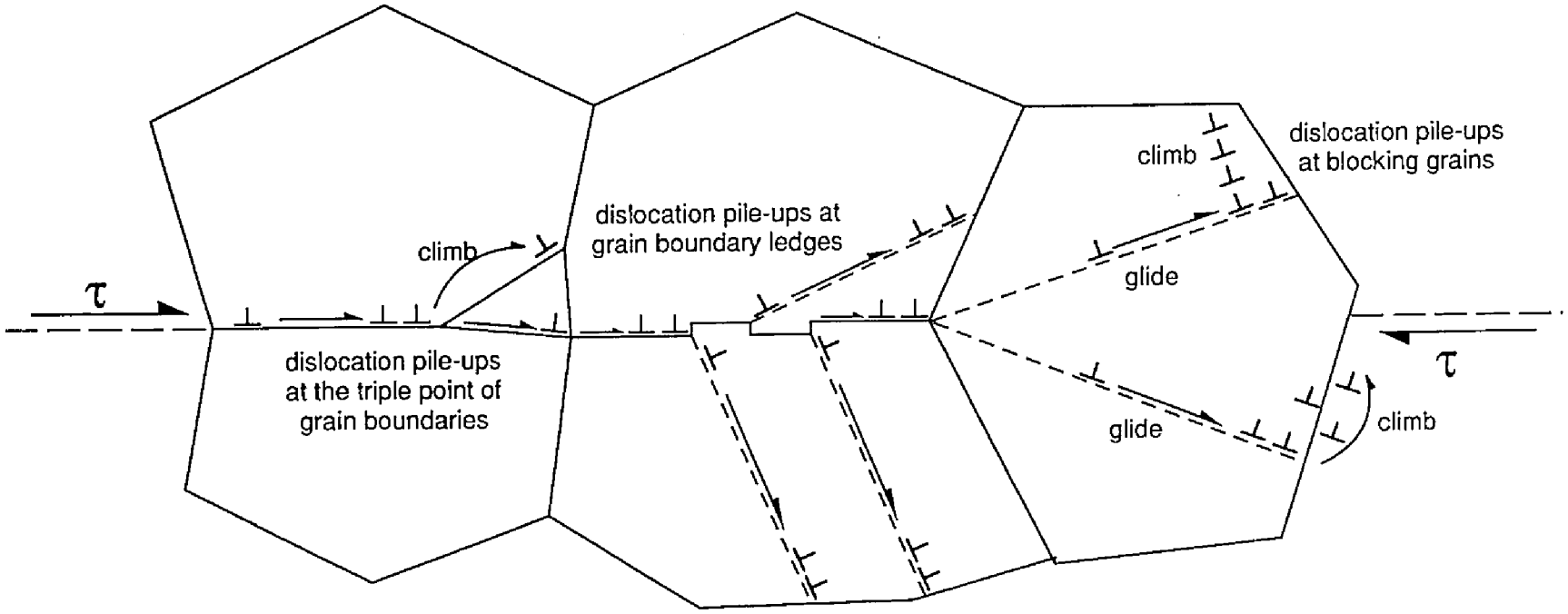

Fig. 1.7 Schematic illustration of the accommodation mechanisms by dislocation movement for superplastic flow [14].

accommodation processes. The models may be divided into two categories: the diffusion model [32] and the dislocation model [33-39]. When grain boundary sliding is accommodated by diffusion, a value of the strain rate sensitivity is predicted to be unity. On the other hand, when grain boundary sliding is accommodated by dislocation movement, a value of the strain rate sensitivity is predicted to be 0.5.

Schematic illustration of the accommodation mechanisms by dislocation movement for superplastic flow is shown in Fig. 1.7 [14]. Dislocations are piled-up at the triple points and ledges of grain boundaries during grain boundary sliding. The piled-up dislocations are removed by climb along grain boundaries or by glide along the most favorable slip planes. The dislocations moving along the most favorable slip planes pile up at the opposite grain boundaries. Climb of the leading dislocation from the pile-up into grain boundary would allow another dislocation to be emitted and enable a small increment of grain boundary sliding to be accumulated. The activation energy for superplastic flow is equal to the one for grain boundary diffusion or lattice diffusion [9]. It depends on the dominant diffusion process in the accommodation processes.

1.2.5 Superplastic metal matrix composites

Ceramic whisker- or particulate- reinforced metal matrix composites exhibit a unique combination of high specific room temperature strength and elastic modulus, and therefore the composites show considerable promise as structural materials. However the composites have low tensile ductility and poor workability, compared to the matrix materials, which gives rise to high costs in the final forming of the composites. It is therefore desirable to improve poor workability of the composites for many structural applications.

The original work by Nieh *et al.* [5] revealed that the SiC_w/Al-Cu-Mg (2124) composite (the subscript *w* represents whiskers) behaved in a superplastic-like manner at a high strain rate of 3.3 x 10^{-1} s^{-1}. Also, Mahoney and Ghosh [40] showed superplastic behavior of the SiC_p/Al-Zn-Mg-Cu (PM64) composite (the subscript *p* represents particulates). After these demonstrations, some superplastic aluminum matrix composites have been studied [41-45]. Recently, a few of superplastic magnesium matrix composites were reported [46,47]. It is noted that some composites exhibited superplasticity at high strain rates of more than 10^{-2} s^{-1}.

1.2.6 Cavitation in superplasticity

When a superplastic material fails during tensile deformation, the fracture is attributed to unstable plastic flow, that is, the development of necking, or the growth and interlinkage of internally nucleated cavities. It is recognized that cavitation occurs during superplastic flow, despite large elongations, in many materials [14]. Excessive cavity formation causes poor properties of the deformed products. Therefore it is important to investigate cavitation characteristics and to control cavitation.

When grain boundary sliding is not sufficiently accommodated, cavities are formed. Schematic illustration of cavity nucleation is shown in Fig. 1.8. In general, cavities are nucleated at the triple points and ledges of grain boundaries and at the particles on a sliding grain boundary, as shown in Fig. 1.8, because stress concentrations are caused at these sites during the sliding process.

1.3 Aim of the present study

The present study describes microstructural control for high strain rate superplasticity and deformation characteristics of high strain rate

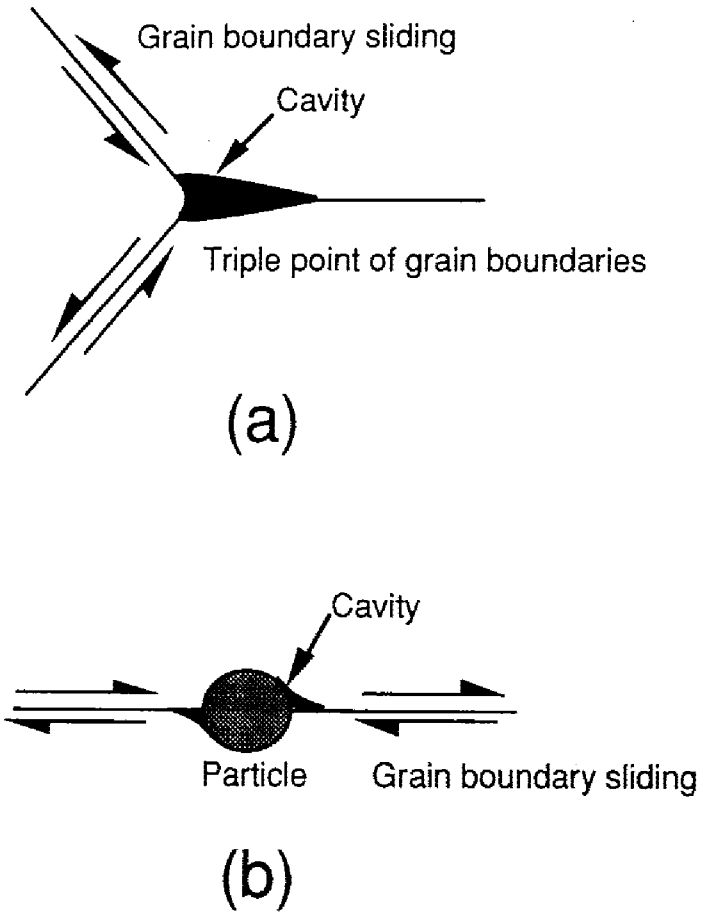

Fig. 1.8 Schematic illustration of cavity formation, (a) at the triple point of grain boundaries and (b) at a particle on a sliding grain boundary.

superplasticity. In the previous studies [6-8], high stain rate superplasticity has been demonstrated for metals. However, the microstructural control for high strain rate superplastic materials is less advanced, compared to for conventional superplastic materials [16-23], and deformation characteristics of high strain rate superplasticity are still unclear. In the present study, aluminum matrix composites and magnesium matrix composites with discontinuous reinforcements have been investigated for the microstructural control for high strain rate superplasticity and the deformation characteristics. High stain rate superplasticity for materials containing a second hard phase such as metal matrix composites is very attractive not only for scientific aspects but also for industrial applications because the materials containing a second hard phase generally show poor workability.

Chapter 2 describes materials preparation, tensile testing methods and cavitation study methods. In the present investigation, constant strain rate tensile tests are carried out to investigate the deformation characteristics and constant stress tensile tests are conducted for the cavitation study.

Chapter 3 describes processing of aluminum matrix composites and magnesium matrix composites exhibiting high strain rate superplasticity. In addition, the mechanisms of grain refinement by hot extrusion are investigated for aluminum matrix composites.

In Chapter 4, the deformation characteristics of high strain rate superplasticity for aluminum matrix composites are investigated by constant strain rate tensile tests. The experimental data are analyzed through the threshold stress concept, and the activation energy for superplastic flow and a rate-controlling process are investigated.

Chapter 5 investigates the deformation characteristics of high strain rate superplasticity for magnesium matrix composites. Similarly, the threshold

stress concept is applied to estimate the activation energy for superplastic flow and a constitutive equation.

Chapter 6 deals with partial melting at matrix/reinforcement interfaces and grain boundaries at elevated temperatures by *in situ* TEM observation and DSC measurements.

Chapter 7 describes the origins of high strain rate superplasticity from the viewpoint of the grain size dependence and the accommodation mechanisms. A new concept of the accommodation mechanism by a liquid phase for superplastic flow is proposed.

In Chapter 8, cavitation characteristics in a state including a liquid phase are investigated, in addition, recovery of cavity damages by static annealing after superplastic deformation is examined.

Chapter 9 summarizes the studies conducted here and describes an overall achievement of the present thesis.

References

1. K.Higashi, Materia Japan, **34**, 1002 (1995).
2. C.E.Pearson, J. Inst. Met., **54**, 111 (1934).
3. F.Wakai, S.Sakaguchi and Y.Matsuno, Advanced Ceram. Mater., **1**, 259 (1986).
4. S.Hanada, T.Sato, S.Watanabe and O.Izumi, J. Jpn. Inst. Met., **45**, 1293 (1981).
5. T.G.Nieh, C.A.Henshall and J.Wadsworth, Scripta Metall., **18**, 1405 (1984).
6. T.G.Nieh, P.S.Gilman and J.Wadsworth, Scripta Metall., **19**, 1375 (1985).
7. T.R.Bieler, T.G.Nieh, J.Wadsworth and A.K.Mukherjee, Scripta Metall., **22**, 81 (1988).

8 K.Higashi, Mater. Sci. Eng., **A166**, 109 (1993).

9. O.D.Sherby and J.Wadsworth, Prog. Mater. Sci., **33**, 169 (1989).
10. N.Iguchi, J. Jpn. Inst. Light Met., **32**, 421 (1982).
11. M.Y.Wu and O.D.Sherby, Scripta Metall., **18**, 773 (1984).
12. G.-Gonzalez-Doncel, S.D.Karmarkar, A.P.Divecha and O.D.Sherby, Composites Sci. Tech., **35**, 105 (1989).
13. T.G.Langdon, Metall. Trans. A, **13A**, 689 (1982).
14. J.Pilling and N.Ridley, in *Superplasticity in Crystalline Solid*, (The Institute of Metals, London, 1989), pp. 8-15.
15. J.A.Wert, in *Superplastic Forming of Structural Alloys*, edited by N.E.Paton and C.H.Hamilton, (The Metall. Soc. AIME, Warrendale, PA, 1982), p. 69.
16. J.A.Wert, N.E.Paton, C.H.Hamilton and M.W.Mahoney, Metall. Trans. A, **12A**, 1267 (1981).
17. B.M.Watts, M.J.Stowell, B.L.Baikie and D.G.E.Owen, Metal Sci., **10**, 189 (1976).

18. B.M.Watts, M.J.Stowell, B.L.Baikie and D.G.E.Owen, Metal Sci., **10**, 198 (1976).
19. E.Nes, J. Mater. Sci., **13**, 2052 (1978).
20. T.R.McNelley, E.-W.Lee and M.E.Mills, Metall. Trans. A, **17A**, 1035 (1986).
21. E.-W.Lee, T.R.McNelley and A.F.Stengle, Metall. Trans. A, **17A**, 1043 (1986).
22. S.J.Hales and T.R.McNelley, Acta Metall., **36**, 1229 (1988).
23. S.J.Hales, T.R.McNelley and H.J.McQueen, Metall. Trans. A, **22A**, 1037 (1991).
24. D.A.Woodford, Trans. Am. Soc. Met., **62**, 291 (1969).
25. E.W.Hart, Acta Metall., **15**, 351 (1967).
26. R.C.Gifkins, J. Mater. Sci., **13**, 1926 (1978).
27. R.Z.Valiev and O.A.Kaibyshev, Acta Metall., **31**, 2121 (1983).
28. Z.-R.Lin, A.H.Chokshi and T.G.Langdon, J. Mater. Sci., **23**, 2712 (1988).
29. T.G.Langdon, Mater. Sci. Eng., **A174**, 225 (1994).
30. F.A.Mohamed, J. Mater. Sci., **18**, 583 (1983).
31. P.K.Chaudhury and F.A.Mohamed, Acta Metall., **36**, 1099 (1988).
32. M.F.Ashby and R.A.Verrall, Acta Metall., **21**, 149 (1973).
33. A.Ball and M.M.Hutchison, Met. Sci. J., **3**, 1 (1969).
34. A.K.Mukherjee, Mater. Sci. Eng., **8**, 83 (1971).
35. H.W.Hayden, S.Floreen and P.D.Goodell, Metall. Trans., **3**, 833 (1972).
36. R.C.Gifkins, Metall. Trans. A, **7A**, 1225 (1976).
37. J.H.Gittus, J. Eng. Mater. Tech., **99**, 244 (1977).
38. B.Burton, Philos. Mag. A, **48**, L9 (1983).
39. M.Suery and B.Baudelet, Philos. Mag. A, **41**, 41 (1980).
40. M.W.Mahoney and A.K.Ghosh, Metall. Trans. A, **18A**, 653 (1987).
41. J.Pilling, Scripta Metall., **23**, 1375 (1989).

42. H.Xiaoxu, L.Qing, C.K.Yao and Y.Mei, J. Mater. Sci. Lett., **10**, 964 (1991).

43. T.Imai, M.Mabuchi, Y.Tozawa and M.Yamada, J. Mater. Sci. Lett., **9** , 255 (1990).

44. K.Matsuki, H.Matsumoto, M.Tokizawa, N.Takatsuji, M.Isogai, S.Murakami and Y.Murakami, in *Science and Engineering of Light Metal*, edited by K.Hirano, H.Oikawa and K.Ikeda (The Japan Institute of Light Metals, Tokyo, 1991), p. 205.

45. K.Higashi, T.Okada, T.Mukai, S.Tanimura, T.G.Nieh and J.Wadsworth, Scripta Metall. Mater., **26**, 185 (1992).

46. T.G.Nieh and J.Wadsworth, Scripta Metall. Mater., **32**, 1133 (1995).

47. S.-W.Lim, T.Imai, Y.Nishida and T.Choh, Scripta Metall. Mater., **32**, 1713 (1995).

2. CHAPTER

EXPERIMENTAL PROCEDURE

2.1 Materials

Experiments were conducted on ten kinds of aluminum matrix composites reinforced either with Si_3N_4 particulates or Si_3N_4 whiskers and two kinds of magnesium matrix composites reinforced with Mg_2Si particulates.

Scheme of processing of Si_3N_4/Al alloy composites is shown in Fig. 2.1. Air atomized powders of four kinds of aluminum alloys (Al-Cu-Mg (2124), Al-Mg (5052), Al-Mg-Si (6061) and Al-Zn-Mg (7064)) were prepared. The chemical compositions of the aluminum alloys are shown in Table 2.1. The air atomized Al-Mg-Si (6061) alloy powder is shown in Fig. 2.2. A kind of Si_3N_4 whisker and three kinds of Si_3N_4 particulates were prepared as reinforcements. The characteristics of the Si_3N_4 reinforcements are listed in Table 2.2. The Si_3N_4 whiskers and the Si_3N_4 particulates (~ 1 μm in diameter) are shown in Fig. 2.3 and in Fig. 2.4, respectively. The aluminum alloy powder and the reinforcement powder of either Si_3N_4 whiskers or Si_3N_4 particulates were ultrasonically mixed for more than 3.6×10^3 s in an alcoholic solvent prior to drying. The volume fraction of the reinforcements was 20 vol.%. The mixed powders were sintered at 873 K with a pressure of 390 MPa for 1.2×10^3 s by a hot press machine and the billets of 40 mm in diameter were processed. The sintering was performed in vacuum because a degassing treatment is necessary in order to suppress harmful effects of hydrogen [1,2]. The sintered billet was then extruded (100 to one reduction)

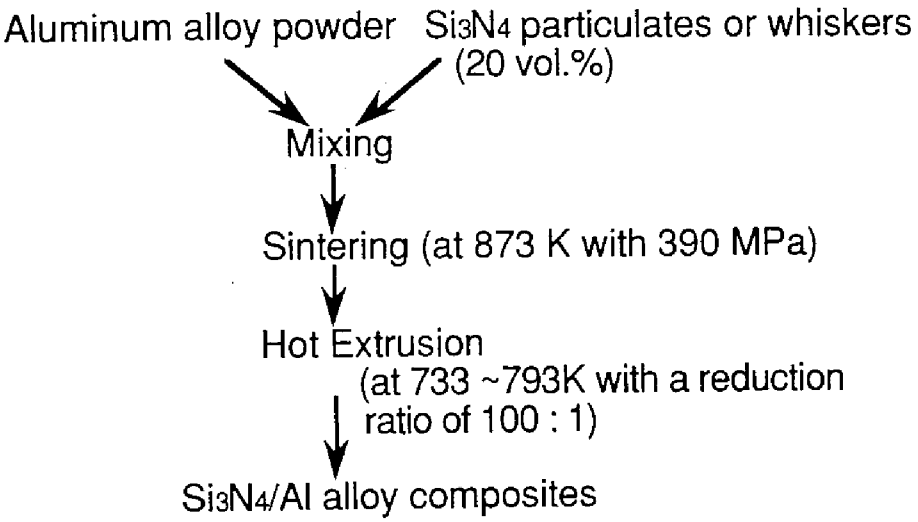

Fig. 2.1 Scheme of processing of Si 3N4/Al alloy composites.

Table 2.1 Chemical composition of the aluminum alloys used in the present investigation.

	Cu	Mg	Zn	Mn	Ti	Cr	Zr	Co	Si	Fe	Al
Al-Cu-Mg (2124)	4.20	1.48	0.12	0.64	0.06	0.06			0.12	0.09	Bal.
Al-Mg (5052)	0.04	2.46				0.25			0.16	0.16	Bal.
Al-Mg-Si (6061)	0.39	1.03				0.15			0.75	0.47	Bal.
Al-Zn-Mg (7064)	0.24	2.38	0.03	0.01		0.07	0.09	0.15	0.03	0.03	Bal.

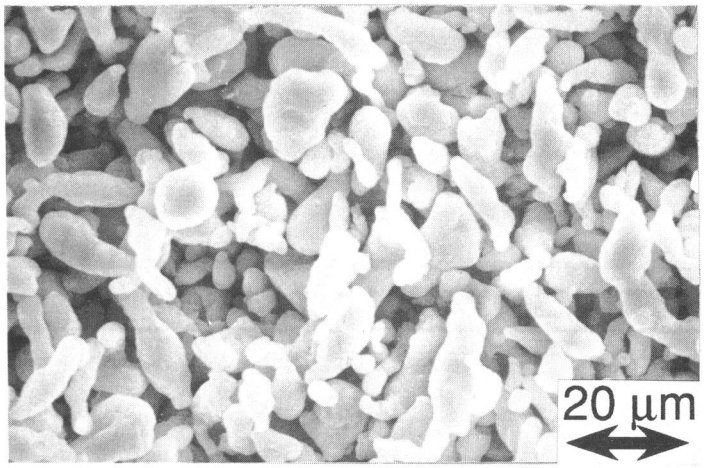

Fig. 2.2 Air atomized Al-Mg-Si (6061) alloy powder.

Table 2.2 Characteristics of the Si_3N_4 reinforcements used in the present investigation.

	Crystal phase	Diameter(μm)
Si_3N_4 particulate	α-phase	~ 0.2
	α-phase	~ 0.5
	α-phase	~ 1.0
Si_3N_4 whisker	β-phase	0.1~1.5 (10 ~30)[a)]

a) length (μm)

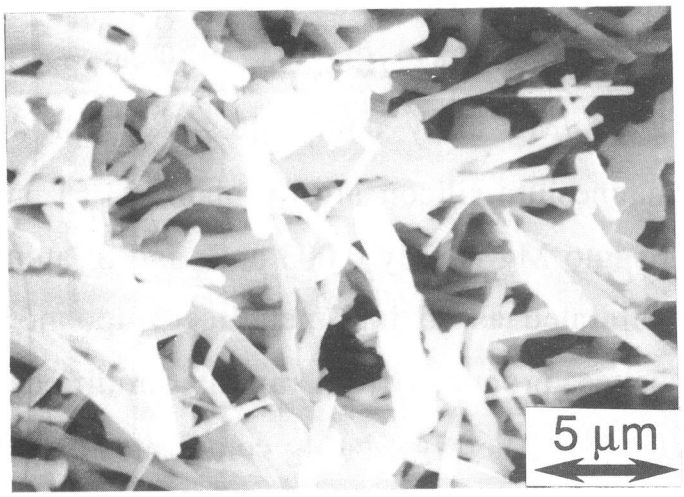

Fig. 2.3 Si_3N_4 whiskers used in the present investigation.

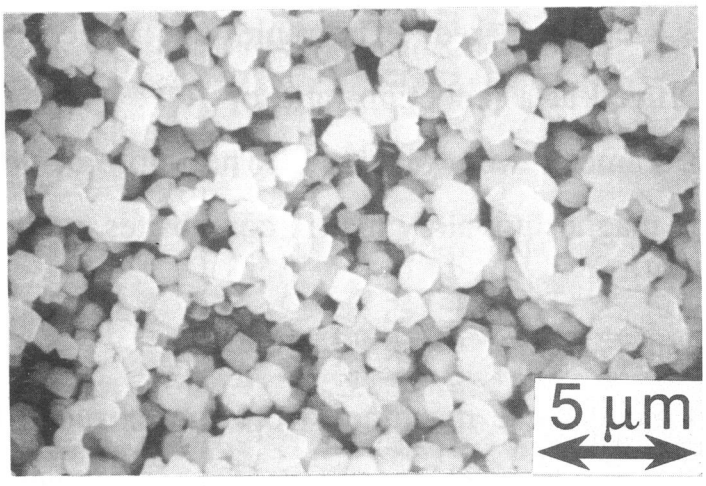

Fig. 2.4 Si_3N_4 particulates (~ 1 μm in diameter) used in the present investigation.

at 733 ~ 793 K in air and the extruded bars of 4 mm in diameter were obtained. The reinforcements and extrusion conditions for the aluminum alloy matrix composites are listed in Table 2.3.

Scheme of processing of Mg_2Si_p/Mg alloy composites is shown in Fig. 2.5. The Mg_2Si_p/Mg alloy composites were produced as *in-situ* composites from magnesium-silicon alloy ribbons [3-5], since a maximum solid solubility of Si into Mg is only 0.003 at.% and Si atoms react with Mg atoms and are precipitated as an intermetallic compound of Mg_2Si. The Mg_2Si_p/Mg composites, produced from rapidly solidified ribbons, showed very small grain sizes [5]. The Mg_2Si_p/Mg composites have high potential as structural materials because an intermetallic compound of Mg_2Si exhibits a high melting temperature, low density, high hardness and a low thermal expansion coefficient [6]. Recently, it was reported [3-5] that the Mg_2Si_p/Mg composites exhibited higher specific strength than AZ91(T4), 7075Al(T6) and Ti-6Al-4V(T6) alloys. In the present investigation, two kinds of rapidly solidified magnesium-silicon alloy ribbons (the chemical compositions: Mg-10.6wt.%Si-4.0wt.%Al and Mg-11.0wt.%Si-4.0wt.%Zn) with less than 0.1 mm in thickness were prepared. The rapidly solidified magnesium-silicon ribbons were extruded at a reduction ratio of 100 : 1 in air and the extruded bars of 4 mm in diameter were obtained. The reinforcements and extrusion conditions for the magnesium alloy matrix composites are listed in Table 2.3.

2.2 Tensile testing

Tensile specimens were machined from the extruded bars without any additional thermo-mechanical treatment for refinement of grain size. Geometry and dimension of a tensile test specimen are shown in Fig. 2.6.

Constant true strain rate tensile tests were carried out to investigate the deformation characteristics. Two kinds of testing machines were used to

Table 2.3 Reinforcements and extrusion conditions of the aluminum matrix composites and the magnesium matrix composites used in the present investigation.

	Reinforcement		Extrusion	
	size, kind and morphology	volume fraction, %	extrusion ratio	extrusion temperature, K
Si_3N_4*p*(0.2μm)/Al-Cu-Mg (2124)	~ 0.2μm Si_3N_4 particulate	20	100	733
Si_3N_4*p*(1μm)/Al-Cu-Mg (2124)	~ 1.0μm Si_3N_4 particulate	20	100	733
Si_3N_4*w*/Al-Cu-Mg (2124)	Si_3N_4 whisker	20	100	733
Si_3N_4*p*(0.2μm)/Al-Mg (5052)	~ 0.2μm Si_3N_4 particulate	20	100	763
Si_3N_4*p*(0.2μm)/Al-Mg-Si (6061)	~ 0.2μm Si_3N_4 particulate	20	100	773
Si_3N_4*p*(0.5μm)/Al-Mg-Si (6061)	~ 0.5μm Si_3N_4 particulate	20	100	773
Si_3N_4*p*(1μm)/Al-Mg-Si (6061)	~ 1.0μm Si_3N_4 particulate	20	100	773
Si_3N_4*w*/Al-Mg-Si (6061)	Si_3N_4 whisker	20	100	773
Si_3N_4*p*(1μm)/Al-Zn-Mg (7064)	~ 1.0μm Si_3N_4 particulate	20	100	793
Si_3N_4*w*/Al-Zn-Mg (7064)	Si_3N_4 whisker	20	100	793
Mg_2Si*p*/Mg-Al	0.7μm Mg_2Si particulate	28	100	623
Mg_2Si*p*/Mg-Zn	0.8μm Mg_2Si particulate	28	100	573

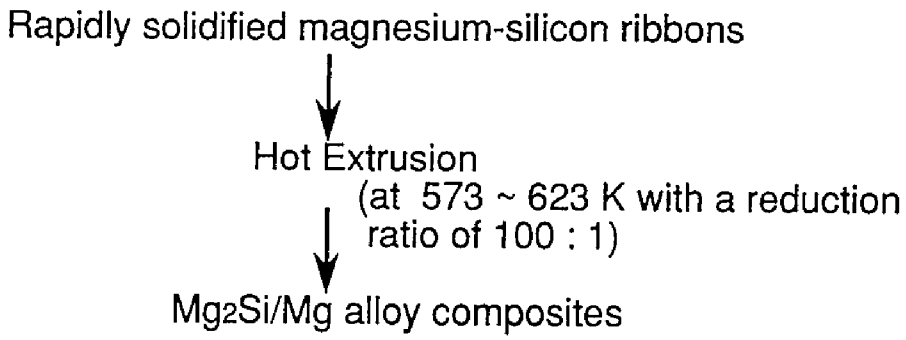

Fig. 2.5 Scheme of processing of Mg2Si/Mg alloy composites.

conduct tensile tests in a wide strain rate range. An Instron type of testing machine driven mechanically was used for tests at strain rates $< 1\ s^{-1}$, and an Instron type of testing machine driven hydraulically was used for tests at strain rates $\geq 1\ s^{-1}$. These two testing machines are shown schematically in Fig. 2.7 and Fig. 2.8, respectively.

The cavitation characteristics strongly depend on the stress for the high strain rate superplastic composite [7]. In the present investigations, constant true stress tensile tests were conducted for cavitation studies. The tensile testing machine is shown schematically in Fig. 2.9. Testing temperatures were attained using a three-zone furnace for all the tensile tests. In each zone, the temperature was controlled separately so that the required temperature was maintained constant for long periods in the range of $\pm$ 1 K. Specimens were deformed after holding 1.8×10^3 s in the furnace at the testing temperature.

2.3 Microstructural observation

Conventional metallographic techniques, scanning electron microscopy (SEM), and transmission electron microscopy (TEM) were used to investigate the microstructures. Samples for microscopic observation were cut such that the sample surface was parallel to the extrusion direction, as shown in Fig. 2.10. Disc specimens for TEM observation were cut from the samples annealed at a given testing temperature. They were mechanically ground to ~ 20 μm in thickness, and ion-milled to perforation with 3 keV argon ions. The grain sizes were determined on the basis of TEM observation. An apparent mean grain size was measured from a measurement of more than 100 grains, and the mean grain size was given by multiplication of the apparent mean grain size by a constant (=1.74).

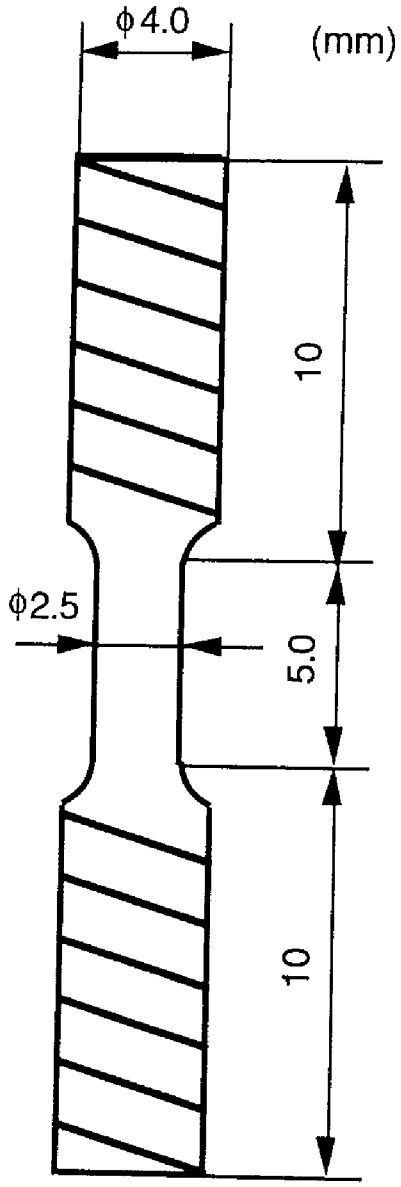

Fig. 2.6 Geometry and dimension of a tensile test specimen.

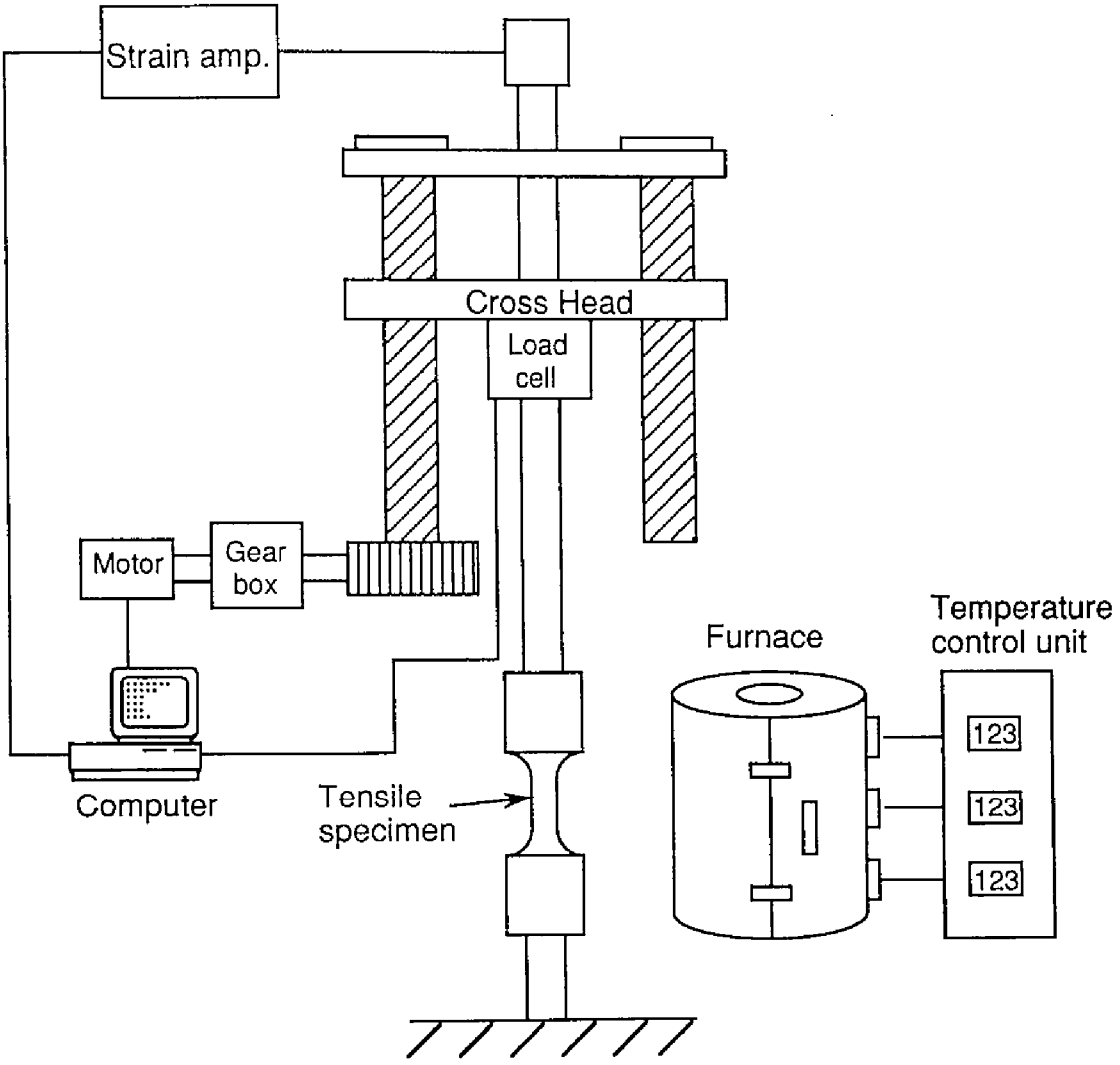

Fig. 2.7 Tensile testing machine for constant true strain rate tests in a low strain rate range < 1 s^{-1}.

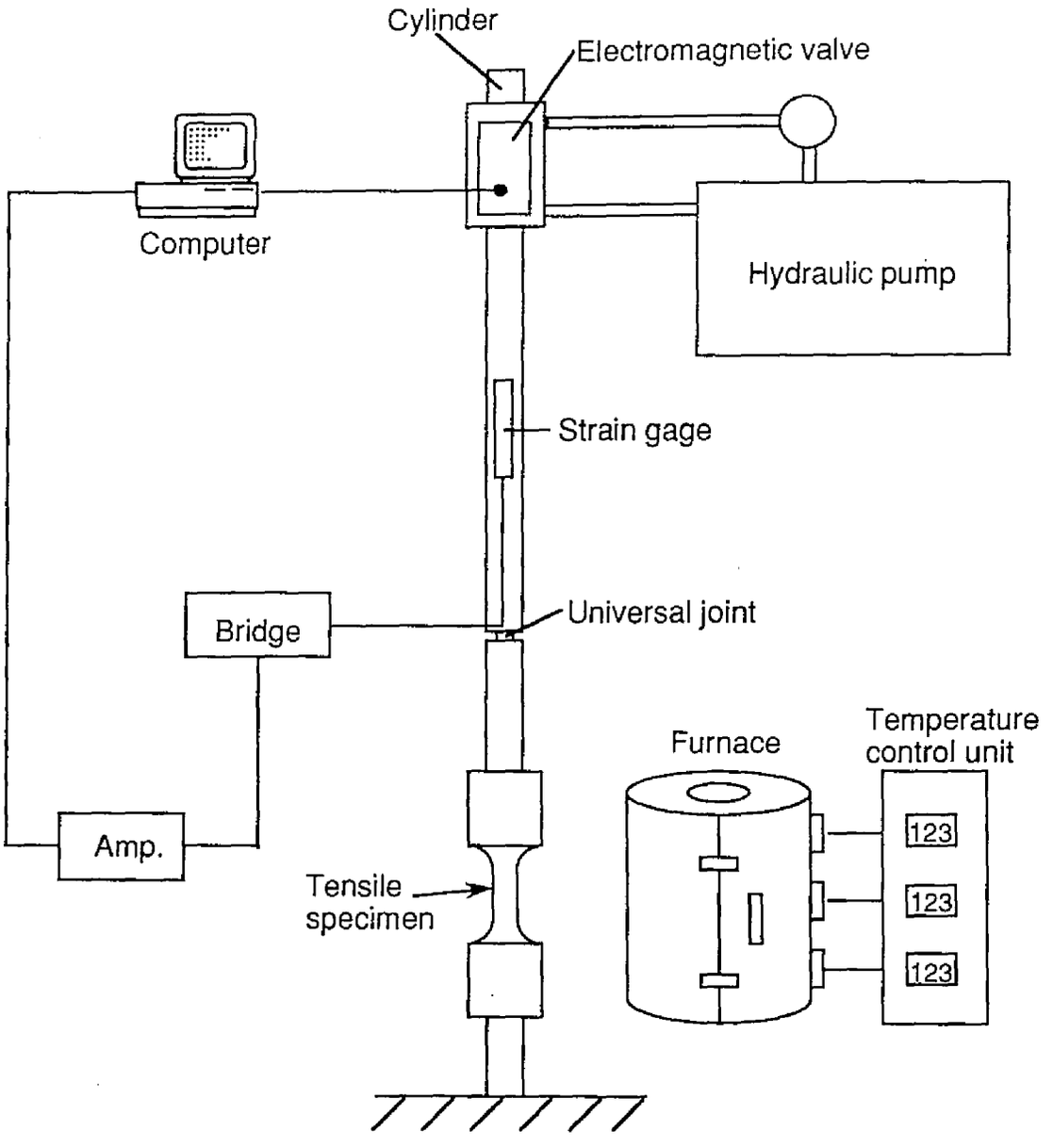

Fig. 2.8 Tensile testing machine for constant true strain rate tests in a high strain rate range $\geq 1\ s^{-1}$.

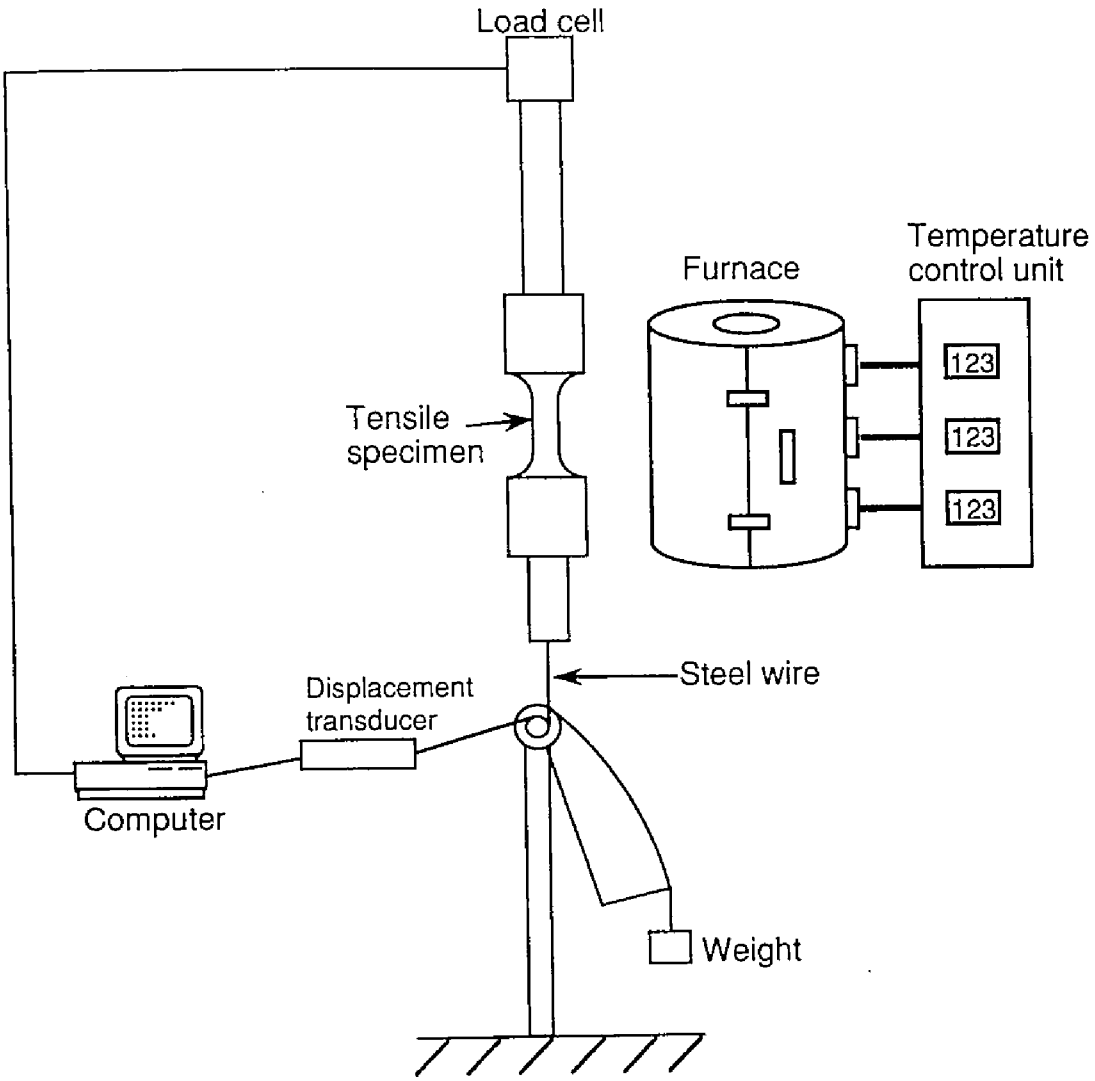

Fig. 2.9 Tensile testing machine for constant true stress tests.

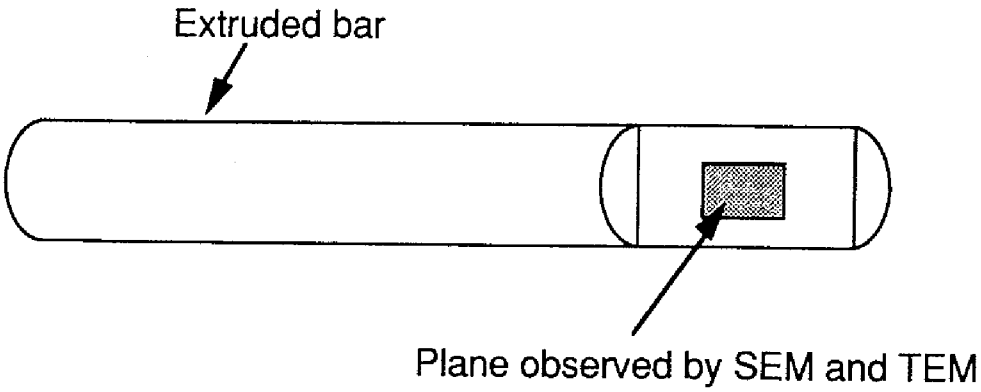

Fig. 2.10 Schematic illustration of a plane observed by SEM and TEM.

2.4 Cavitation studies

After specimens were deformed to a given strain, the specimens were removed from the furnace as soon as possible and were water-quenched. From these specimens, the cavity volumes were investigated by the density measurement method. The cavity volume is given by

$$C_v\,(\%) = \left[1 - \frac{M_{A1}(M_{A0} - M_{L0})}{M_{A0}(M_{A1} - M_{L1})}\right] \times 100 \qquad (2.1)$$

where C_v is the cavity volume (%), M_{A0} and M_{L0} are respectively the weight of the sample in air and in water prior to deformation, M_{A1} and M_{L1} are respectively the weight of the sample in air and in water after deformation.

In addition, the deformed specimens were polished on 240, 600 and 1000 mesh sand papers, and finally were polished with 1.0 and 0.05 μm Al_2O_3 powders, and microstructural observation was carried out. The cavitation was quantitatively analyzed on the basis of the microstructural observation.

References

1. J.R.Pickens, J. Mater. Sci., **16**, 1437 (1981).
2. P.D.Liddiard, Powder Metall., **27**, 193 (1984).
3. M.Mabuchi, K.Kubota and K.Higashi, Scripta Metall. Mater., **33**, 331 (1995).
4. M.Mabuchi, K.Kubota and K.Higashi, in *Light Weight Alloys for Aerospace Applications III*, edited by E.W.Lee, N.J.Kim, K.V.Jata and W.E.Frazier, (TMS, Warrendale, PA, 1995), p. 317.
5. M.Mabuchi and K.Higashi, Acta Mater., in press (1996).
6. S.Beer, G.Frommeyer and E.Schmid, in *Magnesium Alloys and Their Applications*, edited by B.L.Mordike and F.Hehmann, (DGM Informationsgesellschaft m.b.H, Oberursel, Germany, 1992), p. 317.
7. H.Iwasaki, M.Mabuchi and K.Higashi, Mater. Sci. Tech., in press (1996).

CHAPTER 3

MICROSTRUCTURAL CONTROL AND MECHANISM OF GRAIN REFINEMENT

3.1 Introduction

Recently, high strain rate superplastic metals have been developed from special methods or special materials such as mechanical alloying (MA) [1-4], physical vapor deposition [4] and amorphous powders [4]. However, it is of interest to note that high strain rate superplastic aluminum alloy matrix composites were processed by thermo-mechanical treatment [5] or hot extrusion [6-13] without special methods such as MA. For metallic materials containing a second hard phase such as metal matrix composites with high volumes of ceramic reinforcements, recrystallization is expected to be more accelerated by hot working, compared to metallic materials containing no second phase, because a second hard phase causes high dislocation density.

A very small grain size (less than $3 \sim 5$ μm) is required to attain high strain rate superplasticity, as will be shown in Chapter 7. However, the processing conditions and the mechanisms of grain refinement for attaining such a very small grain size are not clear. In this chapter, at first, typical microstructures are shown for aluminum matrix composites and magnesium matrix composites exhibiting high strain rate superplasticity. In addition, factors influencing grain refinement such as extrusion reduction are investigated by tensile tests and microstructural investigation in a Si_3N_{4w}/Al-Mg-Si (6061) composite, and the mechanisms of grain refinement are discussed on the basis of these results. The results in the present chapter can

give important information to the processing of high strain rate superplastic materials.

3.2 Experimental procedure

Al-Mg-Si (6061) alloy as a matrix and Si_3N_4 whisker as a reinforcement were used. The aluminum alloy powder and Si_3N_4 whisker (20 vol.%) were mixed in an alcohol-based solvent under ultrasonic waves prior to drying. The mixed powders were sintered at 873 K for 1.2×10^3 s with a pressure of 390 MPa in a hot press. A part of the sintered billets was preheated at 773 K for 3.6×10^4 s prior to hot extrusion. The sintered billets were then extruded at 773 K with reduction ratios of 4 : 1, 44 : 1 and 100 : 1. In addition, a whisker free Al-Mg-Si (6061) matrix alloy was processed at the same sintering and extrusion conditions.

Tensile tests were carried out in air mainly from 10^{-4} to 40 s^{-1} and at 818 K. The testing temperature of 818 K is an optimum temperature where a large elongation (600 %) was attained [8]. The samples required about 1.8×10^3 s to equilibrate at the test temperature prior to initiation of straining. The flow stress at each strain rate was determined at a fixed small strain of 0.1. Scanning electron microscopy (SEM) and transmission electron microscopy (TEM) were used to investigate the microstructures.

3.3 Results and discussion

3.3.1 Microstructures of high strain rate superplastic materials

High strain rate superplastic aluminum matrix composites and magnesium matrix composites have been processed by hot extrusion with a high reduction ratio of 100 : 1 [6-14]. Typical microstructures of the high strain rate superplastic composites are shown in Figs 3.1 ~ 3.4, where Fig. 3.1 and Fig. 3.2 are for the $Si_3N_{4p(1\mu m)}$/Al-Mg-Si composite, and Fig. 3.3 and

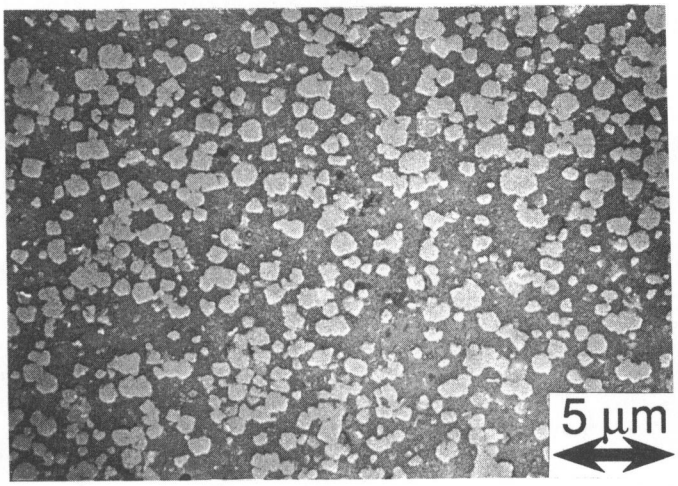

Fig. 3.1 Microstructure (scanning electron micrograph) of a high strain rate superplastic Si3N4*p*(1µm)/Al-Mg-Si (6061) composite.

Fig. 3.2 Microstructure (transmission electron micrograph) of a high strain rate superplastic $Si_3N_4p(1\mu m)$/Al-Mg-Si (6061) composite.

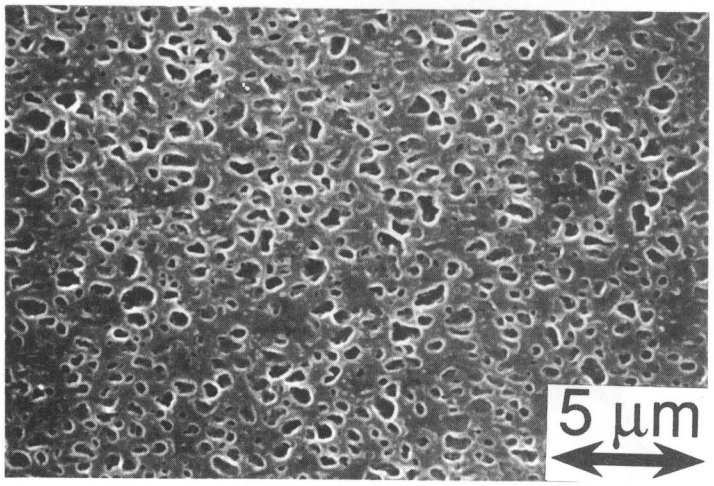

Fig. 3.3 Microstructure (scanning electron micrograph) of a high strain rate superplastic Mg2Si*p*/Mg-Al composite.

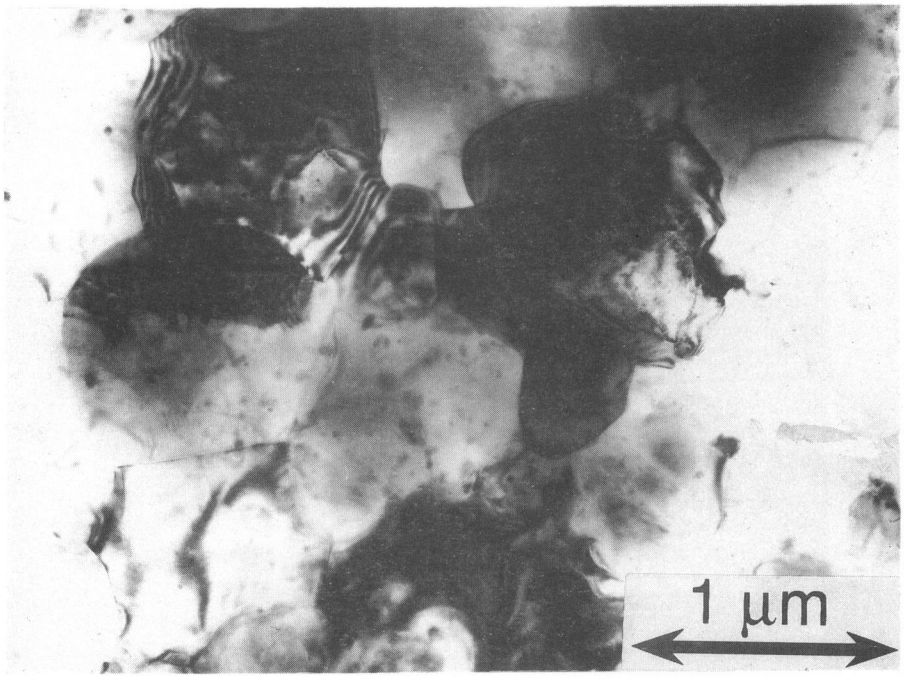

Fig. 3.4 Microstructure (transmission electron micrograph) of a high strain rate superplastic Mg_2Si_p/Mg-Al composite.

Fig. 3.4 are for the Mg_2Si_p/Mg-Al composite, respectively. It is found that the reinforcements were dispersed reasonably homogeneously. Dutta *et al.* [15] showed that the dispersion of particulates became more homogeneous by hot working for a SiC_p/Al-Mg (5083) composite. Hot extrusion at a high reduction ratio of 100 : 1 is likely to have a significant effect on the homogeneous dispersion of the fine reinforcements. This effect will be investigated later.

In general, breaking the oxide coating of the metallic powders is necessary in order to achieve good consolidation of aluminum powders [16,17]. Hot extrusion is one of the effective processes for compacting aluminum powders because a high shear stress, which is caused during extrusion with a high reduction ratio, makes clean surfaces in matrix powders and then can allow them to contact each other. In addition, there were few pores and cracks at interfaces between the reinforcement and the matrix. Hot extrusion at a high reduction ratio is supposedly effective for the consolidation of metallic powder and ceramic reinforcement as well as the consolidation of metallic powder and metallic powder.

It is found from Fig. 3.2 and Fig. 3.4 that the grains were almost equiaxed and were very small (less than 3 μm in grain size) for the composites. Hot extrusion is effective for grain refinement as well as for good consolidation of both powders and reinforcements. All high strain rate superplastic materials show very small grain sizes, as shown in Chapter 7. Therefore it is concluded that microstructural requirements for high strain rate superplasticity in materials containing reinforcements are (i) uniform distribution of reinforcements and (ii) a very small grain size.

3.3.2 Mechanism of grain refinement

3.3.2.1 Factors influencing grain refinement

A. Effects of reduction

Tensile properties were examined at 818 K for the as-sintered Si_3N_{4w}/Al-Mg-Si composite and the as-extruded Si_3N_{4w}/Al-Mg-Si composites, where hot extrusion was conducted at 773 K with different reduction ratios of 4 : 1, 44 : 1 and 100 : 1 to investigate effects of reduction on grain refinement. The variation in flow stress (top figure) and elongation to failure (bottom figure) as a function of strain rate at 818 K is shown in Fig. 3.5. It is accepted that one of the mechanical characteristics for superplastic flow is a high m value, where m is the strain rate sensitivity, and a value of m should be 0.5 or at least greater than 0.3 for superplastic flow. Another important characteristic of superplastic flow is grain size dependence of the mechanical properties [18-22]. The flow stress decreases and a superplastic region shifts to a higher strain rate range with decreasing grain size for superplastic flow. It is found from Fig. 3.5 that the extruded composites exhibited high m (> 0.3) and large elongations. However, the sintered composite showed a low m value of 0.24 and relatively low elongations (≤ 75 %). It appears that the superplastic region is displaced to a higher strain rate range with increasing reduction ratio in the range investigated. It is noted that a large elongation of about 600 % was attained at a high strain rate of 2×10^{-1} s^{-1} for the composite extruded at a high reduction ratio of 100 : 1.

Microstructures of the as-sintered composite and the as-extruded composite with a reduction ratio of 100 : 1 are shown Fig. 3.6. The composite extruded at a high reduction ratio of 100 : 1 showed a very small grain size of about 3 μm. On other hand, the sintered composite had coarser grains (about 20 μm). The grain size of the sintered composite is roughly the same as the powder diameter. The variation in the grain size as a function of a reduction ratio is shown in Fig. 3.7. It is found that the grain size decreased with increasing reduction. Pinned dislocations, dislocation networks and

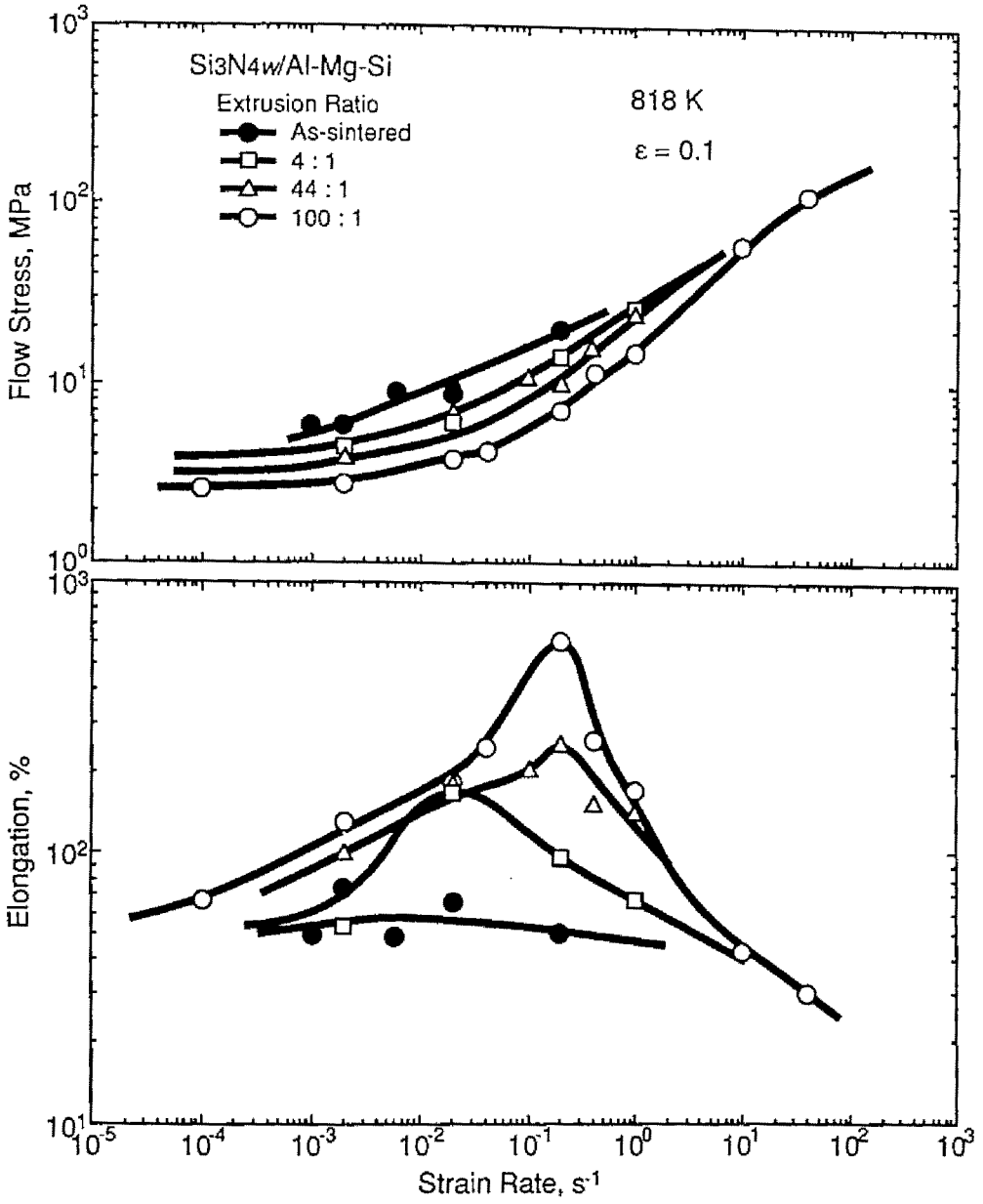

Fig. 3.5 The variation in flow stress (top figure) and elongation to failure (bottom figure) as a function of strain rate at 818 K for the sintered Si_3N_4w/Al-Mg-Si composite and the extruded Si_3N_4w/Al-Mg-Si composites with reduction ratios of 4 : 1, 44 : 1 and 100 : 1.

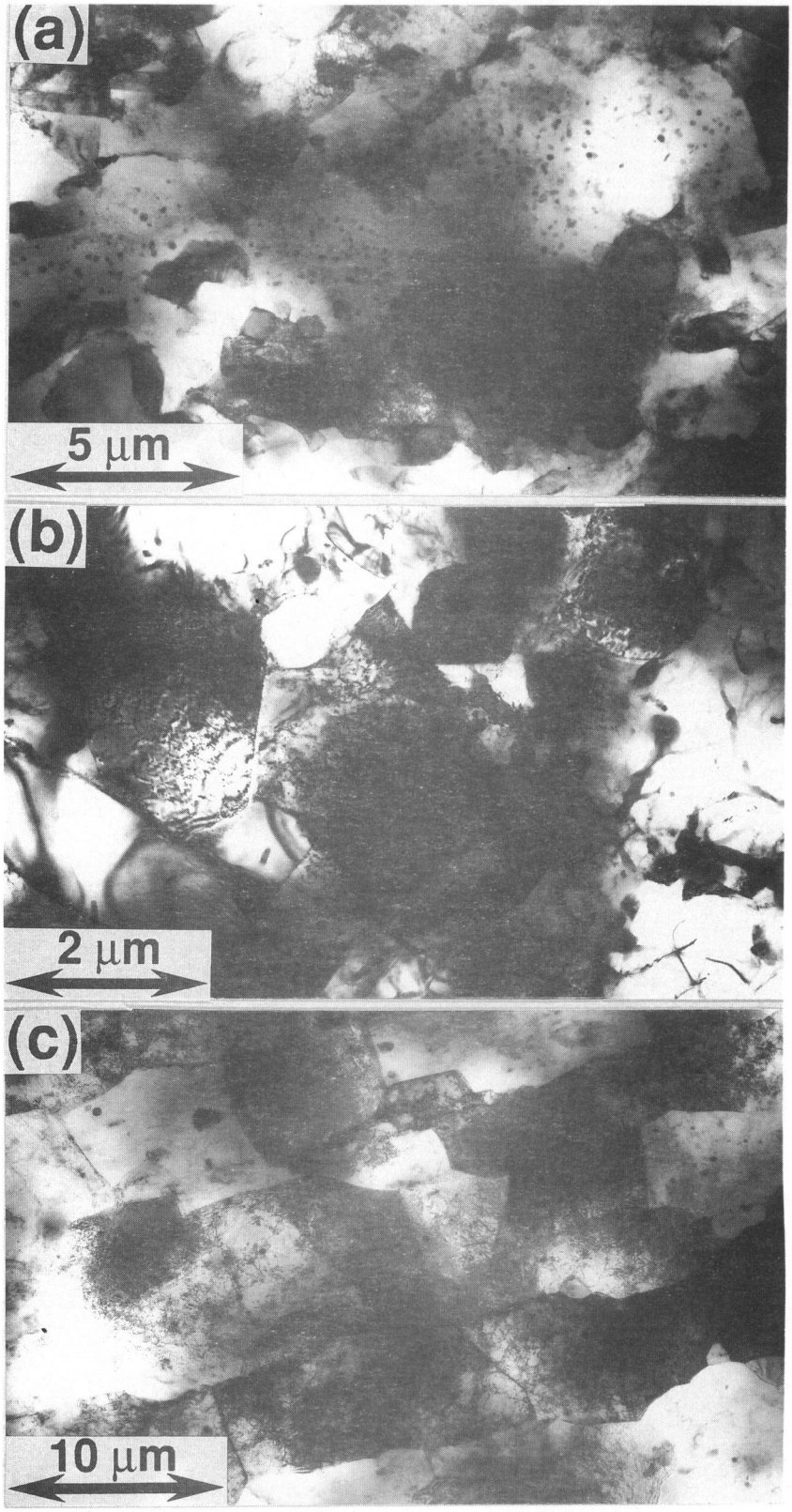

Fig. 3.6 Microstructures of (a) the Si_3N_4*w*/Al-Mg-Si composite sintered at 873 K, (b) the Si_3N_4*w*/Al-Mg-Si composite extruded at 773 K with a reduction ratio of 100 : 1, and (c) the Al-Mg-Si matrix alloy extruded at 773 K with a reduction ratio of 100 : 1.

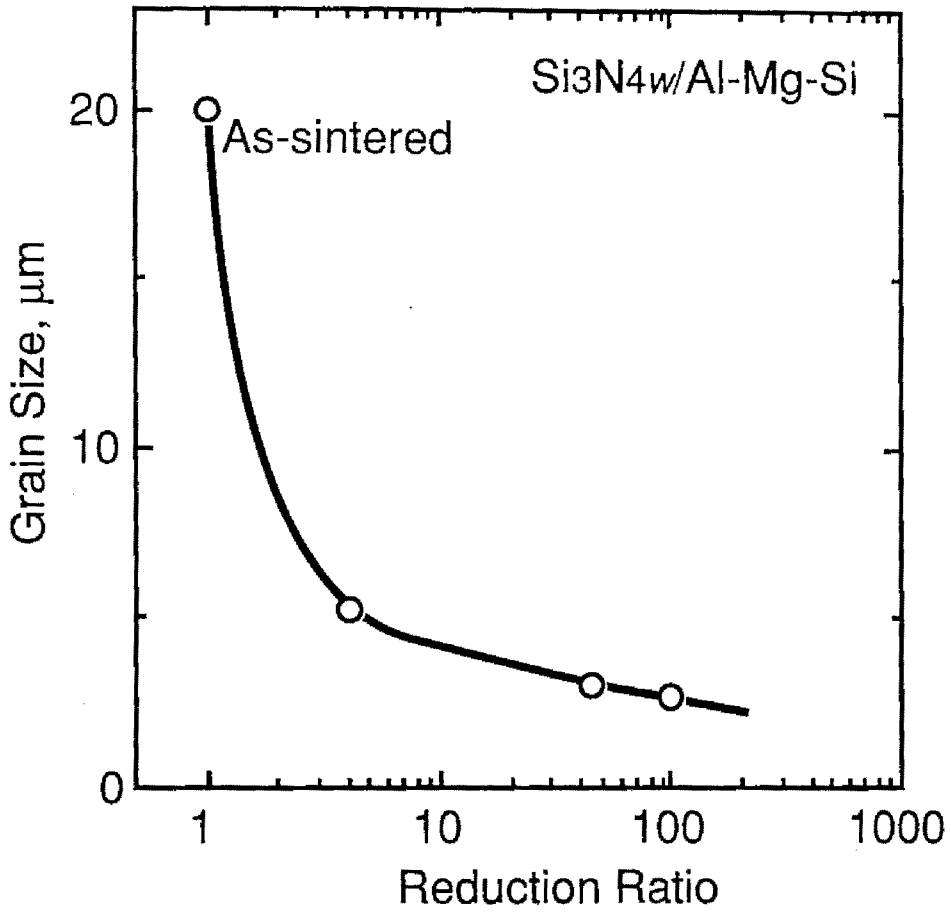

Fig. 3.7 The variation in the grain size as a function of a reduction ratio.

precipitates of 0.1 ~ 1 μm in diameter were observed for the extruded composites. On the other hand, there were fewer dislocations and fewer precipitates of about 0.1 ~ 1 μm for the as-sintered composite.

Scanning electron micrographs of the sintered composite and the extruded composite are shown in Fig. 3.8. It was found that the whiskers were fractured, resulting in a reduction in the aspect ratio and that they were aligned in the extrusion direction. The average length and diameter of the whiskers were respectively 8 and 0.5 μm for the composite extruded at a reduction ratio of 100 : 1. It appears that there were fewer voids and cracks at the matrix/reinforcement interface for the extruded composite than for the sintered composite. It has been reported that hot working gives rise to fracture of reinforcements and uniform distribution of reinforcements, on the other hand, a degradation of the interface is caused [23]. In the present investigation, however, the whiskers were dispersed reasonably uniformly without degradation of the interfaces by hot extrusion.

B. Effects of reinforcements

The variation in flow stress (top figure) and elongation to failure (bottom figure) as a function of strain rate at 818 K is shown in Fig. 3.9 for the extruded Si_3N_{4w}/Al-Mg-Si composite and the extruded Al-Mg-Si matrix alloy. The composite and the matrix alloy were extruded at the same temperature of 773 K and at the same reduction ratio of 100 : 1. The extruded composite exhibited a high m value (> 0.3) at 4 x 10^{-2} ~ 10 s^{-1} and a maximum elongation of about 600 % at 2 x 10^{-1} s^{-1}. However, the extruded matrix alloy showed a high m value at lower strain rates of 5 x 10^{-4} ~ 2 x 10^{-2} s^{-1} and a maximum elongation of about 200 % at a lower strain rate of 10^{-2} s^{-1}. It follows that the extruded composite had higher superplastic potential than the extruded matrix alloy.

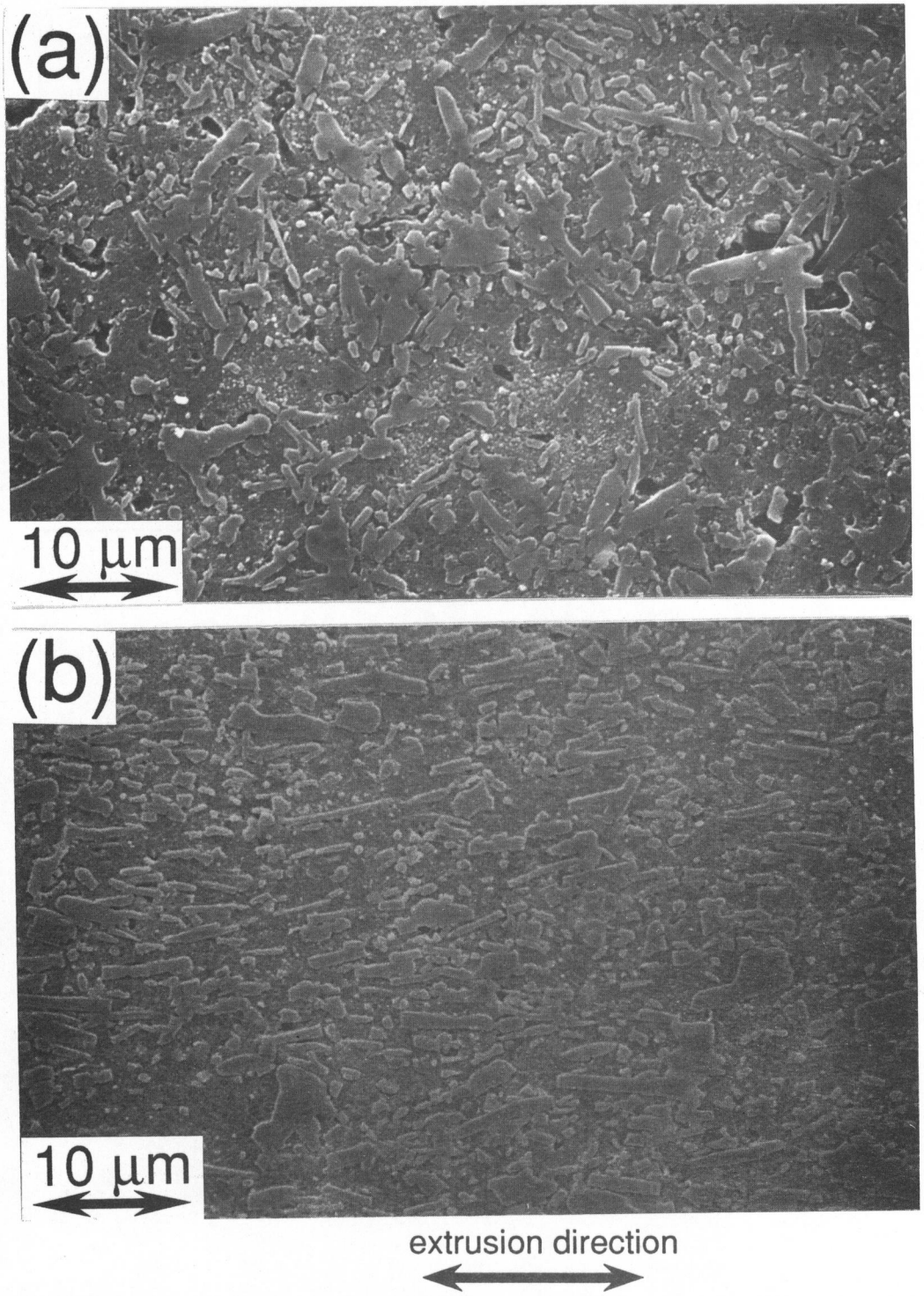

Fig. 3.8 Scanning electron micrographs of (a) the Si_3N_4w/Al-Mg-Si composite sintered at 873 K, (b) the Si_3N_4w/Al-Mg-Si composite extruded at 773 K with a reduction ratio of 100 : 1.

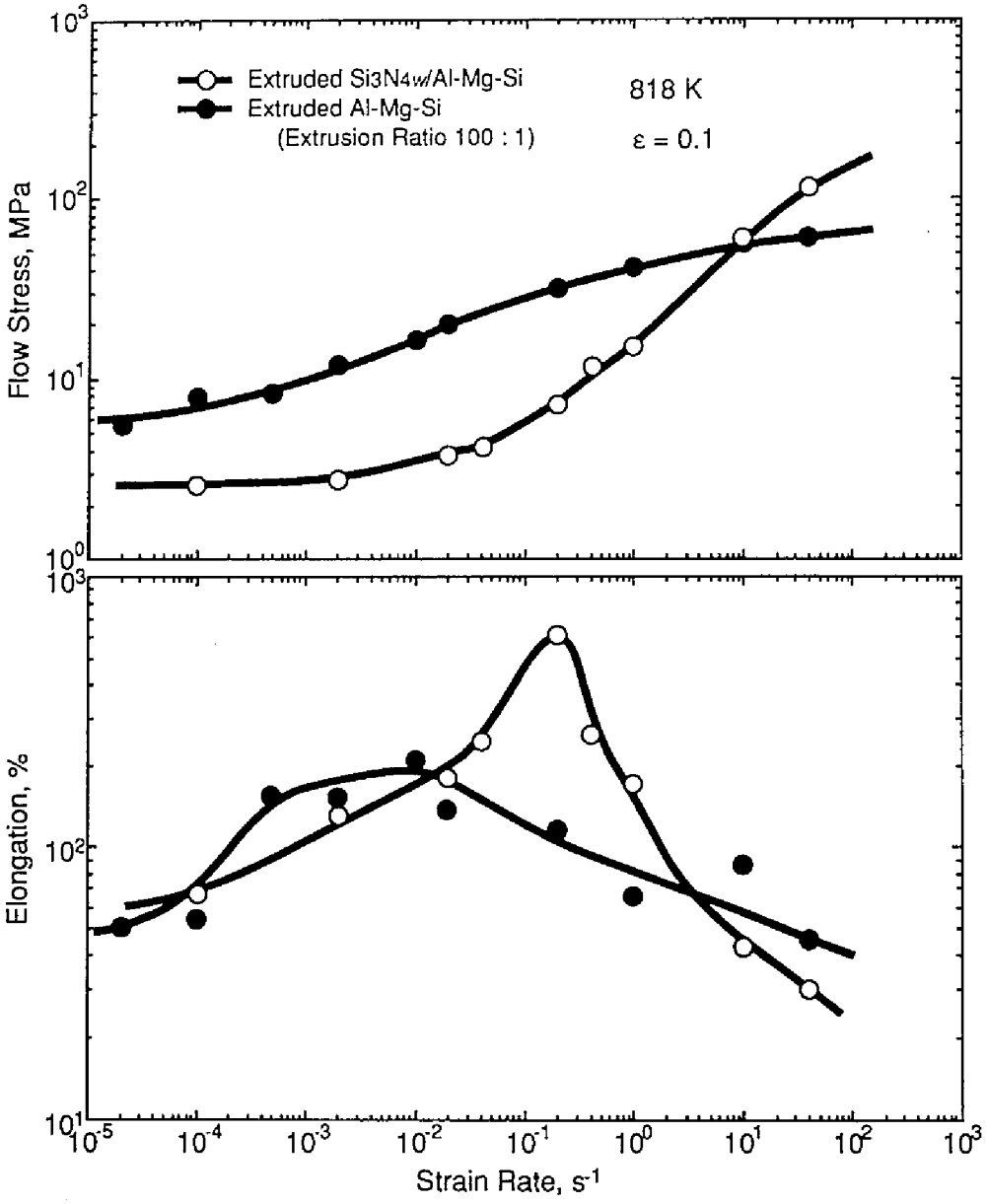

Fig. 3.9 The variation in flow stress (top figure) and elongation to failure (bottom figure) as a function of strain rate at 818 K for the extruded Si3N4w/Al-Mg-Si composite and the extruded Al-Mg-Si matrix alloy, where hot extrusion is carried out at 773 K with a reduction ratio of 100 : 1.

For the extruded matrix alloy, grains were elongated to the extrusion direction and were coarser than those of the extruded composites (Fig. 3.6). Also, many low angle grain boundaries were observed for the extruded matrix alloy. These results indicate that reinforcements played an important role in grain refinement.

C. Effects of dynamic precipitation

It is suggested in the previous works [10,11] that fine particles were precipitated dynamically during hot extrusion and limited grain growth during hot extrusion. It is worthwhile investigating a non-dynamically precipitated composite in order to demonstrate the effect of dynamic precipitation. A part of the sintered billet was preheated at 773 K for 3.6×10^4 s to cause precipitation prior to the hot extrusion. A TEM micrograph of the preheated composite prior to hot extrusion is shown in Fig. 3.10. It is found that a large number of coarse particles of about 1 μm in diameter were precipitated during the preheat. The preheated composite was extruded at 773 K with a reduction ratio of 100 : 1. The variation in flow stress (top figure) and elongation to failure (bottom figure) as a function of strain rate at 818 K is shown in Fig. 3.11 for the extruded composite and the preheated and extruded composite. The extruded composite showed a high m value (> 0.3) at $4 \times 10^{-2} \sim 10$ s^{-1} and a maximum elongation of about 600 % at 2×10^{-1} s^{-1}. However, the preheated and extruded composite showed a high m value at lower strain rates of $2 \times 10^{-2} \sim 2 \times 10^{-1}$ s^{-1} and a maximum elongation of about 265 % at a lower strain rate of 2×10^{-2} s^{-1}.

Microstructures during hot extrusion were investigated by TEM. Typical micrographs are shown in Fig. 3.12. It is found from Fig. 3.12 (a) that a number of fine particles were precipitated for the extruded composite. The average size of the precipitates was about 20 nm. The fine precipitates were

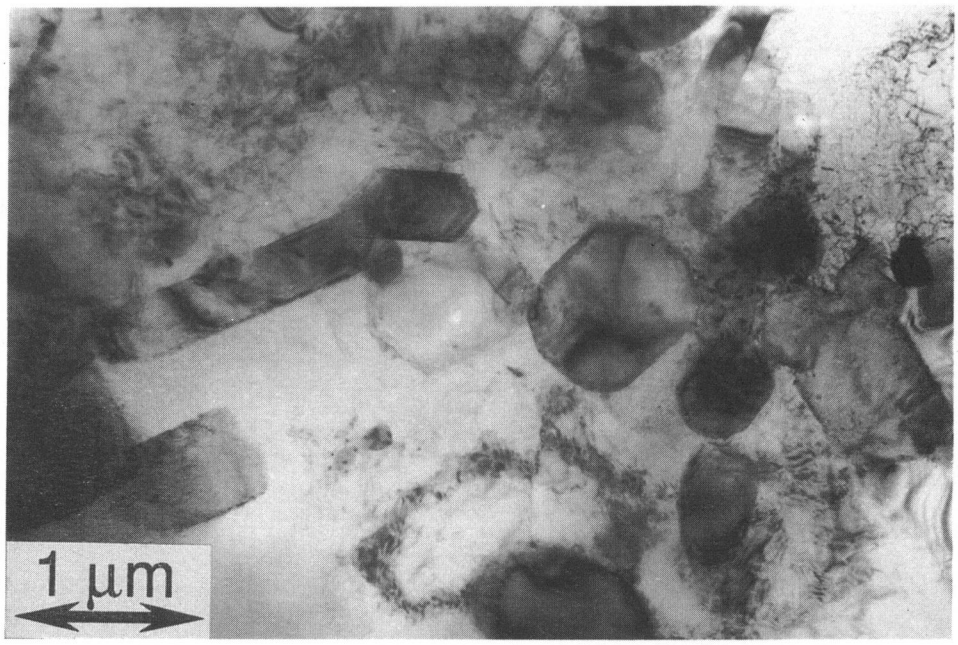

Fig. 3.10 Transmission electron micrograph of the preheat-treated Si_3N_4w/Al-Mg-Si composite, where preheat treatment is performed at 773 K for 3.6×10^4 s.

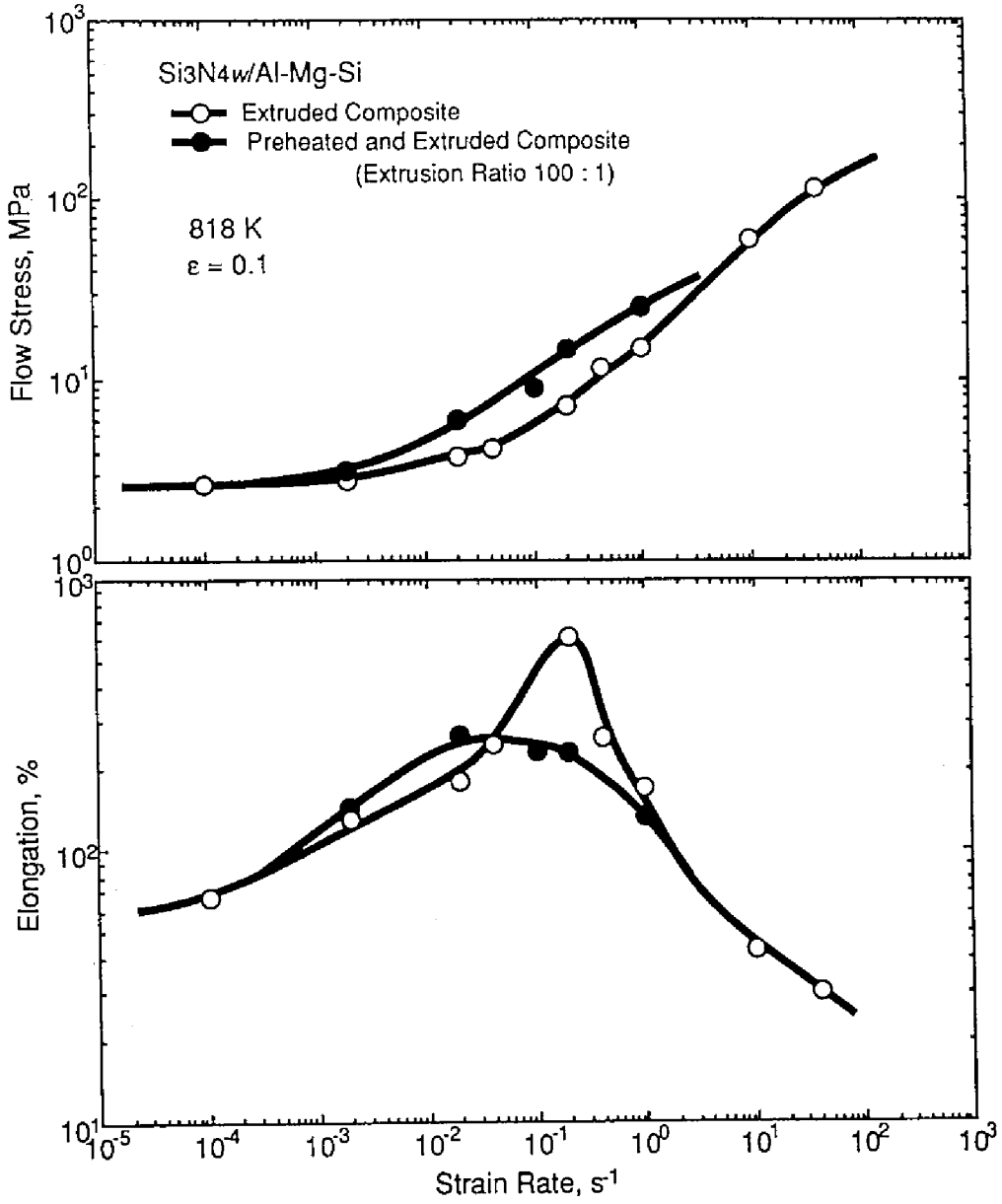

Fig. 3.11 The variation in flow stress (top figure) and elongation to failure (bottom figure) as a function of strain rate at 818 K for the extruded Si3N4w/Al-Mg-Si composite and the preheat-treated and extruded Si3N4w/Al-Mg-Si composite, where the composites are extruded at 773 K with a reduction ratio of 100 : 1.

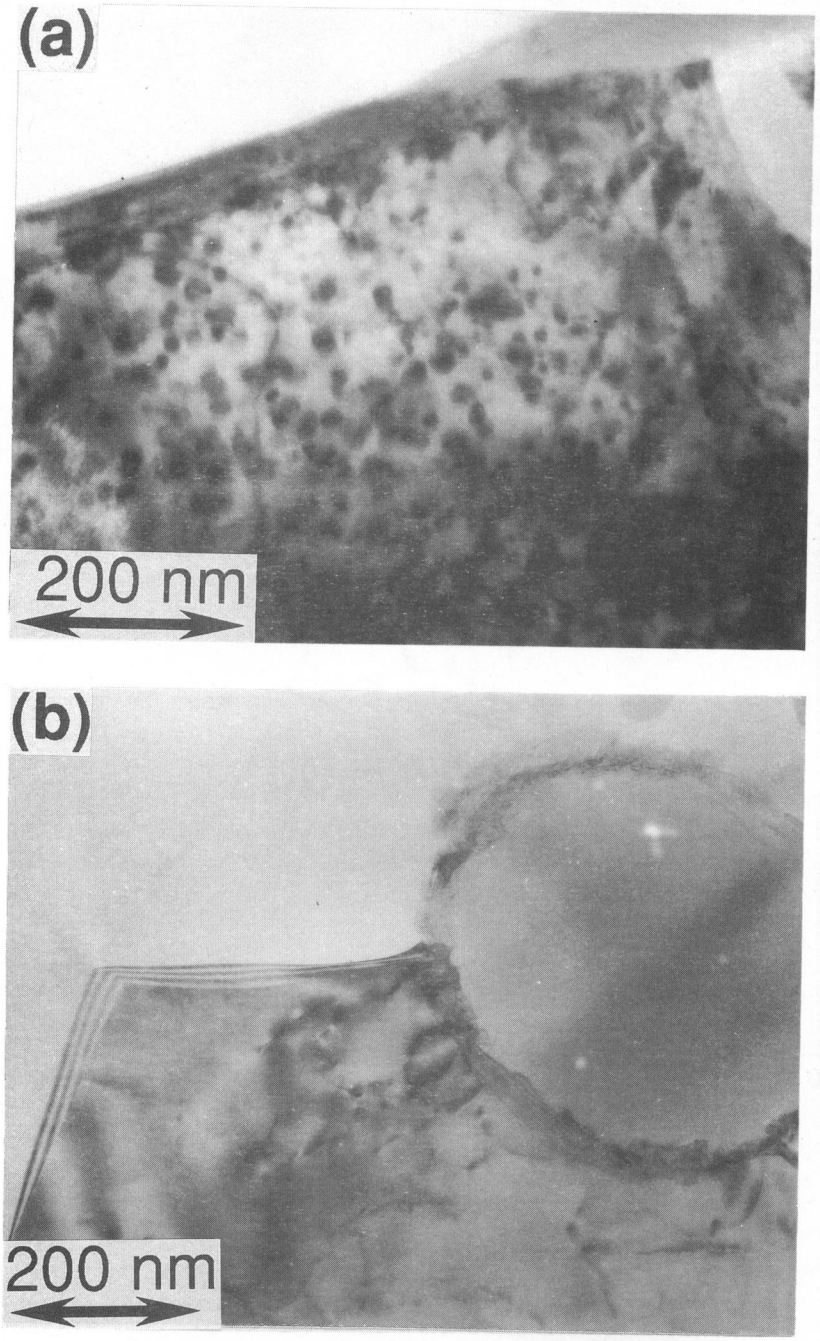

Fig. 3.12 Microstructures during hot extrusion for the Si3N4*w*/Al-Mg-Si composites: (a) the extruded composite and (b)the preheat-treated and extruded composite.

not observed prior to hot extrusion. It is suggested that alloying additions precipitated dynamically during hot extrusion. On the other hand, there were no fine precipitates of a size less than 0.1 μm in the preheated and extruded composite (Fig. 3.12 (b)), indicating that dynamic precipitation did not occur during hot extrusion for the preheated and extruded composite. This is because almost all the alloying additions precipitated out during preheating prior to hot extrusion. The grain size of the preheated and extruded composite was about 5 μm, which is larger than that of the extruded composite. These results clearly point out the importance of dynamic precipitation in grain refinement.

3.3.2.2 Origin of grain refinement

In general, the presence of a dispersed second phase and a considerable quantity of dissolved alloying additions are an important modification to the structure [24,25]. In particular, large (≥ about 1 μm), non-deformable particles cause intense strain gradients around the particles [26] and stimulate recrystallization in the deformed zones adjacent to the particles [26,27]. The fact that there were more low angle grain boundaries for the extruded matrix alloy than for the extruded composites indicates that recrystallization was accelerated by the presence of the reinforcements. It is recognized that when recrystallization occurs continuously, pinned dislocations and dislocation networks remain intact. On the other hand, when recrystallization occurs discontinuously, the sweeping action of high angle boundaries removes pinned dislocations and dislocation networks. In this investigation, the fact that pinned dislocations and dislocation networks were observed in the grains of the extruded composites suggests that the operative mechanism of grain refinement by hot extrusion is continuous recrystallization during hot extrusion.

Christman and Suresh [28] showed that nucleation of precipitates was enhanced for an aluminum alloy matrix composite, compared with that of the matrix alloy, because of preferential precipitation of solute atoms at dislocations generated by the presence of reinforcements. Therefore dynamic precipitation during hot extrusion is likely attributed to enhancement of precipitation through the increased dislocation density resulting from the presence of reinforcements. The limiting grain size to which grains grow, in the absence of abnormal grain growth, is given by [27]

$$d = \frac{2d_p}{3V_f} \tag{3.1}$$

where d is the limiting grain size, d_p is the particle diameter and V_f is the volume fraction of the particles. The limiting grain size is calculated to be 6.7 μm if the whiskers limit grain growth, where the effective reinforcement size for whisker is taken as $\sqrt{L_1 L_2}$, where L_1 is the average length of the whiskers and L_2 is the average diameter of the whiskers. The value of 6.7 μm is larger than the experimentally measured grain size of about 3 μm. When the fine precipitates limit grain growth, the limiting grain size is calculated to be 2.6 μm, where the particle diameter and the volume fraction of the particles are taken to be 20 nm and 0.5 %, respectively. The value is in agreement with the experimentally measured grain size. It is likely that the fine particles, resulting from dynamic precipitation, play a vital role in limiting grain growth during hot extrusion. Therefore it is concluded that an interaction of recrystallization and dynamic precipitation results in very small grain sizes for the aluminum alloy matrix composites, and the mechanism is enhanced by the presence of reinforcements.

3.4 Conclusions

(1) Microstructural requirements for high strain rate superplasticity in materials containing reinforcements are uniform distribution of reinforcements and a very small grain size.

(2) The requirements were attained by hot extrusion with a reduction ratio of 100 : 1 for the aluminum alloy matrix composites with Si_3N_4 reinforcements.

(3) Recrystallization was accelerated by the presence of reinforcements and grain growth was limited by fine particles precipitated dynamically during hot extrusion. An interaction of recrystallization and dynamic precipitation resulted in grain refinement, which was enhanced by the presence of reinforcements.

References

1. T.G.Nieh, P.S.Gilman and J.Wadsworth, Scripta Metall., **19**, 1375 (1985).
2. T.R.Bieler, T.G.Nieh, J.Wadsworth and A.K.Mukherjee, Scripta Metall., **22**, 81 (1988).
3. K.Higashi, T.Okada, T.Mukai and S.Tanimura, Scripta Metall. Mater., **25**, 2053 (1991).
4. K.Higashi, Mater. Sci. Eng. A, **A166**, 109 (1993).
5. T.G.Nieh, C.A.Henshall and J.Wadsworth, Scripta Metall., **18**, 1405 (1984).
6. T.Imai, M.Mabuchi, Y.Tozawa and M.Yamada, J. Mater. Sci. Lett., **9**, 255 (1990).
7. H.Xiaoxu, L.Qing, C.K.Yao and [illegible]Mei, J. Mater. Sci. Lett., **10**, 964 (1991).
8. M.Mabuchi, T.Imai, K.Kubo, K.Higashi, Y.Okada and S.Tanimura, Mater. Lett., **11**, 339 (1991).
9. M.Mabuchi, T.Imai, K.Kubo, K.Higashi and S.Tanimura, Mater. Lett., **12**, 330 (1991).
10. M.Mabuchi, T.Imai and K.Higashi, Mater. Sci. Forum, **113-115**, 545 (1993).
11. M.Mabuchi and K.Higashi, in *Advanced Composites '93*, edited by T.Chandra and A.K.Dhingra, (TMS, Warrendale, PA, 1993), p. 1141.
12. M.Mabuchi, T.Imai and K.Higashi, J. Mater. Sci., **28**, 6582 (1993).
13. M.Mabuchi and K.Higashi, J. Mater. Res., **10**, 2494 (1995).
14. M.Mabuchi, K.Kubota and K.Higashi,, Scripta Metall. Mater., **33**, 331 (1995).
15. I.Dutta, C.F.Tiedemann and T.R.McNelley, Scripta Metall., **24**, 1233 (1990).
16. F.V.Lenel and G.S.Ansell, J. Met., **34**, 17 (1982).

17. F.H.Froes and J.R.Pickens: J. Met., **36**, 14 (1984).
18. F.A.Mohamed and T.G.Langdon, Acta Metall., **23**, 117 (1975).
19. R.C.Gifkins, Metall. Trans. A, **7A**, 1225 (1976).
20. S.-A.Shei and T.G.Langdon, Acta Metall., **26**, 639 (1978).
21. A.Arieli, A.K.S.Yu and A.K.Mukherjee, Metall. Trans. A, **11A**, 181 (1980).
22. C.H.Hamilton, C.C.Bampton and N.E.Paton, in *Superplastic Forming of Structural Alloys,* edited by N.E.Paton and C.H.Hamilton, (The Metall. Soc. AIME, Warrendale, PA, 1982), p. 173.
23. I.Dutta, C.F.Tiedemann and T.R.McNelley, Scripta Metall. Mater., **24**, 1233 (1990).
24. M.A.Zaidi and T.Sheppard, Metal Sci., **16**, 229 (1982).
25. T.Sheppard and M.G.Tutcher, Metal Sci, **14**, 579 (1980).
26. F.J.Humphreys, Metal Sci., **13**, 136 (1979).
27. F.J.Humphreys, Mater. Sci. Eng. A, **A135**, 267 (1991).
28. T.Christman and S.Suresh, Acta Metall., **36**, 1691 (1988).

CHAPTER 4

DEFORMATION CHARACTERISTICS IN HIGH STRAIN RATE SUPERPLASTIC ALUMINUM MATRIX COMPOSITES

4.1 Introduction

Deformation characteristics of dislocation creep behavior for aluminum matrix composites reinforced with ceramic whiskers or particulates have been extensively investigated [1-12]. It was shown that the stress exponent values for the composites are very high (for example, $n > 10$, where n is the stress exponent) and the activation energy values for dislocation creep in the composites are higher than the one for lattice diffusion. Recently, however, an analysis through the threshold stress concept revealed that the activation energy values for dislocation creep in the composites are almost equal to the one for lattice diffusion [7,9,12]. Thus, understanding of deformation characteristics of dislocation creep behavior for aluminum matrix composites has advanced.

There are some studies [13-19] on deformation characteristics of superplasticity for metal matrix composites, however, understanding of deformation characteristics of superplastic behavior for metal matrix composites is not sufficient and the deformation mechanisms are the subject in some debate. Mishra and Mukherjee [17] investigated elevated temperature mechanical properties of the superplastic aluminum alloy composites reinforced with discontinuous SiC and they showed that the activation energy for superplastic flow was 313 kJ/mol, which was near the one for diffusion creep in SiC. On the other hand, Nieh *et al.* [18,19] suggested that a liquid

phase might play an important role in high strain rate superplasticity for the composites. Recently, Higashi *et al.* [20,21] investigated effect of temperature on the mechanical properties of mechanically-alloyed metals exhibiting high strain rate superplasticity and they revealed that the presence of a liquid phase strongly affected the mechanical properties. These studies indicate that the deformation characteristics of high strain rate superplasticity are affected by the presence of a liquid phase.

This chapter describes the deformation characteristics of a variety of aluminum matrix composites exhibiting high strain rate superplasticity. As will be shown in Chapter 6, partial melting occurs at elevated temperature for the aluminum matrix composites investigated. In the present investigation, constant strain rate tensile tests were carried out in a wide temperature range including temperatures above and below the onset temperature for partial melting of each composite. The activation energy is analyzed through the threshold stress concept on the basis of the results of the tensile tests. In addition, a rate-controlling process of superplastic deformation is investigated in a temperature range below the onset temperature for partial melting from the viewpoint of effects of reinforcements.

4.2 Experimental procedure

Ten kinds of aluminum matrix composites listed in Table 2.3 were prepared, and constant true strain rate tensile tests were carried out. To investigate the grain size dependence, parts of the as-extruded bar of the Si_3N_{4w}/Al-Mg-Si composite were exposed at a temperature of 818 K for 36×10^3 and 86.4×10^3 s in order to produce samples with different grain sizes. As a result, the samples with grain sizes of 2.7, 4.0 and 4.7 μm were obtained, where the grain sizes were examined from the samples annealed at 818 K for 1.8×10^3 s.

Constant true strain rate tensile tests were carried out in air in a wide temperature range including the onset temperature for partial melting of each composite, where the onset temperature for partial melting was determined by DSC measurements. The partial melting behavior will be investigated in detail in Chapter 6. The tensile axis was selected to be parallel to the extrusion direction for all tests. The flow stress for each strain rate was determined at the fixed small true strain of 0.1.

4.3 Results and discussion

4.3.1 Mechanical properties

4.3.1.1 Strain rate dependence

A. Al-Cu-Mg (2124) alloy matrix composites

Representative plots of true stress *vs.* true strain are shown in Figs 4.1 ~ 4.3 for three Al-Cu-Mg (2124) alloy matrix composites tested at different temperatures and at strain rates of the order of, or close to, 10^{-1} s^{-1}: the selected strain rates are within the ranges where each material is reasonably superplastic. Three conclusions may be drawn from inspection of these curves. First, each composite exhibits excellent ductility at these high stain rates. Second, the curve for the Si_3N_{4w}/Al-Cu-Mg composite shows strain hardening almost up to the point of failure, whereas the curves for the Si_3N_{4p}/Al-Cu-Mg composites show both strain hardening and strain softening or with nearly a steady-state flow at the higher testing temperatures. Third, the curves tend to have irregular serrations, especially at the lower temperatures.

By conducting a series of tests over a range of strain rates at different temperatures, it was possible to plot both the flow stress, defined as the stress at a small strain of 0.1, and the elongation to failure against the imposed strain rate. The results are shown in Figs 4.4 ~ 4.6. For each composite, the flow

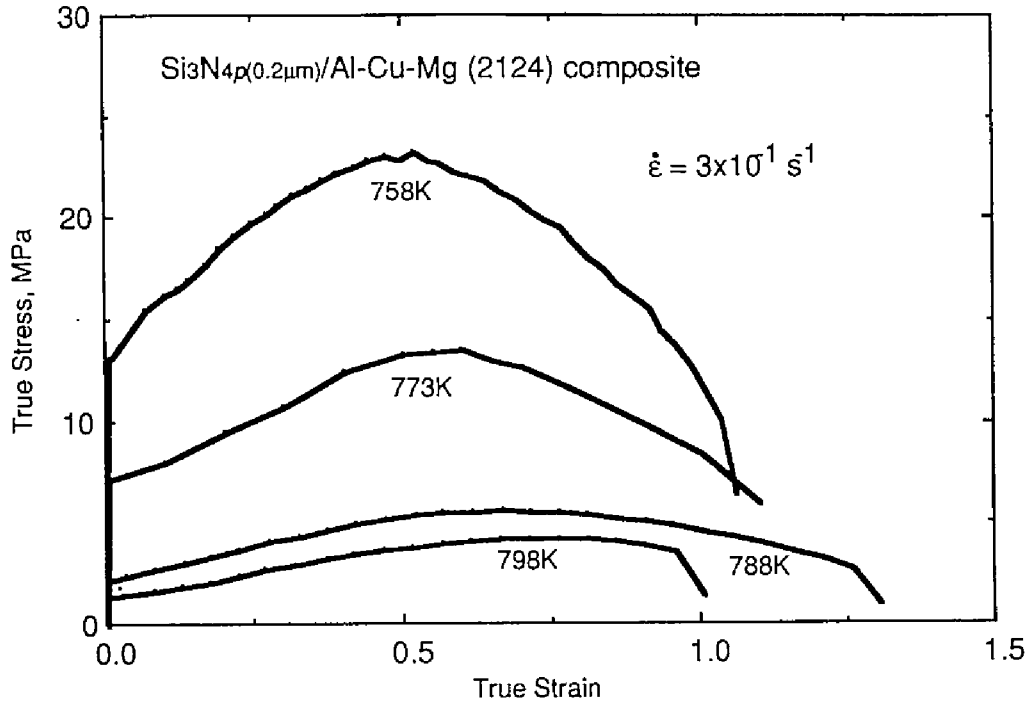

Fig. 4.1 True stress *vs* true strain at a strain rate of 3 x 10^{-1} s^{-1} for the $Si_3N_{4p(0.2\mu m)}$/Al-Cu-Mg (2124) composite.

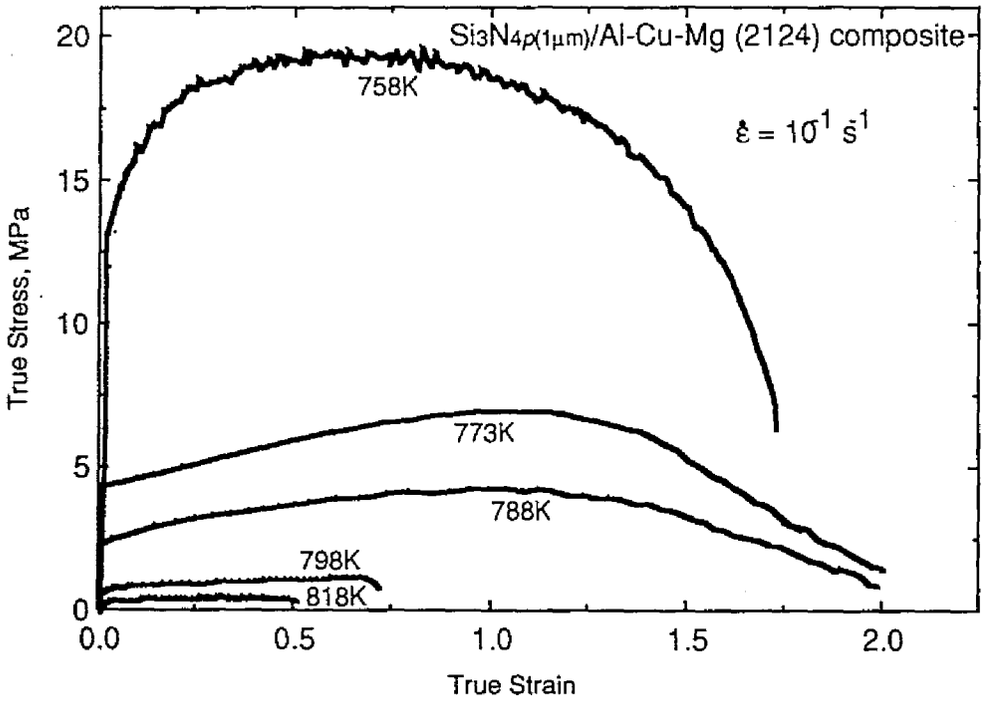

Fig. 4.2 True stress *vs* true strain at a strain rate of 10^{-1} s^{-1} for the $Si_3N_{4p(1\mu m)}$/Al-Cu-Mg (2124) composite.

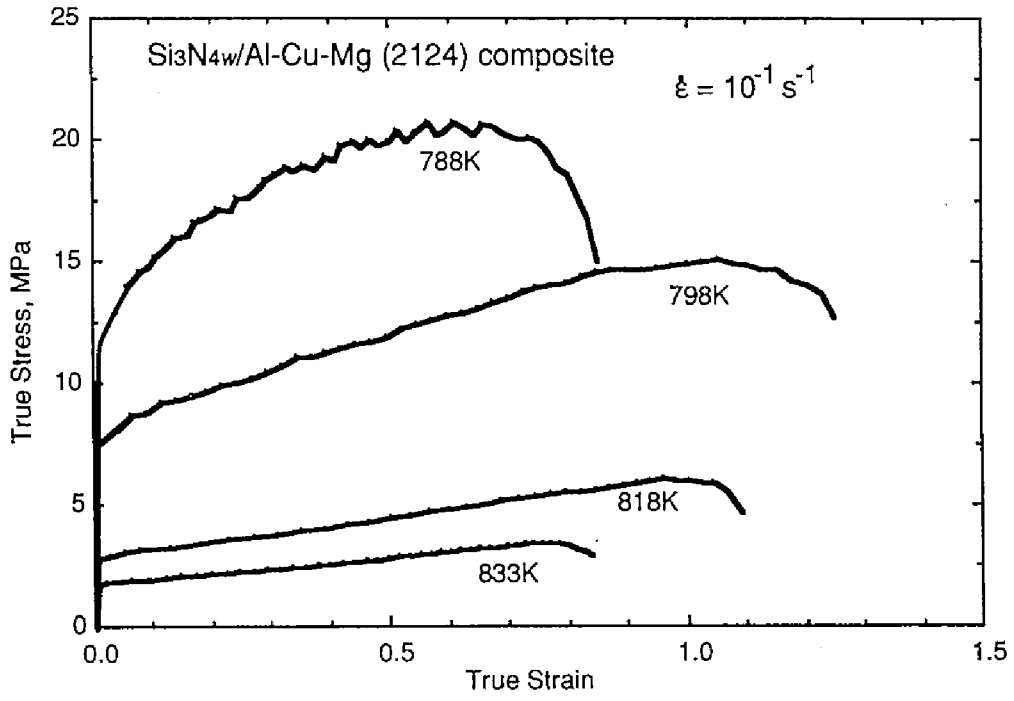

Fig. 4.3 True stress *vs* true strain at a strain rate of 10^{-1} s^{-1} for the Si_3N_{4w}/Al-Cu-Mg (2124) composite.

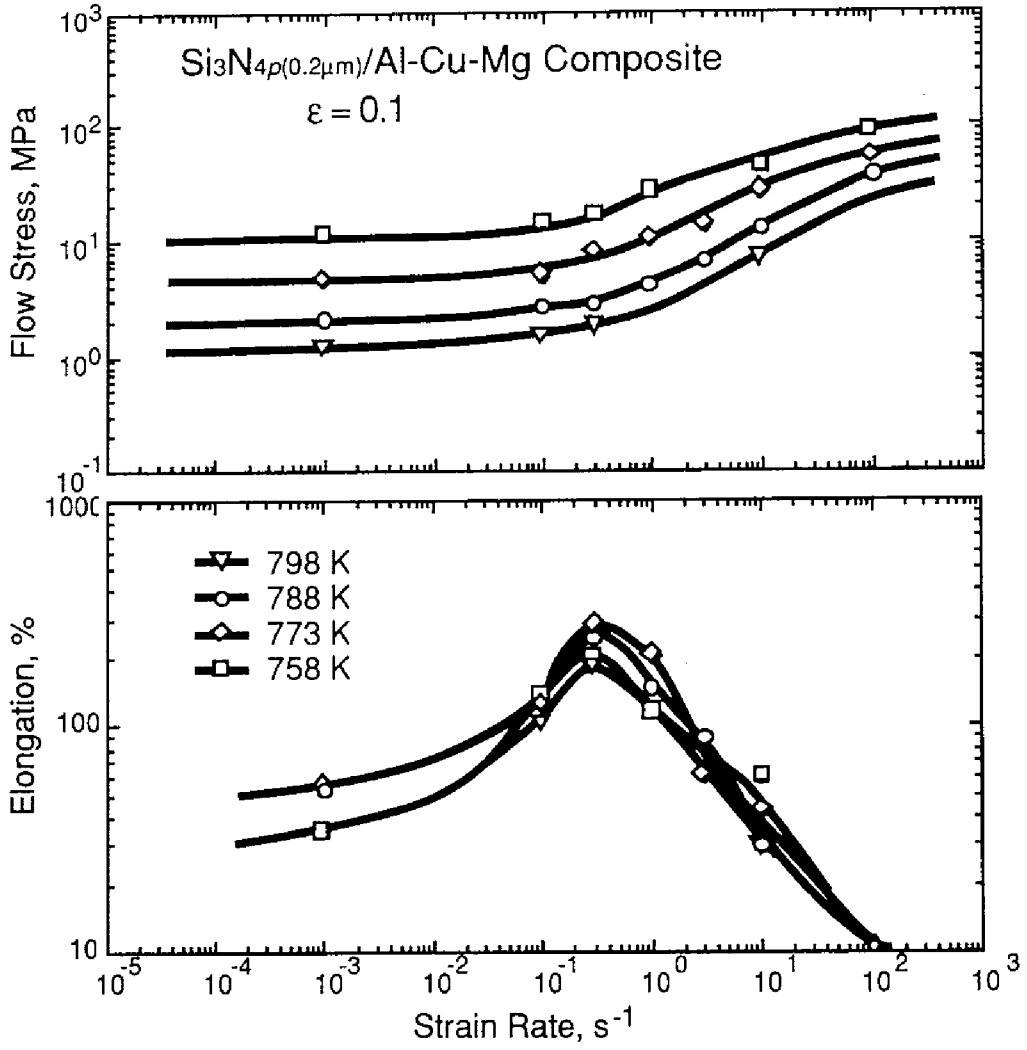

Fig. 4.4 The variation in flow stress (top figure) and elongation to failure (bottom figure) as a function of strain rate for the $Si_3N_{4p(0.2\mu m)}$/Al-Cu-Mg.

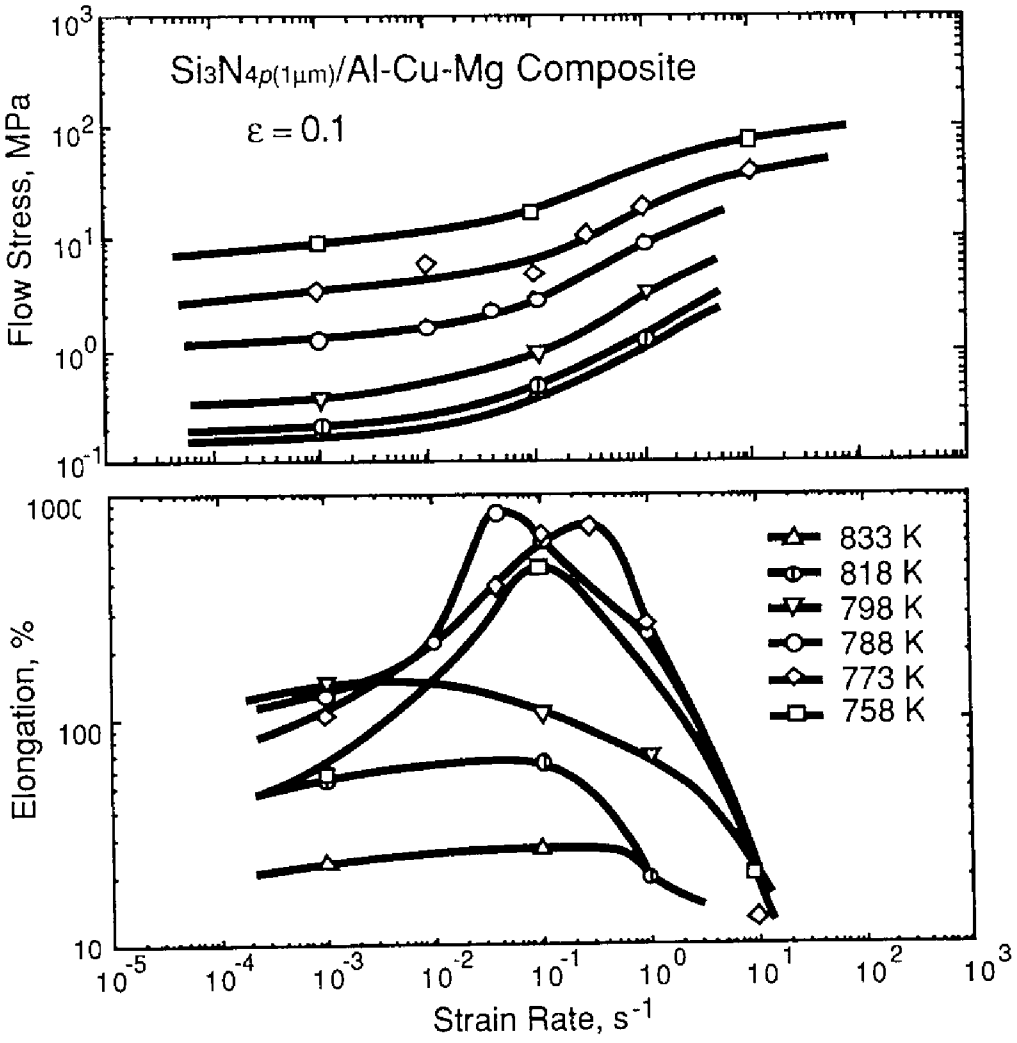

Fig. 4.5 The variation in flow stress (top figure) and elongation to failure (bottom figure) as a function of strain rate for the $Si_3N_{4p(1\mu m)}$/Al-Cu-Mg.

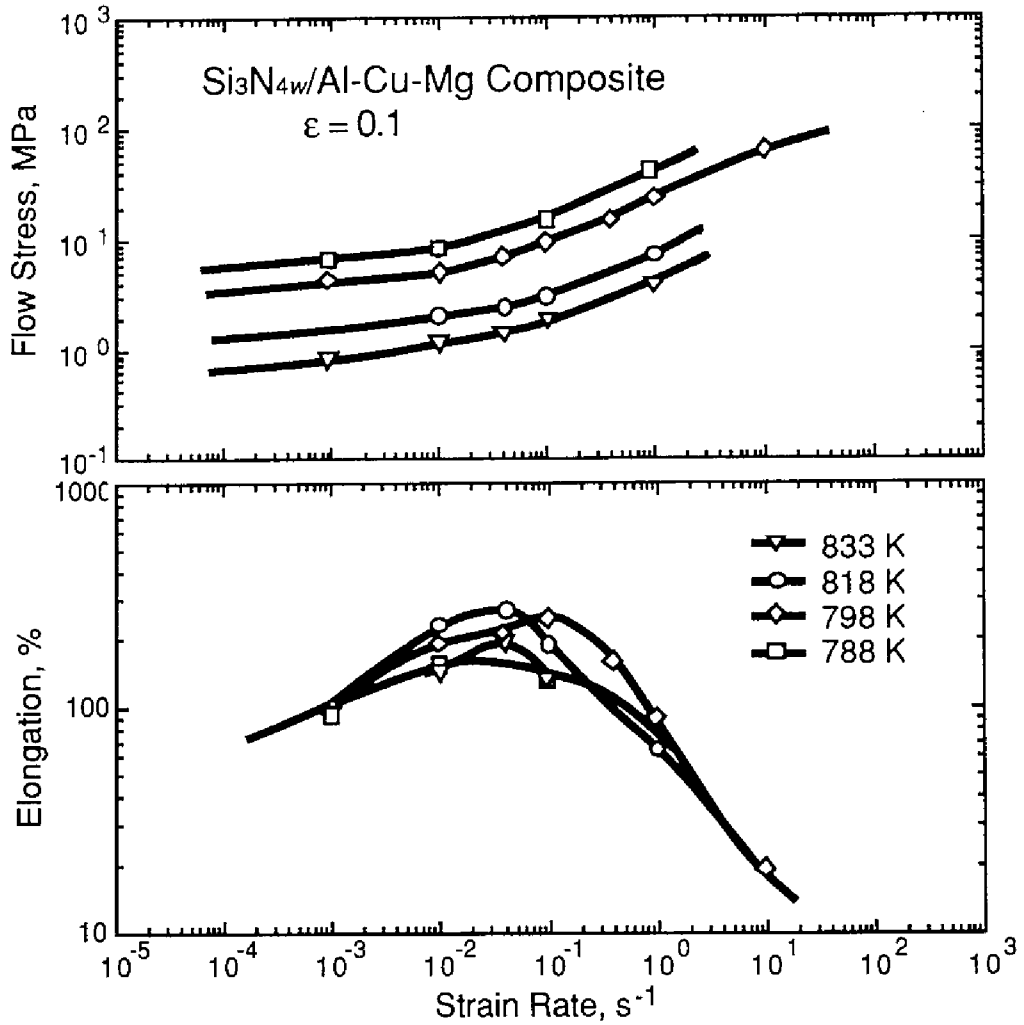

Fig. 4.6 The variation in flow stress (top figure) and elongation to failure (bottom figure) as a function of strain rate for the Si_3N_{4w}/Al-Cu-Mg.

stress increased with the imposed strain rate and there was some evidence, especially in the Si_3N_{4w}/Al-Cu-Mg composites, for a sigmoidal relationship between stress and strain rate. The data show that the strain rate sensitivity was relatively high (0.3 ~ 0.5) over strain rate ranges of approximately 10^{-1} ~ 10 s^{-1} for the $Si_3N_{4p(0.2\mu m)}$/Al-Cu-Mg composite, 4 x 10^{-2} ~ 1 s^{-1} for the $Si_3N_{4p(1\mu m)}$/Al-Cu-Mg composite and 4 x 10^{-2} ~ 1 s^{-1} for the Si_3N_{4w}/Al-Cu-Mg composite, respectively. It is noted that the strain rate sensitivity values were very low ($\leq$ 0.1 ~ 0.2) in a low strain rate range for the composites.

The plots of elongation to failure *vs.* strain rate show that these three composites exhibited very good superplastic properties over a range of strain rates. It is noted that large elongations were attained in a strain rate range where the high strain rate sensitivity was found. This trend is the same as conventional superplastic metals. A maximum elongation was 280 % at 3 x 10^{-1} s^{-1} with 773 K for the $Si_3N_{4p(0.2\mu m)}$/Al-Cu-Mg composite, 840 % at 4 x 10^{-2} s^{-1} with 788 K for the $Si_3N_{4p(1\mu m)}$/Al-Cu-Mg composite and 280 % at 4 x 10^{-2} s^{-1} with 818 K for the Si_3N_{4w}/Al-Cu-Mg composite, respectively. It should be noted that the optimum temperatures where a maximum elongation was attained for each composite were different from each other, in spite of the same chemical composition of the matrix.

B. Al-Mg (5052) alloy matrix composite

The variation in flow stress (top figure) and elongation to failure (bottom figure) at testing temperatures from 773 to 833 K as a function of strain rate is shown in Fig. 4.7 for the $Si_3N_{4p(0.2\mu m)}$/Al-Mg composite. The flow stresses at all temperatures increased with imposed strain rate, and a typical sigmoidal curve was observed. In a low strain rate range, the strain rate sensitivity was a very low value, corresponding to low values in elongation. In a high strain rate range from 1 to 10 s^{-1}, however, a relatively high strain rate sensitivity of

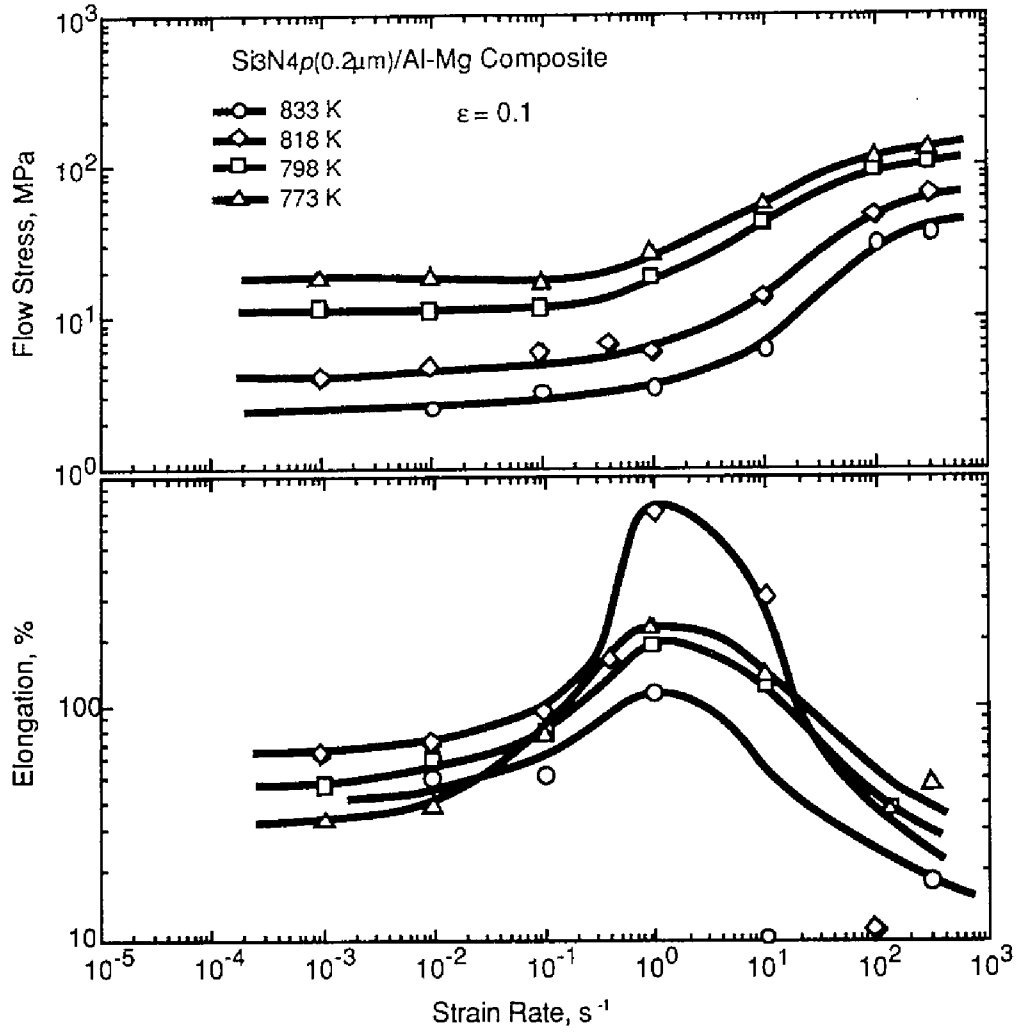

Fig. 4.7 The variation in flow stress (top figure) and elongation to failure (bottom figure) as a function of strain rate for the $Si_3N_{4p(0.2\mu m)}$/Al-Mg.

0.3 ~ 0.5 was obtained, corresponding to large elongations. It is noted that a large elongation of 700 % was attained at an extremely high strain rate of 1 s^{-1} and at 818 K.

C. Al-Mg-Si (6061) alloy matrix composite

Superplastic behaviors of three Si_3N_{4p}/Al-Mg-Si composites and one Si_3N_{4w}/Al-Mg-Si composite were investigated. The variation in flow stress (top figure) and elongation (bottom figure) as a function of strain rate is shown in Figs 4.8 ~ 4.11 for the Si_3N_4/Al-Mg-Si composites. There are some similarities in superplastic behavior in the composites: the flow stress at all testing temperatures increased with strain rate, and the curves were of typical sigmoidal shape, as has been observed for conventional superplastic materials. In a low strain rate range, the strain rate sensitivities were less than 0.1, on the other hand, relatively high strain rate sensitivities of 0.3 ~ 0.5 were obtained in a high strain rate range, with corresponding relatively large elongations..

Small elongations were obtained at low strain rates, however, the elongation increased with strain rate and large elongations were attained in a high strain rate range from 0.1 to 2 s^{-1}. Especially, for the $Si_3N_{4p(0.2\mu m)}$/Al-Mg-Si composite tested at 833 K, a large elongation of 620 % was obtained at a very high strain rate of 2 s^{-1}. The $Si_3N_{4p(0.2\mu m)}$/Al-Mg-Si composite sample deformed to 620 % is shown in Fig. 4.12. Recently, Higashi *et al.* [22,23] showed evidences of superplasticity at very high stain rates $\geq$ 1 s^{-1} for aluminum alloys and they named the high strain rate superplasticity "*positive exponent strain rate superplasticity*". Therefore the sample shown in Fig. 4.12 is labeled as positive exponent strain rate superplasticity.

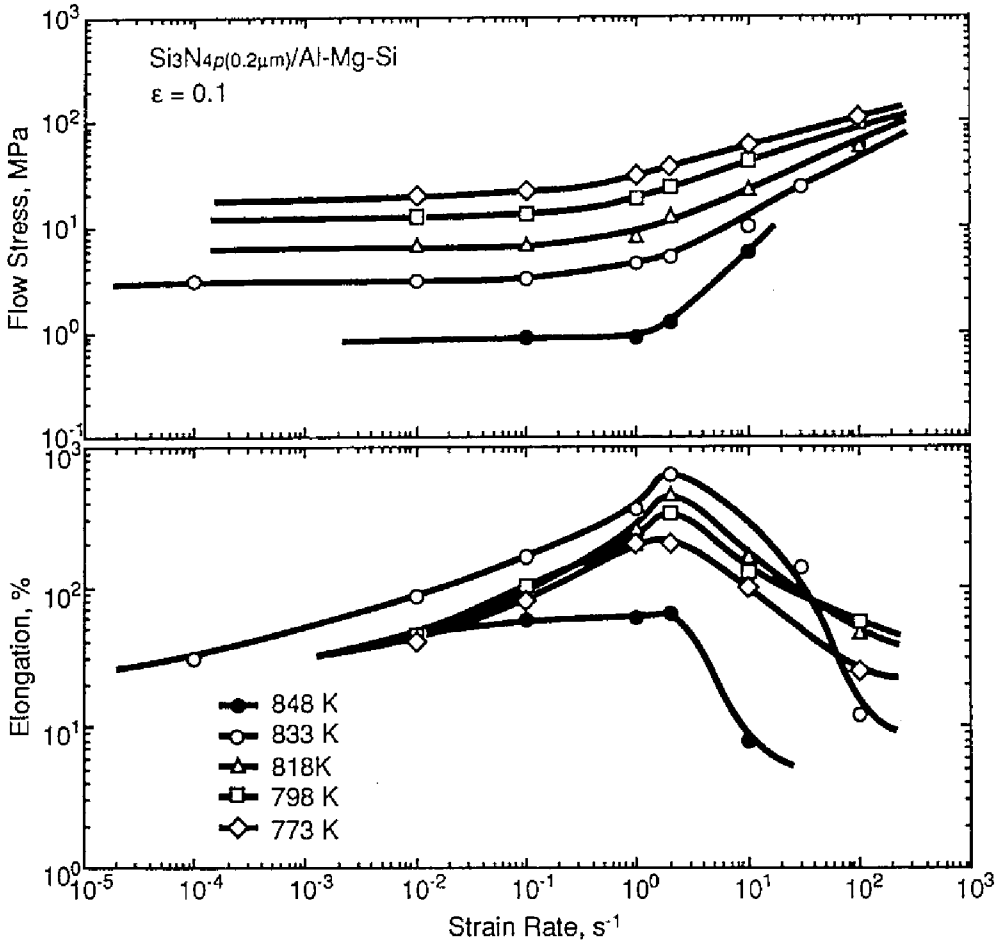

Fig. 4.8 The variation in flow stress (top figure) and elongation to failure (bottom figure) as a function of strain rate for the $Si_3N_{4p(0.2\mu m)}$/Al-Mg-Si.

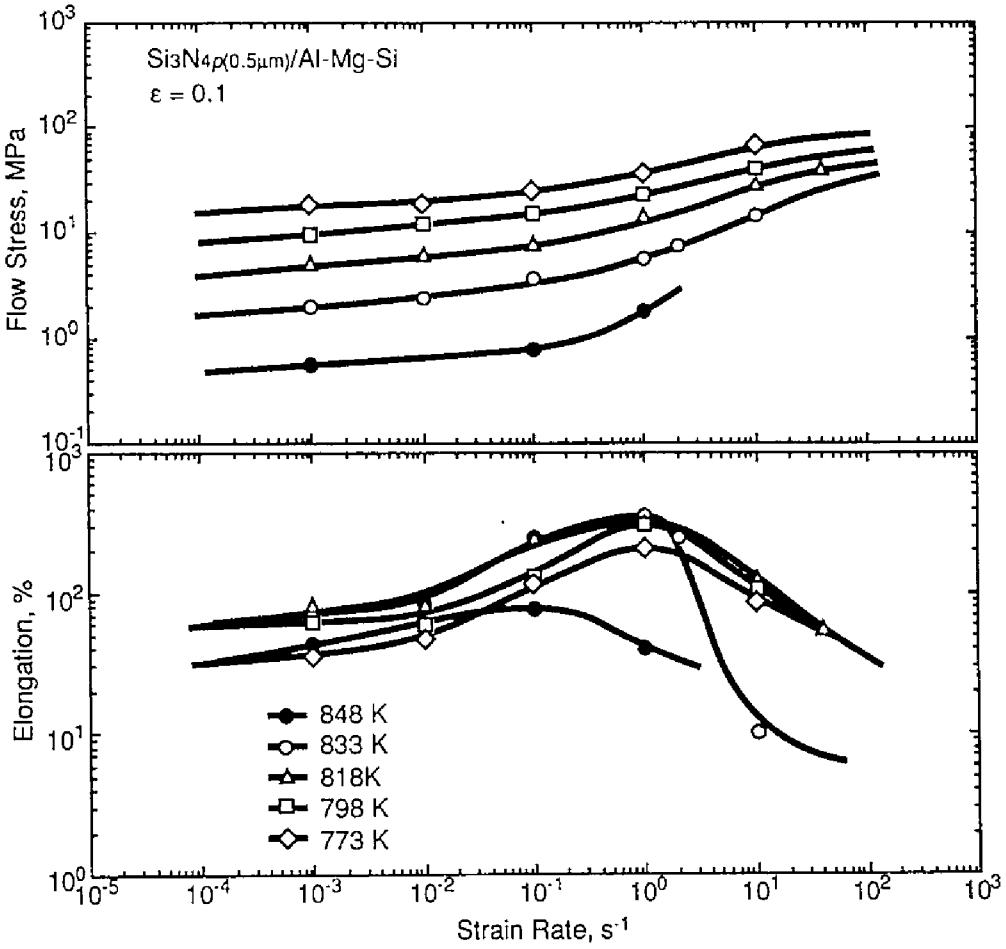

Fig. 4.9 The variation in flow stress (top figure) and elongation to failure (bottom figure) as a function of strain rate for the $Si_3N_{4p(0.5\mu m)}$/Al-Mg-Si.

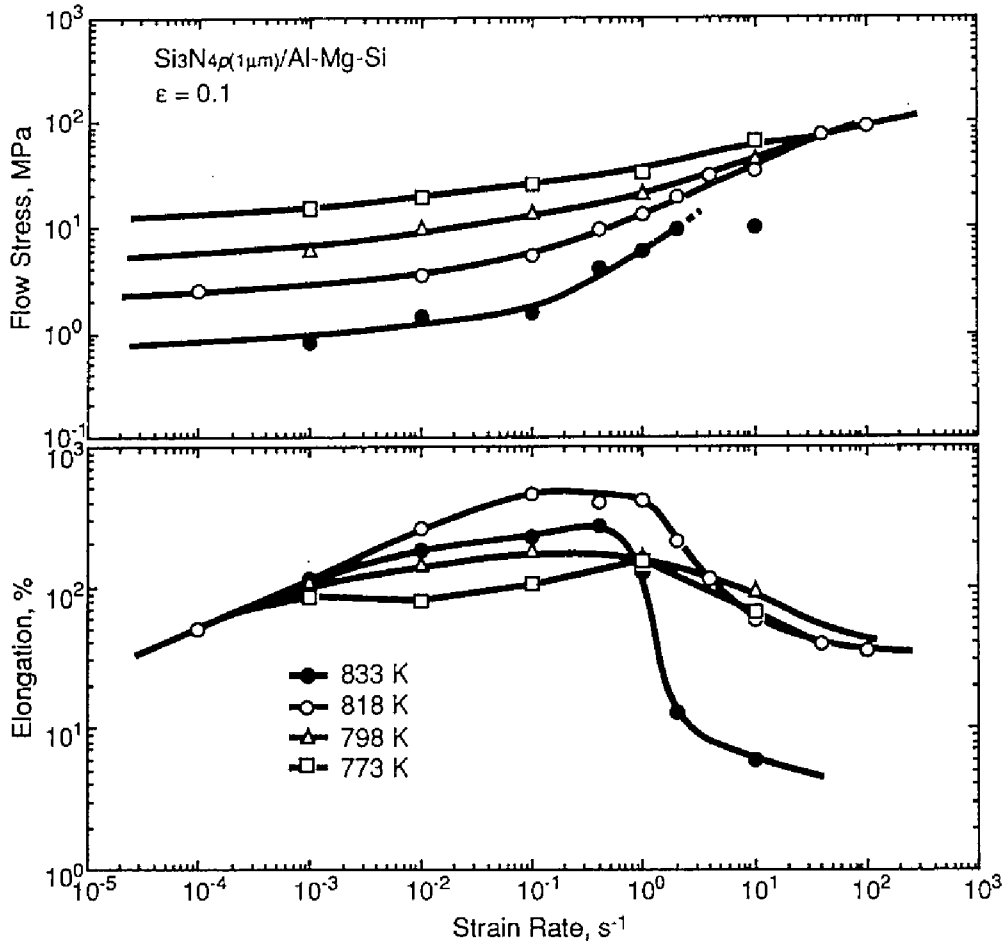

Fig. 4.10 The variation in flow stress (top figure) and elongation to failure (bottom figure) as a function of strain rate for the $Si_3N_{4p(1\mu m)}$/Al-Mg-Si.

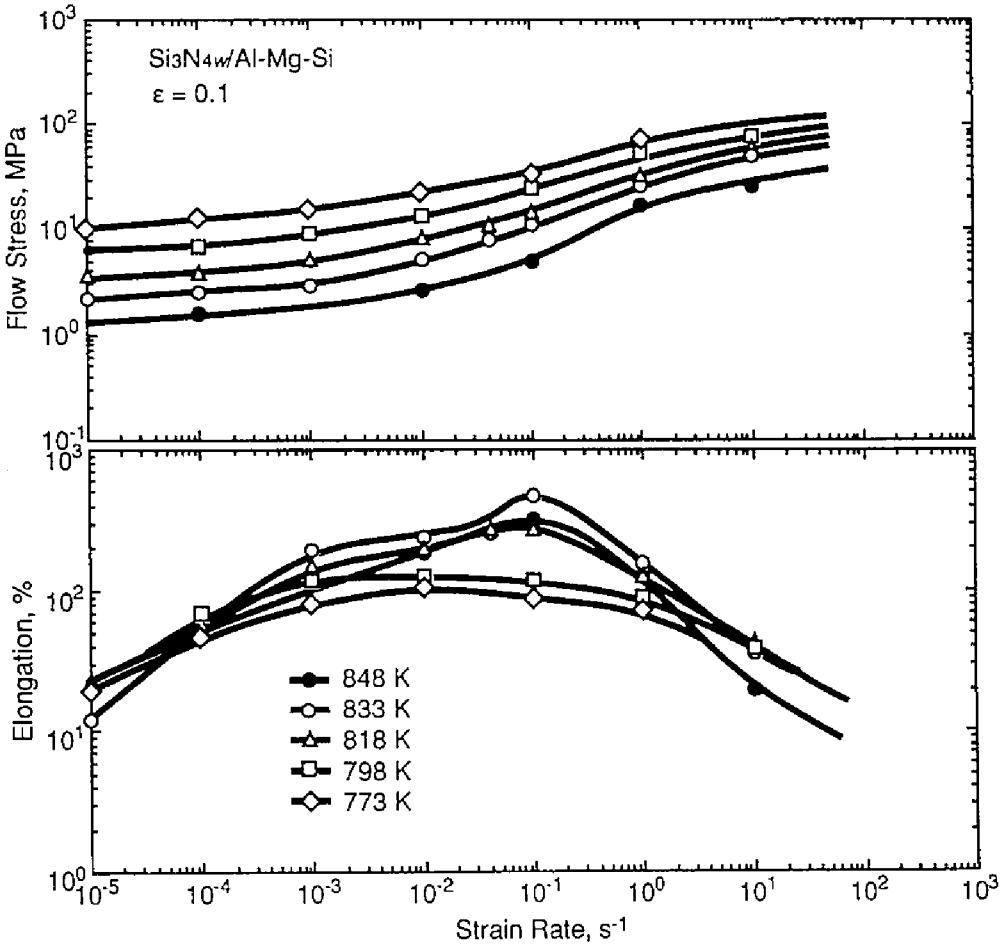

Fig. 4.11 The variation in flow stress (top figure) and elongation to failure (bottom figure) as a function of strain rate for the Si_3N_4w/Al-Mg-Si.

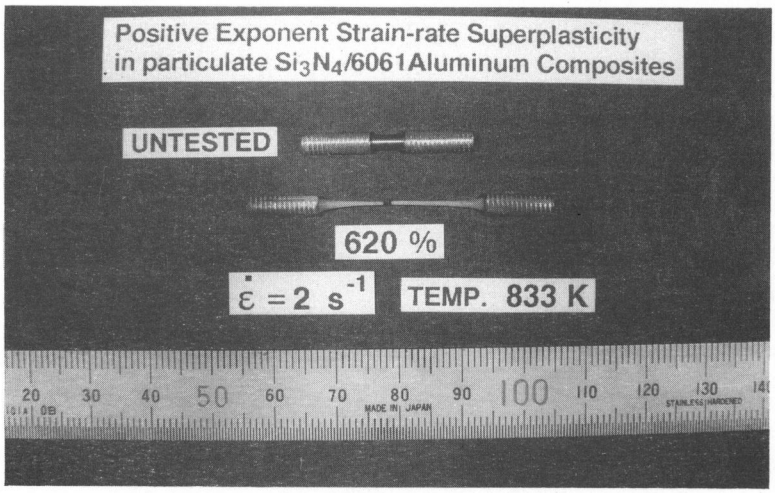

Fig. 4.12 Example of positive exponent strain rate superplasticity in $Si_3N_{4p(0.2\mu m)}$/Al-Mg-Si (6061). This composite exhibited a large elongation of 620 % at a high strain rate of 2 s^{-1}.

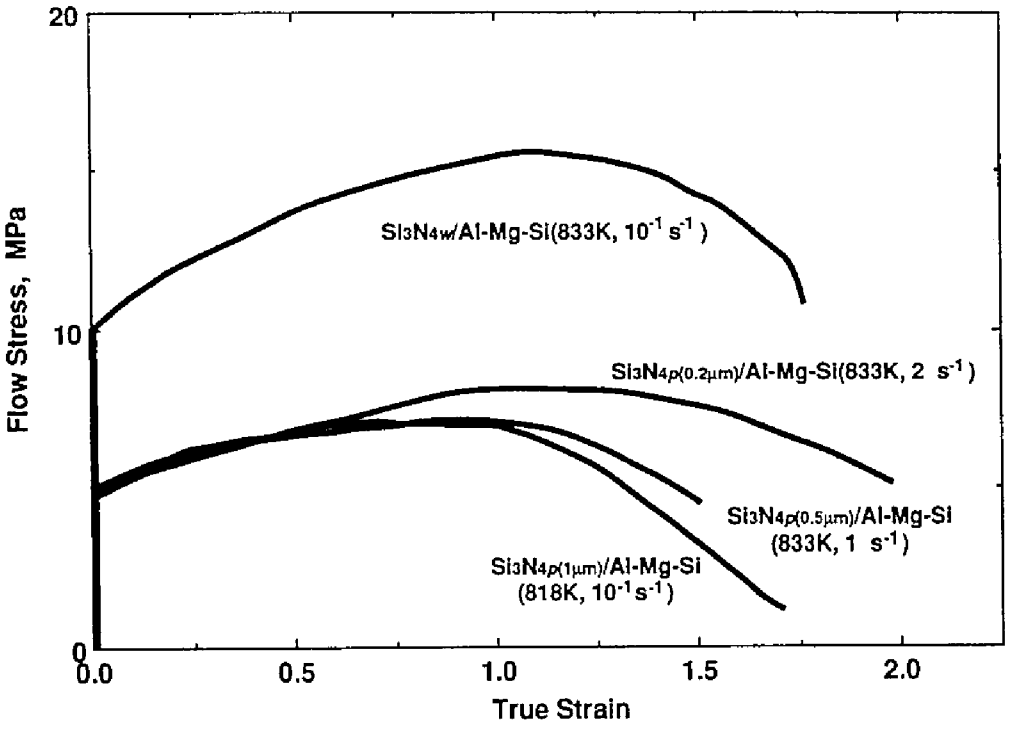

Fig. 4.13 Typical true stress - true strain curves of the Si_3N_4/Al-Mg-Si composites under optimum superplastic deformation conditions.

Typical true stress - true strain curves of the Si_3N_4/Al-Mg-Si composites are shown in Fig. 4.13 under optimum superplastic deformation conditions for a maximum elongation, which are 833 K and 2 s^{-1} for the $Si_3N_{4p(0.2\mu m)}$/Al-Mg-Si composite, 833 K and 1 s^{-1} for the $Si_3N_{4p(0.5\mu m)}$/Al-Mg-Si composite, 818 K and 10^{-1} s^{-1} for the $Si_3N_{4p(1\mu m)}$/Al-Mg-Si composite, and 833 K and 10^{-1} s^{-1} for the Si_3N_{4w}/Al-Mg-Si composite, respectively. The curves, corresponding to the optimum superplastic conditions, exhibited stain hardening and strain softening during superplastic flow for the Si_3N_{4p}/Al-Mg-Si composites. The stain hardening behavior is probably related to grain growth during superplastic deformation, which has been found in superplastic alloys [24-27]. The apparent strain softening may be attributed to development of necking. It is interesting to note that the optimum superplastic flow stress of the Si_3N_{4w}/Al-Mg-Si composite is higher than those of the other Si_3N_{4p}/Al-Mg-Si composites, on the other hand, the stress level in three Si_3N_{4p}/Al-Mg-Si composites is almost identical until the initial deformation stage of $\varepsilon < 0.8$, where ε is the true strain.

D. Al-Zn-Mg (7064) alloy matrix composite

The variation in flow stress (top figure) and elongation to failure (bottom figure) as a function of strain rate is shown in Fig. 4.14 for the $Si_3N_{4p(1\mu m)}$/Al-Zn-Mg composite and in Fig. 4.15 for the Si_3N_{4w}/Al-Zn-Mg composite, respectively. The flow stresses increased with strain rate, and the relationship between the logarithmic flow stress and the logarithmic strain rate showed sigmoidal shape as has been often observed for many superplastic metallic alloys. Low strain rate sensitivity values of less than about 0.1 were obtained in a low strain rate range, but relatively high strain rate sensitivity values of 0.3 ~ 0.5 were attained at high strain rates above 10^{-1} s^{-1} for the

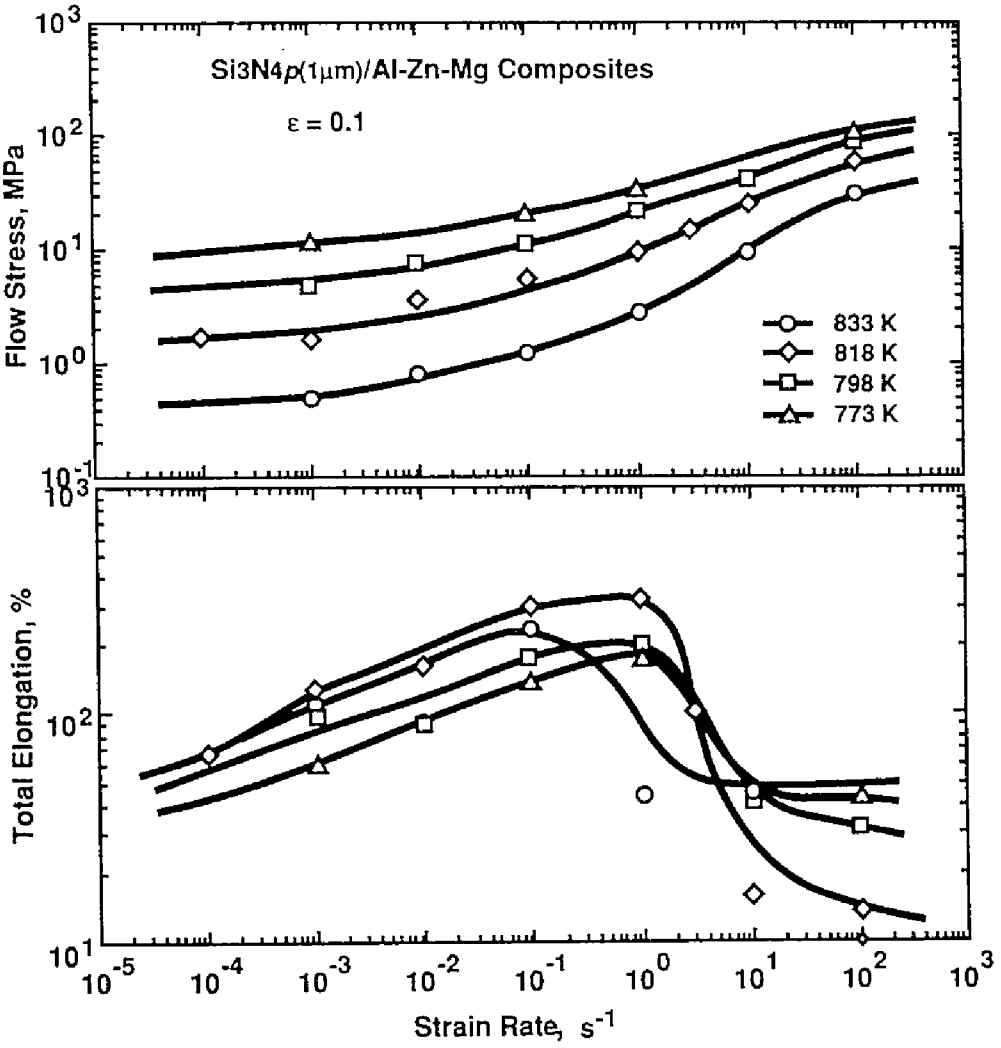

Fig. 4.14 The variation in flow stress (top figure) and elongation to failure (bottom figure) as a function of strain rate for the Si3N4p(1μm)/Al-Zn-Mg.

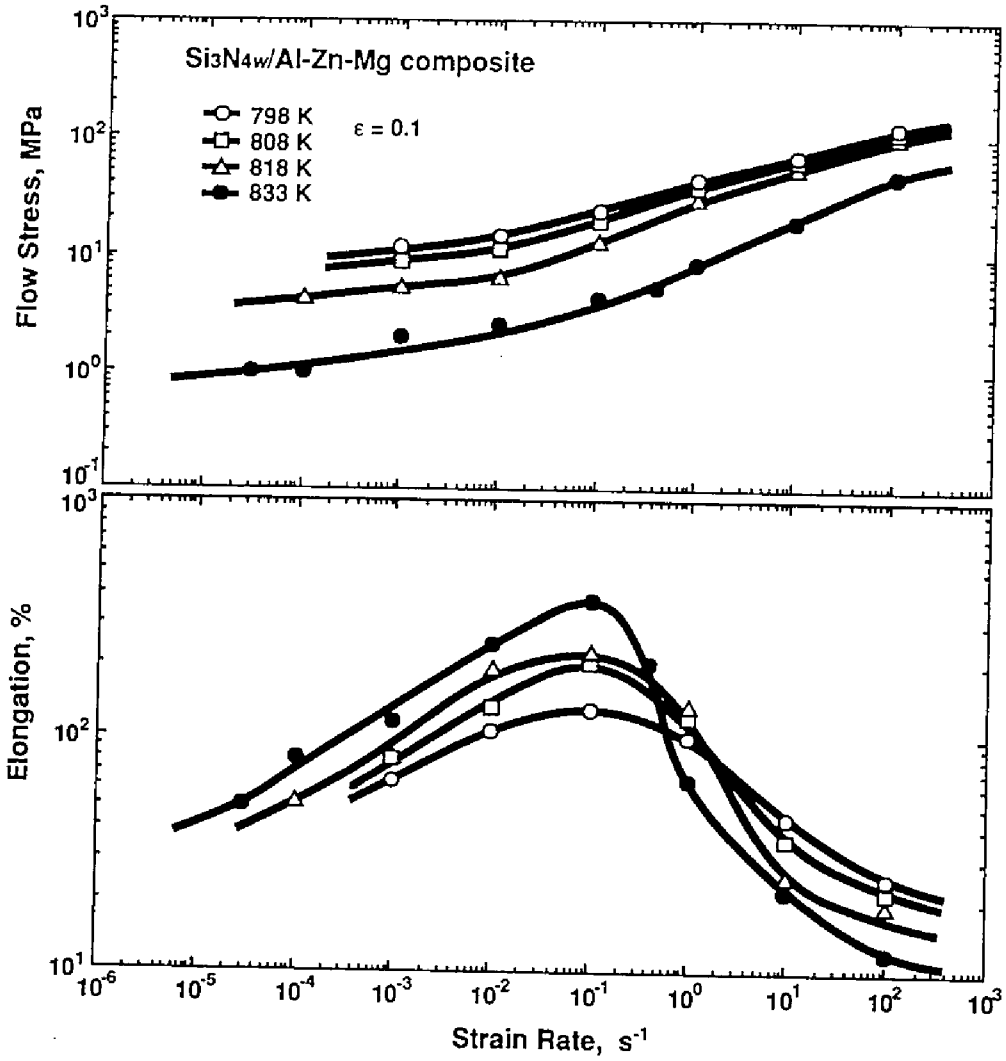

Fig. 4.15 The variation in flow stress (top figure) and elongation to failure (bottom figure) as a function of strain rate for the Si_3N_{4w}/Al-Zn-Mg.

$Si_3N_{4p(1\mu m)}$/Al-Zn-Mg composite and at high strain rates above 10^{-2} s^{-1} for the Si_3N_{4w}/Al-Zn-Mg composite.

Elongations to failure were small values of less than about 100 % at low strain rates below 10^{-3} s^{-1} for both the composites, corresponding to the low strain rate sensitivity values. The elongations to failure increased with an increase in strain rate, and the $Si_3N_{4p(1\mu m)}$/Al-Zn-Mg composite showed a maximum elongation of 330 % at a high strain rate of 1 s^{-1} and at 818 K, and the Si_3N_{4w}/Al-Zn-Mg composite showed a maximum elongation of 380 % at a high strain rate of 10^{-1} s^{-1} and at 833 K. The elongations to failure at all temperatures decreased rapidly to values ≤ about 30 ~ 50 % beyond the strain rate where the maximum elongation was attained.

E. Summary of experimental results

Summary of superplastic properties for aluminum matrix composites is shown in Table 4.1, where the data of other superplastic aluminum matrix composites in the previous papers [13-16,28-36] are added. The phenomenological deformation characteristics of the superplastic aluminum matrix composites are concluded as follows:

(1) All the aluminum matrix composites in the present investigation exhibited superplastic behavior at high strain rates (> 10^{-2} s^{-1}).

(2) There was a sigmoidal relationship between the logarithmic flow stress and the logarithmic strain rate and the high strain rate sensitivity (0.3 ~ 0.5) was attained in an intermediate strain rate range, where large elongations were attained. This phenomenon is the same as that for conventional superplastic metals.

(3) The strain rate sensitivity was very low (for example, less than 0.1) in a low stain rate range.

Table 4.1 Summary of superplastic properties for aluminum matrix composites.

Materials	Temperature (K)	Strain Rate (s^{-1})	m Value	Elongation (%)	Grain Size (μm)	Reference
Al/SiC Composites						
Al-Cu-Mg(2124)/20% SiC_w	798	$3x10^{-1}$	0.3	300		13
Al-Cu-Mg(2014)/15% SiC_p(p=6-10μm)	753	$2x10^{-4}$	0.4	349	14	15
Al-Mg-Si(6061)/20% SiC_w	823	$2x10^{-1}$	0.3	300		28
Al-Zn-Mg-Cu(7475)/10-15% SiC_w	793	$2x10^{-4}$	> 0.5	350	6-8	16
Al-Zn-Mg-Cu(PM64)/10-15% SiC_p(p=5μm)	773	$2x10^{-4}$	0.3	450	6	14
Al-Zn-Mg-Cu(7475)/15% SiC_p(p=6-10μm)	788	$2x10^{-4}$	0.4	310	7	15
Al-Cu-Mg-C-O(IN9021)/15% SiC_p	823	5	> 0.5	600	0.5	29
Al-Zn-Mg-Cu(7075)/10% SiC_p(p=2μm)	793	5	0.5	300		30
Al/Si_3N_4 Composites						
Al-Cu-Mg(2124)/20% Si_3N_{4p}(p=0.2μm)	773	$3x10^{-1}$	0.3~0.5	280	1	This work
Al-Cu-Mg(2124)/20% Si_3N_{4p}(p=1μm)	788	$4x10^{-2}$	0.3~0.5	840	2	This work
Al-Cu-Mg(2124)/20% βSi_3N_{4w}	798	$2x10^{-1}$	0.5	200-250		31
Al-Cu-Mg(2124)/20% βSi_3N_{4w}	818	$4x10^{-2}$	0.3~0.5	280	4	This work
Al-Mg(5052)/20% Si_3N_{4p}(p=0.2μm)	818	1	0.3~0.5	700	1	This work
Al-Mg-Si(6061)/20% Si_3N_{4p}(p=0.2μm)	833	2	0.3~0.5	620	1	This work
Al-Mg-Si(6061)/20% Si_3N_{4p}(p=0.5μm)	833	1	0.3~0.5	350	2	This work
Al-Mg-Si(6061)/20% Si_3N_{4p}(p=1μm)	818	$1x10^{-1}$	0.3~0.5	450	3	This work
Al-Mg-Si(6061)/20% αSi_3N_{4w}	818	$3x10^{-1}$	0.3	150	3	33
Al-Mg-Si(6061)/20% βSi_3N_{4w}	818	$2x10^{-1}$	0.5	260	3	33
Al-Mg-Si(6061)/20% βSi_3N_{4w}	818	$2x10^{-1}$	0.5	600	3	32
Al-Mg-Si(6061)/20% βSi_3N_{4w}	833	$1x10^{-1}$	0.3~0.5	480	3	This work
Al-Zn-Mg(7064)/20% Si_3N_{4p}(p=1μm)	818	1	0.3~0.5	330	2	This work
Al-Zn-Mg(7064)/20% αSi_3N_{4w}	798	$8x10^{-1}$	0.4	160	> 4	34
Al-Zn-Mg(7064)/20% βSi_3N_{4w}	818	$2x10^{-1}$	0.4	230	4	34
Al-Zn-Mg(7064)/20% βSi_3N_{4w}	818	$5x10^{-1}$	0.5	240	> 4	35
Al-Zn-Mg(7064)/20% βSi_3N_{4w}	833	$1x10^{-1}$	0.3~0.5	380	4	This work
Al-Zn-Mg-Cu-0.7%Zr(7475)/20% Si_3N_{4p}(p=0.2μm)	798	4	0.3~0.5	220	1	
Al/AlN Composites						
Al-Mg-Si(6061)/15% AlN_p(p=0.7μm)	873	1	0.5	200		36
Al-Zn-Mg(7064)/20% AlN_p(p=0.7μm)	788	1.5	0.4	200		36

p : particulate diameter

(4) The optimum temperatures where a maximum elongation was attained for each composite were different from one another, in spite of the same chemical composition of a matrix material.

4.3.1.2 Threshold stress

The strain rate sensitivity values were very low in a low strain rate range for all the superplastic composites. This is attributed either to the presence of a threshold stress or to deformation mechanism changes. It is reported that a change in the strain rate sensitivity results from a threshold stress, not the deformation mechanism changes [37,38]. The threshold stress can be given by extrapolation to zero strain rate of a straight line which the data give as $\dot{\varepsilon}^{1/n}$ against σ on a double-linear scale [37], where σ is the flow stress, $\dot{\varepsilon}$ is the strain rate and n is the stress exponent. Many theories on superplasticity postulate the stress exponent of 2 [39-43]. Hence it is reasonable in the present investigation that the threshold stress is calculated from the data plotted as σ against $\dot{\varepsilon}^{1/2}$ on a double-linear scale [37]. The procedure for calculating the threshold stress at 798, 808, 818 and 833 K for the Si_3N_{4w}/Al-Zn-Mg composite is shown in Fig. 4.16. The linearity of the data in this plot indicates that the presence of a threshold stress is responsible for the change in the strain rate sensitivity and that the value of $n = 2$ is correct for the stress exponent for superplastic deformation. The same trend was found for all the composites in the present investigation. Therefore all values of threshold stresses were given by extrapolation to zero strain rate of a line which the data gave as σ against $\dot{\varepsilon}^{1/2}$ on a double-liner scale.

The variation in threshold stress for the Si_3N_{4w}/Al-Zn-Mg composite as a function of temperature is plotted in Fig. 4.17. It should be noted that the threshold stress decreased with an increase in temperature. Such a strong temperature dependence of threshold stress was found for all the superplastic

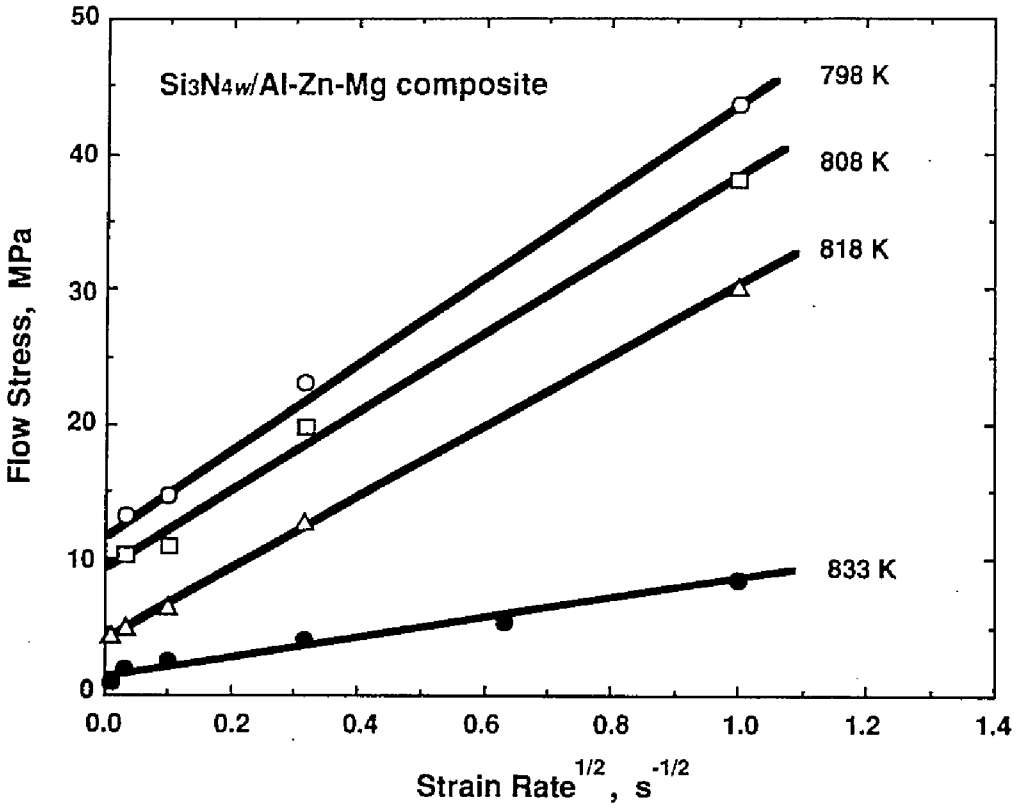

Fig. 16 Calculation of the threshold stress for the Si_3N_{4w}/Al-Zn-Mg.

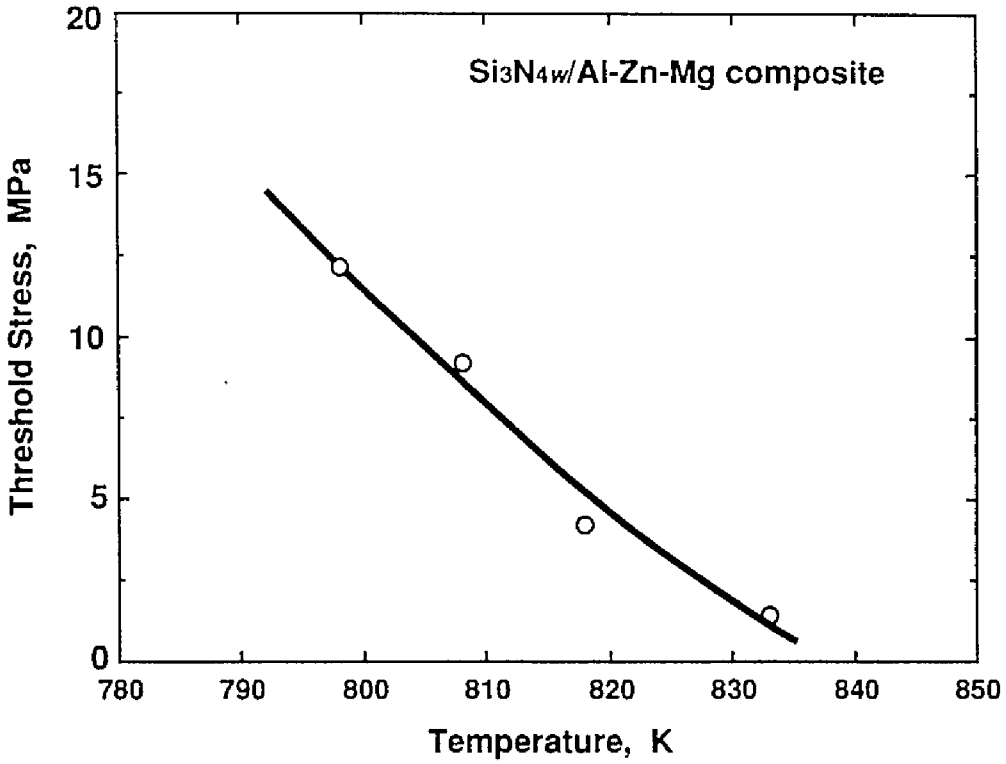

Fig. 17 The variation in threshold stress as a function of temperature for the Si_3N_{4w}/Al-Zn-Mg.

composites in the present investigation. The similar results have been reported for creep behavior of the aluminum matrix composites [8,9].

The origin of the threshold stress has been discussed from the viewpoint of dislocation - particle interaction, such as Orowan stress [44], additional dislocation line length due to climb [45], and detachment of the dislocation from a dispersion particle [46] in dispersion-strengthened alloys. These interpretations about the origin of the threshold stress, however, can not explain the strong temperature dependence of the threshold stresses for the superplastic composites. Arzt and Wilkinson [46] presented the model that the threshold stress might depend on the factor by which the dislocation line tension was lowered, and showed that possible magnitude of the threshold stress σ_{th} might be roughly $0.4\sigma_o \leq \sigma_{th} \leq \sigma_o$, where σ_o is the Orowan stress. However, the results obtained in the present work can not be explained by this theory because the magnitude of a change in the threshold stress was more tremendous than the magnitude postulated by the model. For the composites, there are other possibilities as the origin of the threshold stress: internal stress associated with subgrain size [7] and load transfer to the stiffer reinforcement [7]. However, subgrains are unlikely formed for the superplastic composites since the superplastic composites have a fully recrystallized fine-grained microstructure. Also, the strong temperature dependence of threshold stress can not be explained by load transfer to the stiffer reinforcement.

On the other hand, the threshold stress can be interpreted from the viewpoint of grain boundary sliding for superplastic materials since grain boundary sliding is the dominant deformation process of superplasticity [47-49]. Mohamed [37] pointed out that the threshold stress might result from the interaction between impurity atom segregation and boundary dislocations for superplastic metals and that the interaction might be responsible for the strong

temperature dependence of the threshold stress. For the superplastic composites, segregation of alloying elements such as Mg and Cu was reported around reinforcements [50,51]. In addition, a microchemical analysis by a field-emission TEM reveals, as shown in Chapter 6, that the boundaries are segregated mostly by Si, O, and N and the interfaces are segregated mostly by Mg and O. The interaction between dislocations and such segregation may be responsible for the threshold stress. Further research is required to understand the origin of the threshold stress for the superplastic composites.

4.3.1.3 Grain size dependence

Tensile tests were carried out at 818 K in a strain rate range $10^{-3} \sim 10\ s^{-1}$ for the Si_3N_{4w}/Al-Mg-Si with grain sizes of 2.7, 4.0 and 4.7 μm. The variation in strain rate at 818 K as a function of stress is shown in Fig. 4.18 for the Si_3N_{4w}/Al-Mg-Si with different grain sizes. The grain size dependence of the mechanical properties has been investigated for superplastic metals [52-55]. These studies show that the stress decreases with decreasing grain size when the strain rate is constant and a superplastic strain rate range shifts to a higher strain rate range with decreasing grain size. It is found from Fig. 4.18 that for the composite, similarly, the stress decreased and a superplastic strain rate range shifted to a higher strain rate range with decreasing grain size.

When an effective stress σ-σ_{th} and a temperature are constant, the grain size exponent can be given in the form.

$$p = \frac{\partial \ln \dot{\varepsilon}}{\partial \ln d^{-1}} \qquad (4.1)$$

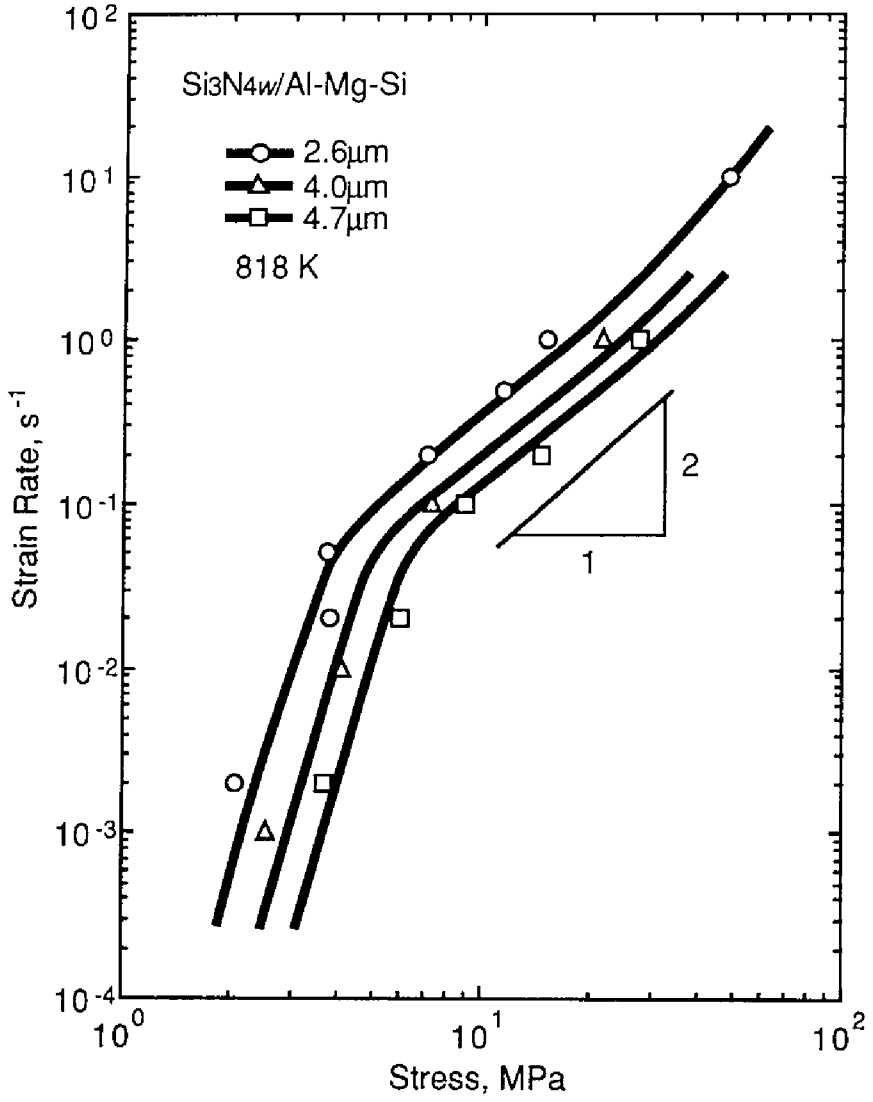

Fig. 4.18 The variation in strain rate at 818 K as a function of stress for the Si3N4*w*/Al-Mg-Si with different grain sizes.

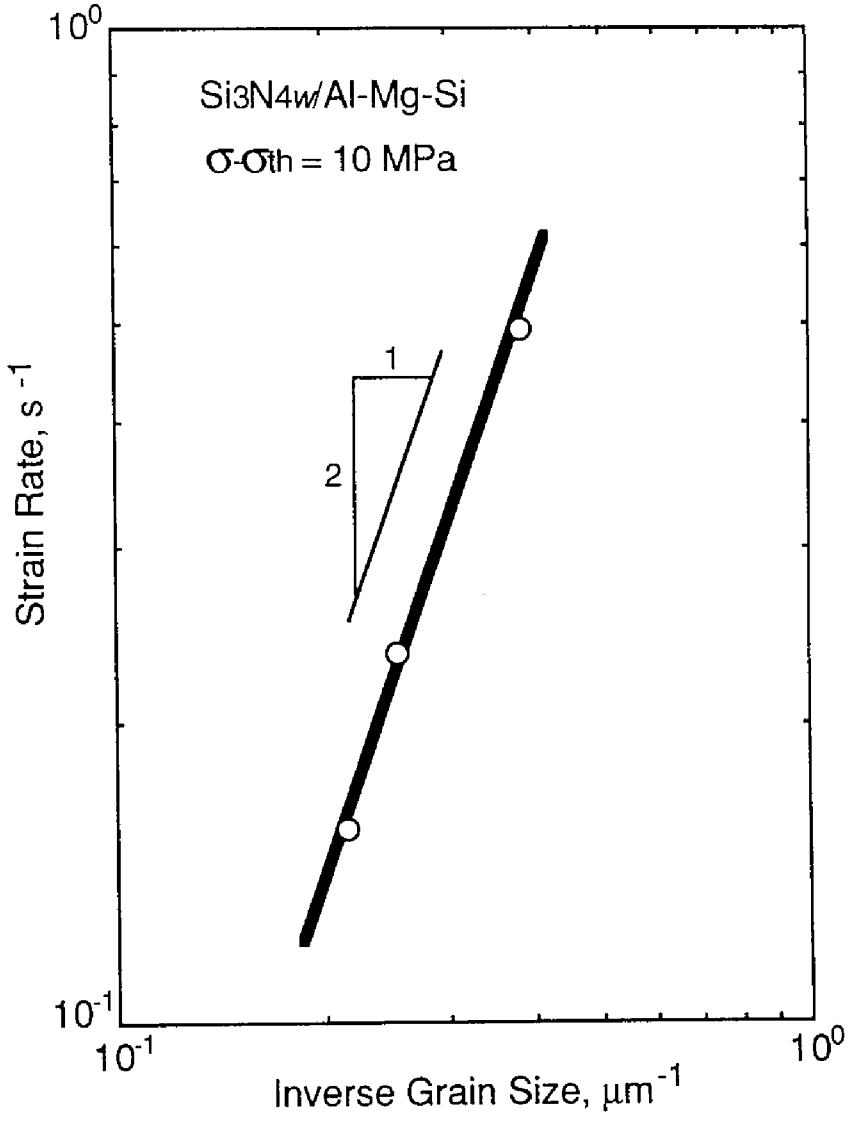

Fig. 4.19 The relationship between the strain rate and the inverse of the grain size for the Si_3N_{4w}/Al-Mg-Si.

The relationship between the strain rate and the inverse of grain size is shown in Fig. 4.19, where the strain rate is determined at σ-σ_{th} = 10 MPa. Inspection of the result in Fig. 4.19 reveals that the grain size exponent is about 2.

4.3.1.4 Activation energy

Elevated temperature mechanical properties in a superplastic region for metal matrix composites with discontinuous reinforcements may be represented in the following form [38]

$$\dot{\varepsilon} = A\left(\frac{\sigma-\sigma_{th}}{G}\right)^{n}\left(\frac{b}{d}\right)^{p} exp\left(\frac{-Q}{RT}\right) \tag{4.2}$$

where A is a constant, G is the shear modulus, b is the Burgers vector, d is the grain size, p is the inverse grain size exponent, Q is the activation energy for superplastic flow, R is a gas constant and T is the absolute temperature. When $(\sigma-\sigma_{th})/G$ is constant, Eq. 4.3 is given from Eq. 4.2.

$$Q = -R\frac{\partial \ln\left[\dot{\varepsilon}\left(\frac{d}{b}\right)^{p}\right]}{\partial (1/T)}. \tag{4.3}$$

Higashi *et al.* [56] analyzed the activation energy for superplastic flow for aluminum alloys and they showed that an apparent value of the activation energy was similar to the activation energy for grain boundary diffusion by incorporation of the temperature dependence of threshold stress and shear modulus, however, the true activation energy was equal to the activation energy for lattice diffusion by additional incorporation of the temperature dependence of grain size. This suggests that it is important to take account of the influence of the grain size to estimate the activation energy for superplastic

flow when the grain size depends on testing temperature due to grain growth during heating for equilibrating at a testing temperature. In the present investigation, the grain sizes were measured from the samples annealed for 1.8×10^3 s at a given testing temperatures, and the activation energy was estimated with the grain size data. The grain size exponent p was 2 for the Si_3N_{4w}/Al-Mg-Si composite, as shown above. Hence, p is taken to be 2 for all the composites in the present investigation.

The variations in $\dot{\varepsilon}(d/b)^2$ as a function of $1/T$ are shown in Fig. 4.20 for the Al-Cu-Mg composites, in Fig. 4.21 for the Al-Mg composite, in Fig. 4.22 for the Al-Mg-Si composites and in Fig. 4.23 for the Al-Zn-Mg composites, respectively, where $(\sigma-\sigma_{th})/G$ for each composite is taken to be the value in Table 4.2. Inspection of Figs 4.20 ~ 4.23 reveals that the superplastic flow is divided into two regions from the viewpoint of the activation energy: Region I (= a low temperature range) showing the low activation energy and Region II (= a high temperature range) showing the high activation energy, for all the composites except the Al-Cu-Mg composites. The behaviors for the Al-Cu-Mg composites are discussed later. Very recently, it was reported [20] that an apparent value of the activation energy for superplastic flow was increased at the onset temperature for partial melting for mechanically-alloyed metals exhibiting high strain rate superplasticity. Therefore it is suggested that it is important to estimate the activation energy for superplastic flow from the viewpoint of effects of a liquid phase. The onset temperatures for partial melting for the superplastic composites were investigated by DSC measurements, which is described in detail in Chapter 6. The optimum conditions where a maximum elongation is attained, $\dot{\varepsilon}$, σ, $(\sigma-\sigma_{th})/G$ and T ($\dot{\varepsilon}$ the strain rate, σ the flow stress at ε=0.1, σ_{th} the threshold stress, G the shear modulus, T the testing temperature), and the onset temperature for partial melting T_m are listed in Table 4.2. The onset temperature for partial melting

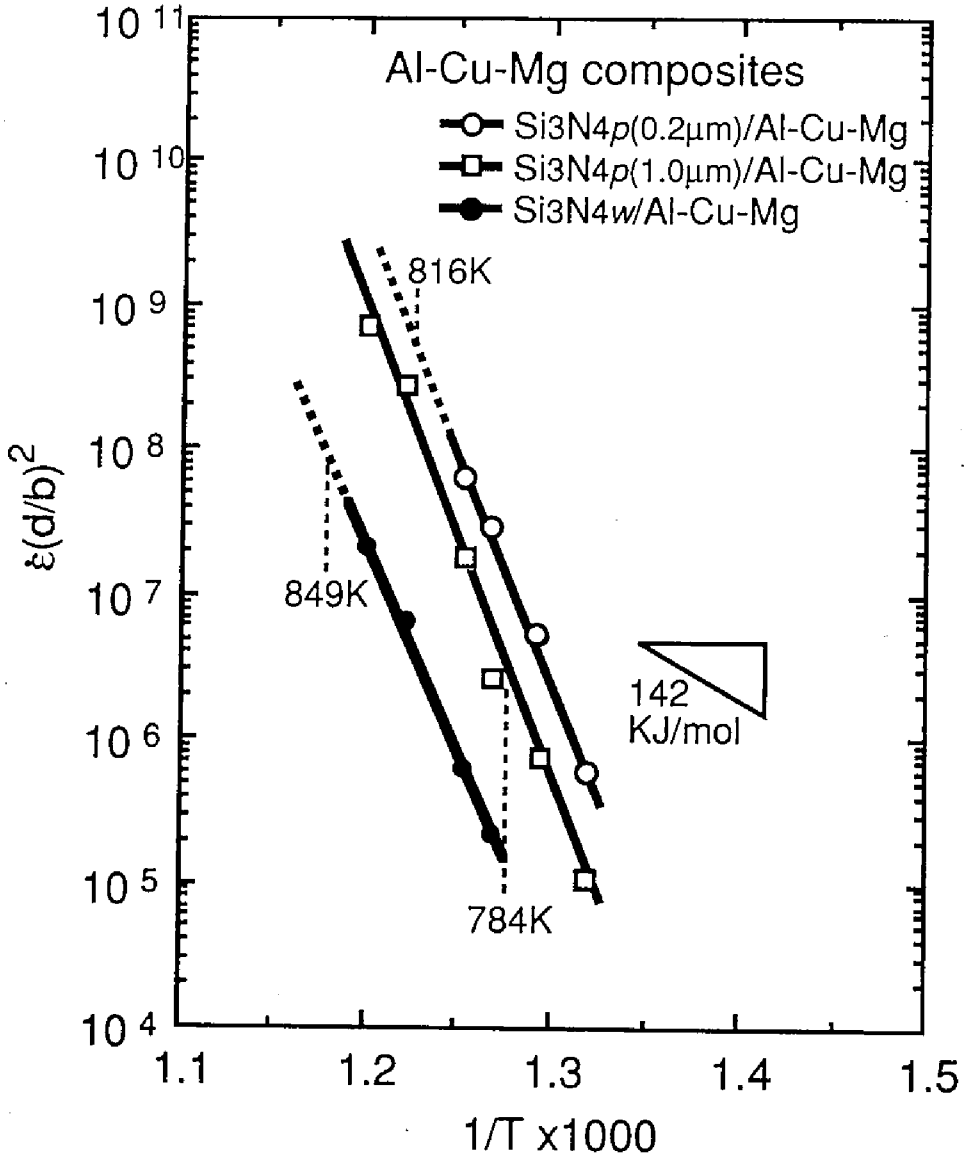

Fig. 20 The variation in $\dot{\varepsilon}(d/b)^2$ as a function of $1/T$ for the Al-Cu-Mg composites.

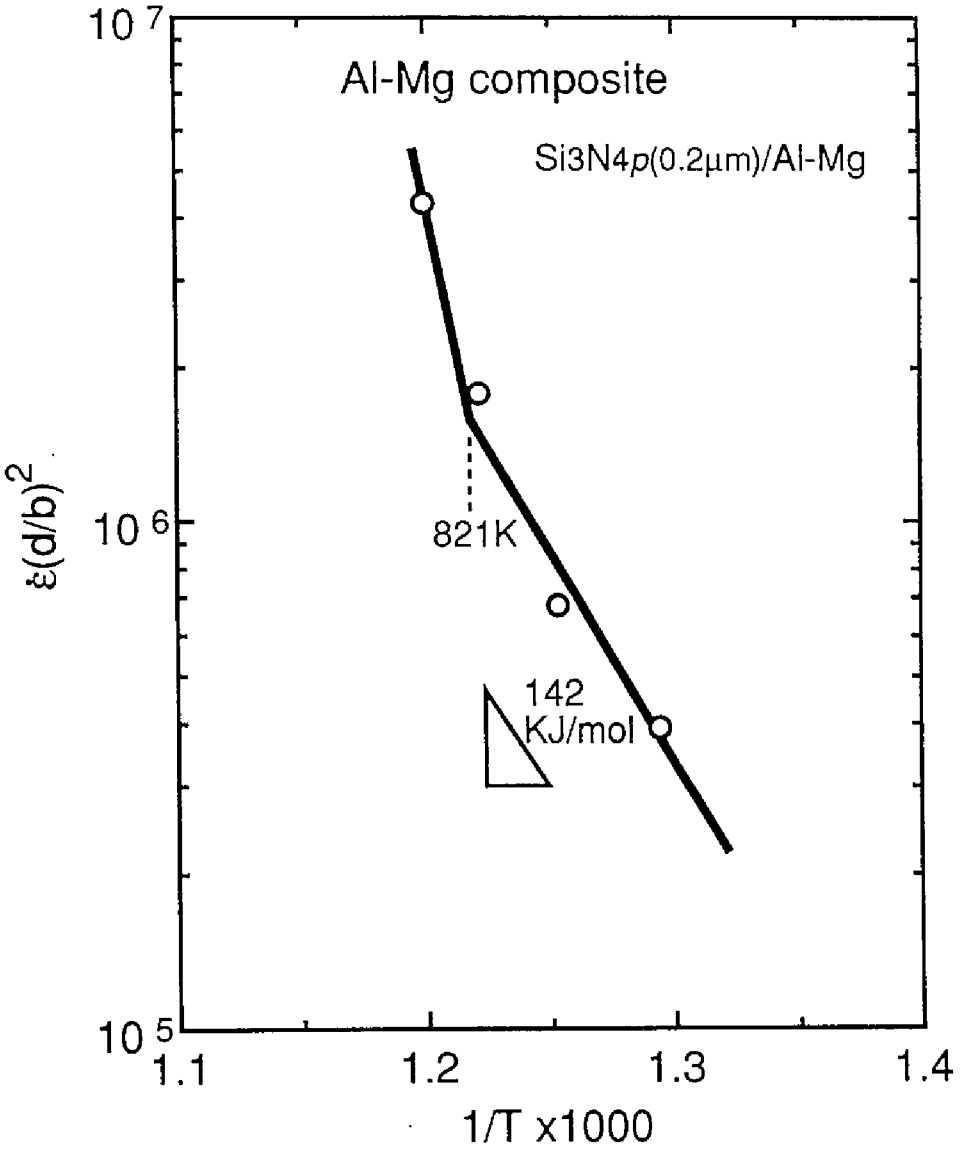

Fig. 21 The variation in $\dot{\varepsilon}(d/b)^2$ as a function of $1/T$ for the Al-Mg composite.

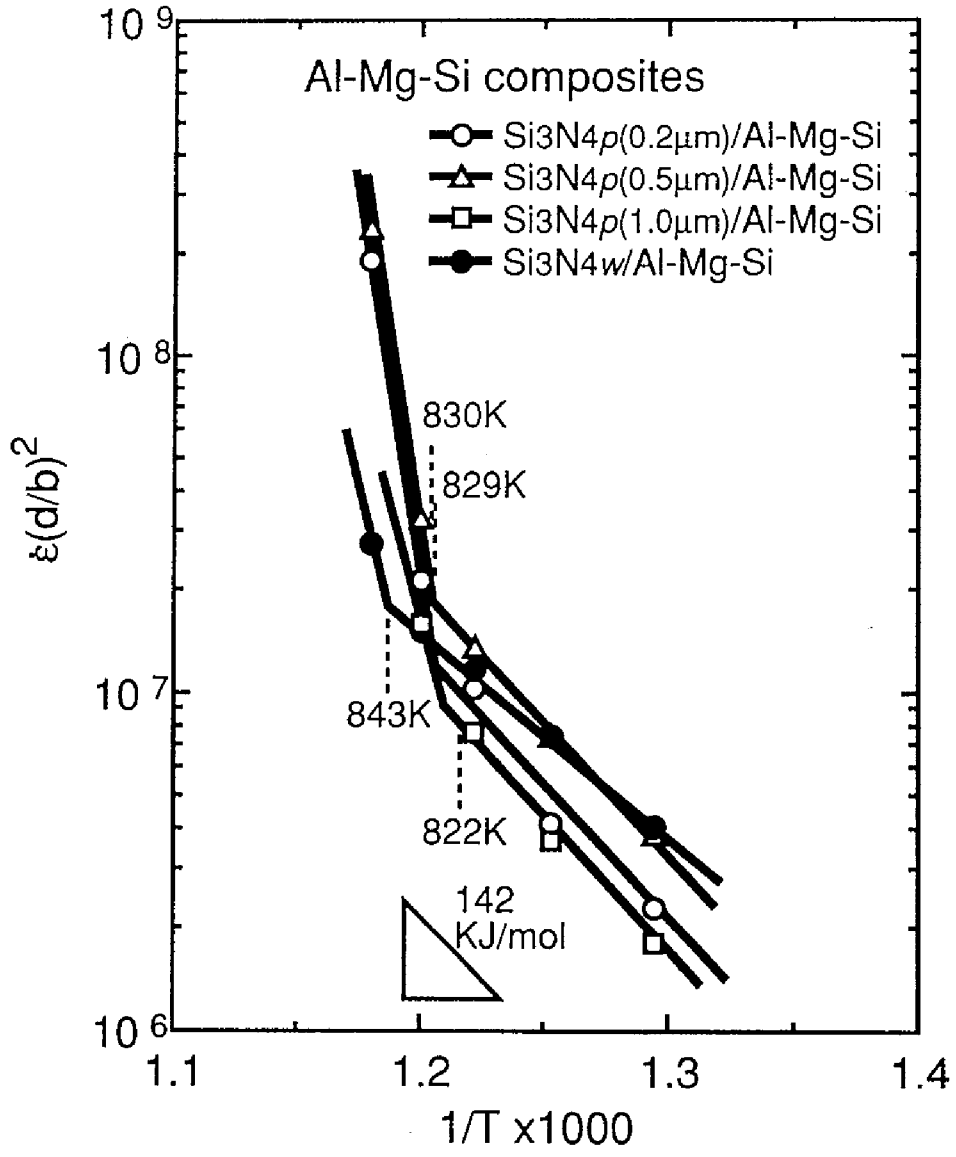

Fig. 22 The variation in $\dot{\varepsilon}(d/b)^2$ as a function of $1/T$ for the Al-Mg-Si composites.

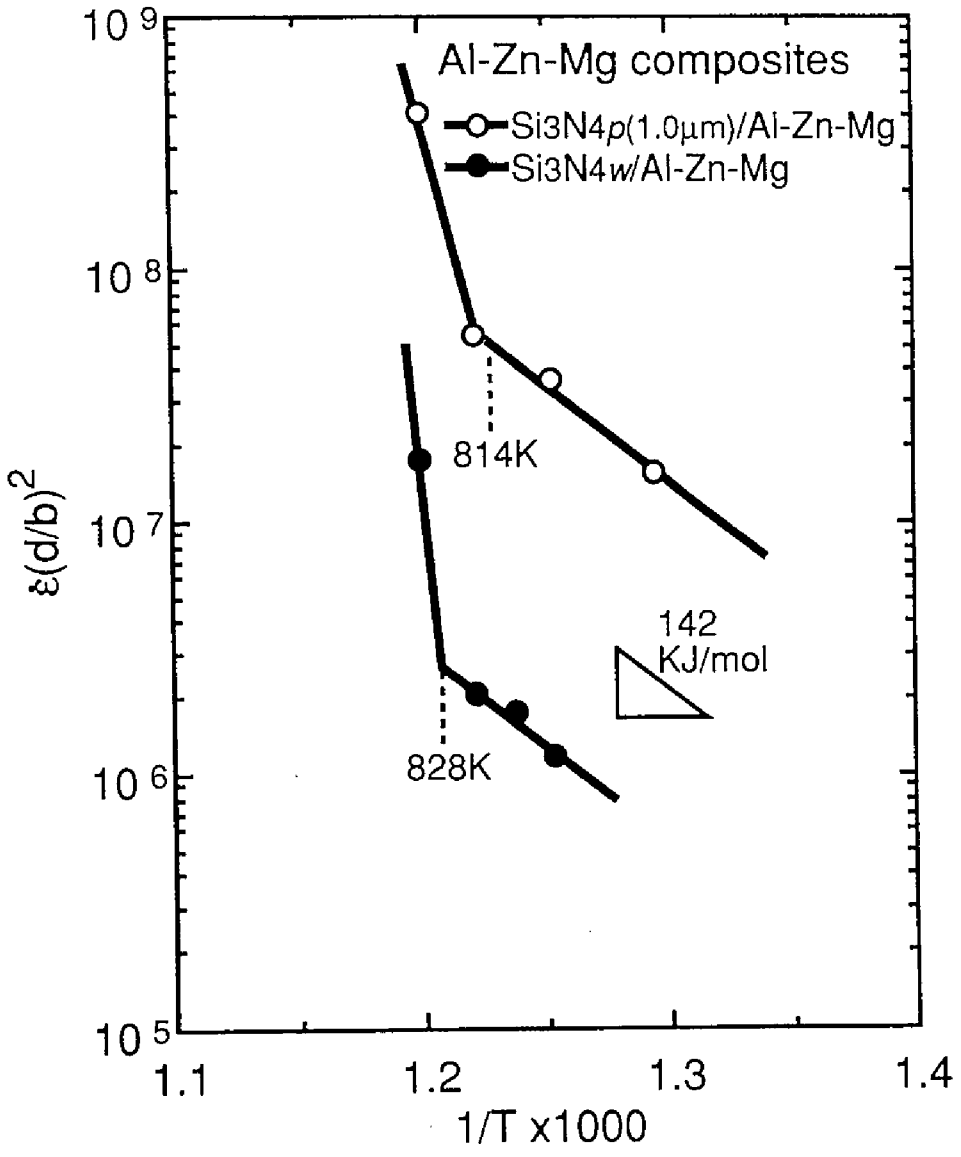

Fig. 23 The variation in $\dot{\varepsilon}(d/b)^2$ as a function of $1/T$ for the Al-Zn-Mg composites.

Table 4.2 Superplastic properties and activation energy for superplastic flow in the Si3N4/Al alloy matrix composites.

Materials	$\dot{\varepsilon}$ /s^{-1}	σ /MPa	$(\sigma-\sigma_{th})/G$	T /K	Tm /K	Q/KJmol^{-1} (Region I)	Q/KJmol^{-1} (Region II)
Si3N4*p*(0.2μm)/Al-Cu-Mg	$3x10^{-1}$	8	$1.37x10^{-4}$	773	816	- - -	581
Si3N4*p*(1.0μm)/Al-Cu-Mg	$4x10^{-2}$	2	$6.22x10^{-5}$	788	784	- - -	638
Si3N4*w*/Al-Cu-Mg	$4x10^{-2}$	2	$1.58x10^{-5}$	818	849	- - -	567
Si3N4*p*(0.2μm)/Al-Mg	1	6	$1.18x10^{-4}$	818	821	174	327
Si3N4*p*(0.2μm)/Al-Mg-Si	2	5	$3.03x10^{-4}$	833	830	171	> 860
Si3N4*p*(0.5μm)/Al-Mg-Si	1	6	$3.01x10^{-4}$	833	829	149	772
Si3N4*p*(1.0μm)/Al-Mg-Si	$1x10^{-1}$	5	$1.80x10^{-4}$	818	822	165	282
Si3N4*w*/Al-Mg-Si	$1x10^{-1}$	11	$2.61x10^{-4}$	833	843	122	> 223
Si3N4*p*(1.0μm)/Al-Zn-Mg	1	10	$4.50x10^{-4}$	818	814	150	> 752
Si3N4*w*/Al-Zn-Mg	$1x10^{-1}$	4	$6.56x10^{-5}$	833	828	148	806

of each composite is shown as the dashed line in Figs 4.20 ~ 4.23. It should be noted that the temperature for a transition from Region I to Region II is very close to the onset temperature for partial melting. The values of the activation energy in Regions I and II are listed in Table 4.2. The activation energy in Region I is roughly in agreement with the activation energy for lattice diffusion of aluminum (= 142 kJ/mol [57]). However, the activation energy in Region II is much higher than the activation energy for lattice diffusion. The fact that the activation energy was increased above the onset temperature for partial melting clearly shows that the high activation energy in Region II is attributed to the presence of a liquid phase.

If the deformation is controlled by viscosity of a liquid phase, for example, Newtonian flow or lubricated flow [58], the activation energy for the deformation is in agreement with the one for viscosity of a liquid phase. The activation energy for viscosity in melt aluminum is very low (= 16.5 kJ/mol [59]). Therefore the high activation energy can not be explained from the viewpoint of viscosity of a liquid phase. It was suggested [20] that an increase in strain rate due to the presence of a liquid phase resulted in an apparent high value of the activation energy. The schematic representation for the high activation energy due to an increase in strain rate caused by the presence of a liquid phase is shown in Fig. 4.24. Region II exhibiting the high activation energy is likely a transition region from superplastic flow in a solid state including no liquid to viscosity flow of liquid.

The behaviors of the Al-Cu-Mg alloy matrix composites were different from those of the other composites. It is found from Fig. 4.20 that the activation energy was higher than that for lattice diffusion even in the temperature range below the onset temperature for partial melting for the Al-Cu-Mg alloy matrix composites. This is probably because partial melting occurred at a temperature lower than the apparent partial melting temperature

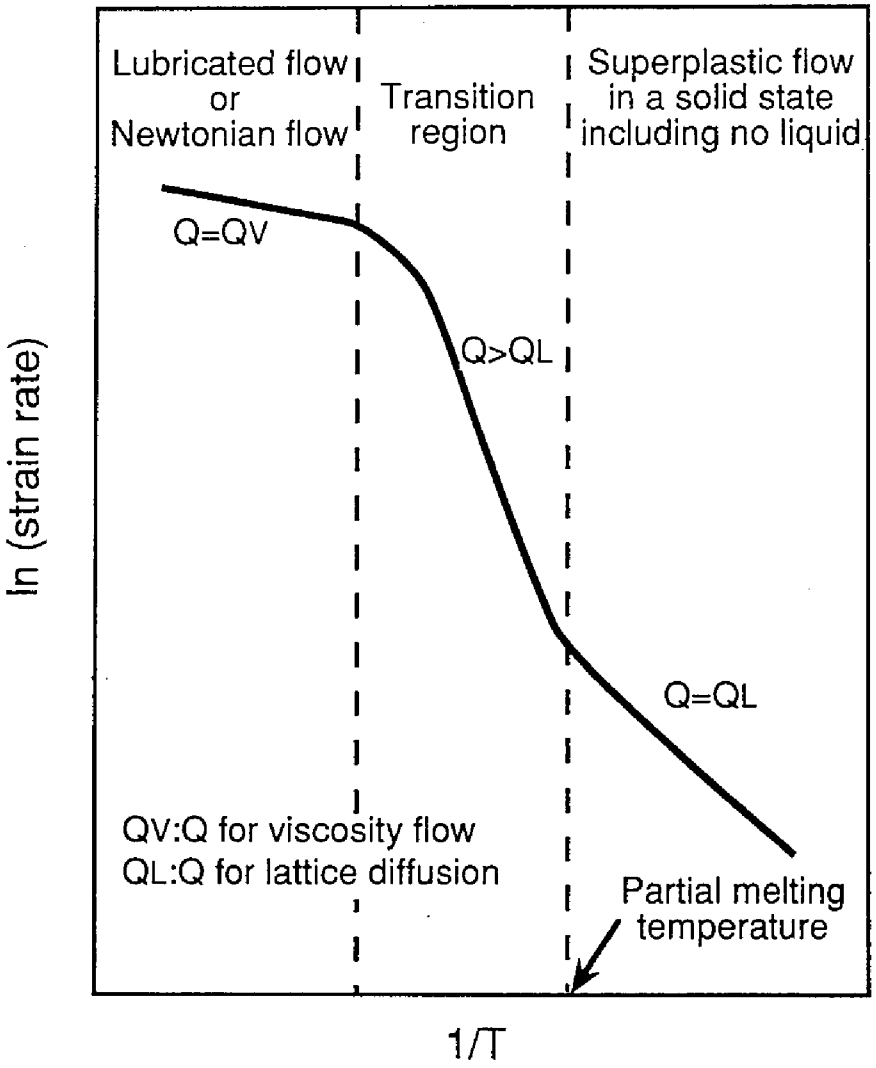

Fig. 4.24 Schematic representation for the high activation energy due to an increase in strain rate caused by the presence of a liquid phase.

determined by the DSC investigation, however, the volume of liquid was too small to be measured by the DSC investigations for the Al-Cu-Mg alloy matrix composites. Differences in the onset temperature for partial melting for identical matrix composites were about 20 K for the Al-Zn-Mg and Al-Mg-Si alloy matrix composites, however, a difference in the onset temperature for partial melting was more than 60 K for the Al-Cu-Mg alloy matrix composites. A large difference in the onset temperature for partial melting for the Al-Cu-Mg alloy matrix composites may be associated with ability of the DSC investigations. Namely, when the volume of liquid is too small, evidence for partial melting can not be exactly checked by DSC investigations, as mentioned above. In such a case, the apparent partial melting temperatures determined by the DSC investigations may differ so greatly. Solute atoms such as Mg and Si are segregated at the matrix/reinforcement interfaces and grain boundaries, as shown in Chapter 6. Such segregation is likely responsible for partial melting for the Al-Mg, the Al-Mg-Si and the Al-Zn-Mg alloy matrix composites. On the other hand, pseudo-ternary eutectics consisting of Al, Mg and Cu are often formed for Al-Cu-Mg alloys. The pseudo-ternary eutectics may be related to partial melting for the Al-Cu-Mg alloy matrix composites. Further research is required to exactly investigate the partial melting behavior for the Al-Cu-Mg alloy matrix composites.

4.3.2 Rate-controlling process

In this section, a rate-controlling process of superplastic flow is investigated in a temperature range below the onset temperature for partial melting for the aluminum matrix composites from the viewpoint of effects of the reinforcements on the basis of the experimental results of the mechanical properties in the present investigation and the previous works [13-16].

4.3.2.1 Accommodation process

Mishra and Mukherjee [60] showed that the activation energy values for superplastic flow for aluminum matrix composites with high volume fraction of reinforcements were significantly higher than the one for lattice diffusion of aluminum and that the deformation process was controlled by interface diffusion. However, this result was obtained from the data in both temperature ranges below and above the partial melting temperature. As shown above, on the other hand, the activation energy for superplastic flow was in agreement with the one for lattice diffusion of aluminum in a temperature range below the onset temperature for partial melting, although the activation energy was much higher than the one for lattice diffusion of aluminum in a temperature range above the onset temperature for partial melting. This indicates that a rate-controlling process of superplastic flow in a temperature range below the onset temperature for partial melting for the composites is controlled not by interface diffusion, but by lattice diffusion of a matrix material.

It is accepted that grain boundary sliding is the dominant deformation process of superplastic flow [47-49]. Because grain boundary sliding generally causes stress concentrations at triple points and ledges of grain boundaries, grain boundary sliding is required to be accommodated in order to attain superplasticity. Therefore the accommodation process is considered to be a rate-controlling process of superplastic flow. Many models on superplastic flow [39-43,61-64] have been proposed from the viewpoint of the accommodation process of grain boundary sliding. Summary of the models is shown in Table 4.3. The experimental results of $n = 2$, $p = 2$ and $Q = Q_L$ in a temperature range below the onset temperature for partial melting for the superplastic aluminum matrix composites in the present investigation are in agreement with the one proposed by Sherby and Wadsworth [63] and

Table 4.3 Summary of the constitutive equations and parametric dependencies for superplastic flow.

Constitutive equation	Stress exponent	Grain size exponent	Activation energy	References
Model				
$\dot{\varepsilon} \propto \left(\frac{\sigma - \sigma_{th}}{G}\right)\left(\frac{b}{d}\right)^2 D_{eff}$	1	2 or 3	QL or QGB	[61]
$\dot{\varepsilon} \propto \left(\frac{\sigma}{G}\right)^2\left(\frac{b}{d}\right)^2 D_{GB}$	2	2	QGB	[39,40,42,62]
$\dot{\varepsilon} \propto \left(\frac{\sigma}{G}\right)^2\left(\frac{b}{d}\right)^3 D_{GB}$	2	3	QGB	[63]
$\dot{\varepsilon} \propto \left(\frac{\sigma}{G}\right)^2\left(\frac{b}{d}\right)^3 D_P$	2	3	QP	[41]
$\dot{\varepsilon} \propto \left(\frac{\sigma}{G}\right)^2\left(\frac{b}{d}\right)^2 D_L$	2	2	QL	[41,63]
$\dot{\varepsilon} \propto \left(\frac{\sigma - \sigma_{th}}{G}\right)^2\left(\frac{b}{d}\right)^2 D_{IPB}$	2	2	QIPB	[43,64]
Result investigated experimentally for MMC				
$\dot{\varepsilon} \propto \left(\frac{\sigma - \sigma_{th}}{\mathbf{G}}\right)^2\left(\frac{\mathbf{b}}{\mathbf{d}}\right)^2 \mathbf{D_L}$	**2**	**2**	**QL**	This investigation

D_L : lattice self-diffusion coefficient
D_{GB}: grain boundary diffusion coefficient
D_P : pipe diffusion coefficient
D_{eff}: $=D_L(1+3.3\delta D_{GB}/dD_L)$
D_{IPB}: diffusion coefficient along an interphase boundary

Hayden *et al.* [41]. The experimental result of $n = 2$ indicates that grain boundary sliding is accommodated by dislocation movement [39-43,62-64], not by diffusion [61]. Furthermore, the fact that the activation energy for superplastic flow in the composites was in agreement with the activation energy for lattice diffusion of a matrix material indicates that the dislocation movement is controlled by lattice diffusion of a matrix material. It is therefore concluded that the dominant deformation process of superplastic flow in a temperature range below the onset temperature for partial melting for the aluminum matrix composites is grain boundary sliding accommodated by dislocation movement controlled by lattice diffusion.

The strain rate for superplastic flow in the composites is lower than that in reinforcement-free metals when the stress is constant, as shown later, indicating that the strengthening due to the presence of reinforcements is retained for superplastic flow and the rate-controlling process is affected by the presence of reinforcements. Schematic illustration of the accommodation process of grain boundary sliding by dislocation movement for metal matrix composites is shown in Fig. 4.25. Dislocations generated at triple points of grain boundaries move on the most favorable slip plane for relaxing the stress concentrations caused by grain boundary sliding. The dislocations are piled up around the reinforcements located in a grain and at the opposite grain boundaries. Finally the piled-up dislocations disappear by climb controlled by lattice diffusion.

4.3.2.2 Effects of reinforcements

The $(\dot{\varepsilon}/D_L)(d/b)^2$ - $(\sigma-\sigma_{th})/G$ relation was analyzed from the data in a temperature range below the onset temperature for partial melting for the superplastic aluminum matrix composites, where D_L is the lattice diffusion coefficient. The plot is shown in Fig. 4.26. For reference, the relation for

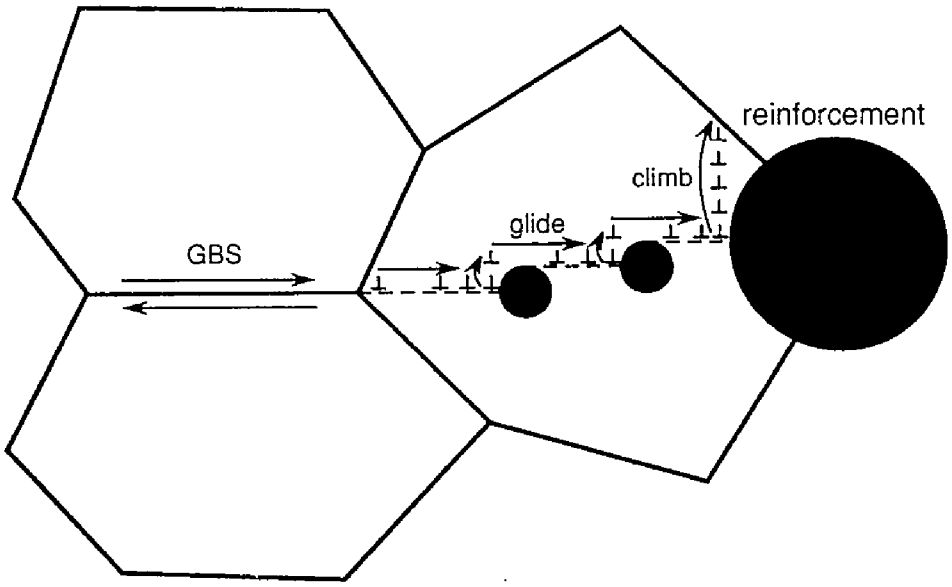

Fig. 4.25 Schematic illustration of the accommodation process of grain boundary sliding by dislocation movement for metal matrix composites.

superplastic metals [63] is superimposed in the figure. It should be noted that as a whole, the strengthening for the particle-reinforced composites is lower than that for the whisker-reinforced composites. It is suggested that the superplastic behavior for the composites depends on the morphology of reinforcements. This trend is similar to the creep behavior of aluminum matrix composites [9].

In general, large triaxial stresses develop in a matrix material due to the presence of reinforcements and these stresses have a strong effect on reducing the deformation rate at elevated temperatures [65]. In such a case, the strain rate of composites may be given by [66]

$$\dot{\varepsilon} = \dot{\varepsilon}_0 \left(\frac{\sigma}{a\sigma_0} \right)^n \tag{4.4}$$

where a is the strengthening coefficient, $\dot{\varepsilon}_0$ is the creep coefficient and σ_0 is the reference stress. For $n = \infty$, the strengthening coefficient a is approximated by [66]

$$a \approx 1+2(2+c)V_f^{3/2} \tag{4.5}$$

for fibers, where c and V_f are the aspect ratio and the volume fraction of the reinforcements, respectively. The strengthening coefficient depends on the morphology and volume fraction of reinforcements. Therefore the mechanical properties of composites may be given by

$$\dot{\varepsilon} = B\left(\frac{\sigma-\sigma_{th}}{\alpha G} \right)^n \left(\frac{b}{d} \right)^p D \tag{4.6}$$

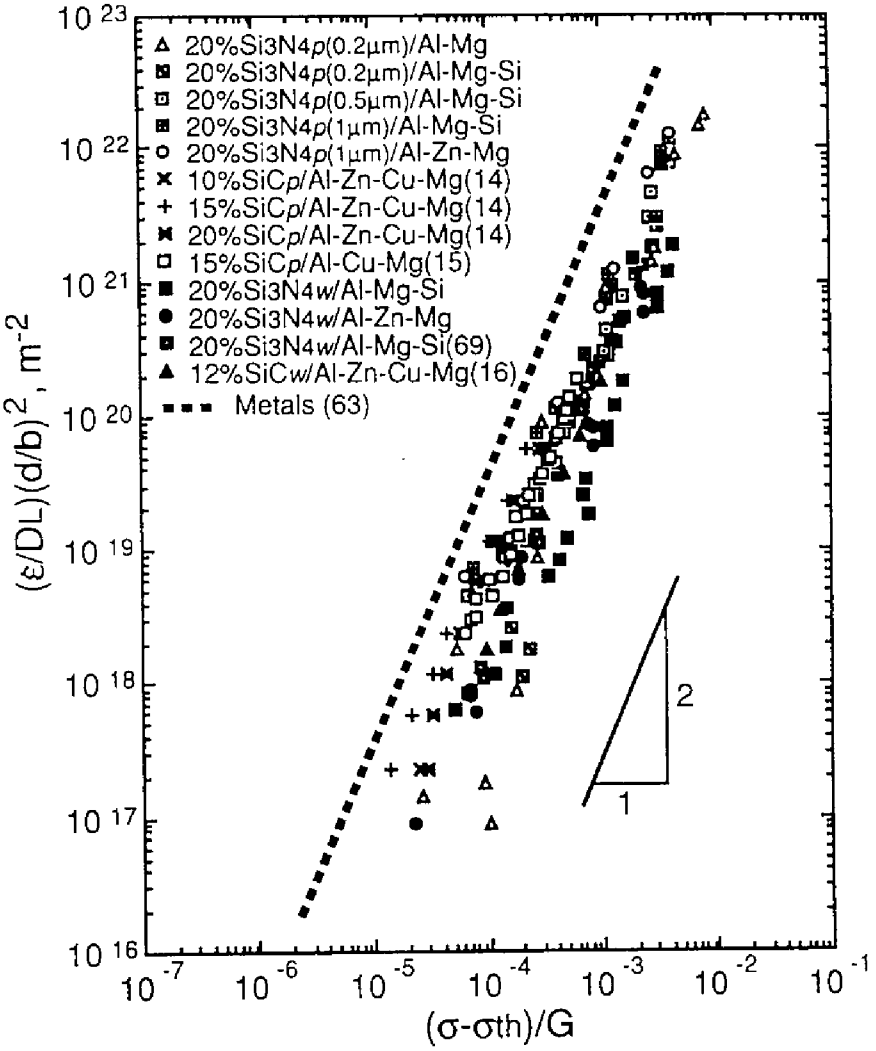

Fig. 4.26 The variation in $(\dot{\varepsilon}/DL)(d/b)^2$ as a function of $(\sigma-\sigma th)/G$ for the aluminum matrix composites.

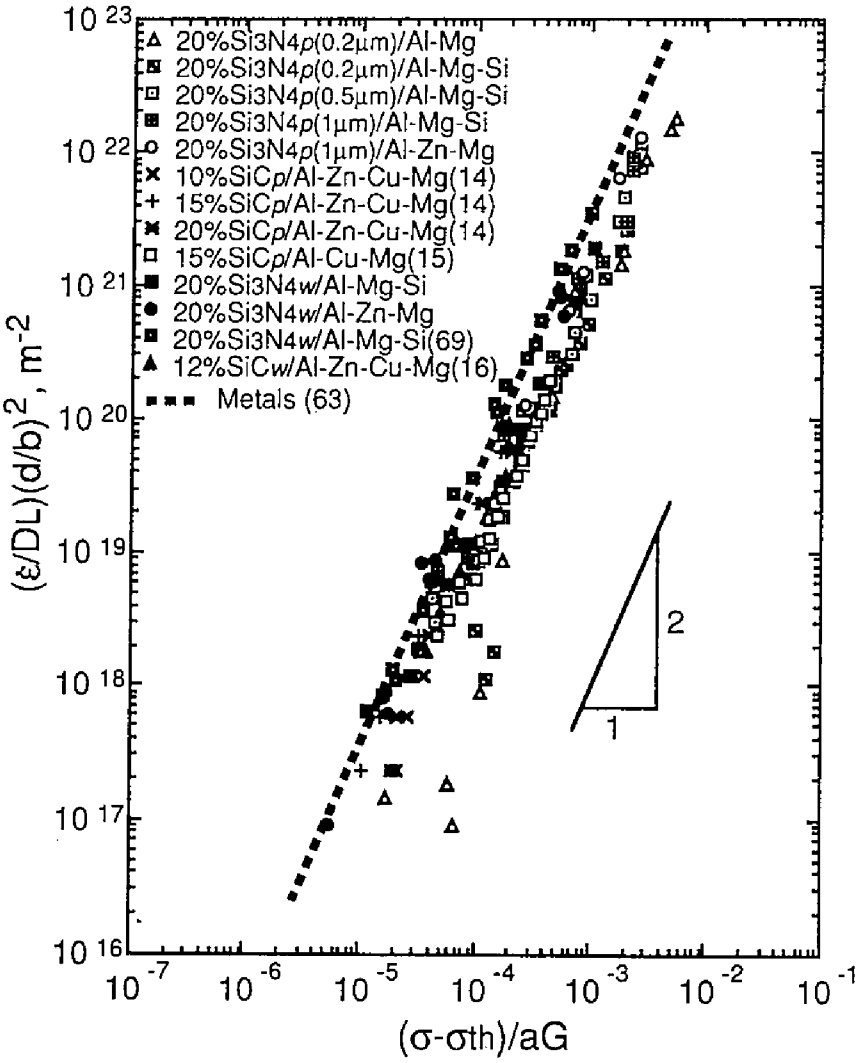

Fig. 4.27 The variation in $(\dot{\varepsilon}/DL)(d/b)^2$ as a function of $(\sigma-\sigma th)/aG$ for the aluminum matrix composites.

where B is a constant and D is the adequate diffusion coefficient. The variation in $(\dot{\varepsilon}/D_L)(d/b)^2$ as a function of $(\sigma-\sigma_{th})/aG$ is shown in Fig. 4.27. It is found that the mechanical properties of the particulate-reinforced composites are roughly in agreement with those of the whisker-reinforced composites, compensated by the strengthening coefficient, though the plots show some deviations.

The strengthening coefficient defined by Eq. 4.5 does not depend on the reinforcement spacing and size, and effects of the reinforcement spacing and size are not taken into consideration in the above analysis. However, there is no reason why the reinforcement spacing and size have no effect on the deformation process. Pandy *et al.* [7] experimentally revealed that the reinforcement size affected the creep behavior of an aluminum matrix composite. As mentioned above, the moving dislocations are expected to pile up due to the presence of reinforcements during superplastic deformation for metal matrix composites. This situation is similar to the case of dislocation pile-ups at grain boundary at low temperatures, for example, at room temperature for metals. Hence, the strengthening may be increased with decreasing reinforcement spacing. On the other hand, Rösler *et al.* [66] analyzed limitation in relaxation of stress concentrations by diffusion and they revealed that the critical strain rate, below which the strengthening is eliminated and above which the strengthening is retained, increases with decreasing reinforcement size. This suggests that the strengthening is retained more easily for larger reinforcement size. Also, Artz *et al.* [67] theoretically analyzed by-pass of dislocations over a reinforcement and they suggested that the strain rate is inversely proportional to the reinforcement size. In these cases, the strengthening is expected to be increased with increasing reinforcement size.

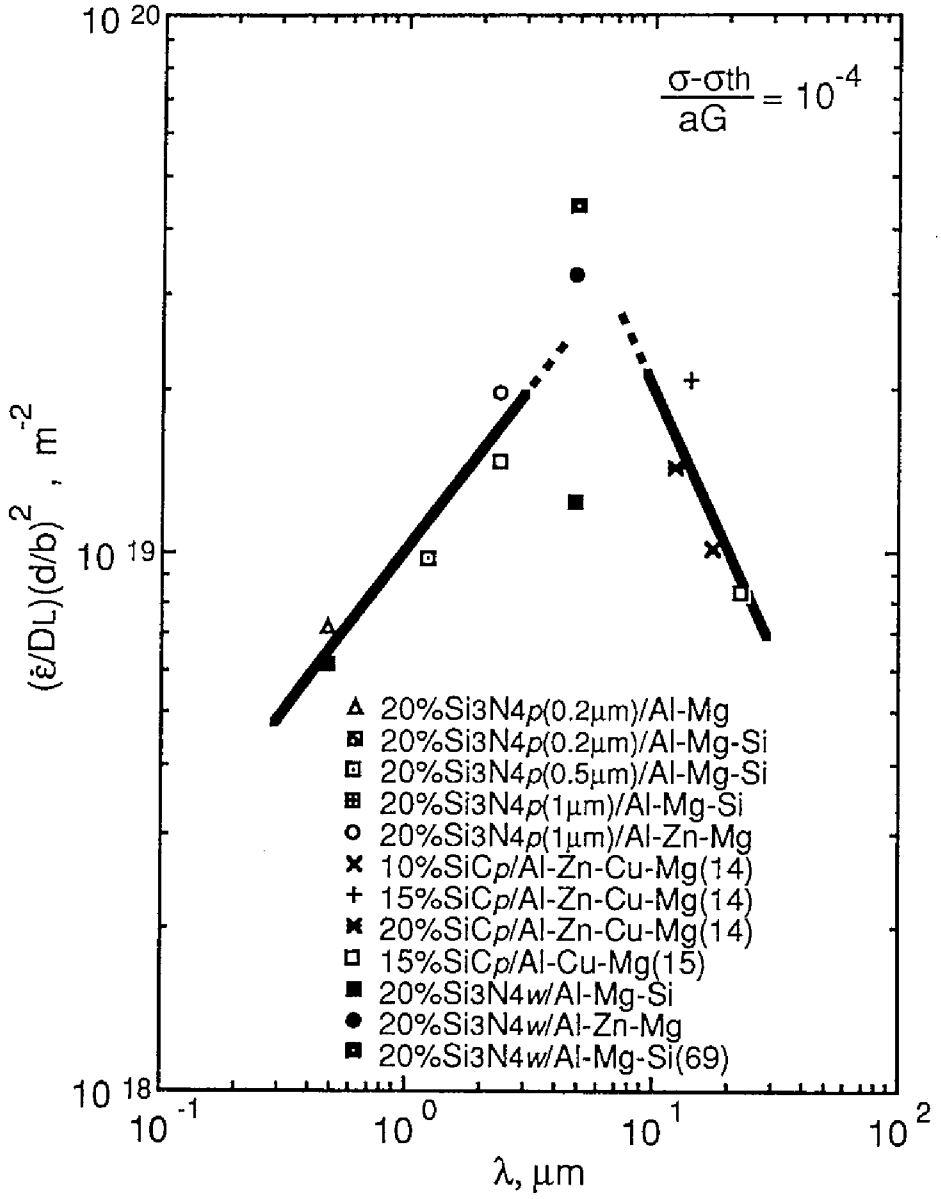

Fig. 4.28 The variation in $(\dot{\varepsilon}/DL)(d/b)^2$ as a function of the reinforcement spacing λ for the superplastic aluminum matrix composites.

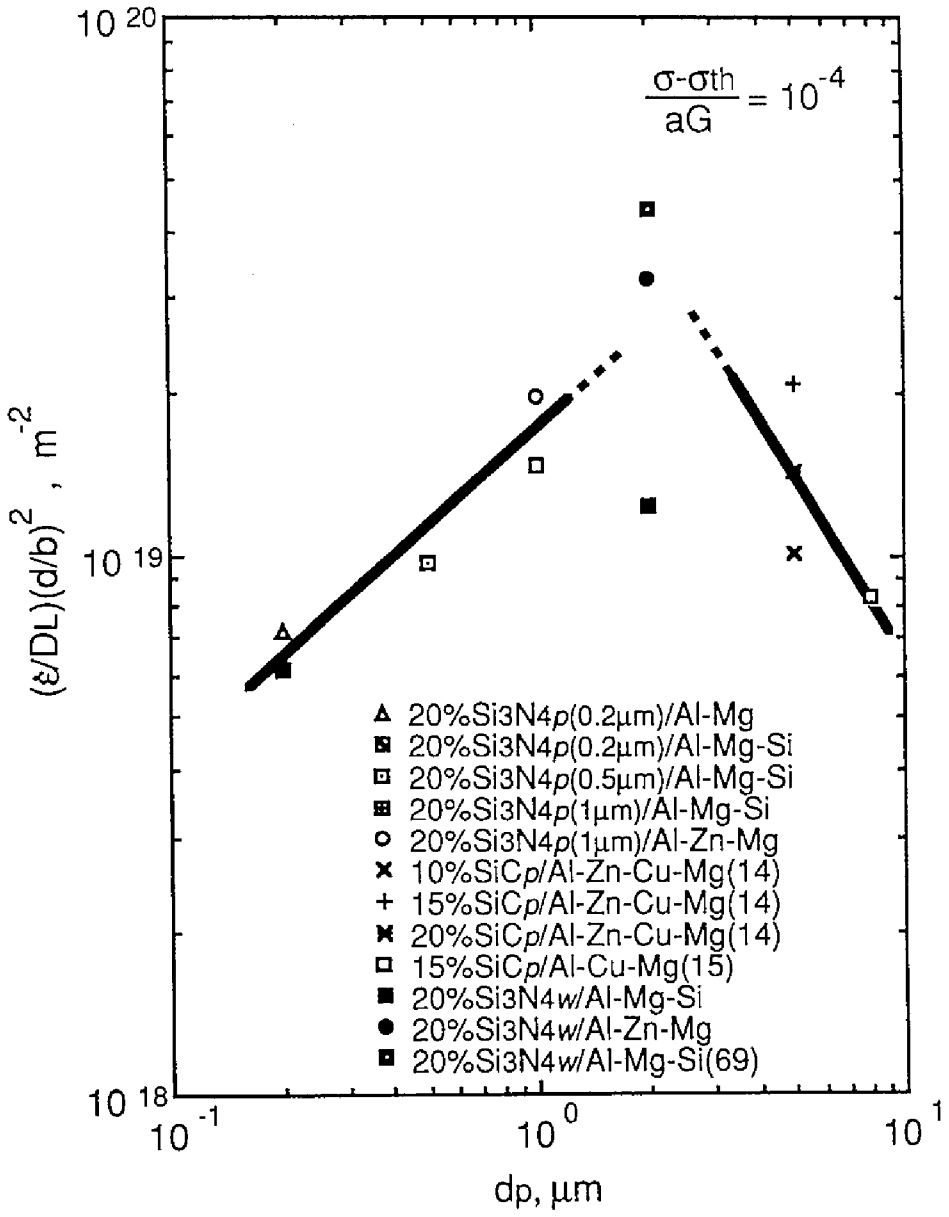

Fig. 4.29 The variation in $(\dot{\varepsilon}/DL)(d/b)^2$ as a function of the reinforcement size *dp* for the superplastic aluminum matrix composites.

The variation in $(\dot{\varepsilon}/D_L)(d/b)^2$ as a function of the reinforcement spacing λ is shown in Fig. 4.28, where λ is given by $(d_p/2)\sqrt{3\pi/2V_f}$ [68], and the variation in $(\dot{\varepsilon}/D_L)(d/b)^2$ as a function of the reinforcement size d_p is shown in Fig. 4.29, respectively, where a value of $(\dot{\varepsilon}/D_L)(d/b)^2$ is determined at $(\sigma-\sigma_{th})/aG = 10^{-4}$. A value of d_p is taken to be $\sqrt{d_1 d_2}$ for the whisker-reinforce composites, where d_1 is the diameter of whiskers and d_2 is the length of whiskers. Inspection of Figs 4.28 and 4.29 reveals that a value of $(\dot{\varepsilon}/D_L)(d/b)^2$ increases with increasing reinforcement spacing in a range $\lambda \leq 2$ μm and it decreases with increasing reinforcement size in a range $d_p \geq 5$ μm. This indicates that the dislocation-pileup mechanism affects the rate-controlling process for a small reinforcement spacing, on the other hand, the diffusional relaxation-limitation or dislocation-bypass mechanism affects the rate-controlling process for a large reinforcement size. It is suggested that the strongest strengthening process among these processes affects the rate-controlling process of superplastic flow for the composites.

4.4 Conclusions

(1) The phenomenological deformation characteristics of the superplastic aluminum matrix composites are summarized as follows: (i) all the aluminum matrix composites in the present investigation exhibited superplastic behavior at high strain rates (> 10^{-2} s^{-1}), (ii) the high strain rate sensitivity was attained in an intermediate strain rate range, where large elongations were attained, (iii) the strain rate sensitivity was very low (for example, less than 0.1) in a low stain rate range, which is attributed to the presence of threshold stress, and (iv) the optimum temperatures where a maximum elongation was attained for each composite were different from one another, in spite of the same chemical composition of a matrix alloy.

(2) The threshold stress strongly depended on the testing temperature. The interaction between grain boundary dislocations and segregation of solute additions may be responsible for the threshold stress. Further research is required to understand the origin of the threshold stress for the superplastic composites.

(3) The superplastic flow was divided into two regions from the viewpoint of the activation energy: Region I (= a low temperature range) showing the low activation energy and Region II (= a high temperature range) showing the high activation energy. The activation energy in Region I was roughly in agreement with the activation energy for lattice diffusion of aluminum, on the other hand, the activation energy in Region II was much higher than the activation energy for lattice diffusion. The high activation energy in Region II is likely attributed to the presence of a liquid phase.

(4) The experimental results showed that $n = 2$, $p = 2$ and $Q = Q_L$ in a temperature range below the onset temperature for partial melting for the superplastic composites. The dominant deformation process in a temperature range below the onset temperature for partial melting for the superplastic aluminum matrix composites is likely grain boundary sliding accommodated by dislocation movement controlled by lattice diffusion of a matrix material.

(5) The strengthening due to the presence of reinforcements was retained for superplastic flow and the mechanical properties of superplastic flow were affected by the presence of reinforcements. It is suggested that there are strengthening processes of the dislocation-pileup mechanism, the diffusional relaxation-limitation and dislocation-bypass mechanism, so that the strongest strengthening process among these processes affects the rate-controlling process of superplastic flow for the composites.

(6) The mechanical properties in a solid state for the superplastic aluminum matrix composites were made clear by the present work. However, the mechanical properties in a state including a liquid phase are not clear. It is important to understand the superplastic deformation mechanisms in a state including a liquid phase because a liquid phase plays an important role in superplastic flow, as shown in Chapter 7. Further research is required to investigate the superplastic properties in a state including a liquid phase.

References

1. T.G.Nieh, Metall. Trans. A, **15A**, 139 (1984).
2. V.C.Nardone and J.R.Strife, Metall. Trans. A, **18A**, 109 (1987).
3. T.G.Nieh, K.Xia and T.G.Langdon, J. Eng. Mater. Tech., **110**, 77 (1988).
4. K.-T. Park, E.J.Lavernia and F.A.Mohamed, Acta Metall. Mater., **38**, 2149 (1990).
5. R.B.Bhagat and M.B.House, Mater. Sci. Eng., **A144**, 319 (1991).
6. T.L.Dragon and D.Nix, Acta Metall. Mater., **40**, 2781 (1992).
7. A.B.Pandey, R.S.Mishra and Y.R.Mahajan, Acta Metall. Mater., **40**, 2045 (1992).
8. F.A.Mohamed, K.-T. Park and E.J.Lavernia, Mater. Sci. Eng., **A150**, 21 (1992).
9. G.G.-Doncel and O.D.Sherby, Acta Metall. Mater., **41**, 2797 (1993).
10. X.Xia, P.Sakaris and J.McQueen, Mater. Sci. Tech., **10**, 487, (1994).
11. K.-T. Park, E.J.Lavernia and F.A.Mohamed, Acta Metall. Mater., **42**, 667 (1994).
12. J.Cadek, H.Oikawa and V.Sustek, Mater. Sci. Eng., **A190**, 9 (1995).
13. T.G.Nieh, C.A.Henshall and J.Wadsworth, Scripta Metall., **18**, 1405 (1984).
14. M.W.Mahoney and A.K.Ghosh, Metall. Trans. A, **18A**, 653 (1987).
15. J.Pilling, Scripta Metall., **23**, 1375 (1989).
16. M.W.Mahoney, A.K.Ghosh and C.C.Bampton, in *Proc. 6th Int. Conf. on Composite Materials*, edited by F.L.Matthew, N.C.R.Buskell, J.M.Hodgkinson and J.Monton (Elesier Applied Science, London, 1986), vol. 2, p.372.
17. R.S.Mishra and A.K.Mukherjee, Scripta Metall. Mater., **25**, 271 (1991).
18. T.G.Nieh, J.Wadsworth and T.Imai, Scripta Metall. Mater., **26**, 703 (1992).

19. T.G.Nieh and J.Wadsworth, Mater. Sci. Eng., **A147**, 129 (1991).

20. K.Higashi, T.G.Nieh and J.Wadsworth, Acta Metall. Mater., **43**, 3275 (1995).

21. K.Higashi, T.G.Nieh, M.Mabuchi and J.Wadsworth, Scripta Metall. Mater., **32**, 1079 (1995).

22. K.Higashi, T.Okada, T.Mukai and S.Tanimura, Scripta Metall. Mater., **25**, 2053 (1991).

23. K.Higashi, Mater. Sci. Eng., **A166**, 109 (1993).

24. B.M.Watts and M.J.Stowell, J. Mater. Sci., **6**, 228 (1971).

25. A.K.Ghosh and C.H.Hamilton, Metall. Trans. A, **A10**, 699 (1979).

26. D.S.Wilkinson and C.H.Caceres, Acta Metall., **32**, 1335 (1984).

27. B.P.Kashyap, J. Mater. Sci., **26**, 4657 (1991).

28. H.Xiaoxu, L.Qing, C.K.Yao and Y.Mei, J. Mater. Sci. Lett., **10**, 964 (1991).

29. K.Higashi, T.Okada, T.Mukai, S.Tanimura, T.G.Nieh and J.Wadsworth, Scripta Metall. Mater., **26**, 185 (1992).

30. K.Matsuki, H.Matsumoto, M.Tokizawa, N.Takatsuji, M.Isogai, S.Murakami and Y.Murakami, in *Science and Engineering of Light Metal*, edited by K.Hirano, H.Oikawa and K.Ikeda (The Japan Institute of Light Metals, Tokyo, 1991), p. 205.

31. T.Imai, M.Mabuchi, Y.Tozawa and M.Yamada, J. Mater. Sci. Lett., **9** , 255 (1990).

32. M.Mabuchi, T.Imai, K.Kubo, K.Higashi, Y.Okada and S.Tanimura, Mater. Lett., **11**, 339 (1991).

33. M.Mabuchi, T.Imai, K.Kubo, K.Higashi and S.Tanimura, Mater. Lett., **12**, 276 (1991).

34. M.Mabuchi, K.Higashi, S.Tanimura, T.Imai and K.Kubo, Scripta Metall. Mater., **25**, 1675 (1991).

35. M.Mabuchi, T.Imai, K.Kubo, K.Higashi and S.Tanimura, Mater. Lett., **12**, 330 (1991).

36. T.Imai, G.L'espérance, B.Hong, Y.Tozawa and M.Mabuchi, in *1993 Powder Metallurgy World Congress*, edited by Y.Bando and K.Kosuge, (Japan Society of Powder and Powder Metallurgy, 1993), p. 634.

37. F.A.Mohamed, J. Mater. Sci., **18**, 583 (1983).

38. R.S.Mishra, T.R.Bieler and A.K.Mukherjee, Acta Metall. Mater., **43**, 877 (1995).

39. A.Ball and M.M.Hutchison, Met. Sci. J., **3**, 1 (1969).

40. A.K.Mukherjee, Mater. Sci. Eng., **8**, 83 (1971).

41. H.W.Hayden, S.Floreen and P.D.Goodell, Metall. Trans., **3**, 833 (1972).

42. R.C.Gifkins, Metall. Trans. A, **7A**, 1225 (1976).

43. J.H.Gittus, J. Eng. Mater. Tech., **99**, 244 (1977).

44. R.W.Lund and W.D.Nix, Acta Metall., **24**, 469 (1976).

45. E.Arzt and M.F.Ashby, Scripta Metall., **16**, 1285 (1982).

46. E.Arzt and D.S.Wilkinson, Acta Metall., **34**, 1893 (1986).

47. K.Matsuki, H.Morita, M.Yamada and Y.Murakami, Metal Sci., **11**, 156 (1977).

48. Z.-R.Lin, A.H.Chokshi and T.G.Langdon, J. Mater. Sci., **23**, 2712 (1988).

49. T.G.Langdon, Mater. Sci. Eng., **A174**, 225 (1994).

50. M.Strangwood, C.A.Hippsley and J.J.Lewandowski, Scripta Metall. Mater., **24**, 1483, (1990).

51. G.L'Eseprance, T.Imai and B.Hong, in *Superplasticity in Advanced Materials*, edited by S.Hori, M.Tokizane and N.Furushiro, (Japan Soc. for Res. on Superplasticity, 1991), p. 379.

52. F.A.Mohamed and T.G.Langdon, Acta Metall., **23**, 117 (1975).

53. F.A.Mohamed and T.G.Langdon, Philos. Mag., **32**, 697 (1975).

54. A.Arieli, A.K.S.Yu and A.K.Mukherjee, Metall. Trans. A, **11A**, 181 (1980).

55. C.H.Hamilton, C.C.Bampton and N.E.Paton, in *Superplastic Forming of Structural Alloys*, edited by N.E.Paton and C.H.Hamilton (The Metallurgical Society of AIME, Warrendale, PA, 1982), p.173.

56. K.Higashi, Y.Matsumura and S.Tanimura, Trans. Japan. Soc. Mech. Eng., **59**, 1669 (1993).

57. H.J.Frost and M.F.Ashby, in *Deformation Mechanism Maps*, (Pergamon Press, Oxford, 1982).

58. G.M.Pharr and M.F.Ashby, Acta Metall., **31**, 129 (1983).

59. "*Metals Databook*, 2th Edition", (Maruzen, Tokyo, 1984).

60. R.S.Mishra and A.K.Mukherjee, in *Superplasticity and Superplastic Forming*, edited by A.K.Ghosh and T.R.Bieler (TMS, Warrendale, PA, 1995), p.171.

61. M.F.Ashby and R.A.Verrall, Acta Metall., **21**, 149 (1973).

62. B.Burton, Philos. Mag. A, **48**, L9 (1983).

63. O.D.Sherby and J.Wadsworth, Prog. Mater. Sci., **33**, 169 (1989).

64. M.Suery and B.Baudelet, Philos. Mag. A, **41**, 41 (1980).

65. T.L.Dragone and W.D.Nix, Acta Metall. Mater., **38**, 1941 (1990).

66. J.Rösler, G.Bao and A.G.Evans, Acta Metall. Mater., **39**, 2733 (1991).

67. E.Arzt, M.F.Ashby and R.A.Verrall, Acta Metall., **31**, 1977 (1983).

68. G.Le Roy, J.D.Embury, G.Edward and M.F.Ashby, Acta Metall., **29**, 1509 (1981).

CHAPTER 5

DEFORMATION CHARACTERISTICS IN HIGH STRAIN RATE SUPERPLASTIC MAGNESIUM MATRIX COMPOSITES

5.1 Introduction

High strain rate superplasticity was originally demonstrated in aluminum based materials [1,2]. To date, there have been some studies on high strain rate superplasticity for aluminum based materials [3-6]. For magnesium based materials, however, there are fewer studies on superplasticity, in particular, high strain rate superplasticity, compared to aluminum based materials and it is not sufficient to understand the deformation characteristics for superplastic magnesium based materials.

Very recently, a few of works on high strain rate superplasticity for magnesium matrix composites with ceramic reinforcements were reported [7-9]. As shown in Chapter 4, the activation energy value was apparently changed by the presence of a liquid phase for the high strain rate superplastic aluminum matrix composites. On the other hand, Nieh *et al.* [9] revealed that the activation energy for superplastic flow in the high strain rate superplastic SiC_p/Mg-Zn (ZK60) composite was equal to the one for grain boundary diffusion and they showed no evidence of a drastic change in the activation energy for the magnesium matrix composite.

The aim in the present chapter is to investigate deformation characteristics of high strain rate superplasticity for magnesium matrix composites exhibiting partial meting behavior or not. Since partial melting behavior is attributed to segregation [10], a difference in chemical compositions of a matrix affects

partial melting behavior. In this investigation, two Mg_2Si particle-reinforced magnesium matrix composites with different chemical compositions (Mg_2Si_p/Mg-Al and Mg_2Si_p/Mg-Zn) were prepared, as shown in Chapter 2. As a result of DSC measurements, the Mg_2Si_p/Mg-Al composite showed partial melting at 794 K, on the other hand, the Mg_2Si_p/Mg-Zn composite showed no partial melting. The superplastic properties have been investigated by constant strain rate tensile tests in a temperature range from 653 to 813 K, including temperatures below and above the onset temperature for partial melting of the Mg_2Si_p/Mg-Al composite.

5.2 Experimental procedure

The Mg_2Si_p/Mg-Al and Mg_2Si_p/Mg-Zn composites listed in Table 2.3 were prepared by rapidly solidification and hot extrusion routes, as shown in Chapter 2, and constant strain rate tensile tests were carried out in a strain rate range of 10^{-3} ~ 10 s^{-1} from 733 to 813 K for the Mg_2Si_p/Mg-Al composite and from 653 to 788 K for the Mg_2Si_p/Mg-Zn composite, respectively. The testing temperature range for the Mg_2Si_p/Mg-Al composite includes temperatures below and above the onset temperature for partial melting of the composite (= 794 K).

5.3 Results and discussion

5.3.1 Mechanical properties

5.3.1.1 Strain rate dependence

The variation in flow stress (top figure) and elongation to failure (bottom figure) as a function of strain rate is shown in Fig. 5.1 for the Mg_2Si_p/Mg-Al composite and in Fig. 5.2 for the Mg_2Si_p/Mg-Zn composite, respectively. In general, large elongations are attained in the range of both temperatures and strain rates where the strain rate sensitivity is high. For the Mg_2Si_p/Mg

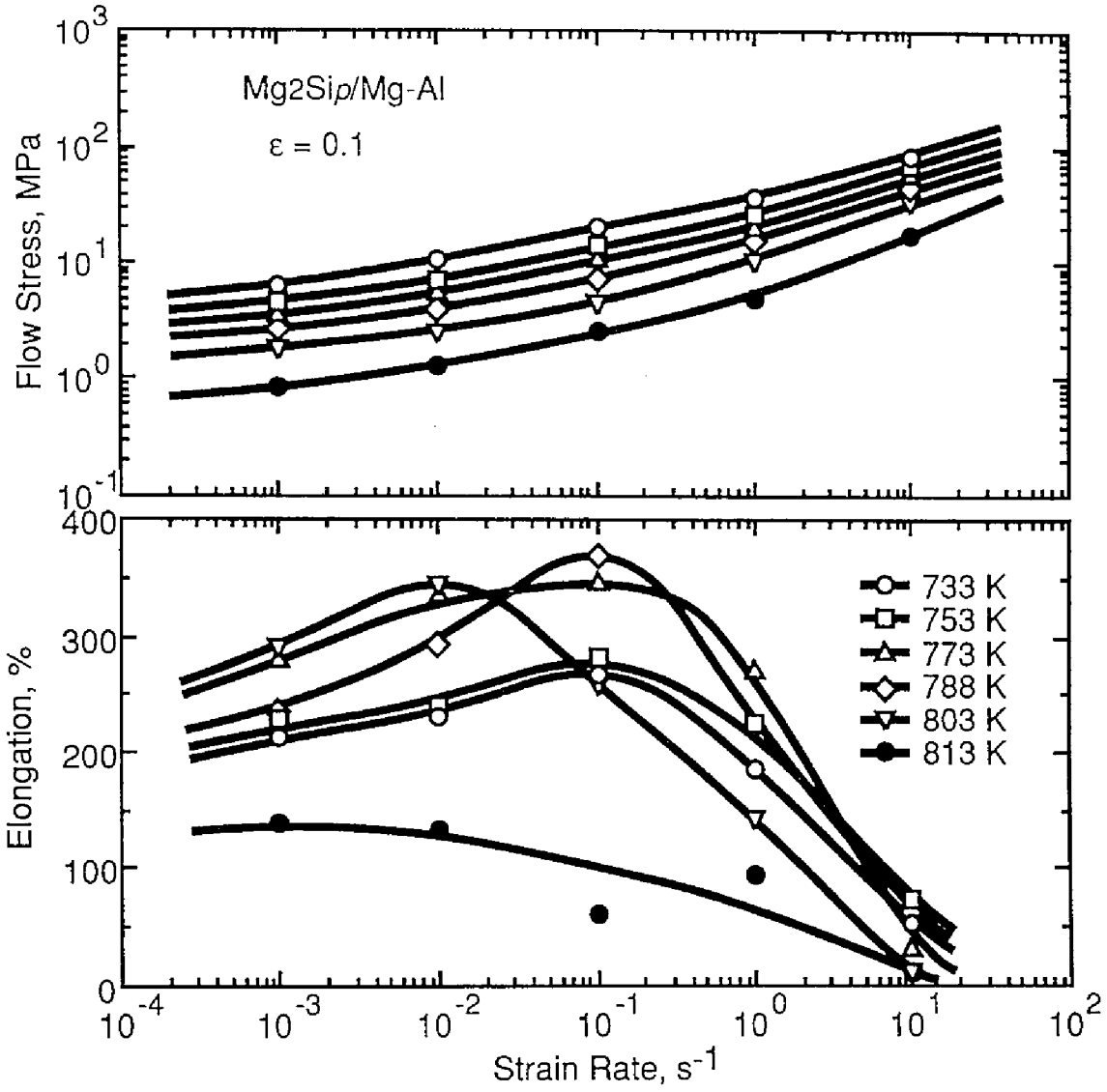

Fig. 5.1 The variation in flow stress (top figure) and elongation to failure (bottom figure) as a function of strain rate for the Mg_2Si_p/Mg-Al composite.

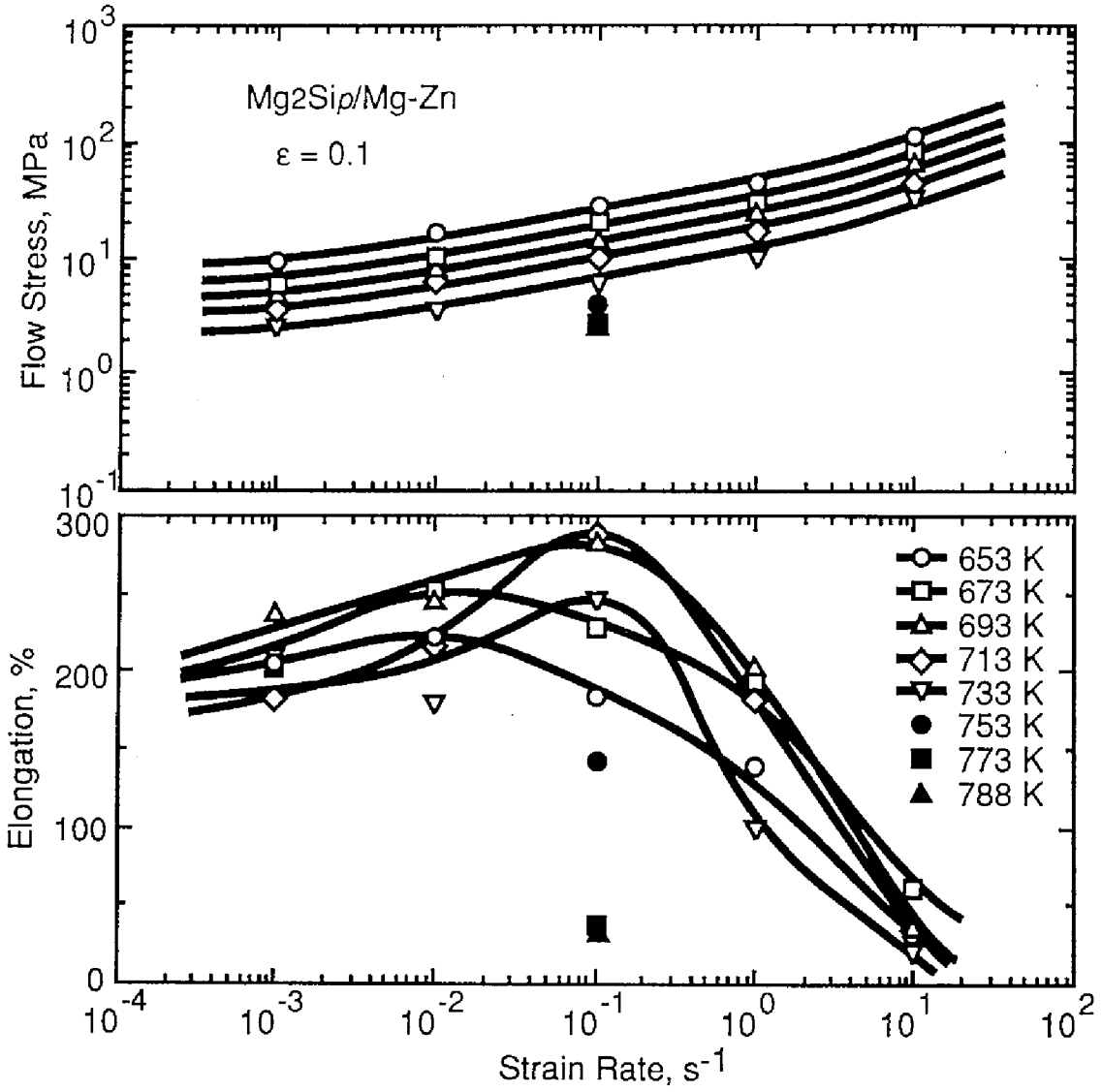

Fig. 5.2 The variation in flow stress (top figure) and elongation to failure (bottom figure) as a function of strain rate for the Mg_2Si_p/Mg-Zn composite.

composites, high values of the strain rate sensitivity (≥ 0.3) were attained at high strain rates above 10^{-2} s^{-1}. The strain rate sensitivity tended to decrease with decreasing strain rate. This trend for the superplastic magnesium matrix composites is the same as that for the superplastic aluminum matrix composites. The low strain rate sensitivity in a low strain rate range for the magnesium matrix composites is likely attributed to the presence of a threshold stress as well as for the aluminum matrix composites.

The Mg_2Si_p/Mg-Al composite exhibited a maximum elongation of 370 % at 788 K and at a high strain rate of 10^{-1} s^{-1}, and the Mg_2Si_p/Mg-Zn composite showed a maximum elongation of 290 % at 713 K and at a high strain rate of 10^{-1} s^{-1}. It should be noted that a maximum elongation of 290 % was attained at 713 K, where no partial melting occurred, for the Mg_2Si_p/Mg-Zn composite.

5.3.1.2 Threshold stress

The strain rate sensitivity tended to decrease with decreasing strain rate for the superplastic magnesium matrix composites, as shown in Figs 5.1 & 5.2. This is probably attributed to the presence of a threshold stress. A threshold stress can be estimated by extrapolation to zero strain rate of a line which the data give as σ against $\dot{\varepsilon}^{1/n}$ on a double-liner scale [11], as shown in Chapter 4, where σ is the flow stress, $\dot{\varepsilon}$ is the strain rate and n is the stress exponent. For example, plots of σ against $\dot{\varepsilon}^{1/2}$, $\dot{\varepsilon}^{1/3}$, $\dot{\varepsilon}^{1/5}$ and $\dot{\varepsilon}^{1/8}$ at 788 K for the Mg_2Si_p/Mg-Al composite are shown in Fig. 5.3. The linearity of the data in this plot indicates that the presence of a threshold stress is responsible for the change in the strain rate sensitivity and that the value of $n = 2$ is correct for the stress exponent for superplastic deformation. The same trend was found at other testing conditions for the Mg_2Si_p/Mg composites in the present investigation. Therefore all values of threshold stresses were given by

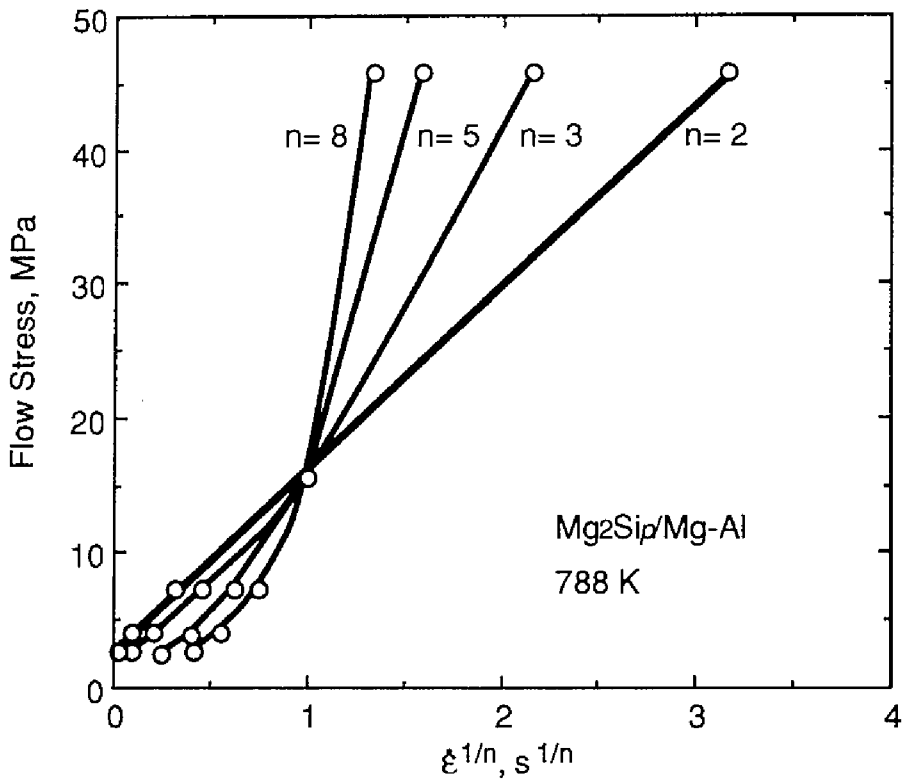

Fig. 5.3 Plots of σ against $\dot{\varepsilon}^{1/2}$, $\dot{\varepsilon}^{1/3}$, $\dot{\varepsilon}^{1/5}$ and $\dot{\varepsilon}^{1/8}$ at 788 K for the Mg_2Si_p/Mg-Al composite.

extrapolation to zero strain rate of a line which the data gave as σ against $\dot{\varepsilon}^{1/2}$ on a double-liner scale.

The variation in threshold stress as a function of temperature is plotted in Fig. 5.4. It is noted that the threshold stress decreased with an increase in temperature. This is the same as the result for the aluminum matrix composites, as shown in Chapter 4, in addition, the similar results were reported for superplastic metals in the previous works [11-13]. The stress concentrations around the Mg_2Si particles, which are caused by sliding process, are sufficiently relaxed, as shown later (in Chapter 7), and therefore the origin of the threshold stress is unlikely directly associated with the presence of the Mg_2Si particles. The nature of sliding processes is probably responsible for the threshold stress. Mohamed and co-worker [11,14,15] noted that a possible origin of a threshold stress is interaction between impurities and grain boundary dislocations. In the present investigation, the Mg_2Si_p/Mg-Al composite showed partial melting, on the other hand, the Mg_2Si_p/Mg-Zn composite showed no evidence of partial melting from the results of DSC measurements, indicating that concentrations of segregation for the Mg_2Si_p/Mg-Al composite are higher than for the Mg_2Si_p/Mg-Zn composite. It is of interest to note that the threshold stresses for the Mg_2Si_p/Mg-Al composite were higher than those for the Mg_2Si_p/Mg-Zn composite. It may be that high concentrations of segregation lead to the higher threshold stresses for the Mg_2Si_p/Mg-Al composite, compared to the Mg_2Si_p/Mg-Zn composite.

5.3.1.3 Activation energy

When a threshold stress is taken into consideration, the mechanical properties for superplastic deformation may be described by an equation for power-law creep of the form [13]

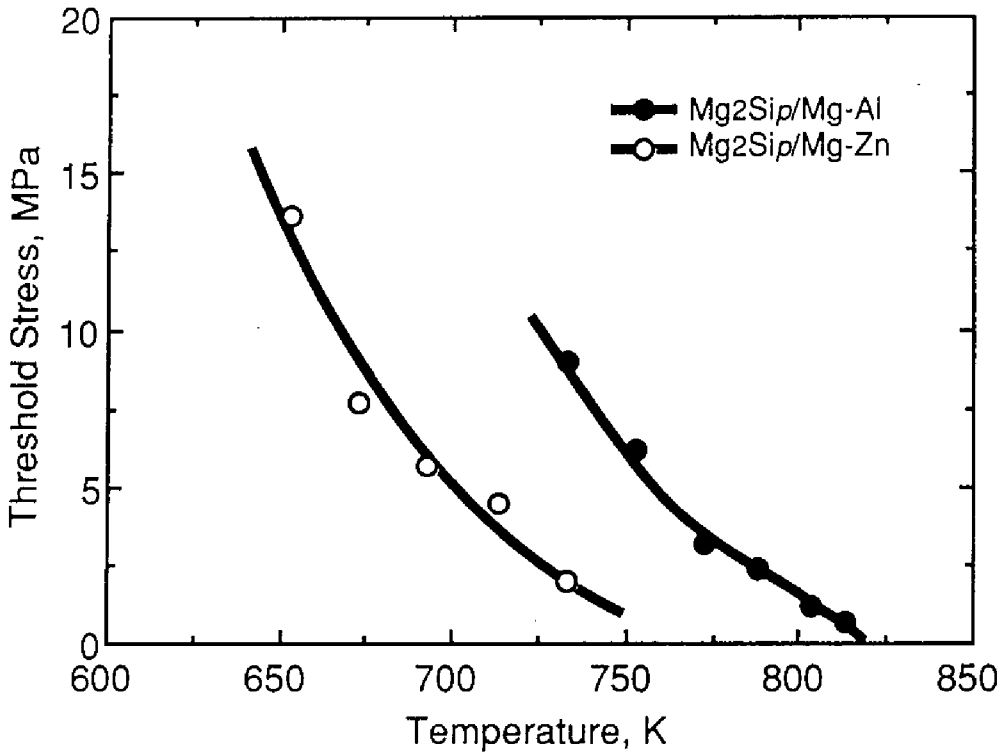

Fig. 5.4 The variation in threshold stress as a function of temperature for the Mg_2Si_p/Mg-Al and Mg_2Si_p/Mg-Zn.

$$\dot{\varepsilon} = \frac{AD_oGb}{kT}\left(\frac{\sigma-\sigma_{th}}{G}\right)^n\left(\frac{b}{d}\right)^p exp\left(\frac{-Q}{RT}\right) \quad (5.1)$$

where A is a constant, G is the shear modulus, b is the Burgers vector, k is the Boltzmann constant, T is the absolute temperature, σ_{th} is the threshold stress, d is the grain size, p is the grain size exponent, D_o is the frequency factor, Q is the activation energy of an appropriate diffusion process and R is the gas constant. When $(\sigma-\sigma_{th})/G$ is constant, the activation energy Q is evaluated as

$$Q = -R\frac{\partial[ln\dot{\varepsilon}(T/G)(d/b)^p]}{\partial(1/T)}. \quad (5.2)$$

Theoretical models on superplasticity [16-21] predict $p = 2$ or 3. A value of p was about 3 for high strain rate superplastic Mg-Al-Zn (AZ91) and Mg-Zn-Zr (ZK61) alloys [22]. Hence, in this investigation, p is taken to be 3. The variation in $\dot{\varepsilon}(T/G)(d/b)^3$ as a function of $1/T$ is shown in Fig. 5.5. As shown in Chapter 4, an apparent value of the activation energy for superplastic flow was drastically increased by the presence of a liquid phase for the high strain rate superplastic aluminum matrix composites. Therefore it is important to check the onset temperature for partial melting. In this investigation, the onset temperature for partial melting was measured by DSC. From the DSC investigations, a small endothermic peak appeared at 794 K for the Mg_2Si_p/Mg-Al composite, however, there was no endothermic reaction to 823 K for the Mg_2Si_p/Mg-Zn composite. These results revealed that partial melting occurred at 794 K for the Mg_2Si_p/Mg-Al composite, on the other hand, melting did not occur at least in the testing temperature range from 653 to 788 K for the Mg_2Si_p/Mg-Zn composite. The onset temperature for partial melting for the Mg_2Si_p/Mg-Al composite (= 794 K) is shown as the dashed line in Fig. 5.5. Inspection of Fig. 5.5 reveals that there is a transition point

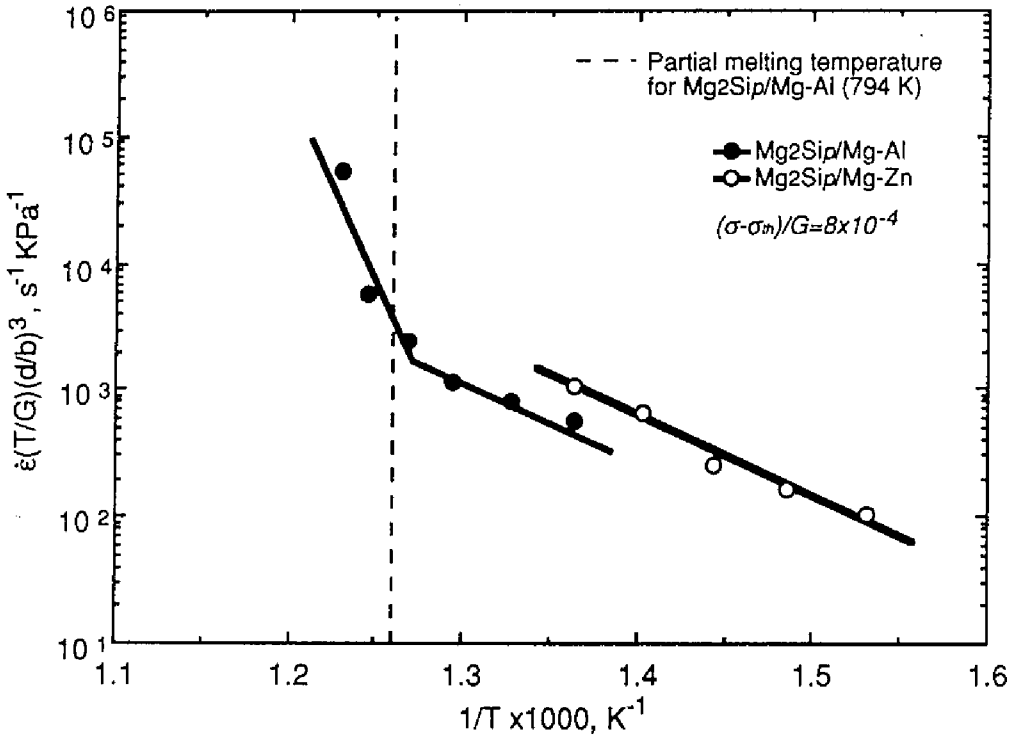

Fig. 5.5 The variation in $\dot{\varepsilon}(T/G)(d/b)^3$ as a function of $1/T$ for the Mg_2Si_p/Mg-Al and Mg_2Si_p/Mg-Zn.

for the Mg_2Si_p/Mg-Al composite and the behavior is divided into two regions: one is a temperature region of 733 ~ 773 K and another is a temperature region of 788 ~ 813 K. The activation energy for superplastic flow was 85 kJ/mol in a temperature region of 733~ 773 K and was 620 kJ/mol in a temperature region of 788 ~ 813 K. On the other hand, for the Mg_2Si_p/Mg-Zn composite, there was no transition point and the activation energy for superplastic flow was 117 kJ/mol. The activation energy for the Mg_2Si_p/Mg-Zn composite is between the one for grain boundary diffusion of magnesium (= 92 kJ/mol [23]) and the one for lattice diffusion of magnesium (= 135 kJ/mol [23]), and the activation energy in a temperature region of 733 ~ 773 K for the Mg_2Si_p/Mg-Al composite is close to the one for grain boundary diffusion. However, the activation energy in a temperature region of 788 ~ 813 K for the Mg_2Si_p/Mg-Al composite is much higher than the ones for grain boundary diffusion and for lattice diffusion of magnesium. It should be noted that the transition point for the Mg_2Si_p/Mg-Al composite is very close to the onset temperature for partial melting. Therefore, the high value of the activation energy in a temperature region of 788 ~ 813 K for the Mg_2Si_p/Mg-Al composite is likely attributed to the presence of a liquid phase. This trend is the same as the results of the aluminum matrix composites and mechanically-alloyed materials [24].

It is recognized that superplastic flow is controlled by grain boundary diffusion or lattice diffusion [25]. A dominant diffusion process for superplastic flow may be evaluated through the effective diffusion concept. The effective diffusion coefficient D_{eff} involving the lattice diffusion coefficient D_L and the grain boundary diffusion coefficient D_{GB} is given by [26]

$$D_{eff} = D_L + x\frac{\pi\delta D_{GB}}{d} \tag{5.3}$$

where x is an unknown constant and δ is the grain boundary width. If the diffusion processes in superplastic flow are analogous with those in diffusion creep, a value of x is unity. On the other hand, Metenier *et al.* [26] noted that $x = 10^{-2}$ for superplastic flow. The critical grain size, above which a dominant diffusion process is lattice diffusion and below which it is grain boundary diffusion, can be evaluated by the effective diffusion concept. The critical grain size d_c may be given by

$$d_c = \frac{x\pi\delta D_{GB}}{D_L} . \tag{5.4}$$

The variation in the critical grain size as a function of temperature is shown for magnesium base materials in Fig. 5.6, where x is taken to be 10^{-2} and 1. The measured grain sizes for the Mg_2Si_p/Mg composites (= about 1 μm) are lower than the critical grain size at $x = 10^{-2}$ at most of testing temperatures. It is therefore suggested that the effective grain boundary diffusion $x\pi\delta D_{GB}/d$ is faster than the lattice diffusion and so that a dominant diffusion process for superplastic flow in a solid state for the Mg_2Si_p/Mg composites is grain boundary diffusion.

5.3.2 Constitutive equation

The experimental results in the present investigation showed that the deformation characteristics of high strain rate superplasticity for the magnesium matrix composites were changed by the presence of a liquid phase as well as for the aluminum matrix composites. In this session, superplastic deformation mechanisms in a solid state are mainly discussed.

It was found from the experimental investigation that $n = 2$, $p = 3$ and $D = D_{GB}$, taking into consideration a threshold stress, for superplastic flow in a

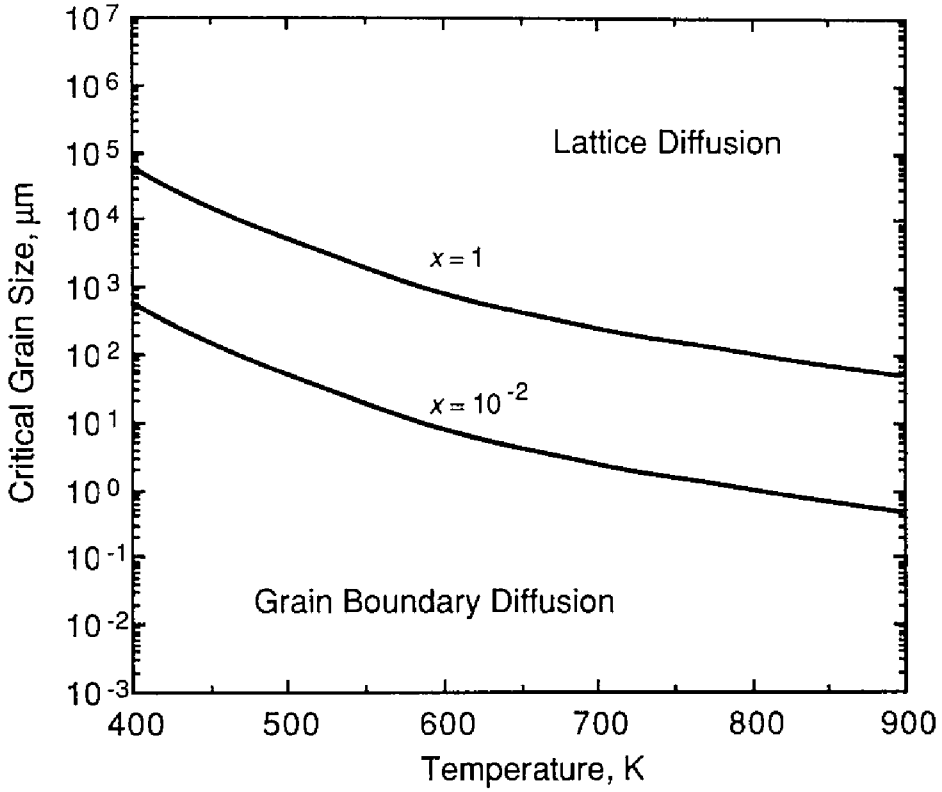

Fig. 5.6 The variation in the critical grain size as a function of temperature for magnesium base materials.

solid state for the Mg_2Si_p/Mg composites. Hence, the mechanical properties for superplastic flow in a solid state for the Mg_2Si_p/Mg composites are described as

$$\dot{\varepsilon} \propto \frac{Gb}{kT}\left(\frac{\sigma-\sigma_{th}}{G}\right)^2\left(\frac{b}{d}\right)^3 D_{GB} \quad . \tag{5.5}$$

It is therefore concluded that a dominant superplastic deformation process in a solid state for the Mg_2Si_p/Mg composites is grain boundary sliding accommodated by dislocation movement controlled by grain boundary diffusion [25].

The variation in diffusion- and grain size-compensated strain rate as a function of modulus- and threshold stress-compensated stress for magnesium base materials is shown in Fig. 5.7, where the shear modulus is taken to be the shear modulus of pure magnesium. In the figure, the data of superplastic magnesium alloys without reinforcements [27-30] are superimposed. It is found from Fig. 5.7 that the composites exhibit lower diffusion- and grain size-compensated strain rate than the alloys when modulus- and threshold stress-compensated stress is constant.

The stress concentrations around the Mg_2Si particles, which are caused due to sliding process, are sufficiently relaxed by diffusion and/or diffusion-controlled dislocation movement for the Mg_2Si_p/Mg composites, as will be shown in Chapter 7. Hence, it is suggested that strengthening mechanisms due to the particles are not operative. The lower strain rates for the composites may be related to a change in the elastic stress field due to a large volume fraction of particles with a high shear modulus because the speeds of dislocation glide and climb are strongly influenced by the elastic stress field of dislocations [31]. The lower strain rates for the composites may be approximately estimated using the shear modulus of the composite by the role

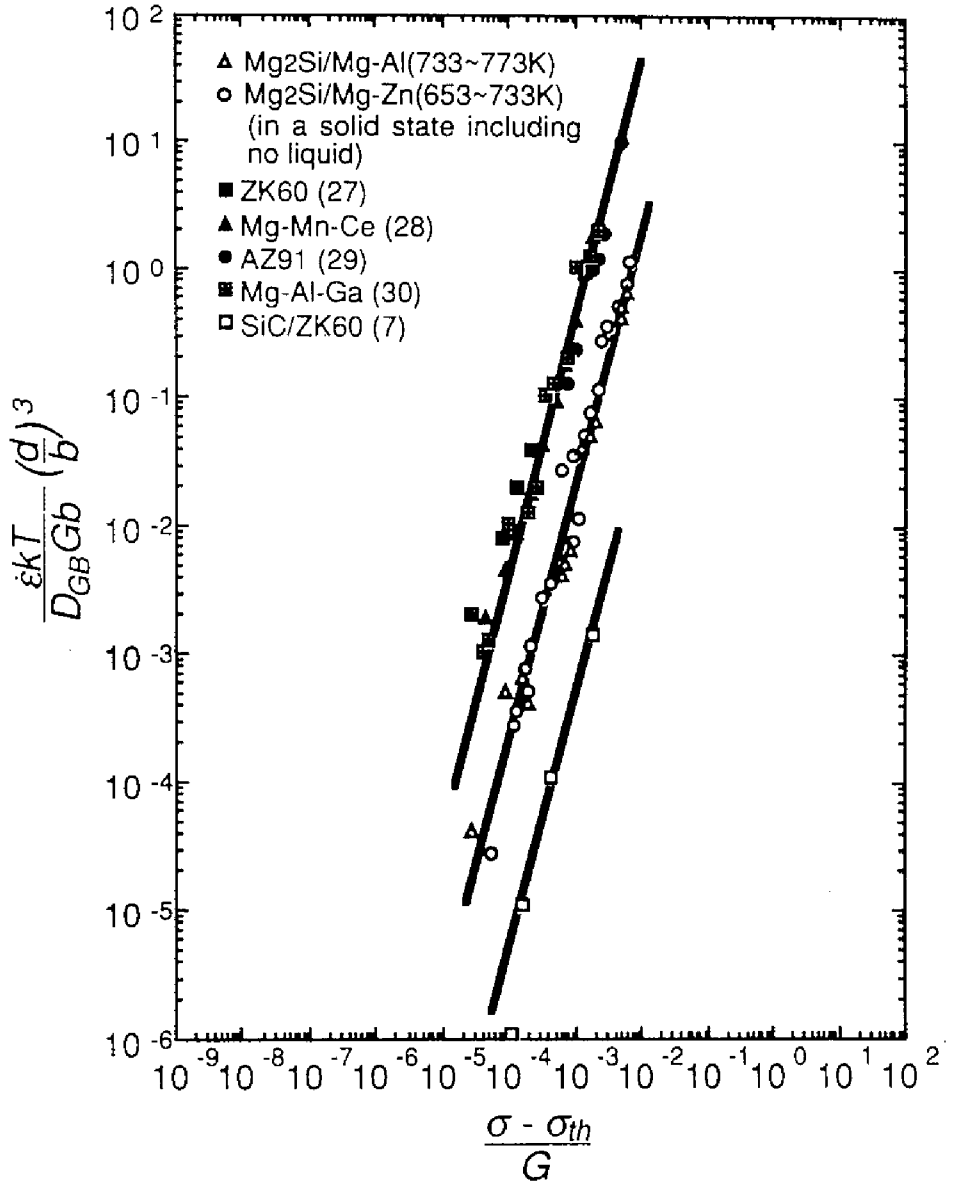

Fig. 5.7 The variation in $(\dot{\varepsilon}kT/D_{GB}Gb)(d/b)^3$ as a function of $(\sigma-\sigma_{th})/G$ for magnesium base materials, where G is taken to be the shear modulus of pure magnesium.

of mixture equation, though the estimate is not rigid. The shear modulus of the composite G_C is given by the role of mixture equation,

$$G_c = (1-V_f)G_m + V_fG_p \tag{5.6}$$

where V_f is the volume fraction of particles, G_m and G_p are the shear modulus of a matrix and a particle, respectively. The variation in diffusion- and grain size-compensated strain rate as a function of modulus- and threshold stress-compensated stress for magnesium base materials is shown in Fig. 5.8, where the shear modulus is taken to be the shear modulus by the role of mixture equation. It is found from Fig. 5.8 that the data for the composites are roughly in agreement with the data for the alloys, taking into consideration a threshold stress and an increase in the shear modulus due to a large volume fraction of particles. It is therefore suggested that the superplastic deformation mechanism in a solid state for the composites is the same as that for the alloys. The slight deviations between the composites and the alloys after taking into consideration an increase in the shear modulus may be attributed to a difference in texture since the mechanical properties of a superplastic magnesium alloy strongly depend on texture [32]. It is recognized that deformation in regions adjacent to hard particles is different from deformation of materials containing no particles [33,34]. The complicated deformation due to the presence of hard particles probably results in unusual texture for the composites.

At temperatures above the onset temperature for partial melting, the activation energy was much higher than the ones for grain boundary diffusion and for lattice diffusion for the Mg_2Si_p/Mg-Al composite. The high activation energy for superplastic flow for the magnesium matrix composite as well as for the aluminum matrix composites is because the rate is faster in a state

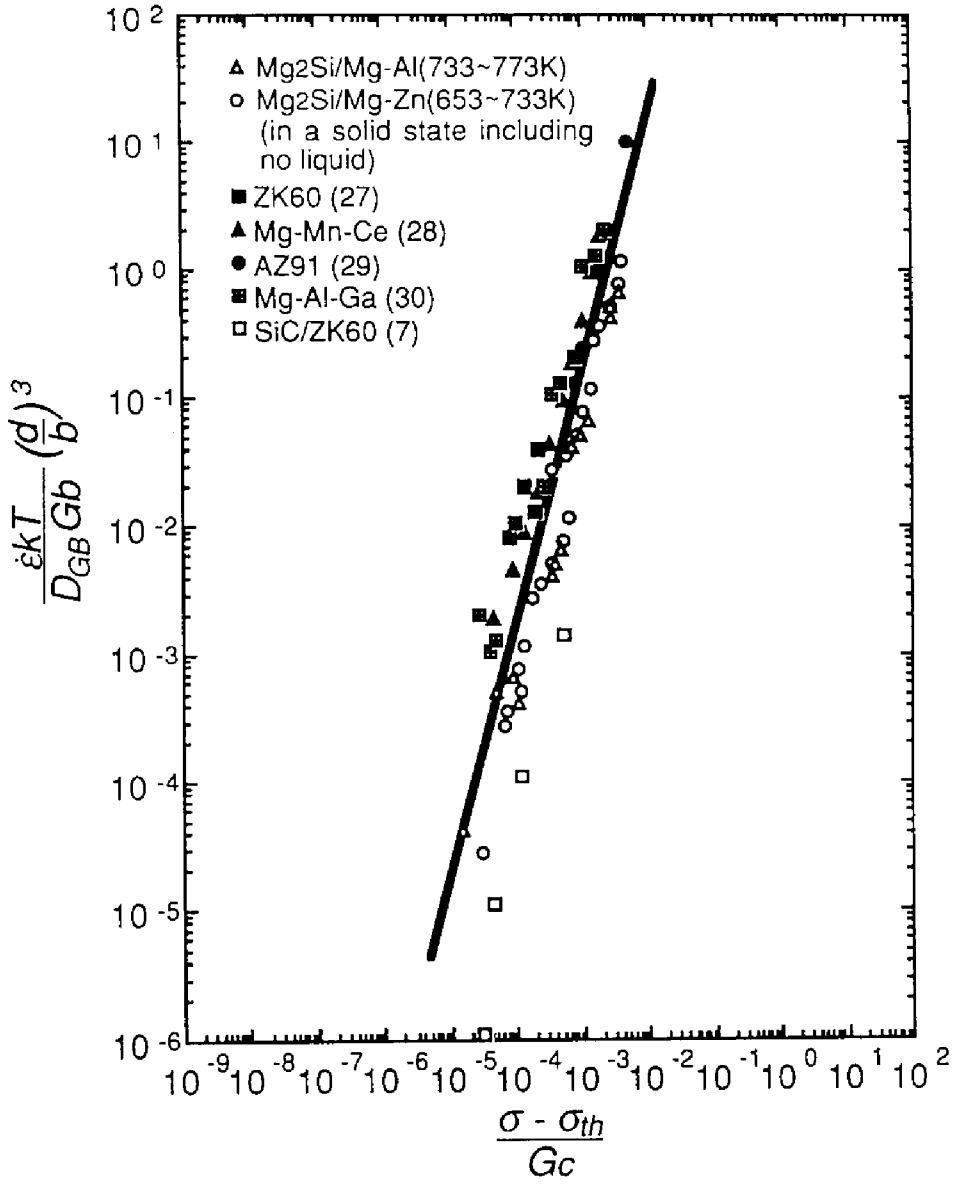

Fig. 5.8 The variation in $(\dot{\varepsilon}kT/D_{GB}Gb)(d/b)^3$ as a function of $(\sigma-\sigma_{th})/Gc$ for magnesium base materials, where $Gc=(1-Vf)Gm+VfGp$; Vf is the volume fraction of particles, Gm and Gp are the shear modulus of a matrix and a particle, respectively.

including liquid than in a state including no liquid and the activation energy is apparently increased by the presence of liquid phases [24]. It was reported in the previous papers [12,13] that the activation energy for superplastic flow in a high strain rate superplastic SiC_w/Al-Cu-Mg (2124) composite was 313 kJ/mol and that the deformation mechanism of superplasticity in aluminum matrix composites exhibiting high strain rate superplasticity was different from conventional superplasticity. However, the high value of the activation energy for the composite is probably attributed to the presence of a liquid phase because the testing temperature range was above the melting point of the composite [1]. It should be noted that the deformation characteristics of superplasticity for the composites are intrinsically the same as those for metals without reinforcements, though the deformation characteristics are drastically changed by the presence of a liquid phase.

5.4 Conclusions

(1) The Mg_2Si_p/Mg-Al composite exhibited a maximum elongation of 370 % at 788 K and at a high strain rate of 10^{-1} s^{-1}, and the Mg_2Si_p/Mg-Zn composite showed a maximum elongation of 290 % at 713 K and at a high strain rate of 10^{-1} s^{-1}. It is noted that a maximum elongation of 290 % was attained at 713 K, where no partial melting occurred, for the Mg_2Si_p/Mg-Zn composite.

(2) The superplastic flow in a solid state including no liquid is likely controlled by grain boundary diffusion. On the other hand, an apparent value of the activation energy was increased by the presence of a liquid phase.

(3) The relationship between the diffusion- and grain size-compensated strain rate and the modulus- and threshold stress-compensated stress for the magnesium matrix composites was roughly in agreement with the

relationship for magnesium alloys, taking into consideration a threshold stress and an increase in the shear modulus due to the presence of hard particles. It should be noted that the deformation characteristics of superplasticity for the composites are intrinsically the same as those for metals without reinforcements, at least in a state including no liquid phase.

References

1. T.G.Nieh, C.A.Henshall and J.Wadsworth, Scripta Metall., **18**, 1405 (1984).
2. T.G.Nieh, P.S.Gilman and J.Wadsworth, Scripta Metall., **19**, 1375 (1985).
3. K.Higashi and M.Mabuchi, in *Advanced Composites '93*, edited by T.Chandra and A.K.Dhingra, (TMS, Warrendale, PA, 1993), p. 35.
4. K.Higashi, Mater. Sci. Eng., **A166**, 109 (1993).
5. K.Higashi, Mater. Sci. Forum, **170/172**, 131 (1994).
6. M.Mabuchi, J.Koike, H.Iwasaki, K.Higashi and T.G.Langdon, Mater. Sci. Forum, **170/172**, 503 (1994).
7. T.G.Nieh and J.Wadsworth, Scripta Metall. Mater., **32**, 1133 (1995).
8. S.-W.Lim, T.Imai, Y.Nishida and T.Choh, Scripta Metall. Mater., **32**, 1713 (1995).
9. T.G.Nieh, A.J.Schwartz and J.Wadsworth, Mater. Sci. Eng., **A208**, 30 (1996).
10. J.Koike, M.Mabuchi and K.Higashi, J. Mater. Res., **10**, 133 (1995).
11. F.A.Mohamed, J. Mater. Sci., **18**, 582 (1983).
12. R.S.Mishra and A.K.Mukherjee, Scripta Metall. Mater., **25**, 271 (1991).
13. R.S.Mishra, T.R.Bieler and A.K.Mukherjee, Acta Metall. Mater., **43**, 877 (1995).
14. P.K.Chaudhury and F.A.Mohamed, Acta Metall., **36**, 1099 (1988).
15. P.K.Chaudhury, K.-T.Park and F.A.Mohamed, Metall. Trans. A, **25A**, 2391 (1994).
16. A.Ball and M.M.Hutchison, Metal. Sci. J., **3**, 1 (1969).
17. A.K.Mukherjee, Mater. Sci. Eng., **8**, 83 (1971).
18. H.W.Hayden, S.Floreen and P.D.Goodell, Metall. Trans., **3**, 833 (1972).
19. M.F.Ashby and R.A.Verrall, Acta Metall., **21**, 149 (1973).
20. R.C.Gifkins, Metall. Trans. A, **7A**, 1225 (1976).

21. J.H.Gittus, J. Eng. Mater. Tech., **99**, 244 (1977).
22. M.Mabuchi, T.Asahina, H.Iwasaki and K.Higashi, Mater. Sci. Tech., in press.
23. H.J.Frost and M.F.Ashby, in *Deformation-Mechanism Maps*, (Pergamon Press, Oxford, 1982).
24. K.Higashi, T.G.Nieh and J.Wadsworth, Acta Metall. Mater., **43**, 3275 (1995).
25. O.D.Sherby and J.Wadsworth, Prog. Mater. Sci., **33**, 169 (1989).
26. P.Metenier, G.G.Doncel, O.A.Ruano, J.Wolfenstine and O.D.Sherby, Mater. Sci. Eng., **A125**, 195 (1990).
27. A.-U.Karim and W.A.Bachofen, Metall. Trans., **3**, 709 (1972).
28. R.Z.Valiev and O.A.Kaibyshev, phys. stat. sol. (a)., **44**, 65 (1977).
29. M.Mabuchi., K.Kubota, and K.Higashi, in *Aspects of High Temperature Deformation and Fracture in Crystalline Materials*, edited by Y.Hosoi, H.Yoshinaga, H.Oikawa and K.Maruyama, (The Japan Institute of Metals, Sendai, 1993), p.279.
30. T.Shibata, A.Uoya, K.Higashi, Y.Yamaguchi, A.Inoue and K.Masumoto, in *Superplasticity: 60 Years after Pearson*, edited by N.Ridley, (The institute of Materials, London, 1995), p.113.
31. O.D.Sherby, R.H.Klundt and A.K.Miller, Metall. Trans. A, **8A**, 843 (1977).
32. O.A.Kaibyshev, I.V.Kazachkov and N.G.Zaripov, J. Mater. Sci., **23**, 4369 (1988).
33. F.J.Humphreys, Acta Metall., **27**, 1801 (1979).
34. F.J.Humphreys and M.G.Ardakani, Acta Metall. Mater., **42**, 749 (1994).

CHAPTER 6

PARTIAL MELTING AT INTERFACES AND GRAIN BOUNDARIES

6.1 Introduction

The mechanical properties of metal matrix composites are strongly affected by the nature of interfaces between a matrix and a reinforcement as well as by the chemical composition and grain size of a matrix and the morphology, volume fraction and chemistry of a reinforcement. In superplastic deformation for metal matrix composites, the interfaces appear to provide the sites for cavity formation. If excessive cavities are formed at the interfaces, superplasticity (large elongation) is not attained. The nature of the interfaces is expected to affect superplastic potential. Hence an investigation of the interfaces may give important information to make clear the deformation mechanisms of high strain rate superplasticity for the composites.

The microstructure and chemical segregation at interfaces, which are not superplastic materials, have been extensively investigated for aluminum matrix composites [1-9]. These studies revealed that phase formation and segregation occurred at the interfaces by heat treatment after hot extrusion. Suganuma *et al.* [2] showed that segregation of magnesium was severely caused and that the segregated areas were the order of micro-meter by heat treatment at 853 K for 1.8×10^4 s for the Al_2O_3/Al-Mg-Si (6061) composite. Also, a variety of precipitates such as MgO, Mg_2Si, $MgAl_2O_4$, $CuMgAl_2$, Al_3Mg_2 and $MgAl_{26}O_{40}$ were frequently observed for many aluminum matrix composites. When a molten-alloy-mixing technique was used to form a SiC/Al

alloy composite, Al_4C_3 was observed in addition of $MgAl_2O_4$. These interface precipitates are highly stable at elevated temperatures and anticipated to hamper interfacial sliding.

The deformation characteristics of high strain rate superplasticity for the aluminum matrix composites and the magnesium matrix composites were strongly changed by the presence of a liquid phase, as shown in Chapters 4 & 5. The presence of a liquid phase in the superplastic composites probably results from partial melting occurring at elevated temperatures. In the present chapter, partial melting at the interfaces and grain boundaries is evidenced by *in situ* TEM observations and DSC measurements, in addition, the origins of partial melting are discussed.

6.2 Experimental procedure

The composites used in the present chapter are the same as the ones in Chapter 4. *In situ* TEM observation was carried out for the $Si_3N_{4p(0.2\mu m)}$/Al-Mg (5052) composite. Disc specimens for TEM were cut by a low speed diamond saw from the as-extruded bar. They were mechanically ground to ~ 20 μm in thickness, and ion-milled to perforation with 3 keV argon ions. During ion milling, specimens were cooled with a liquid nitrogen stage to minimize irradiation damages. A perforated specimen was then loaded on a single tilt heating stage for TEM examination. The microstructure was studied at 821 K by *in situ* TEM. The specimen was then slowly cooled in the TEM to room temperature and was removed from the specimen stage. In order to remove surface contamination, formed during *in situ* observation, the specimen was ion-milled with a liquid nitrogen holder for 1.8×10^3 s.

The segregation behavior was subsequently investigated by an electron energy loss spectrometer (EELS) attached to the TEM for microchemical analysis. An electron-beam diameter of ~ 2 nm was obtained by using a field

emission source. The actual beam size was expected to be slightly larger, particularly on the exit surface of the specimen because of scattering of electrons during interaction with the specimen. In order to minimize the multiple scattering effects on inner-shell peaks, a very thin part of the specimen was analyzed by EELS. This also ensured that no other phases were overlapped in the analyzed area. Data acquisition time for each EELS spectrum was 10 s. During acquisition, both the specimen and the electron beam remained at the same position. It was considered that the chemical concentration was not altered noticeably before and after a heating-and-cooling cycle. This was supported by the experiment in a different specimen which showed a similar partial melting behavior at the same temperature during the first and second heating runs that were performed 24 h apart. Therefore, EELS analysis performed at room temperature could be utilized to discuss the effects of chemical composition on the microstructure observed at 821 K.

DSC experiments were carried out for Al-Mg-Si (6061) alloy matrix composites. The powder, the as-extruded matrix alloy, the as-sintered composite and the as-extruded composite were investigated. The samples for DSC were 10 ~ 25 mg in weight. All the DSC runs started at room temperature, ended at about 873 K and were made with a constant heating rate of 10 K/min. The thermal analyzer was connected to a computer with a suitable interface, and the data from each run were continuously stored.

6.3 Results and discussion

6.3.1 *In situ* TEM investigation

Specimen temperature was increased stepwise by controlling an applied voltage of a heater, and the microstructural change was observed *in situ* by TEM. With increasing temperature from 816 to 821 K, a drastic change was

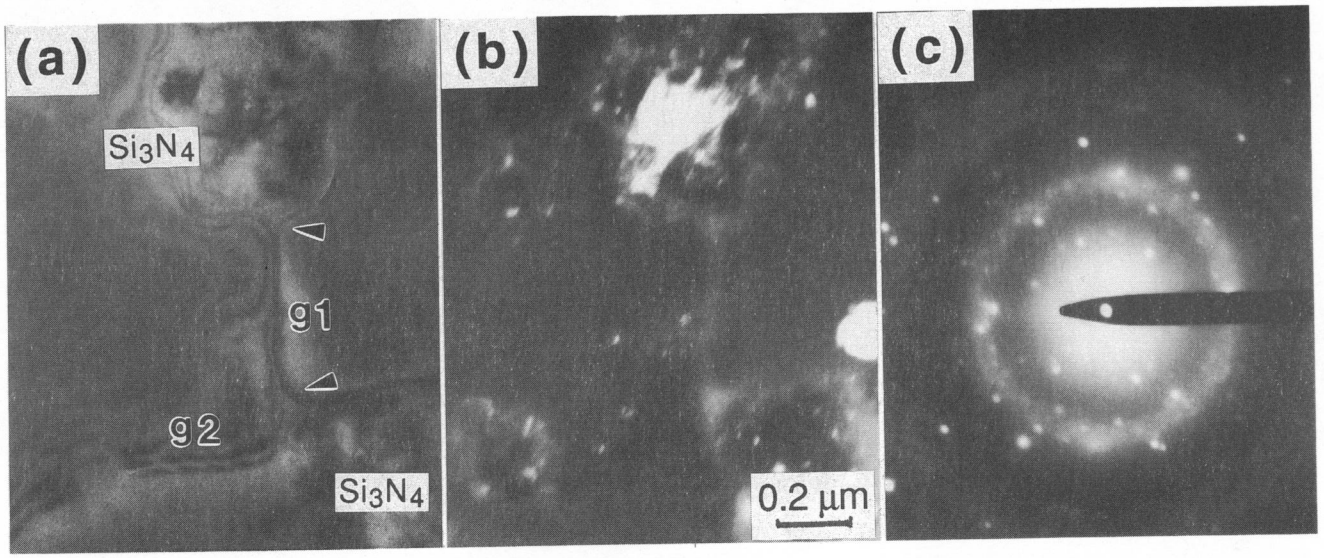

Fig. 6.1 *In situ* TEM investigation at 821 K for the Si3N4*p*(0.2μm)/Al-Mg composite, (a) bright field image, (b) dark field image and (c) selected area diffraction pattern.

observed in the microstructure as shown in Fig. 6.1. In the bright-field image in (a) taken at 821 K, rounded corners of the matrix grains (marked by arrows) appear, indicating the presence of a liquid phase. The diffraction pattern in (c) shows the diffuse ring intensity, superposed with a crystalline spot pattern. The diffuse ring pattern is indicative of the formation of a liquid phase. As soon as the temperature is lowered, the diffuse ring pattern is found to disappear, but the polycrystalline ring remains unchanged. Since no additional phase formation is observed, the polycrystalline ring can be attributed to a thin contamination layer on the surface, formed during *in situ* observation at 821 K. When the specimen is reheated to 821 K, partial melting is observed again, indicating that surface contamination layer does not affect the partial melting temperature. It should be noted that the onset temperature for partial melting by *in situ* TEM observation was almost the same as the ones determined by DSC measurements [10].

Partial melting occurred not only at the interfaces, but also at grain boundaries. It is emphasized that the tendency of melting appears to depend on the nature of grain boundaries, *i.e.*, the type of grain boundary structure characterized by the misorientation between neighboring grains. In the bright-field image, two types of grain boundaries are observed and marked as g1 and g2. In the dark-field image, only the g1 grain boundary has a bright contrast, indicating melting. Quantitatively, the misorientation angle, determined from Kikuchi diffraction pattern, is 18° for the g1 boundary and is 3° for the g3 boundary. The results suggest that the tendency of melting along grain boundaries depends on the misorientation angle between adjacent grains.

6.3.2 DSC investigation

The DSC experimental data to 873 K are shown in Fig. 6.2 for the Al-Mg-Si (6061) powder, the as-extruded Al-Mg-Si matrix alloy and the as-extruded Al-Mg-Si alloy matrix composites. A flat area was found in both $Si_3N_{4p(0.2\mu m)}$/Al-Mg-Si and $Si_3N_{4p(0.5\mu m)}$/Al-Mg-Si composites, and then a sharp endothermic peak and finally a continuous endothermic curve appeared. For the $Si_3N_{4p(1\mu m)}$/Al-Mg-Si composite, a weak endothermic peak was found, followed by a flat area, and then a sharp endothermic peak was found and finally a continuous endothermic curve appeared. For the Si_3N_{4w}/Al-Mg-Si composite, a weak exothermic peak was found, then followed by a relatively flat area, and finally a continuous endothermic curve appeared.

The sharp endothermic peaks, which were found for the Si_3N_{4p}/Al-Mg-Si composites, are attributed to partial melting. This is evidenced by *in situ* TEM observation [10]. The onset temperature for partial melting of each material is listed in Table 6.1, where the onset temperature for partial melting is determined from an intercept of two dotted lines indicated in Fig. 6.2. The melting points of the powder and the matrix alloy are 855 K, which is the same as the published data of the Al-Mg-Si alloy (6061) [11]. It is found from Table 6.1 that the melting point of the Si_3N_{4w}/Al-Mg-Si composite as well as the Si_3N_{4p}/Al-Mg-Si composites was lower than 855 K. This suggests that partial melting occurred in the Si_3N_{4w}/Al-Mg-Si composite as well as the Si_3N_{4p}/Al-Mg-Si composites. DSC investigations were conducted on all the Si_3N_4/Al alloy composites used in Chapter 4. The results showed that evidence for partial melting was found for all the aluminum alloy matrix composites exhibiting high strain rate superplasticity.

Partial melting is likely attributed to segregation of solute atoms, as shown later. As shown in Table 6.1, the onset temperature for partial melting of the $Si_3N_{4p(1\mu m)}$/Al-Mg-Si composite was different from those of the $Si_3N_{4p(0.2\mu m)}$/Al-Mg-Si and $Si_3N_{4p(0.5\mu m)}$/Al-Mg-Si composites, in spite of

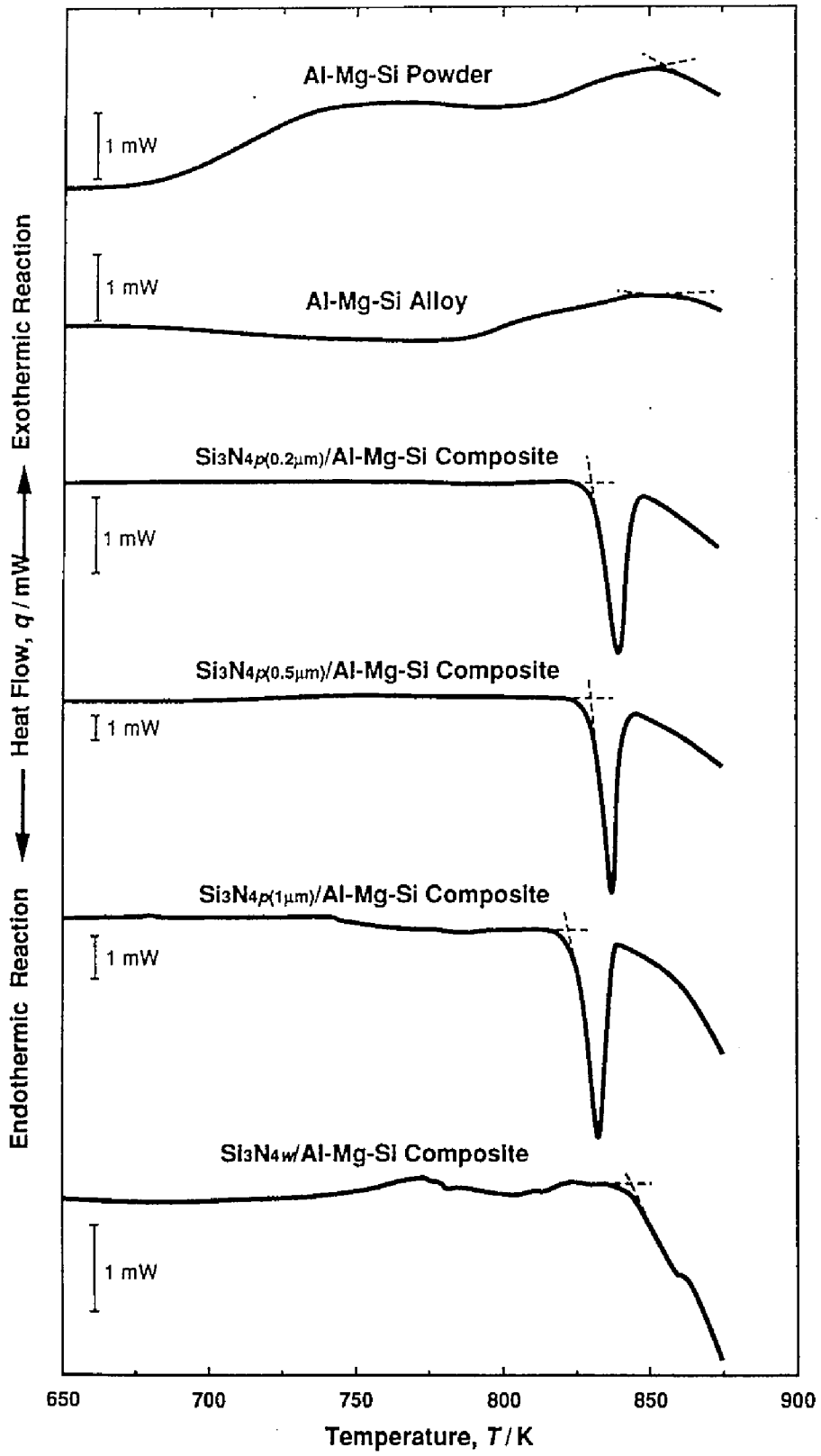

Fig. 6.2 DSC experimental data to 873 K for the Al-Mg-Si matrix alloy and the Al-Mg-Si matrix composites.

Table 6.1 The onset temperature for partial melting obtained from DSC measurements shown in Fig. 6.2.

Al-Mg-Si Powder	855 K
Al-Mg-Si Alloy	855 K
$Si_3N_{4p(0.2\mu m)}$/Al-Mg-Si Composite	830 K
$Si_3N_{4p(0.5\mu m)}$/Al-Mg-Si Composite	829 K
$Si_3N_{4p(1\mu m)}$/Al-Mg-Si Composite	822 K
Si_3N_{4w}/Al-Mg-Si Composite	843 K

the same chemical composition of the matrix alloy. This is probably because of the difference in concentration of solute segregation.

6.3.3 Segregation

Concentrations of segregants at the interfaces and grain boundaries were measured by EELS for the $Si_3N_{4p(0.2\mu m)}$/Al-Mg composite. The result is listed in Table 6.2. The solute concentration measured in the present work may be lower than the true concentration at the interfaces and grain boundaries because of the possibility of the electron beam diameter being larger than the width of the segregation profile. It is found from Table 6.2 that the interfaces are segregated with magnesium and grain boundaries are segregated with silicon. One may argue that the presence of oxygen and nitrogen can consume segregating magnesium and silicon by forming various ceramic compounds as well as intermetallic compounds [1-9]. However, these compounds are all very stable and do not melt in the temperature range where the experimental was conducted. Therefore a substantial amount magnesium and silicon probably remain isolated without forming the compounds.

Segregation was found at most interfaces (6 segregated interfaces out of 7 investigated), on the other hand, segregation was observed at only two of the seven grain boundaries investigated (1 strongly segregated and 1 weakly segregated). Thus, the tendency of melting depended on grain boundaries. This can be understood by the grain-boundary dependent segregation, characterized by the misorientation angle between neighboring grains. Watanabe and co-workers [12,13] have systematically studied the extent of segregation as a function of misorientation angle in Fe(Si) and Fe(Sn). They found that the extent of segregation increased with increasing the tilting angle except for low energy special boundaries. These observations support the view of partial melting that is caused by segregation whose extent depends on

Table 6.2 Concentration of segregation in at. % at the interface and grain boundary in the superplastic Si3N4*p*(0.2μm)/Al-Mg composite.

	Mg	Si	N	O
Interface	9.3	a	a	3.2
Grain Boundary	b	2.5	1.0	3.9

[a]Strong peaks from a Si3N4 particle are detected.
[b]The peak is not detected in all seven grain boundaries.

the grain boundary structure. On the other hand, the tendency of melting appears to be independent of the interface types. This may be associated with a strong chemical interaction of magnesium atoms with Si_3N_4 reinforcements.

Strangwood *et al.* [3] showed that segregation was found for various aluminum alloy matrix composites reinforced with SiC, indicating that segregation was caused for SiC/Al composites as well as for Si_3N_4/Al composites. L'Esperance *et al.* [5] and Nieh and Wadsworth [14] proposed that the solute segregation can lower the melting point of segregated layers. According to the binary phase diagrams [15] of Al-Mg and Al-Si, magnesium addition to pure aluminum up to 18.6 at.% lowers the melting point by 11 K per 1 at.% Mg. Beyond 18.6 at.%, the alloy melts at 723 K. Similarly, silicon addition to pure aluminum up to 1.5 at.% lowers the melting point by 56 K per 1 at.% Si. Beyond 1.5 at.%, the alloy melts at 850 K. Therefore, if the interfaces are segregated with more than 18.6 at.% of magnesium, the interfaces can melt at a eutectic temperature of 723 K.

DSC was carried out on the extruded $Si_3N_{4p(0.2\mu m)}$/Al-Mg-Si composite and the sintered $Si_3N_{4p(0.2\mu m)}$/Al-Mg-Si composite, where the sintered $Si_3N_{4p(0.2\mu m)}$/Al-Mg-Si composite [16] is processed by hot pressing (at 873 K) of mixed powder of the aluminum power and the Si_3N_4 particulates. The results are shown in Fig. 6.3. It should be noted that the extruded composite showed the lower onset temperature for partial melting than the sintered composite, indicating that the concentration of segregation is increased by hot extrusion. Because the extruded matrix alloy showed no evidence of partial melting, as shown in Fig. 6.2, the origin of segregation is probably related to the presence of the reinforcements. Dislocations tend to be attracted to incoherent second phase particles at elevated temperatures [17,18]. Hence segregation may be attributed to core diffusion enhanced by dislocations in contact with the reinforcements during hot extrusion. Another possibility of

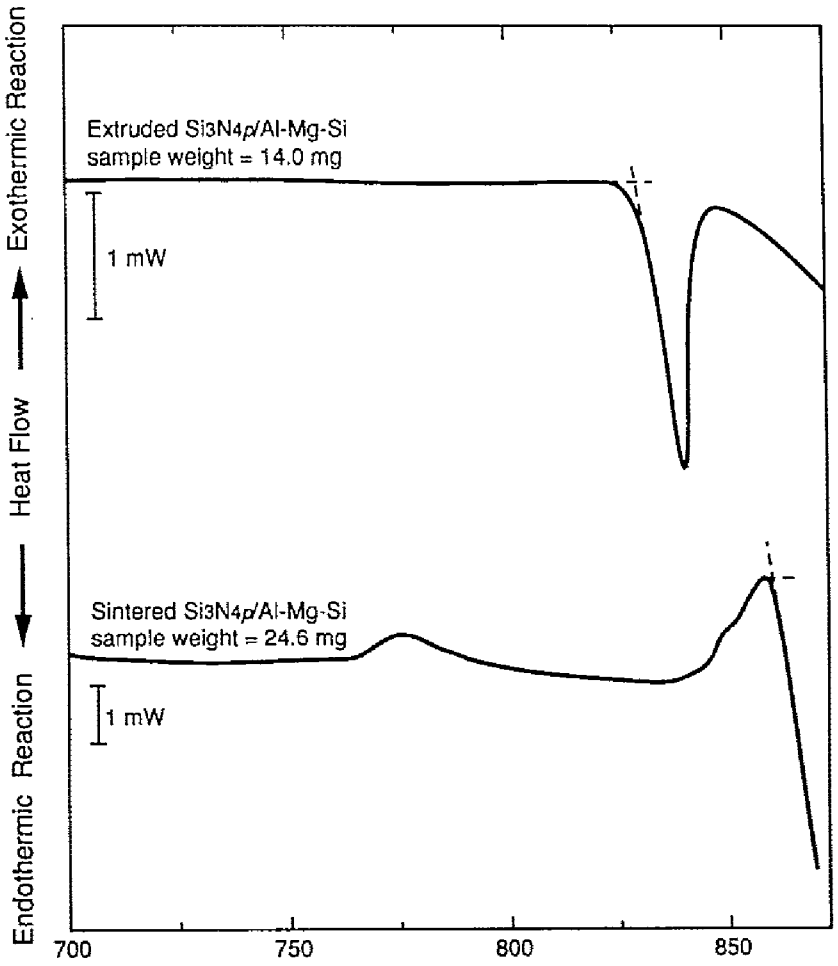

Fig. 6.3 DSC runs from 700 to 873 K for the extruded $Si_3N_{4p(0.2\mu m)}$/Al-Mg-Si and the sintered $Si_3N_{4p(0.2\mu m)}$/Al-Mg-Si.

segregation is the strong chemical interaction of Si_3N_4 with solute atoms such as magnesium. It is reported that there are oxides on the surface of ceramic particles [19,20]. The oxides also may affect segregation behavior.

6.4 Conclusions

(1) *In situ* TEM observation and DSC measurements revealed that partial melting occurred at the interfaces and grain boundaries at elevated temperatures for the high strain rate superplastic Si_3N_4/Al alloy composites.

(2) The tendency of melting depended on grain boundaries, however, was independent of the interfaces.

(3) The partial melting is likely attributed to segregation of solute atoms such as magnesium and silicon.

References

1. S.R.Nutt and R.W.Carpenter, Mater. Sci. Eng., **75**, 169 (1985).
2. K.Suganuma, T.Okamoto, T.Hayami, Y.Oku and N.Suzuki, J. Mater. Sci., **23,** 1317 (1988).
3. M.Strangwood, C.A.Hippsley and J.J.Lewandowski, Scripta Metall. Mater., **24**, 1483, (1990).
4. H.Ribes, M.Suery, G.L'Eseprance and J.G.Legoux, Metall. Trans. A, **21A**, 2489 (1990).
5. G.L'Eseprance, T.Imai and B.Hong, in *Superplasticity in Advanced Materials*, edited by S.Hori, M.Tokizane and N.Furushiro, (Japan Soc. for Res. on Superplasticity, 1991), p. 379.
6. X.G.Ning, J.Pan, K.Y.Hu and H.Q.Ye, Philos. Mag., **66**, 811 (1992).
7. N.Wang, Z.Wang and G.C.Weatherly, Metall. Trans. A, **23A**, 2489 (1992).
8. A.Bardal, Mater. Sci. Eng., **A159**, 119 (1992).
9. P.K.Rohatgi, S.Ray, R.Asthana and C.S.Narendranath, Mater. Sci. Eng., **A161**, 163 (1993).
10. J.Koike, M.Mabuchi and K.Higashi, Acta Metall. Mater., **43**, 199 (1995).
11. *Aluminum Handbook 4th Edition*, (Japan Inst. of Light Metals, Tokyo, 1990), p. 25.
12. T.Watanabe, S.Kitamura and S.Karashima, Acta Metall., **28**, 455 (1980).
13. T.Watanabe, T.Murakami and S.Karashima, Scripta Metall., **12**, 361 (1978).
14. T.G.Nieh and J.Wadsworth, JOM, 11, **46** (1992).
15. *Binary Alloy Phase Diagrams 2nd Edition*, edited by T.B.Massalski, (ASM International, Materials Park, Ohio, 1992).
16. M.Mabuchi and K.Higashi, J. Mater. Res., **10**, 2494 (1995).
17. D.J.Srolovitz, M.J.Luton, R.Petkovic-Luton, D.M.Barnett and W.D.Nix, Acta Metall., **32**, 1079 (1984).

18. V.C.Nardone, D.E.Matejczyk and J.K.Tien, Acta Metall., **32**, 1509 (1984).

19. M.N.Rahaman, Y.Boiteux and L.C.D.Jonghe, Am. Ceram. Soc. Bull., **65**, 1171 (1986).

20. S.M.Pickard, B.Derby and E.A.Feest, J. Mater. Sci., **26**, 6207 (1991).

CHAPTER 7

DEFORMATION MECHANISMS OF HIGH STRAIN RATE SUPERPLASTICITY

7.1 Introduction

It has been demonstrated in Chapters 4 & 5 that the aluminum matrix composites and the magnesium matrix composites exhibit superplastic behavior at high strain rates > 10^{-2} s^{-1}. Higashi [1] noted that the origin of high strain rate superplasticity is associated with ultra-fine grain sizes for metals. However, high strain rate superplasticity is not necessarily attained only by ultra-fine grain sizes for metal matrix composites because excessive cavitation is considered to be caused due to high stress concentrations around reinforcements intersected by grain boundaries during the sliding process. In particular, it appears to be difficult to accommodate the sliding process at high strain rates by the diffusion processes including diffusion-controlled dislocation movement because of too short times.

In Chapter 6, the presence of a small amount of liquid at the matrix/reinforcement interfaces and grain boundaries at elevated temperature was evidenced by DSC measurements and *in-situ* TEM observation for the high strain rate superplastic aluminum matrix composites. The liquid phase may be associated with the deformation mechanisms of high strain rate superplasticity for the composites. In the present chapter, the origins of high strain rate superplasticity are investigated from the viewpoint of the grain size dependence and a role of a liquid phase. In addition, the critical strain rate, below which the accommodation mechanism for superplastic flow is

diffusional flow and/or dislocation movement in a solid state, on the other hand, above which a special accommodation process by an accommodation helper such as a liquid phase is required, is developed, and the theoretical view is compared with the experimental results. Finally, the optimum conditions for the accommodation process by a liquid phase are discussed.

7.2 Analysis and discussion

7.2.1 Grain size dependence

Overview of superplastic behavior for aluminum matrix composites and magnesium matrix composites as a function of strain rate is shown in Fig. 7.1. It should be noted that many composites showed superplastic behavior at high strain rates > 10^{-2} s^{-1}.

The superplastic strain rate range strongly depends on the grain size [7]. The relationship between the superplastic strain rate and the grain size may be expressed by

$$\dot{\varepsilon}_{sp} \propto d^{-p} \tag{7.1}$$

where $\dot{\varepsilon}_{sp}$ is the superplastic strain rate, d is the grain size and p is a constant. The variation in superplastic strain rate as a function of the inverse of grain size is shown in Fig. 7.2 for aluminum matrix composites, where the optimum superplastic strain rate represents to the strain rate where a maximum elongation is obtained. Clearly, high strain rate superplasticity results from very small grain sizes.

There are some studies on superplasticity for magnesium alloys [10-17], however, fewer reports of superplastic magnesium matrix composites [6,18], compared to aluminum matrix composites. Recently, it was reported that a

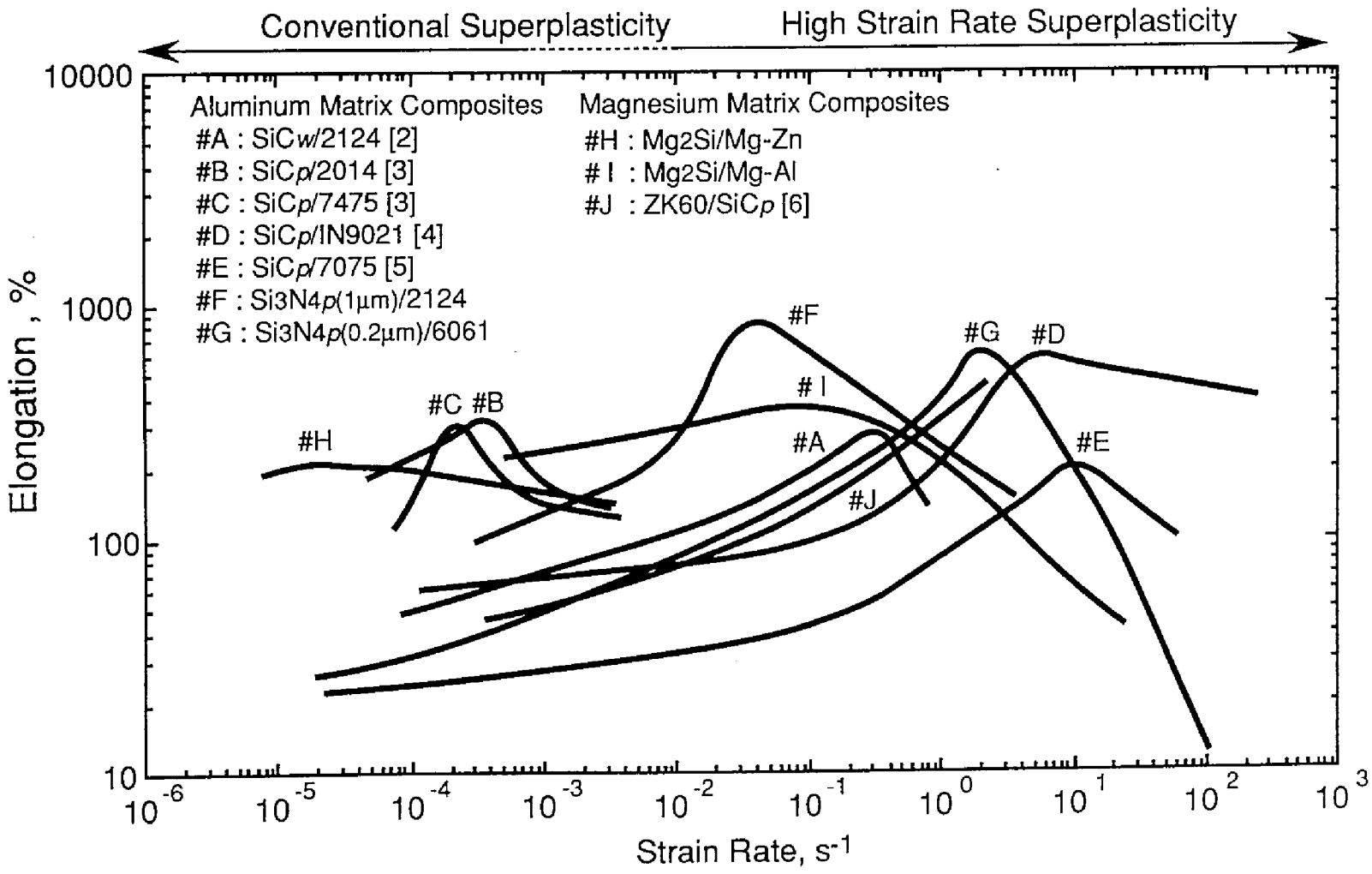

Fig. 7.1 Overview of the relationship between elongation and strain rate in metal matrix composites

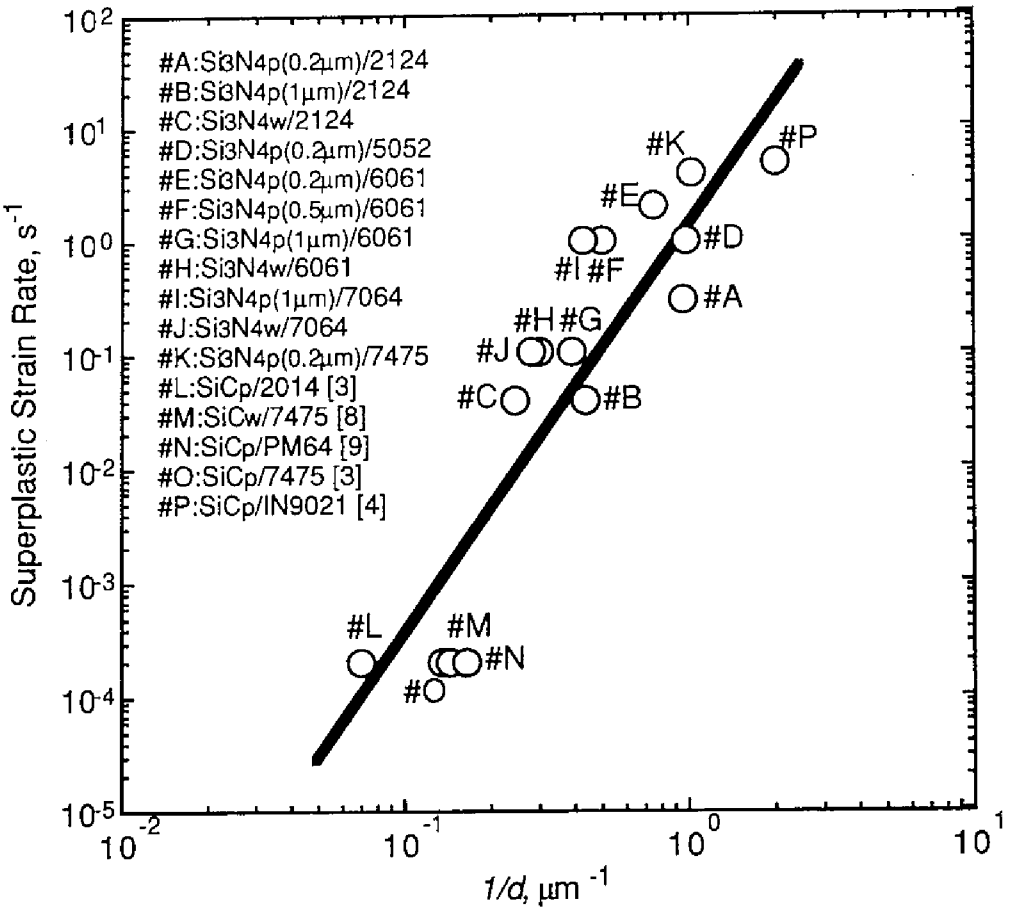

Fig. 7.2 The variation in superplastic strain rate as a function of the inverse of grain size for aluminum matrix composites, where the superplastic strain rate is the one where a maximum elongation is attained.

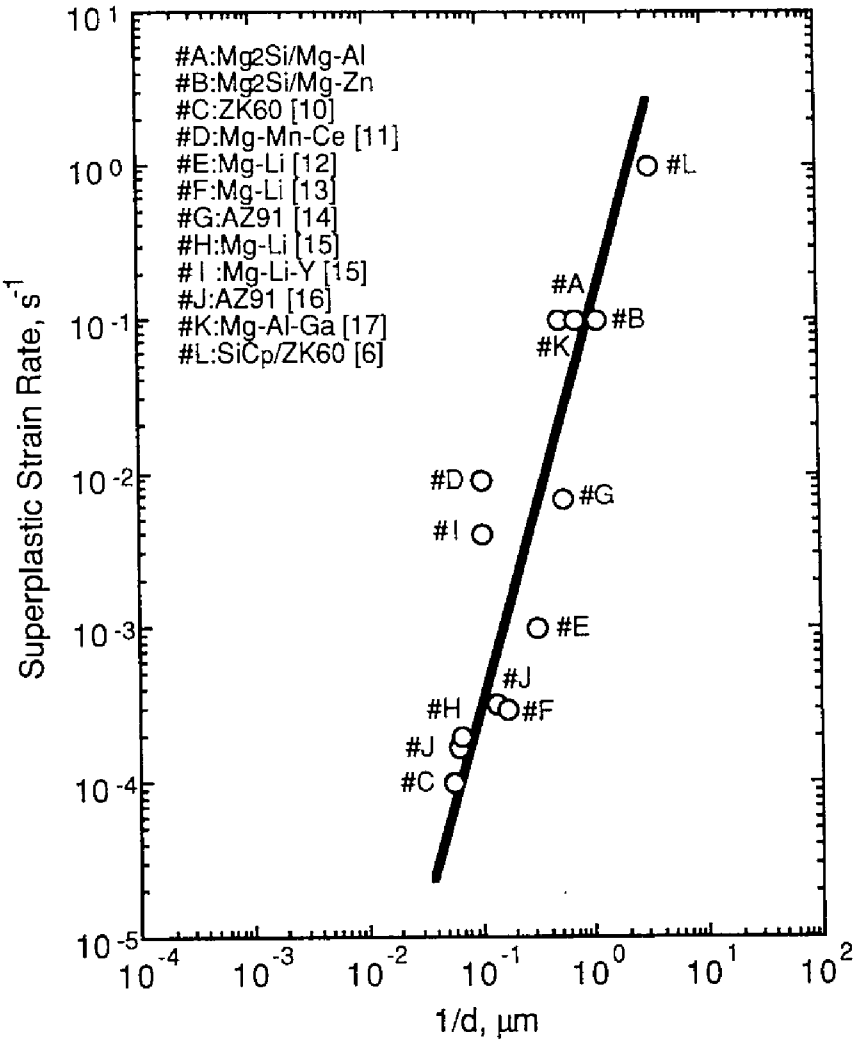

Fig. 7.3 The variation in the superplastic strain rate as a function of the inverse of grain size for magnesium based materials.

few of magnesium based materials [6,17,18] showed superplastic behavior at high strain rates above 10^{-2} s^{-1}. The variation in superplastic strain rate as a function of the inverse of grain size for magnesium based materials is shown in Fig. 7.3 for magnesium based materials. It is clear that an increase in the superplastic strain rate is attributed to a decrease in the grain size for magnesium based materials as well as for aluminum based materials. It appears from Figs 7.2 & 7.3 that $p = 2 \sim 3$. It is concluded that a very small grain size (≤ approximately 4 μm) is required to attain superplasticity at high strain rates above 10^{-2} s^{-1}.

7.2.2 Accommodation helper mechanisms

7.2.2.1 Stress concentrations

It is recognized that grain boundary sliding is the dominant deformation process of superplasticity [19-22]. For the composites as well, the sliding process is the dominant deformation process of superplasticity. Evidence for grain boundary sliding in the $Si_3N_{4p(1\mu m)}$/Al-Cu-Mg composite [23] is shown in Fig. 7.4. The sample is deformed to 100 % at 788 K and at a strain rate of 4×10^{-2} s^{-1}, where the high strain rate sensitivity (> 0.3) is attained. Stress concentrations are expected to be caused around the reinforcements during the sliding process for the composites. Therefore it is required not only to attain a very small grain size, but also to accommodate the sliding process, that is, to relax the stress concentrations in order to attain superplasticity for metal matrix composites because the stress concentrations cause excessive cavity formation, resulting in premature fracture.

Assuming that the sliding displacements are too large to be accommodated elastically and the sliding is accommodated by diffusional or plastic flow, Raj and Ashby [24] developed the equation of the sliding rate. The sliding rate at a

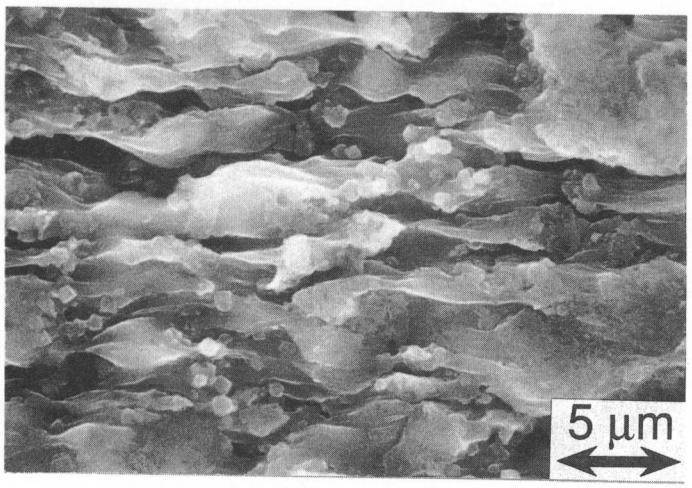

Fig. 7.4 Evidence for grain boundary sliding in the Si3N4*p*(1µm)/Al-Cu-Mg (2124) composite deformed to 100 % at 788 K at 4 x 10^{-2} s^{-1}.

plane boundary containing an array of discrete impermeable particles is given by

$$\dot{\bar{U}} = 1.6\frac{\tau_i \Omega}{kT}\frac{\lambda^2}{{d_p}^3} D_L\left(1+5\frac{\delta D_{GB}}{aD_L}\right) \tag{7.2}$$

where $\dot{\bar{U}}$ is the sliding rate, τ_i is the local shear stress, Ω is the atomic volume, k is the Boltzmann's constant, T is the absolute temperature, λ is the particle spacing, d_p is the reinforcement size, D_L is the lattice diffusion coefficient, δ is the grain boundary thickness and D_{GB} is the grain boundary diffusion coefficient. By substituting $\dot{\bar{U}} = \dot{\varepsilon} d$ [25] into the equation of the sliding rate, the local shear stress around the matrix/reinforcement interfaces is given by

$$\tau_i = \frac{kT{d_p}^3 \dot{\varepsilon} d}{1.6\Omega\lambda^2 D_L\left(1+5\frac{\delta D_{GB}}{aD_L}\right)} \tag{7.3}$$

where $\dot{\varepsilon}$ is the strain rate. It follows from this equation that the local stress increases significantly with increasing particle size. It is therefore expected that clustering of reinforcements gives rise to high stress concentrations. Hence, uniform dispersion of reinforcements is important to reduce the stress concentrations. The relationship between the local tensile stress ($= \sqrt{3}\tau_i$) and the strain rate can be given by Eq. 7.3. The relationship between the local tensile stress and the strain rate at the particle sizes of 0.01, 0.1, 1, 2 and 10 μm for aluminum based materials is shown in Fig. 7.5, where T = 818 K, Ω = $1.66\text{x}10^{-29}$ m^3, λ = 1.7 μm, d = 3 μm, D_L = $1.45\text{x}10^{-13}$ m^2s^{-1}, δD_{GB} = $2.16\text{x}10^{-19}$ m^2s^{-1}. The experimental flow stresses at the optimum superplastic temperature for the Si_3N_4/Al alloy composites are superimposed in the figure,

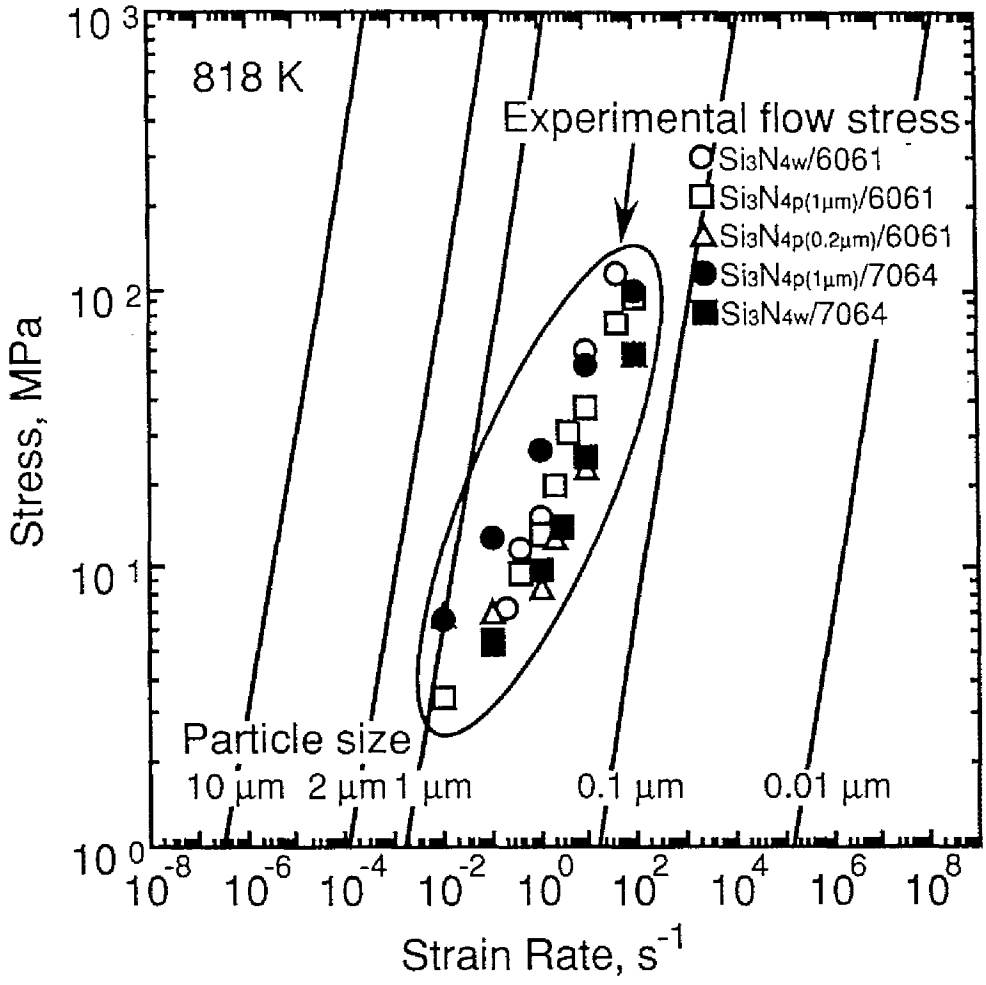

Fig. 7.5 The relationship between the local stress and the strain rate at the particle sizes of 0.01, 0.1, 1, 2 and 10 μm for aluminum based materials, where the experimental flow stresses at 818 K of the Si_3N_4/Al alloy composites are superimposed.

where the optimum superplastic temperature is the temperature where a maximum elongation is attained. The effective reinforcement size of the whisker for the Si_3N_{4w}/Al alloy composites is about 2 μm. Clearly, very high stress concentrations are caused at the interfaces for the composites when the sliding is accommodated only by diffusional or plastic flow. The local tensile stress predicted from Eq. 7.3 and the experimental flow stresses are listed in Table 7.1 for the Si_3N_{4p}/Al alloy composites and the Mg_2Si_p/Mg-Zn composite, where the experimental flow stress is taken to be the flow stress at the testing condition where a maximum elongation is attained. The fact that the experimental flow stress is lower than or almost the same as the local stress for each Si_3N_4/Al alloy composite, except the $Si_3N_{4p(0.2\mu m)}$/Al-Cu-Mg, indicates that the stress concentrations around the reinforcements are relaxed by special accommodation processes for the Si_3N_{4p}/Al alloy composites except the $Si_3N_{4p(0.2\mu m)}$/Al-Cu-Mg. It is of interest to note that the local stress is much lower than the experimental flow stress for the Mg_2Si_p/Mg-Zn composite, indicating that the stress concentrations caused around the reinforcements are sufficiently relaxed by diffusional processes in a solid state for the Mg_2Si_p/Mg-Zn composite.

7.2.2.2 Role of a liquid phase

Stress concentration is expected to be caused around matrix/reinforcement interfaces during superplastic flow for the aluminum matrix composites, as shown above. The cavity nucleation rate increases rapidly with increasing stress [25]. It is therefore suggested that high concentrations in local stress by interfacial sliding cause excessive cavity nucleation at the interfaces easily, so that premature fracture occurs. Therefore special mechanisms should be required for the accommodation process of relaxation in the stress

Table 7.1 The experimental flow stress and the predicted local tensile stress around reinforcements for the aluminum matrix composites and the magnesium matrix composite.

Materials	Experimental flow stress/MPa	Predicted local stress/MPa
Si3N4*p*(1μm)/Al-Cu-Mg	2	10
Si3N4*p*(0.2μm)/A-Cu-Mg	8	3
Si3N4*p*(0.2μm)/Al-Mg	6	5
Si3N4*p*(1μm)/Al-Mg-Si	5	31
Si3N4*p*(0.5μm)/Al-Mg-Si	6	42
Si3N4*p*(0.2μm)/Al-Mg-Si	5	10
Si3N4*p*(1μm)/Al-Zn-Mg	10	225
Mg2Si*p*/Mg-Zn	10	0.1

concentrations at interfaces resulting from the interfacial sliding to limit cavity formation and attain large superplastic elongations.

The variation in elongation to failure as a function of testing temperature is shown in Fig. 7.6 for the high strain rate superplastic Si_3N_4/Al alloy composites, where the strain rate for each composite is the optimum strain rate where a maximum elongation is attained. The onset temperature for partial melting of each composite is shown by an arrow, where the onset temperature for partial melting is determined by DSC measurements. It should be noted that the elongation to failure strongly depended on the testing temperature, and a maximum elongation was attained at the temperature very close to the onset temperature for partial melting.

The optimum superplastic temperature *vs* the onset temperature for partial melting is plotted in Fig. 7.7 for the high strain rate superplastic aluminum matrix composites. It is noted that the optimum superplastic temperature is close to the onset temperature for partial melting, though the optimum superplastic temperature for the $Si_3N_{4p(0.2\mu m)}$/Al-Cu-Mg composite is lower than the onset temperature for partial melting. Therefore it is suggested that a liquid phase due to partial melting plays a vital role in high strain rate superplastic deformation for the composites, except the $Si_3N_{4p(0.2\mu m)}$/Al-Cu-Mg.

Here, I propose a new concept of the accommodation mechanism by a liquid phase for superplastic deformation. The new concept is that a liquid phase relaxes the high stress concentrations caused around the reinforcements during superplastic flow and promotes interfacial sliding occurring without excessive cavity formation at the interfaces, namely, a liquid phase plays an important role as accommodation helpers [1]. Schematic illustrations of (a) cavity formation due to high stress concentrations at the interfaces and (b) relaxation of the stress concentrations by a liquid phase are shown in Fig. 7.8.

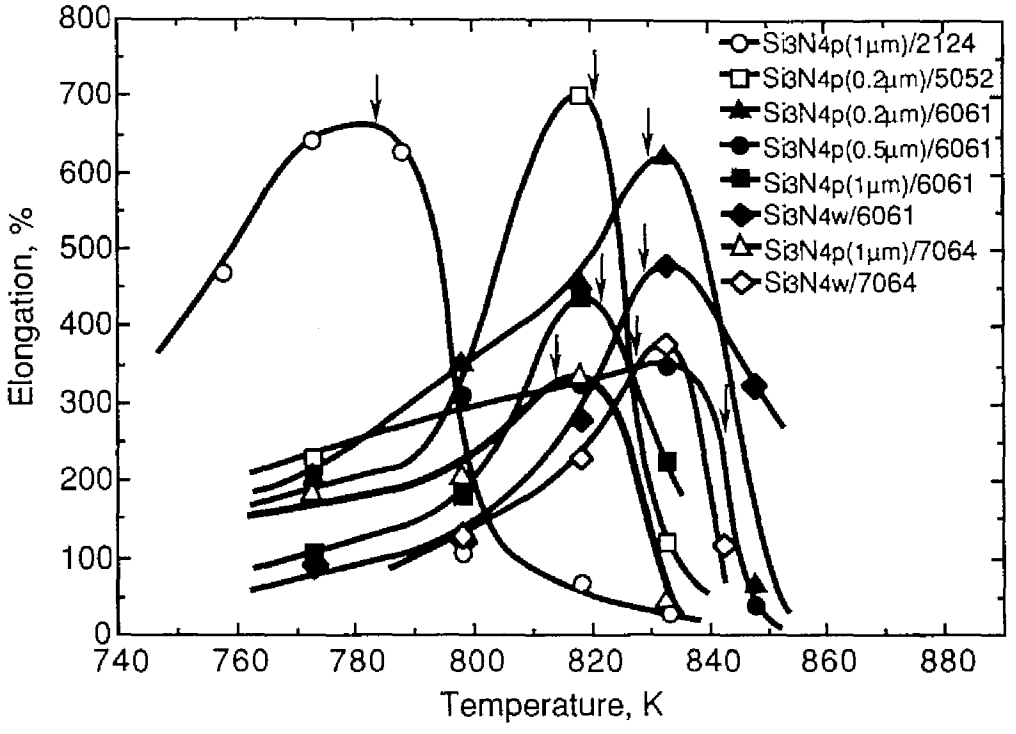

Fig. 7.6 The variation in elongation to failure as a function of testing temperature at the optimum superplastic strain rate for the Si3N4/Al alloy composites, where the onset temperature for partial melting of each composite is shown by an arrow.

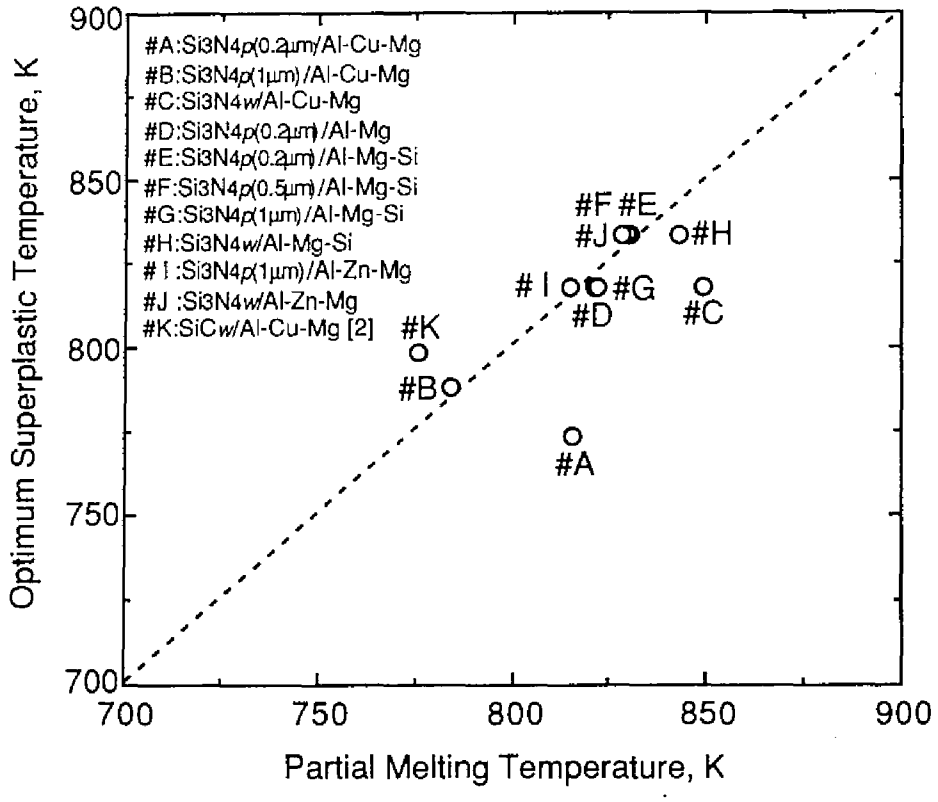

Fig. 7.7 The optimum superplastic temperature versus the partial melting temperature for the high strain rate superplastic aluminum matrix composites, where the partial melting temperature is the onset temperature for partial melting determined by DSC.

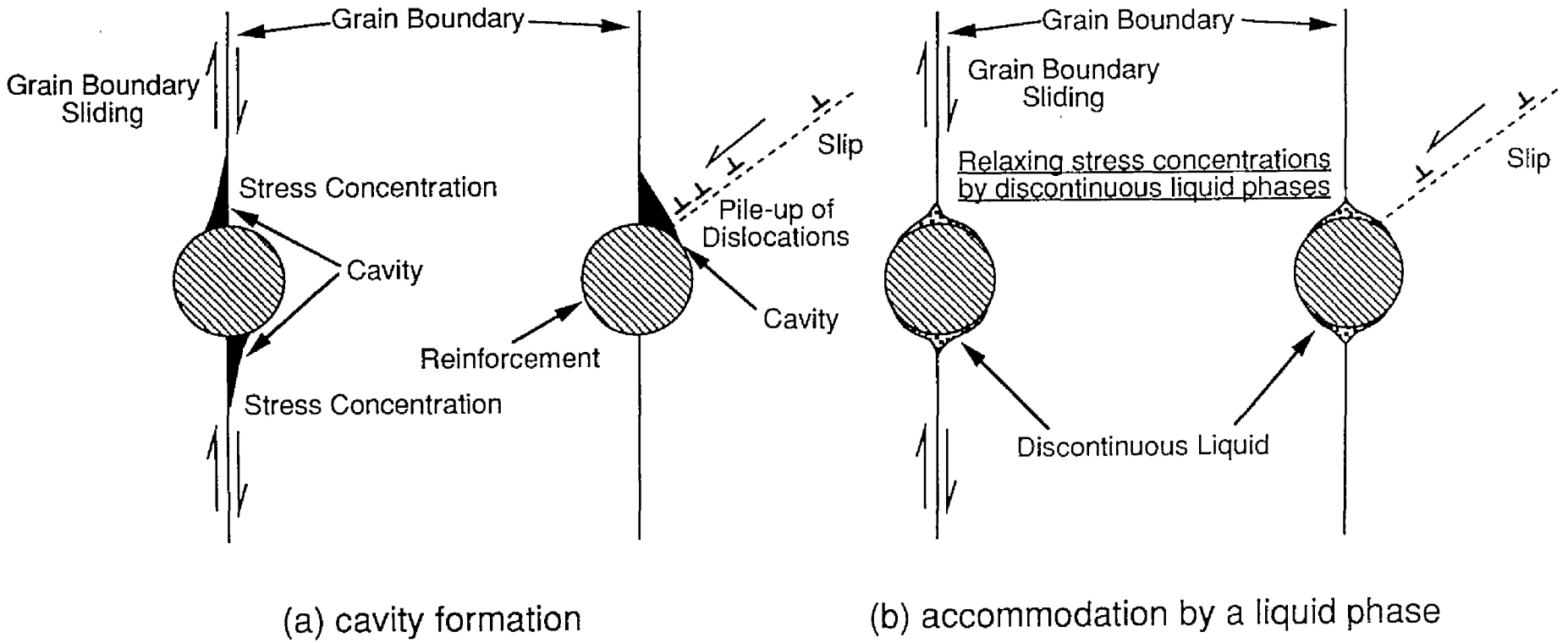

Fig. 7.8 Schematic illustrations of (a) cavity formation due to high stress concentrations at the interfaces and (b) relaxation of the stress concentrations by a liquid phase.

The stress concentrations are relaxed by a liquid phase and cavity formation is limited, and consequently large elongations are attained. If no partial melting is caused and the stress concentrations are not relaxed, excessive cavitation occurs and superplasticity is not attained.

I would like to note that a liquid phase is one of accommodation helpers and the presence of a liquid phase is not needed if the stress concentrations are sufficiently relaxed by diffusional processes in a solid state. As shown in Chapter 5, the Mg_2Si_p/Mg-Zn composite showed superplastic behavior at the testing condition where no partial melting occurred. Also, the optimum superplastic temperature for the $Si_3N_{4p(0.2\mu m)}$/Al-Cu-Mg composite was lower than the onset temperature for partial melting. For these composites, the stress concentrations caused around the reinforcements are sufficiently relaxed by diffusional processes in a solid state, as shown above, and therefore superplasticity can be attained without special accommodation helpers such as a liquid phase. In such a case, the optimum temperature, where a maximum elongation is attained, is often below the melting point because higher testing temperatures cause grain growth.

7.2.2.3 Critical strain rate

A. Critical strain rate

Assuming that the sliding displacements are too large to be accommodated elastically and the sliding is accommodated by diffusional flow in a solid state, the local shear stress around reinforcements caused by sliding can be given by Eq. 7.3. The space between reinforcements can be given by [26]

$$\lambda = \frac{d_p}{2}\sqrt{\frac{3\pi}{2V_f}} \tag{7.4}$$

where V_f is the volume fraction of the reinforcements. Hence the local shear stress is given in the form

$$\tau_i = \frac{0.92kTd_p\dot{\varepsilon}dV_f}{\Omega D_L\left(1+5\frac{\delta D_{GB}}{d_p D_L}\right)} \quad . \tag{7.5}$$

One can explore approximate conditions for stress concentrations occurring around reinforcements or not, using the local tensile stress around reinforcements σ_i ($= \sqrt{3}\tau_i$) and the steady-state stress for metals containing no liquid phase. Sherby and Wadsworth [7] showed a phenomenological relation of the mechanical properties for superplastic metals in the following two forms

$$\dot{\varepsilon} = 10^8\left(\frac{\sigma}{E}\right)^2\left(\frac{bD_{GB}}{d^3}\right) \tag{7.6-a}$$

(for grain boundary diffusion-controlled superplastic flow)

$$\dot{\varepsilon} = 2\times10^9\left(\frac{\sigma}{E}\right)^2\left(\frac{D_L}{d^2}\right) \tag{7.6-b}$$

(for lattice diffusion-controlled superplastic flow)

where σ is the stress and E is the Young's modulus. When $\sigma_i = A\sigma$ using Eqs 7.5 and 7.6, where A is a constant, the critical strain rate $\dot{\varepsilon}_c$, below which the stress concentrations around reinforcements are sufficiently relaxed and highly improbable, can be defined in the forms

$$\dot{\varepsilon}_c = 1.18\times10^{-8}A^2\left(\frac{\Omega E}{kT}\right)^2\left(\frac{d}{b}\right)\left(\frac{1+5\delta a/d_p}{d_p}\right)^2\left(\frac{1}{V_f}\right)^2\frac{D_{GB}}{a^2} \tag{7.7-a}$$

(for grain boundary diffusion-controlled superplastic flow)

$$\dot{\varepsilon}_c = 5.92\times10^{-10} A^2 \left(\frac{\Omega E}{kT}\right)^2 \left(\frac{1+5\delta a/d_p}{d_p}\right)^2 \left(\frac{1}{V_f}\right)^2 D_L \qquad (7.7\text{-b})$$

(for lattice diffusion-controlled superplastic flow)

where a is the ratio of the diffusion coefficient ($= D_{GB}/D_L$). Accommodation mechanisms for superplastic flow in metal matrix composites can be approximately estimated using the critical strain rate: the accommodation mechanism is diffusional flow and/or diffusion-controlled dislocation movement in a strain rate range below the critical strain rate, on the other hand, a special accommodation process by an accommodation helper such as a liquid phase is required in a strain rate range above the critical strain rate because stress concentrations are caused around reinforcements. An estimate of the accommodation mechanisms using the critical strain rate is not a rigid estimate since the surface energy [25], the morphology of reinforcements [27] and the presence of threshold stress [28] are not taken into consideration, however, some trends of the accommodation mechanisms can be approximately examined.

B. Effect of particle size of reinforcements

It is found from Eqs 7.7-a&b that the critical strain rate depends on the reinforcement size parameter $= [(1+5\delta a/d_p)/d_p]^2$. The variation in $(\dot{\varepsilon}_c a^2/D_{GB})(kT/\Omega E)^2(b/d)$ as a function of the particle size d_p for grain boundary diffusion-controlled superplastic flow is shown in the top figure of Fig. 7.9 and the variation in $(\dot{\varepsilon}_c/D_L)(kT/\Omega E)^2$ as a function of the particle size d_p for lattice diffusion-controlled superplastic flow is shown in the bottom figure of Fig. 7.9, where A and δa are taken to be 1 and 10^{-5} m, respectively. It is found that the critical strain rate strongly depends on the particle size for

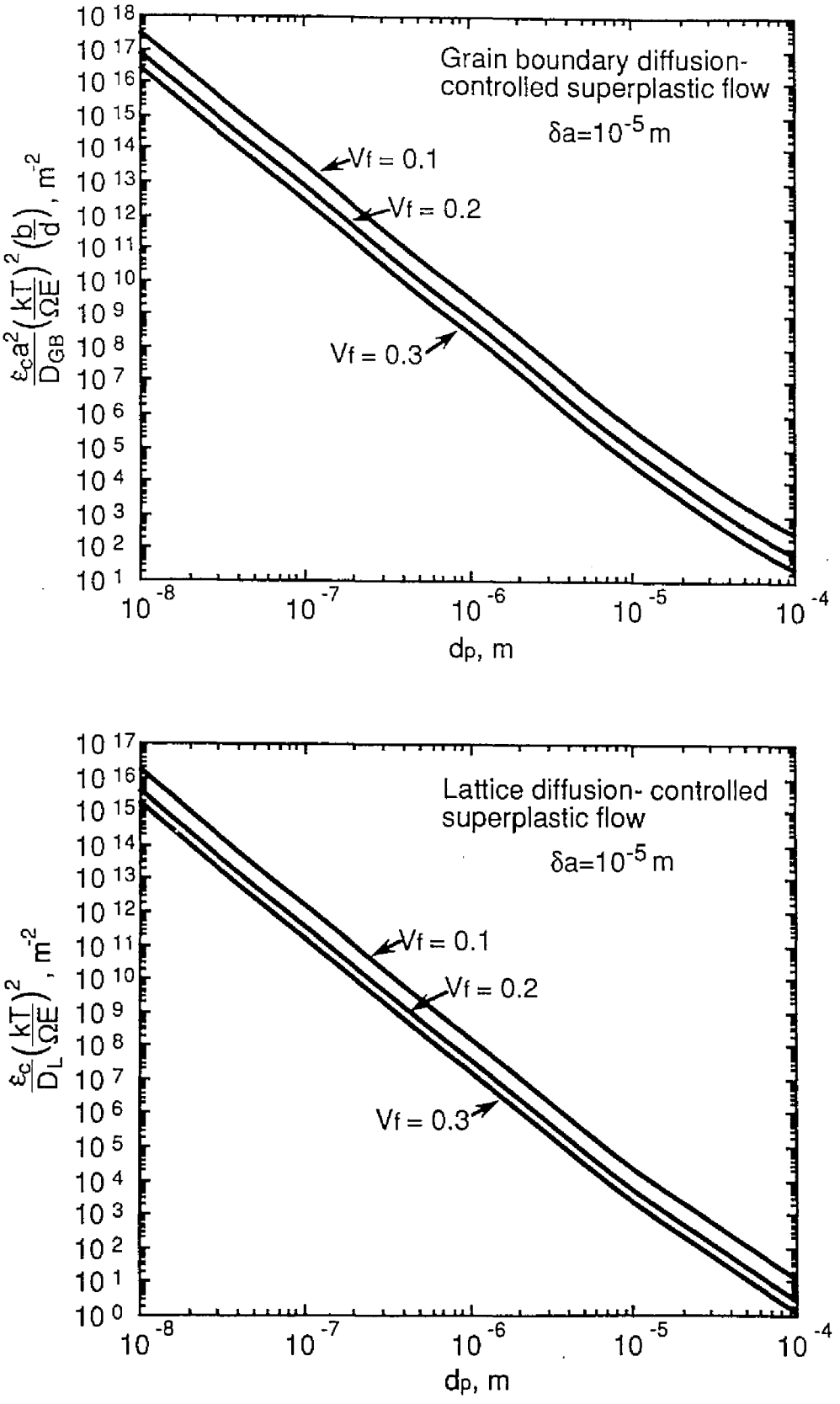

Fig. 7.9 The variation in the critical strain rate as a function of the particle size for grain boundary diffusion-controlled superplastic flow (top figure) and lattice diffusion-controlled superplastic flow (bottom figure).

both the dominant diffusion processes. It is therefore suggested that it is important to use small size reinforcements in order to limit cavity formation caused by the stress concentrations around reinforcements.

C. Effect of volume fraction of reinforcements

The variation in $(\dot{\varepsilon}_c a^2/D_{GB})(kT/\Omega E)^2(b/d)$ as a function of the volume fraction of reinforcements V_f for grain boundary diffusion-controlled superplastic flow is shown in the top figure of Fig. 7.10 and the variation in $(\dot{\varepsilon}_c/D_L)(kT/\Omega E)^2$ as a function of the volume fraction of the reinforcements V_f for lattice diffusion-controlled superplastic flow is shown in the bottom figure of Fig. 7.10, where A and δa are taken to be 1 and 10^{-5} m, respectively. The critical strain rate depends on $(1/V_f)^2$. The volume fractions of the reinforcements are typically 0.1 ~ 0.3 for metal matrix composites. The critical strain rate at $V_f = 0.3$ is approximately one order of magnitude lower than the critical strain rate at $V_f = 0.1$.

D. Effect of grain size of a matrix material

It is found from Eqs 7.7-a&b that there is the grain size dependence of the critical strain rate for grain boundary diffusion-controlled superplastic flow, however, there is no grain size dependence for lattice diffusion-controlled superplastic flow.

7.2.2.4 Accommodation mechanism map

One can develop accommodation mechanism maps for superplastic flow using the critical strain rate concept, where the accommodation mechanism is diffusional flow and/or diffusion-controlled dislocation movement in a solid state in a strain rate range below the critical strain rate, on the other hand, a special accommodation process by an accommodation helper such as a liquid

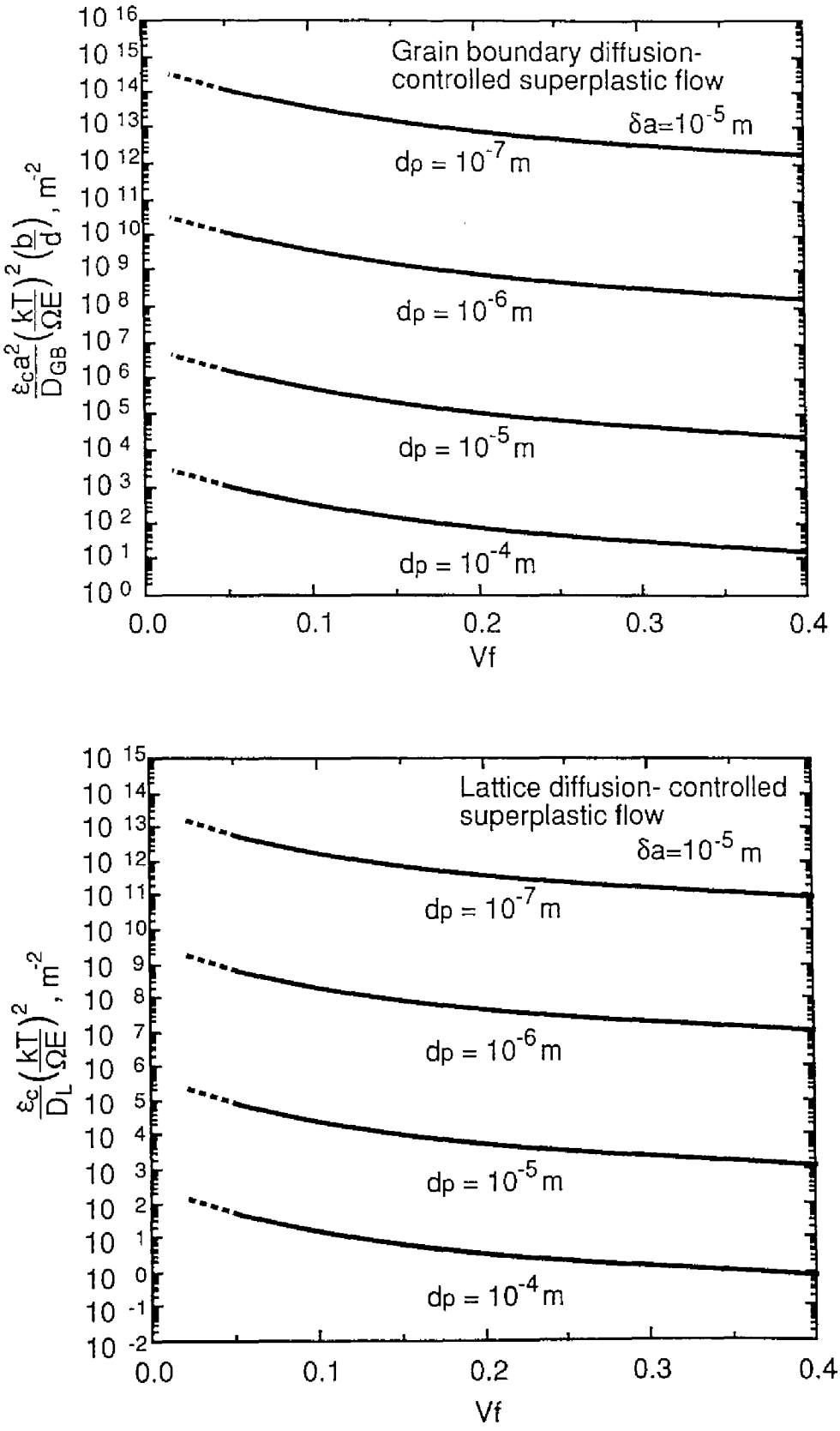

Fig. 7.10 The variation in the critical strain rate as a function of the volume fraction of reinforcements for grain boundary diffusion-controlled superplastic flow (top figure) and lattice diffusion-controlled superplastic flow (bottom figure).

phase is required in a strain rate range above the critical strain rate. Accommodation mechanism maps for aluminum matrix composites and magnesium matrix composites are shown in Fig. 7.11, where effect of the particle size is shown. In the figures, T_m is taken to be the absolute melting point of pure aluminum and pure magnesium, respectively. A value of A in Eqs 7.7-a&b is taken to be 1. These figures indicate that superplasticity can be attained at high strain rates (≥ about 10^{-1} s^{-1}) without special accommodation processes for magnesium matrix composites, independent of the dominant diffusion processes, when d_p and V_f are respectively 1 μm and 20 %, however, special accommodation processes are required in order to attain superplasticity at high strain rates above 10^{-1} s^{-1} in the same testing conditions for aluminum matrix composites.

Other accommodation mechanism maps for aluminum matrix composites and magnesium matrix composites are shown in Fig. 7.12, where effect of the volume fraction of the reinforcements is shown. It is suggested that aluminum matrix composites reinforced with volume fractions ≥ 10 % hardly exhibit superplasticity at high strain rates above 10^{-1} s^{-1} in a solid state when the particle size is 1 μm, however, magnesium matrix composites reinforced with volume fractions of about 20 % can show superplasticity at high strain rates above 10^{-1} s^{-1} in a solid state above $0.6T_m$. It is suggested from these accommodation mechanism maps that a special accommodation mechanism by an accommodation helper such as a liquid phase plays an important role in high strain rate superplasticity for aluminum matrix composites, compared to magnesium matrix composites.

7.2.2.5 Comparison between theoretical analyses and experimental results

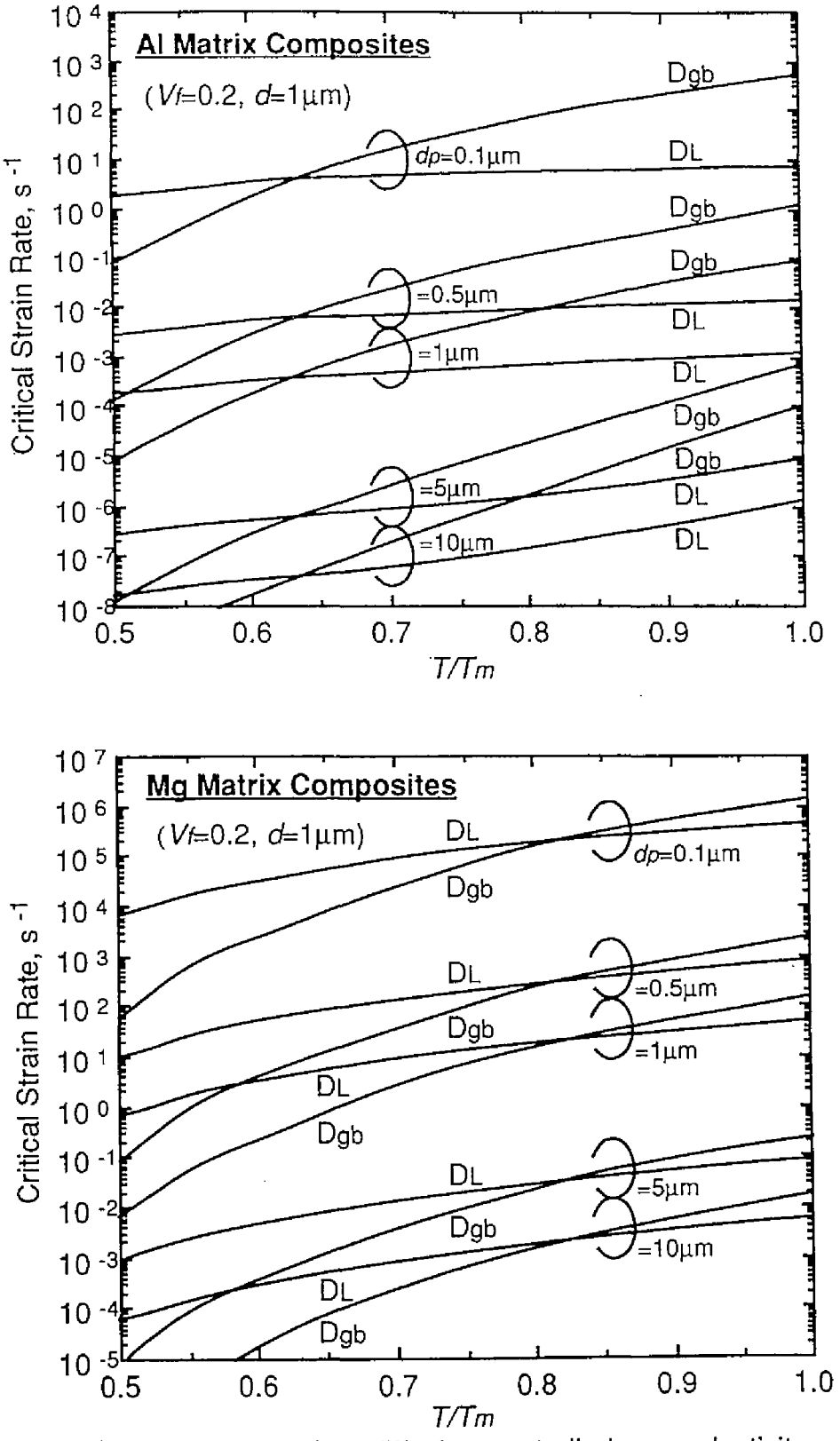

Dgb : grain boundary diffusion-controlled superplasticity
DL : lattice diffusion-controlled superplasticity

Fig. 7.11 Accommodation mechanism maps for aluminum matrix composites and magnesium matrix composites, where effect of the particle size is shown.

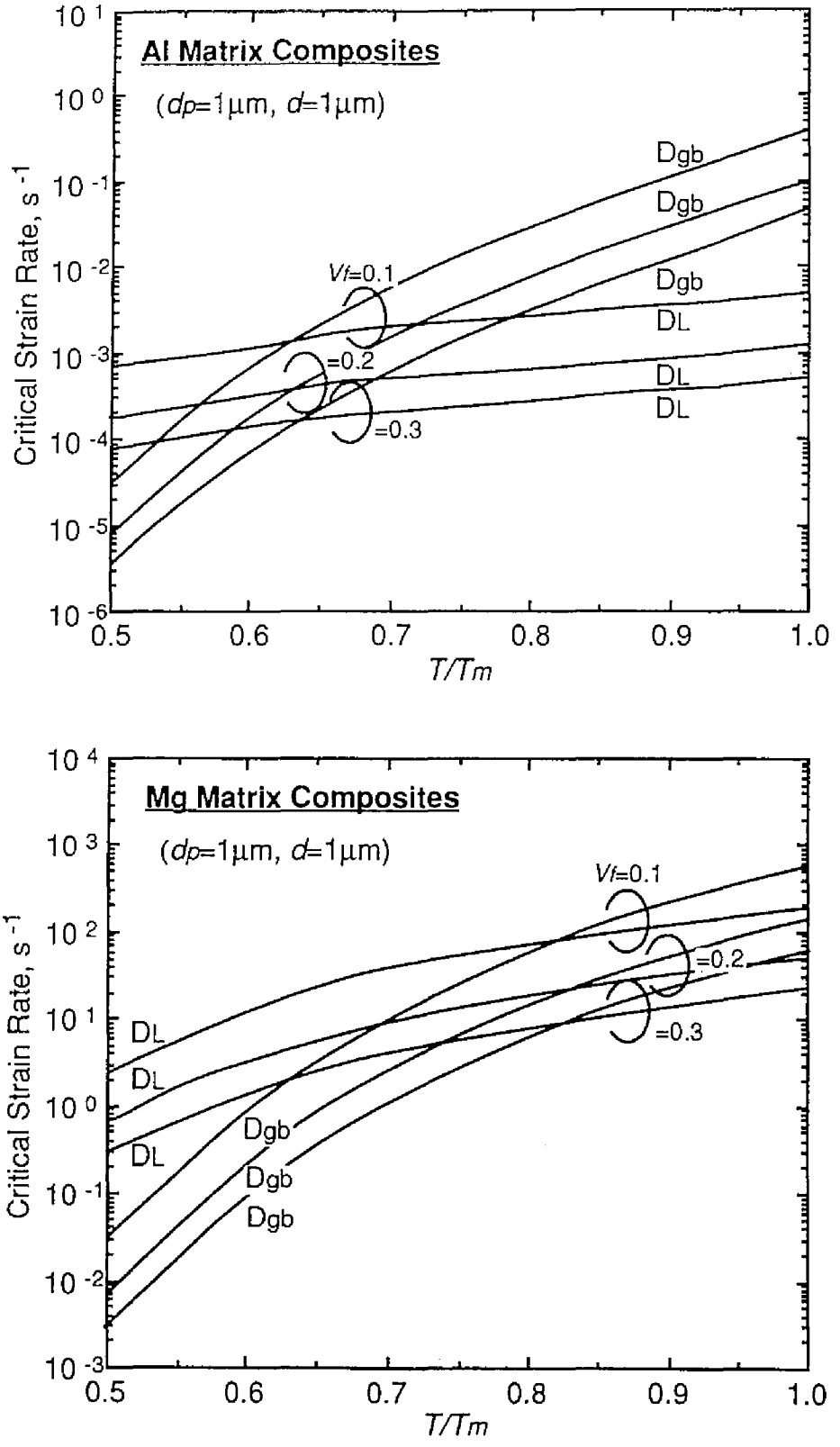

Dgb : grain boundary diffusion-controlled superplasticity
DL : lattice diffusion-controlled superplasticity

Fig. 7.12 Accommodation mechanism maps for aluminum matrix composites and magnesium matrix composites, where effect of the volume fraction of reinforcements is shown.

The experimental results are summarized as follows: (1) All the Si_3N_4/Al alloy composites, except the $Si_3N_{4p(0.2\mu m)}$/Al-Cu-Mg composite, exhibited a maximum elongation at the temperature close to the onset temperature for partial melting and (2) the Mg_2Si_p/Mg-Zn composite showed a maximum elongation at the testing condition where no partial melting occurred. In the present section, the accommodation mechanism maps are compared with the experimental results.

As shown in Chapter 4, the Si_3N_4/Al alloy composites showed the same values of the activation energy, the stress exponent and the grain size exponent, in a solid state including no liquid, as lattice diffusion-controlled superplastic flow as represented by Eq 7.6-b, and the Mg_2Si_p/Mg-Zn composite showed the same values of the activation energy, the stress exponent and the grain size exponent as grain boundary diffusion-controlled superplastic flow as represented by Eq 7.6-a. Hence it is reasonable to use Eq 7.6-b for the Si_3N_4/Al alloy composites and Eq 7.6-a for the Mg_2Si_p/Mg-Zn composite.

The experimental results are superimposed in the accommodation mechanism maps in Fig. 7.13 for the Si_3N_{4p}/Al alloy composites and in Fig. 7.14 for the Mg_2Si_p/Mg-Zn composite, respectively. The experimental data correspond to the optimum testing condition where a maximum elongation is attained. Inspection of Fig. 7.13 reveals that the strain rates obtained experimentally for the Si_3N_{4p}/Al alloy composites are always above the critical strain rates in the deformation condition, except the $Si_3N_{4p(0.2\mu m)}$/Al-Cu-Mg composite, indicating that a special accommodation process by an accommodation helper such as a liquid phase is required for the Si_3N_{4p}/Al alloy composite, except the $Si_3N_{4p(0.2\mu m)}$/Al-Cu-Mg composite. In fact, all the composites except the $Si_3N_{4p(0.2\mu m)}$/Al-Cu-Mg composite exhibited large elongations at the temperatures close to the onset temperature for partial melting, however, only the $Si_3N_{4p(0.2\mu m)}$/Al-Cu-Mg composite

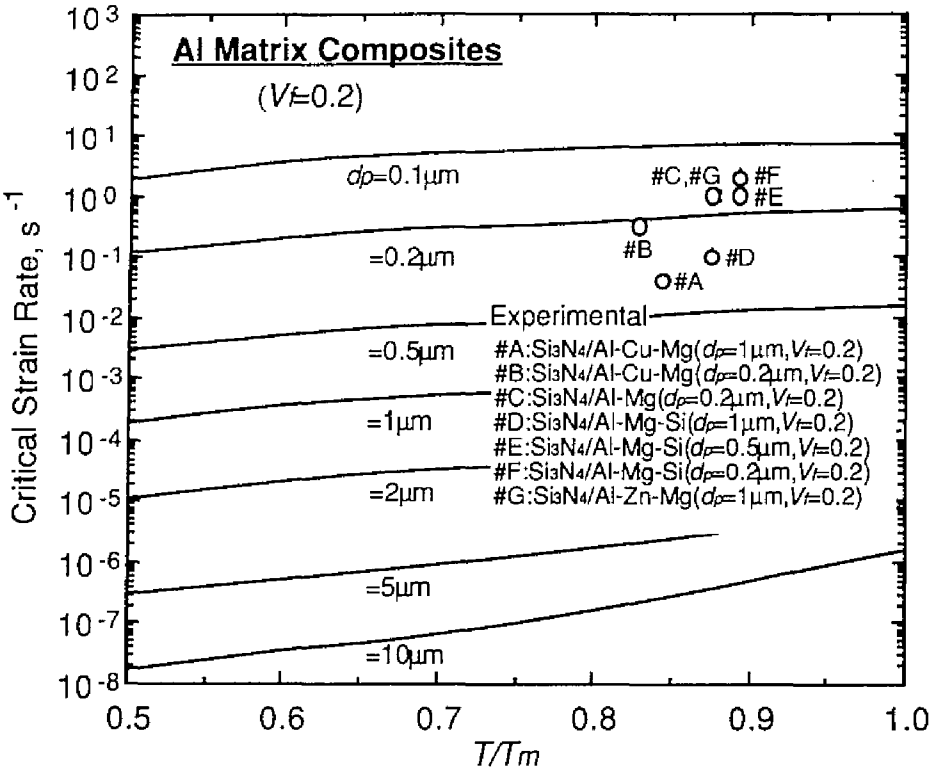

Fig. 7.13 Comparison between the experimental results of the Si3N4p/Al alloy composites and the accommodation mechanism map.

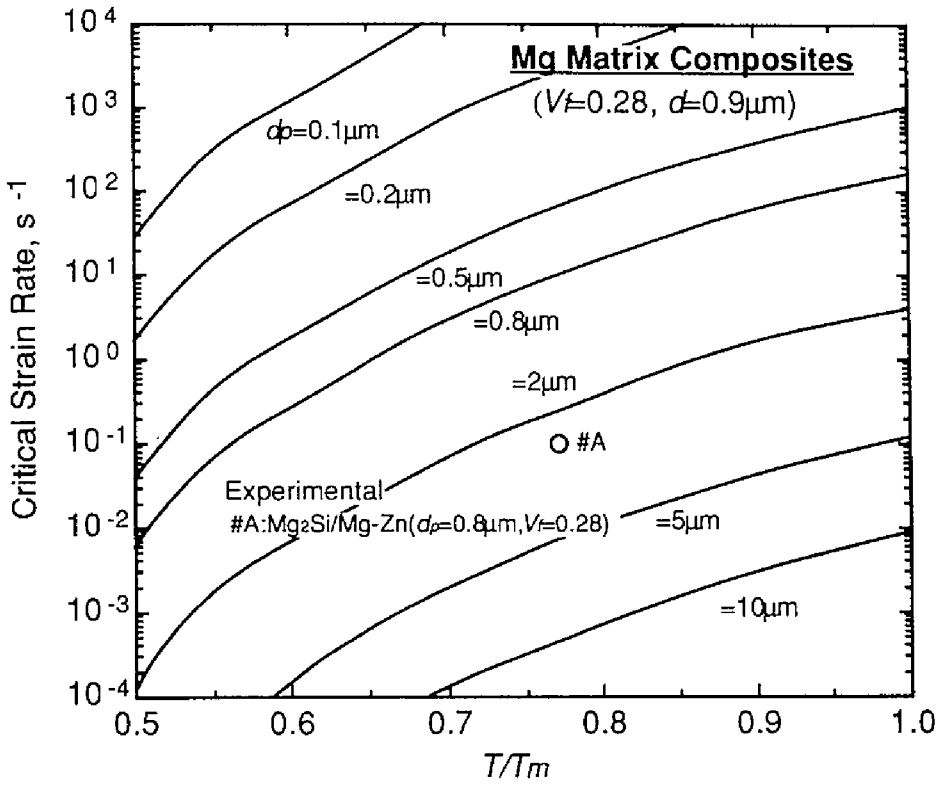

Fig. 7.14 Comparison between the experimental results of the Mg2Si$_p$/Mg-Zn composite and the accommodation mechanism map.

exhibited a maximum elongation at the temperature below the onset temperature for partial melting.

On the other hand, the strain rates obtained experimentally for the Mg_2Si_p/Mg-Zn composite is below the critical strain rate in the deformation condition, indicating that superplasticity can be attained in a solid state including no liquid for the composite. This is in good agreement with the experimental fact. Thus, the theoretical view of the critical strain rate concept is in good agreement with the experimental results.

7.2.2.6 Optimum condition for accommodation by a liquid phase

A liquid phase plays a vital role as accommodation helpers in high strain rate superplasticity for the aluminum matrix composites. However, the presence of a liquid phase does not always lead to the superplasticity. The DSC scan (top figure), the variation in elongation to failure (middle figure) and flow stress (bottom figure) as a function of temperature are shown in Fig. 7.15 for the $Si_3N_{4p(1\mu m)}$/Al-Mg-Si (6061) composite. The sharp endothermic peak is attributed to partial melting, as shown in Chapter 6. The onset temperature for partial melting of the composite was 822 K, which is determined from an intercept of two dotted lines shown in Fig. 7.15. It is found from the middle figure of Fig. 7.15 that the elongation strongly depended on a testing temperature. A maximum elongation was attained at 818 K which is close to the onset temperature for partial melting (= 822 K), however, the elongation significantly decreased at 833 K, which is close to the end temperature for partial melting determined by DSC (= 837 K). It should be noted that large elongations were not obtained when the temperature was too high. The same trend was found for all the high strain rate superplastic Si_3N_4/Al alloy composites. This indicates that a very large volume of liquid does not contribute to large elongations. This may be associated with

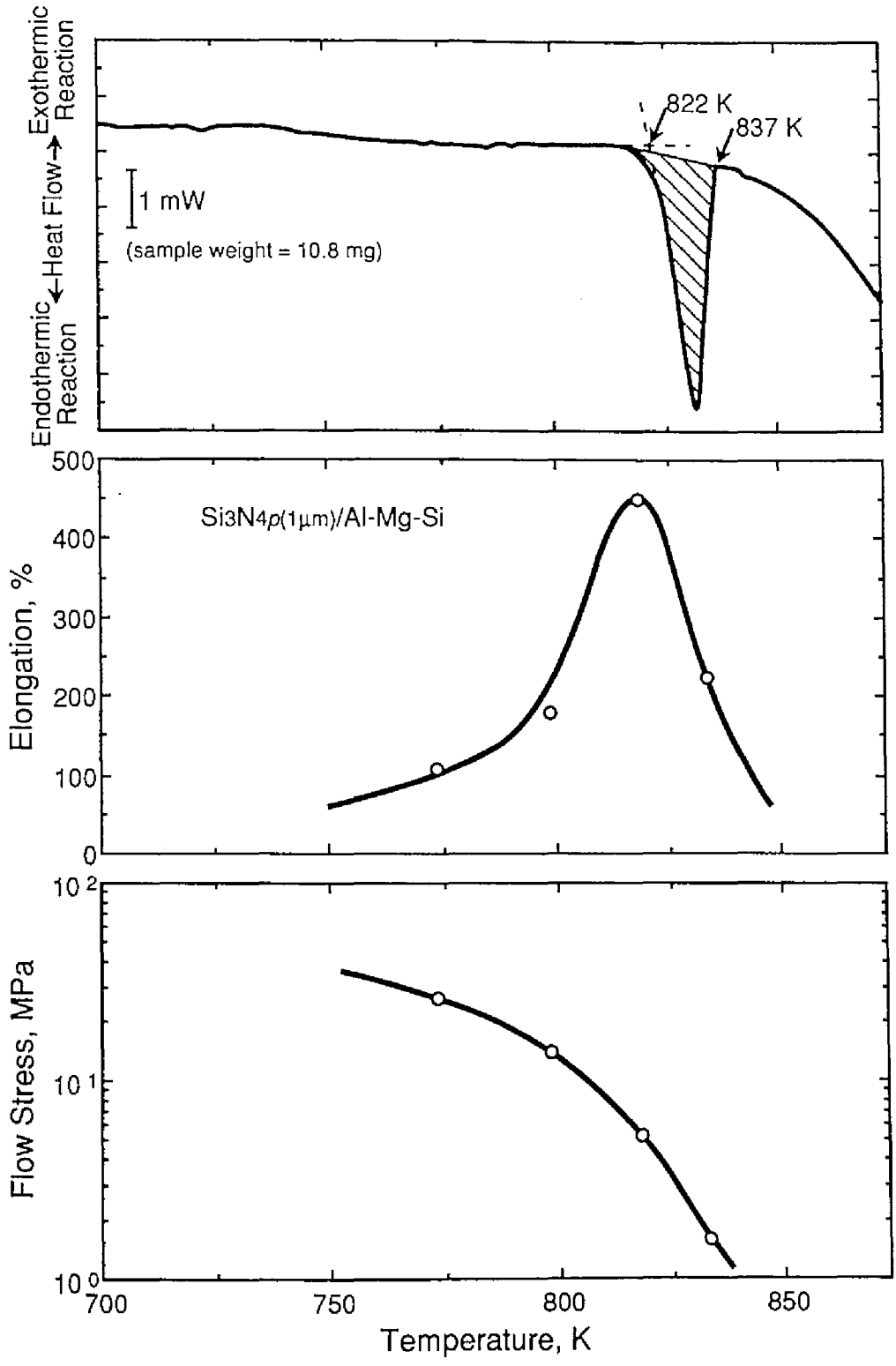

Fig. 7.15 The DSC scan (top figure), the variation in elongation to failure (middle figure) and flow stress (bottom figure) as a function of temperature for the $Si_3N_{4p(1\mu m)}$/Al-Mg-Si composite.

Table 7.2 The optimum superplastic temperature, the partial melting temperature and the volume fractions of a liquid phase at the end temperature for partial melting for the high strain rate superplastic Si_3N_4/Al composites.

	Optimum superplastic temperature /K	Partial melting temperature	Volume fraction of a liquid phase /%
Si_3N_4*p*(0.2μm)/Al-Cu-Mg	773	816	15
Si_3N_4*p*(1.0μm)/Al-Cu-Mg	788	784	6
Si_3N_4*p*(0.2μm)/Al-Mg	818	821	18
Si_3N_4*p*(0.2μm)/Al-Mg-Si	833	830	4
Si_3N_4*p*(0.5μm)/Al-Mg-Si	833	829	10
Si_3N_4*p*(1.0μm)/Al-Mg-Si	818	822	5
Si_3N_4*p*(1.0μm)/Al-Zn-Mg	818	814	5

intergranular decohesion at liquid interfaces and grain boundaries leading to intergranular fractures.

The volume fraction of a liquid phase at the end temperature for partial melting can be approximately estimated from the quantity of heat, as hatched in the top figure of Fig. 7.15. The volume fractions of a liquid phase at the end temperature for partial melting are listed in Table 7.2 for the Si_3N_{4p}/Al alloy composites. The volume fractions of a liquid phase are 4 ~ 18 % at the end temperature for partial melting. It is therefore suggested that the volume fractions of a liquid phase of 4 ~ 18 % are too large for superplastic deformation by tensile straining because of decohesion at a liquid phase. The volume fractions of a liquid phase at the optimum conditions may be a few of percents or less [29].

In general, a tensile stress tends to cause decohesion at a liquid phase and thereby excessive cavity formation. Hence it is required to limit decohesion at a liquid phase in a tensile stress field in order to attain superplasticity by tensile straining. Gee *et al.* [30] investigated the nature of very thin liquid films and they showed that the effective viscosity in very thin liquid films can be 10^5 times the bulk value and molecular relaxation times can be 10^{10} times slower. Such unusual behaviors of very thin liquid films are supported by molecular dynamics simulations [31,32]. Recently, Jeong *et al.* [33] investigated the matrix/reinforcement interfaces of the sample deformed at the optimum testing condition for the high strain rate superplastic Si_3N_{4w}/Al-Mg-Si composite by high-resolution electron microscopy and they found new phases, which were epitaxially grown, with a FCC structure at the interfaces. The new phases were distributed discontinuously and the thicknesses of the new phases were ~ 30 nm for a maximum (the average was about 20 nm). If the origin of the new phase is associated with a liquid phase, it is suggested that a liquid phase is distributed discontinuously and the thickness of the new

phases is very thin (~ 30 nm for a maximum) at the optimum testing condition. I believe that such a discontinuous and thin liquid phase serves both to relax the stress concentrations and to limit decohesion at a liquid phase.

7.3 Conclusions

(1) High strain rate superplasticity is attributed to a very small grain size. However, it is required not only to attain a very small grain size, but also to accommodate the sliding process, that is, to relax the stress concentrations around the reinforcements in order to attain high strain rate superplasticity for metal matrix composites because stress concentrations cause excessive cavity formation, resulting in premature fracture.

(2) The optimum superplastic temperature is close to the onset temperature for partial melting for all the Si_3N_4/Al alloy composites, except for the $Si_3N_{4p(0.2\mu m)}$/Al-Cu-Mg composite. It is therefore suggested that a liquid phase due to partial melting plays a vital role in high strain rate superplasticity for the composites.

(3) On the basis of the above results, a new concept for the accommodation mechanisms of superplastic deformation was proposed. The new concept is that a liquid phase relaxes the high stress concentrations caused around the reinforcements during superplastic flow and promotes interfacial sliding occurring without excessive cavity formation at the interfaces, namely, a liquid phase plays a role as accommodation helpers.

(4) From this view, the critical strain rate, below which the accommodation mechanism for superplastic flow is diffusional flow and/or dislocation movement in a solid state, on the other hand, above which a special accommodation process by an accommodation helper such as a liquid

phase is required, was developed. The theoretical analysis was in good agreement with the experimental results.

(5) However, the presence of a liquid phase does not always lead to superplasticity. A very large volume of liquid does not contribute to large elongations. A discontinuous and thin liquid phase is required both to relax the stress concentrations and to limit intergranular decohesion at liquid interfaces and grain boundaries.

References

1. K.Higashi, Mater. Sci. Forum, **170-172**, 131 (1994).
2. T.G.Nieh, C.A.Henshall and J.Wadsworth, Scripta Metall., **18**, 1405 (1984).
3. J.Pilling, Scripta Metall., **23**, 1375 (1989).
4. K.Higashi, T.Okada, T.Mukai, S.Tanimura, T.G.Nieh and J.Wadsworth, Scripta Metall. Mater., **26**, 185 (1992).
5. K.Matsuki, S.Murakami, H.Matsumoto, M.Tokizawa, N.Takatsuji and M.Isogai, J. Japan Inst. Metals, **59**, 145 (1995).
6. T.G.Nieh and J.Wadsworth, Scripta Metall. Mater., **32**, 1133 (1995).
7. O.D.Sherby and J.Wadsworth, Prog. Mater. Sci., **33**, 169 (1989).
8. M.W.Mahoney, A.K.Ghosh and C.C.Bampton, in *Proc. 6th Int. Conf. on Composite Materials*, edited by F.L.Matthew, N.C.R.Buskell, J.M.Hodgkinson and J.Monton (Elesier Applied Science, London, 1986), vol. 2, p.372.
9. M.W.Mahoney and A.K.Ghosh, Metall. Trans. A, **18A**, 653 (1987).
10. A.-U.Karim and W.A.Bachofen, Metall. Trans., **3**, 709 (1972).
11. R.Z.Valiev and O.A.Kaibyshev, phys. stat. sol. (a)., **44**, 65 (1977).
12. G.G.Doncel, J.Wolfenstine, P.Metenier, O.A.Ruano and O.D.Sherby, J. Mater. Sci., **25**, 4535 (1990).
13. P.Metenier, G.G.Doncel, O.A.Ruano, J.Wolfenstine and O.D.Sherby, Mater. Sci. Eng., **A125**, 195 (1990).
14. J.K.Solberg, J.Torklep, O.Bauger and H.Gjestland, Mater. Sci. Eng., **A134**, 1201 (1991).
15. K.Higashi, K.Kubota and G.Neite, in *Magnesium Alloys and Their Applications*, edited by B.L.Mordike and F.Hehmann, (DGM Informationsgesellschaft mbH, Oberursel), p. 293.

16. M.Mabuchi., K.Kubota, and K.Higashi, in *Aspects of High Temperature Deformation and Fracture in Crystalline Materials*, edited by Y.Hosoi, H.Yoshinaga, H.Oikawa and K.Maruyama, (The Japan Institute of Metals, Sendai, 1993), p. 279.
17. T.Shibata, A.Uoya, K.Higashi, Y.Yamaguchi, A.Inoue and K.Masumoto, in *Superplasticity: 60 Years after Pearson*, edited by N.Ridley, (The institute of Materials, London, 1995), p. 113.
18. S.-W.Lim, T.Imai, Y.Nishida and T.Choh, Scripta Metall. Mater., **32**, 1713 (1995).
19. R.C.Gifkins, J. Mater. Sci., **13**, 1926 (1978).
20. R.Z.Valiev and O.A.Kaibyshev, Acta Metall., **31**, 2121 (1983).
21. Z.-R.Lin, A.H.Chokshi and T.G.Langdon, J. Mater. Sci., **23**, 2712 (1988).
22. T.G.Langdon, Mater. Sci. Eng., **A174**, 225 (1994).
23. M.Mabuchi, K.Higashi and T.G.Langdon, Acta Metall. Mater., **42**, 1739 (1994).
24. R.Raj and M.F.Ashby, Metall. Trans., **2**, 1113 (1971).
25. R.Raj and M.F.Ashby, Acta Metall., **23**, 653 (1975).
26. G.Le Roy, J.D.Embury, G.D.Ward and M.F.Ashby, Acta Metall., **29**, 1509 (1981).
27. J.Rösler, G.Bao and A.G.Evans, Acta Metall. Mater., **39**, 2733 (1991).
28. R.S.Mishra, T.R.Bieler and A.K.Mukherjee, Acta Metall. Mater., **43**, 877 (1995).
29. M.Mabuchi, H.-G.Jeong, K.Hiraga and K.Higashi, Interface Science, in press.
30. M.L.Gee, P.M.McGuiggan and N.Israelachvili, J. Chem. Phys., **93**, 1895 (1990).
31. M.Lupkowski and F.van.Swol, J. Chem. Phys., **95**, 1995 (1991).
32. M.W.Ribrarsky and U.Landman, J. Chem. Phys., **97**, 1937 (1992).

33. H.-G.Jeong, K.Hiraga, M.Mabuchi and K.Higashi, Philos. Mag. Lett., **74**, 73 (1996).

CHAPTER 8

CAVITATION AND CAVITATION CONTROL

8.1 Introduction

The deformation mechanisms of high strain rate superplasticity in the composites are currently the subject of some debate. In Chapter 7, I proposed the new concept that a liquid phase play an important role in high strain rate superplasticity. Recently, Iwasaki *et al.* [1,2] compared the cavity volume of the high strain rate superplastic $Si_3N_{4p(0.5\mu m)}$/Al-Mg-Si (6061) composite with that of a superplastic aluminum alloy and they showed that (i) the evolution in cavity volume with strain for the composite was much lower than that for the alloy and (ii) the cavity sizes for the composite were much smaller than those for the alloy. In their studies, the testing temperature for the composite was slightly above the onset temperature for partial melting. Therefore the presence of a liquid phase appears to affect the cavitation characteristics. However, there are not sufficient date to understand the characteristics and mechanisms of cavitation in a state including a liquid phase for high strain rate superplastic composites.

In general, cavitation has a strong deleterious influence on post-forming service properties [3-8]. Therefore, it is important to control cavitation for structural applications. Several procedures have been applied to reduce the level of cavitation: superimposed hydrostatic pressure during deformation [9,10], annealing before deformation [11,12], and annealing with or without superimposed pressure after deformation [5,11].

Varloteaux *et al.* [11] showed that for superplastic aluminum alloys, small cavities ($\leq$ 6 μm) were eliminated by static annealing without superimposed pressure after deformation, however, large cavities ($\geq$ 8 ~ 9 μm) were only slightly affected by the annealing and they noted that superimposed pressure was required to reduce large cavities. As shown by Iwasaki *et al.* [1], the sizes of most of cavities were very small ($\leq$ 1 μm) for the aluminum matrix composite. Such small cavities may be reduced by static annealing without superimposed pressure after deformation. Cavitation control by static annealing is attractive for commercial applications.

In the present chapter, cavitation in a state including a liquid phase is investigated by density measurements, microstructural observation and quantitative analyses for the $Si_3N_{4p(0.5\mu m)}$/Al-Mg-Si (6061) composite. In addition, recovery of cavity damages by static annealing after superplastic deformation is examined.

8.2 Experimental procedure

The $Si_3N_{4p(0.5\mu m)}$/Al-Mg-Si (6061) composite was investigated for the cavitation study. The particulates were distributed reasonably uniformly and no cracks and no cavities were found before tensile tests by SEM observation. Constant true stress tensile tests were carried out at 4 ~ 12 MPa and at 833 K to examine superplastic behavior. The testing temperature of 833 K is the optimum temperature where a maximum elongation is attained and is slightly above the partial melting temperature of the composite (= 829 K) [1]. A maximum elongation was attained at 8 MPa and the elongation largely decreased at high stresses > 10 MPa [13]. Hence, in the present investigation, a stress of 8 MPa was used for an examination of cavitation.

Specimens were deformed at a constant stress of 8 MPa and at temperatures of 818 and 833 K and the volumes of cavities in the gauge length

of the deformed specimens were determined by hydrostatic weighing in water with a corresponding gauge head being used as a density standard. In addition, the cavities were metallographically observed by high resolution scanning electron microscopy of HITACHI S-900. The high resolution scanning electron microscopy enabled observation with a sizing interval of 0.1 μm. An quantitative analysis was conducted by a LUZEX F Stereo Analyzing System connected to the scanning electron microscope on the basis of the observation. All cavities were assumed to be spherical to investigate the cavity size distributions.

To investigate recovery of cavity damages by a static annealing, specimens were deformed to 50 % elongation at 8 MPa and at 833 K and then were annealed at 793 K prior to aging treatment at 453 K for 28.8×10^3 s, which is the standard T6 heat treatment for the Al-Mg-Si (6061) alloy [14]. The annealing at 793 K was conducted for 1.8×10^3 and 1.08×10^5 s. After the specimens were machined to a constant diameter to eliminate the effect of differing specimen geometry on the tensile properties, room temperature tensile tests were carried out on both deformed and non-deformed specimens with the same thermal history.

8.3 Results and discussion

8.3.1 Cavity nucleation

Microstructure of the specimen deformed to $\varepsilon = 1$ at 833 K and at 8 MPa is shown in Fig. 8.1. It follows that the interfaces are the sites for cavities to nucleate. Iwasaki *et al.* [1] showed that the cavity sizes were much smaller, but the cavity number was much larger for the high strain rate superplastic aluminum matrix composite, compared to those for the superplastic aluminum alloy. As shown later, excessive strain-induced cavity nucleation was not observed during superplastic straining for the composite. This is probably

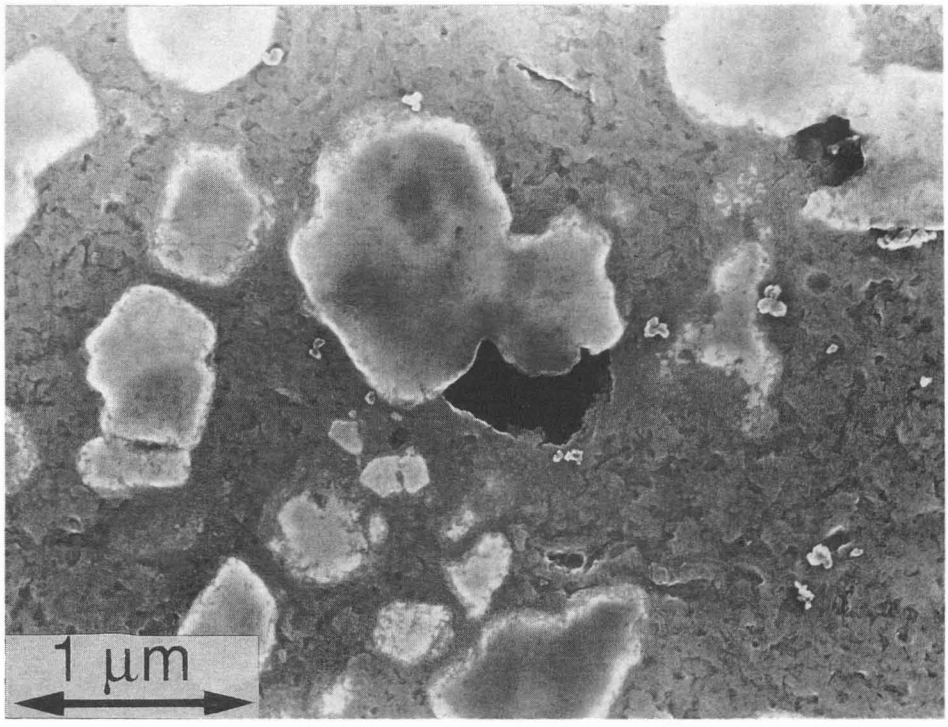

Fig. 8.1 Cavity nucleation in the $Si_3N_{4p(0.5\mu m)}$/Al-Mg-Si (6061) composite deformed to $\varepsilon = 1$ at 833 K and at 8 MPa.

because of relaxation of the stress concentrations by the presence of a liquid phase. In the present investigation, most of cavities were formed during very short straining of $\varepsilon < 0.2$. The cavity formation during very short straining may be attributed to cavity nucleation in a liquid phase.

8.3.2 Cavity growth

8.3.2.1 Cavity volume

The variation in cavity volume fraction as a function of true strain at 833 K and at 8 MPa is shown in Fig. 8.2, where the strain rate is determined at $\varepsilon = 0.1$. In the figure, the date for a superplastic 7475 aluminum alloy, which are measured at the optimum testing condition (for a maximum elongation) of 5 MPa and 788 K, are superimposed. The testing temperature of 788 K for the aluminum alloy is lower than the solidus temperature of the aluminum alloy. It is found that the cavity volume fraction of the composite was larger at $\varepsilon < 1$, but it was smaller at $\varepsilon > 1$, compared with the aluminum alloy. It should be noted that the extent of the cavity volume for the composite was much lower than that for the aluminum alloy. It is suggested that the development of cavities is limited by the presence of a liquid phase for the composite.

The variation in cavity volume with strain was examined at 818 and 833 K with a constant true stress of 8 MPa for the composite. The testing temperatures of 818 and 833 K are lower than and slightly above the onset temperature for partial melting, respectively. The results are shown in Fig. 8.3. It is apparent that the rate of increase in the cavity volume at 833 K is significantly lower than that at 818 K and the cavity development is very minor at 833 K where partial melting occurs. It is therefore suggested that cavity development is minimized by the presence of a liquid phase because a liquid phase serves to relax the stress concentrations.

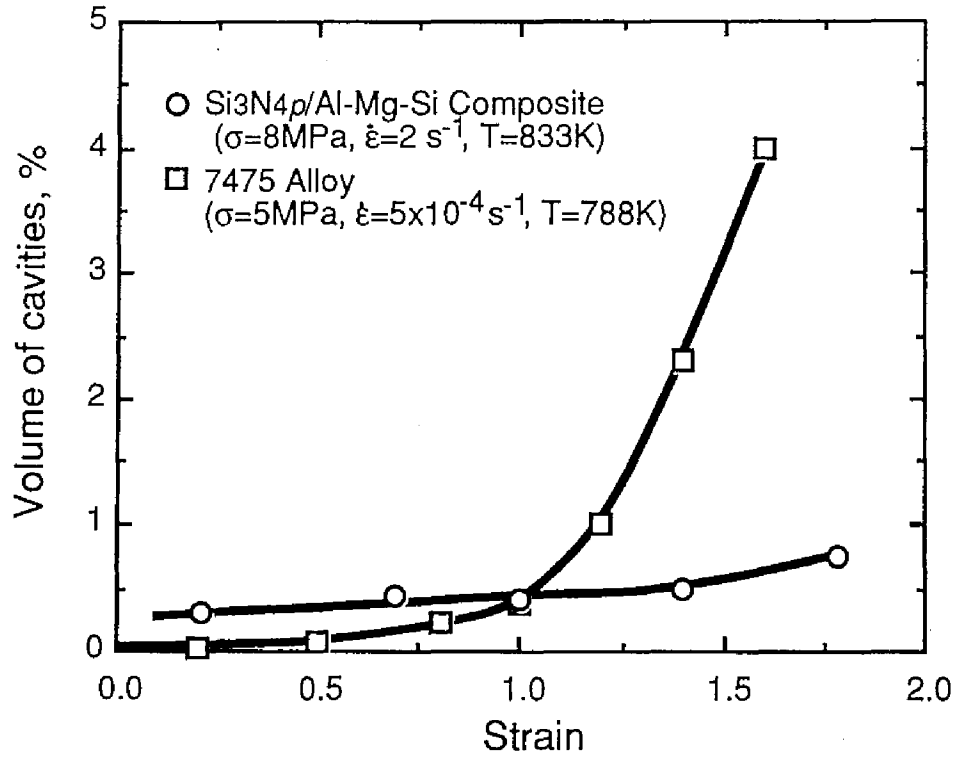

Fig. 8.2 The variation in cavity volume fraction as a function of true strain for the $Si_3N_{4p(0.5\mu m)}$/Al-Mg-Si composite and the 7475 alloy.

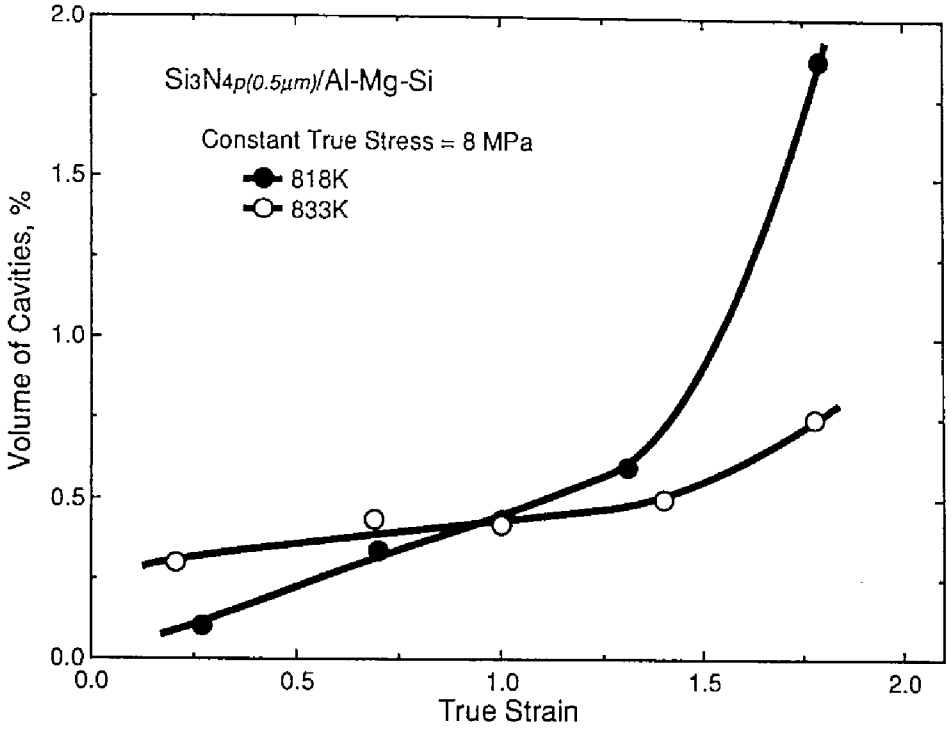

Fig. 8.3 The variation in cavity volume as a function of true strain at 818 and 833 K under a constant true stress of 8 MPa for the Si3N4*p*(0.5μm)/Al-Mg-Si (6061) composite, where the testing temperature of 818 K is lower than the onset temperature for partial melting and the testing temperature of 833 K is slightly above the onset temperature for partial melting.

8.3.2.2 Quantitative analysis

Cavitation characteristics of the specimen deformed at 833 K and at 8 MPa were quantitatively analyzed on the basis of microstructural observation. The variation in number of cavities per unit area as a function of cavity diameter at strains of 0.2, 0.7, 1.0 and 1.4 is shown in Fig. 8.4, where a sizing interval is taken to be 1 μm. It is found that large cavities of more than 2 μm in diameter were very few and there were no cavities of more than 4 μm even at a strain of 1.4. It should be noted that most of cavities were very small for the high strain rate superplastic composite.

It is important to investigate the distribution of small size cavities in order to understand the cavitation characteristics for the high strain rate superplastic composites. In the present investigation, the distributions of small cavities of less than 1 μm were examined with a sizing interval of 0.1 μm. The results are shown in Fig. 8.5. Inspection of the figure reveals that the peak cavity size, which is defined as the cavity size where the number of cavities per unit area at each strain is the largest, increased with increasing strain, indicating that cavities were slowly grown during straining. It is of interest to note that most of cavities were more than 0.1 ~ 0.2 μm and very fine cavities of less than 0. 2 μm were few, indicating that the critical cavity diameter, above which cavities are stable and below which cavities are unstable, is approximately 0.2 μm.

The variation in normalized number of cavities as a function of roundness factor $(L_{max}/L_O)^2$ is shown in Fig. 8.6, where the normalized number of cavities is the number of cavities divided by the total number of cavities and L_{max} is the maximum cavity diameter, which is the longest separation between any two points on the perimeter of a cavity, and L_O is the cavity diameter assuming that a cavity is perfectly round. The roundness factor $(L_{max}/L_O)^2$ is unity if a cavity is a perfect circle. It is accepted that small cavities are almost

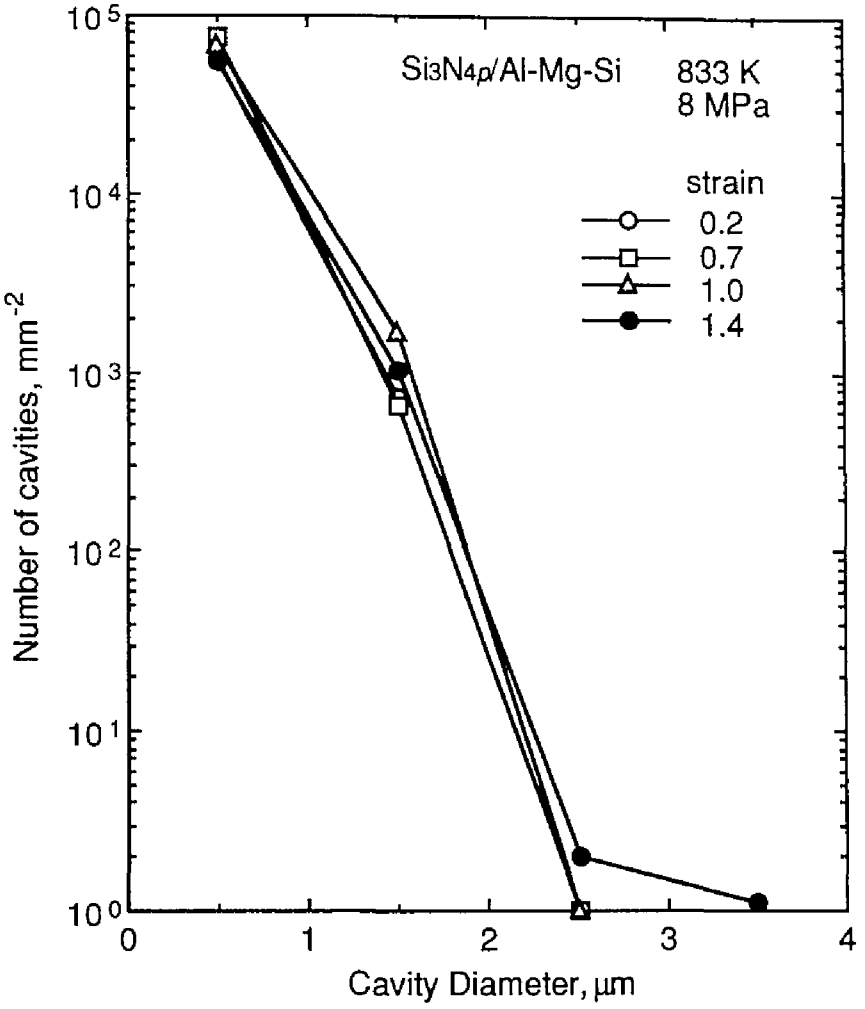

Fig. 8.4 The variation in number of cavities as a function of cavity diameter at strains of 0.2, 0.7, 1.0 and 1.4.

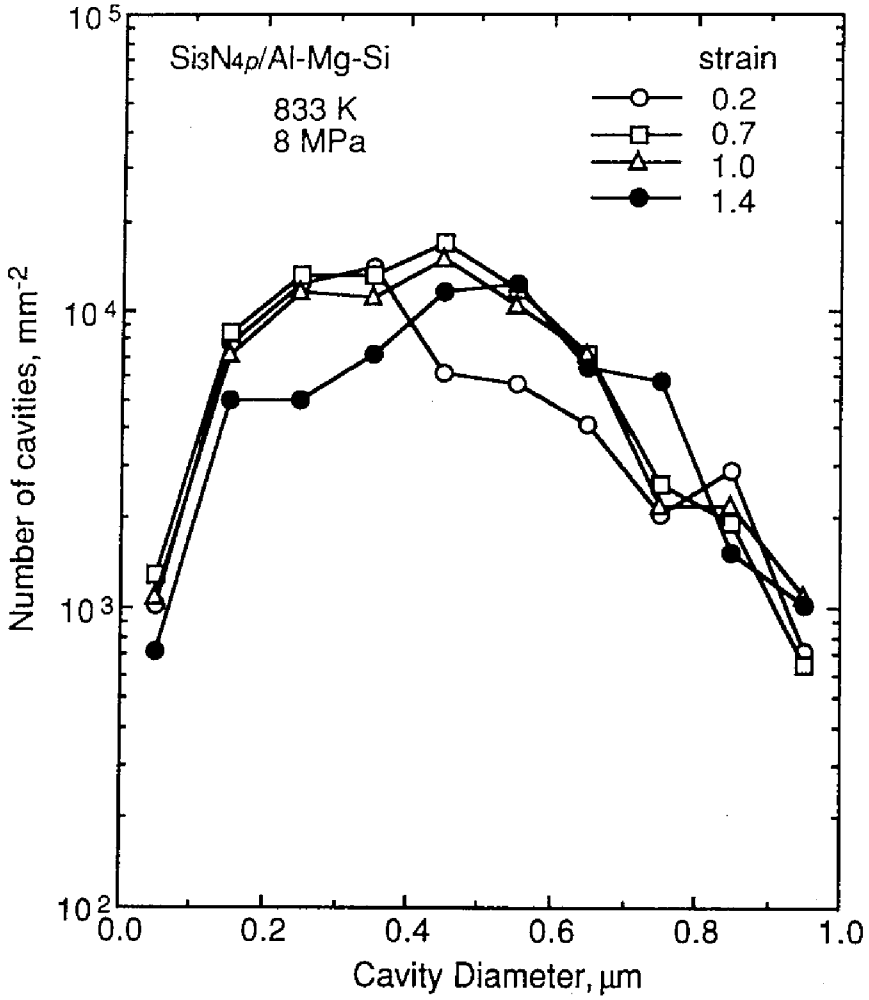

Fig. 8.5 The variation in number of cavities as a function of cavity diameter at strains of 0.2, 0.7, 1.0 and 1.4, where small cavities of less than 1 μm are measured.

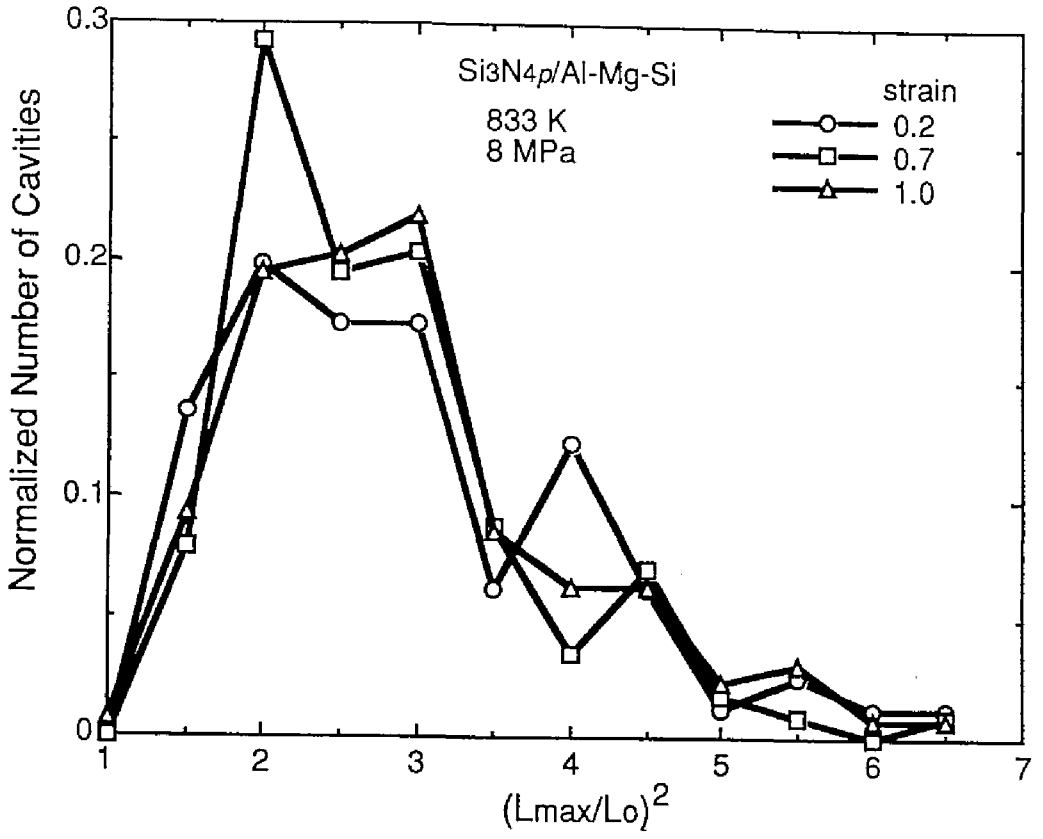

Fig. 8.6 The variation in normalized number of cavities as a function of roundness factor $(Lmax/Lo)^2$, where $Lmax$ is the maximum length of each cavity and Lo is the diameter assuming a cavity is perfectly round.

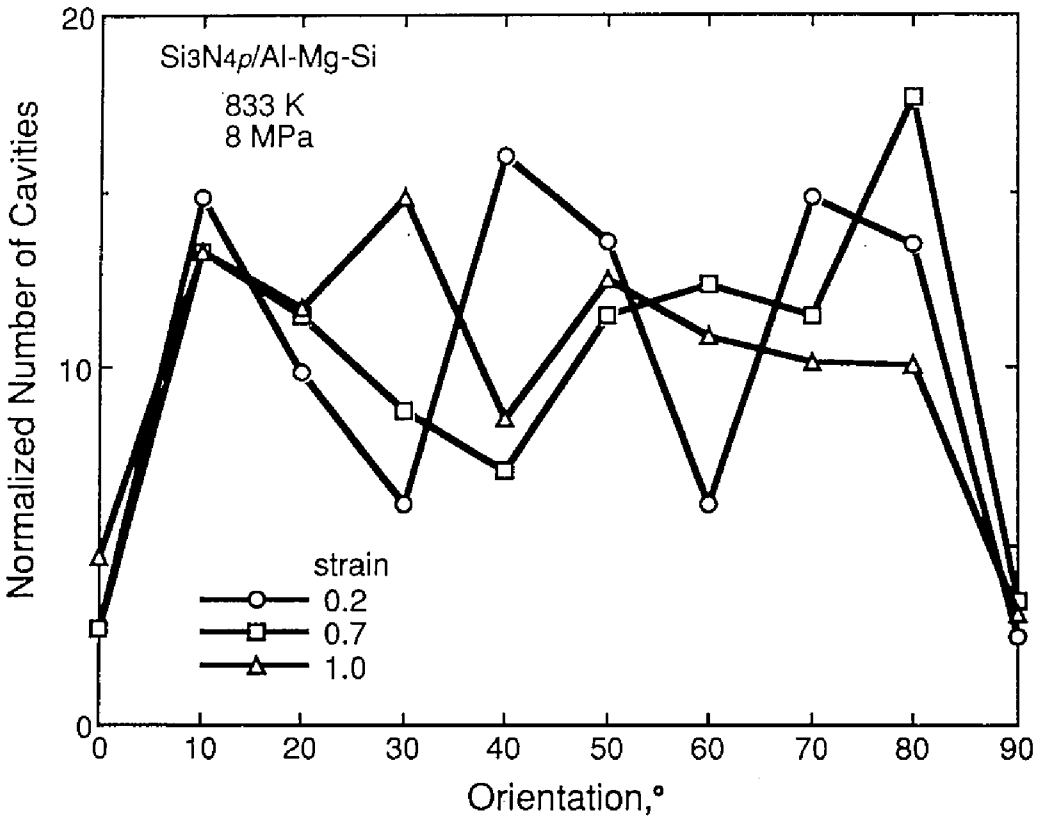

Fig. 8.7 The variation in normalized number of cavities as a function of orientation.

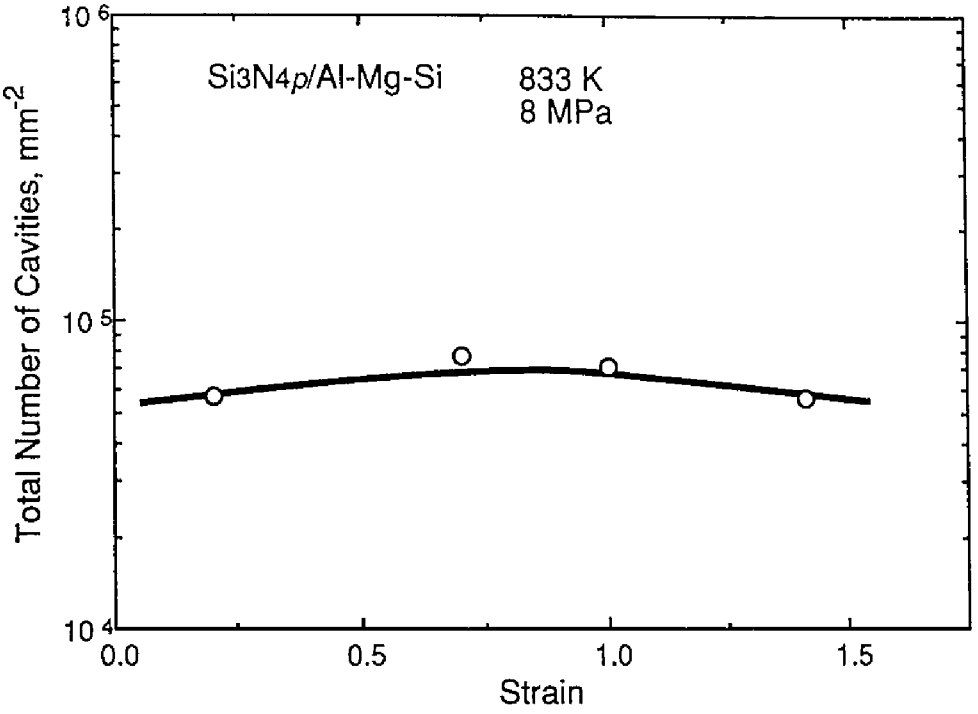

Fig. 8.8 The variation in total number of cavities as a function of strain.

round due to diffusion-controlled cavity growth, on the other hand, large cavities are elongated due to plasticity-controlled cavity growth [15]. The results in the present investigation showed broad distributions of the roundness factor of ~ 7, though most of cavities were very small (< 1 μm). It should be noted that this trend is independent of strains.

The variation in normalized number of cavities as a function of orientation is shown in Fig. 8.7, where the orientation is the angle between the maximum diameter and the tensile axis. There appears to be no preferential directionality of cavities, independent of strains.

The variation in total number of cavities as a function of strain is shown in Fig. 8.8. Excessive strain-induced cavity nucleation is expected to be caused when the stress concentrations, caused by grain boundary sliding, are not sufficiently relaxed. However, the results in Fig. 8.8 show that the total number of cavities is roughly constant and excessive strain-induced cavity nucleation is limited during superplastic straining for the composite. It is found that most of cavities are nucleated at short straining of $\varepsilon < 0.2$.

The cavity growth mechanisms for superplastic materials may be classified into three categories [15]: diffusion-controlled growth [16,17], superplastic diffusion-controlled growth [18] and plasticity-controlled growth [19,20]. The diffusion-controlled growth occurs by the stress directed diffusion of vacancies from a zone in the grain boundary plane adjacent to a cavity. The rate of diffusion-controlled growth is given by [18,21,22]

$$\frac{dr}{d\varepsilon} = \alpha \frac{2D_{GB}\delta\Omega}{kT\dot{\varepsilon}r^2}\left(\sigma - \frac{2\gamma}{r}\right) \tag{8.1}$$

where r is the radius of cavity, ε is the strain, D_{GB} is the grain boundary diffusion coefficient, δ is the grain boundary width, Ω is the atomic volume, k is the Boltzmann's constant, T is the absolute temperature, $\dot{\varepsilon}$ is the strain rate,

σ is the stress, γ is the surface energy and α is the cavity size-spacing parameter. For the composite in the present investigation, a value of α is take to be 1/4 (Appendix).

Chokshi and Langdon [18] proposed superplastic diffusion-controlled growth, that is, the cavity growth due to additional mass transfer along grain boundaries intersecting the surface of the cavity. The growth rate is given by [18, 22]

$$\frac{dr}{d\varepsilon} = 45\frac{D_{GB}\delta\Omega}{kTd^2}\left(\frac{\sigma}{\dot{\varepsilon}}\right) \tag{8.2}$$

where d is the grain size.

Plasticity-controlled growth occurs by plastic deformation of the material surrounding a cavity. The rate of plasticity-controlled growth is given in the form [18,21,22]

$$\frac{dr}{d\varepsilon} = r\text{-}\frac{3\gamma}{2\sigma} \ . \tag{8.3}$$

Since these cavity growth mechanisms operate independently, the fastest process is a dominant process of the cavity growth mechanisms.

Assuming that the sliding displacements are too large to be accommodated elastically and the sliding is accommodated by diffusional flow in a solid state, the local shear stress, caused by sliding, around reinforcements may be given by Eq 7.3. When the accommodation helper mechanisms such as the accommodation by a liquid phase are not operative, the high local tensile stress is caused around reinforcements for the aluminum matrix composites, as shown in Chapter 7. The local tensile stress ($= \sqrt{3}\tau_i$) is calculated to be 108 MPa at the testing conditions of the present investigation for the composite.

The variation in cavity growth rate as a function of cavity radius for the above cavity growth mechanisms in the cases of stress concentrations, that is, $\sigma = 108$ MPa and of no stress concentrations, that is, $\sigma = 8$ MPa is shown in Fig. 8.9. The diffusion growth rate is expected to be low because of short times for high strain rate deformation. However, as shown in Fig. 8.9, when the stress concentrations are caused, the diffusion growth rate is very high in a small cavity radius range < about 0.2 μm because mass transfer due to diffusion is accelerated by the high local stress. On the other hand, when the stress concentrations are relaxed, the diffusion growth is significantly slow and consequently the diffusion growth is negligible even in a small cavity size range. Inspection of Fig. 8.9 reveals that plastic growth is also significantly limited in a cavity radius range ≤ about 0.5 μm by relaxation of the stress concentrations. In addition, fine cavities < 0.2 μm are unstable and disappear in the case of no stress concentrations, though such fine cavities grow very fast by the diffusion growth in the case of stress concentrations. It is suggested from these analyses that the growth rates are significantly decreased and the critical cavity size is increased by relaxation of the stress concentrations.

The experimental growth rates were calculated on the basis of the data of the largest ten cavity radii and the data of the peak cavity size, that is, the cavity radius for the maximum number. The results are superimposed in Fig. 8.9, where a close circle is from the largest ten cavity radii and an open circle is from the cavity radius for the maximum number. The experimental growth rates are in good agreement with the rate predicted by plasticity-controlled growth mechanism in the case of relaxation of the stress concentrations. In addition, the experimental critical cavity radius of approximately 0.1 μm, as shown in Fig. 8.5, is in agreement with the critical cavity radius in the case of no stress concentrations. It is therefore suggested

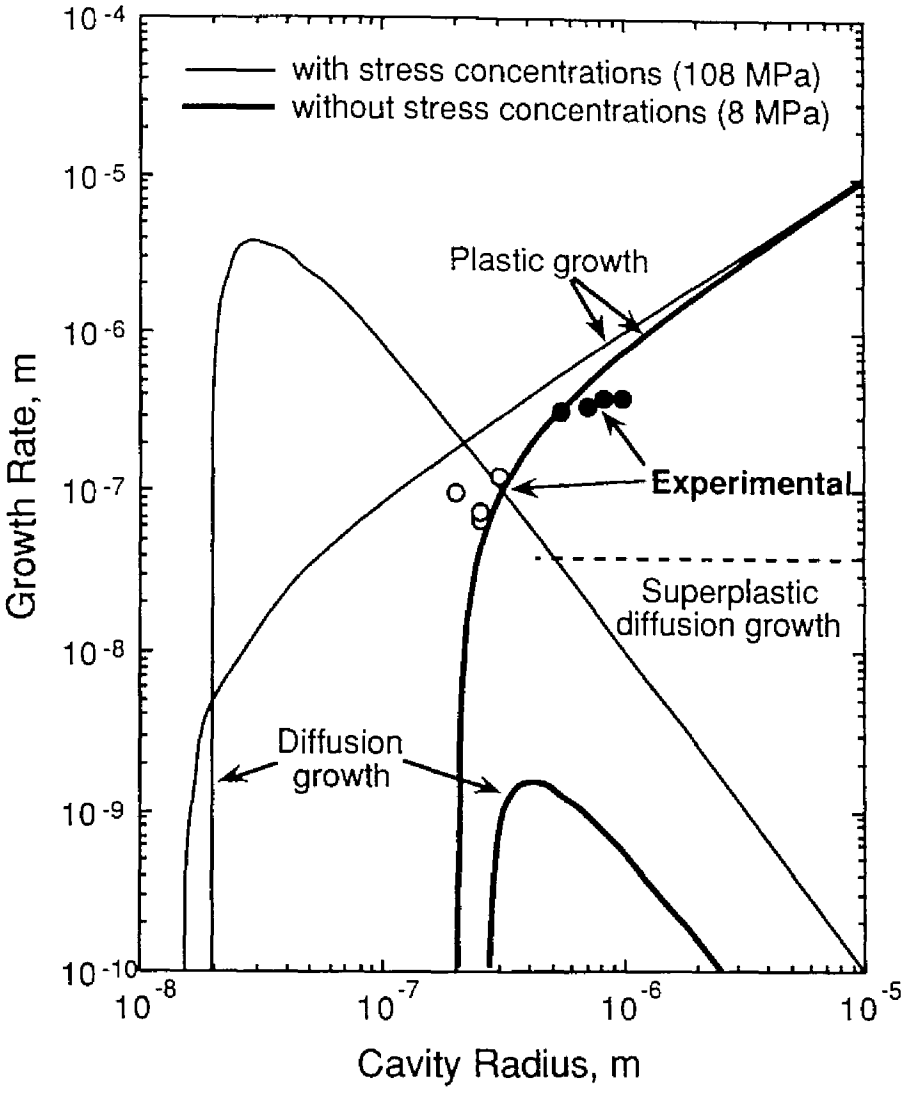

Fig. 8.9 The variation in cavity growth rate as a function of cavity radius for diffusive and plastic mechanisms together with experiment measurements, where ● : the experimental value from the largest ten cavity radii and o : from the cavity radius for the maximum number of cavities.

that the stress concentrations are relaxed by the presence of a liquid phase and consequently the development of cavitation is limited for the composite.

8.3.3 Recovery of cavity damages by static annealing

After specimens were deformed to 50 % elongation at 8 MPa and at 833 K, static annealing at 793 K prior to aging-treatment at 453 K for 28.8 x 10^3 s was conducted and recovery of cavity damages was investigated. The variation in cavity volume as a function of annealing time is shown in Fig. 8.10. It is found that the extent of cavitation was decreased by the static annealing after superplastic deformation.

Quantitative metallographic measurements of cavity size distributions were performed. The result is shown in Fig. 8.11. Clearly, many cavities were reduced and eliminated by the static annealing.

The variation in post-deformation tensile properties at room temperature as a function of annealing time at 793 K is shown in Fig. 8.12 for the non-deformed and the deformed specimens. Since the non-deformed specimens were treated with the same thermal history as the deformed specimens, differences in tensile properties between the non-deformed and the deformed specimens result from cavitation occurring during superplastic flow. Eto *et al.* [8] showed that post-deformation ultimate tensile strength (UTS) and yield stress (YS) strongly depended on superplastic elongation, however, post-deformation elongation did not depend on superplastic elongation for a superplastic Al-Zn-Mg-Cu (7475) alloy. On the other hand, Bampton and Edington [4] revealed that UTS and YS showed no significant deterioration up to superplastic strain of at least 1.0, however, the elongation decreased more rapidly with increasing superplastic strain for a superplastic Al-Zn-Mg-Cu (7475) alloy. For the composite, not only elongation, but also UTS and YS were degraded by superplastic elongation. However, it is found from

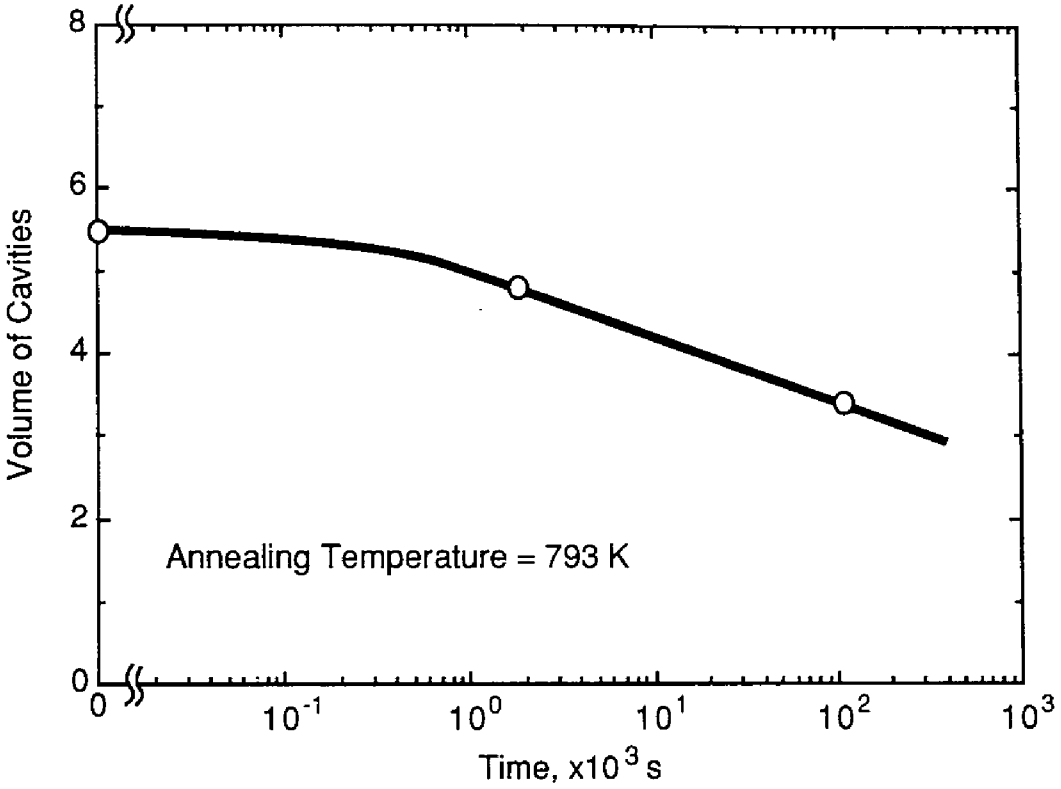

Fig. 8.10 The variation in cavity volume as a function of annealing time at 793 K for the deformed (50%) Si3N4*p*/Al-Mg-Si composite.

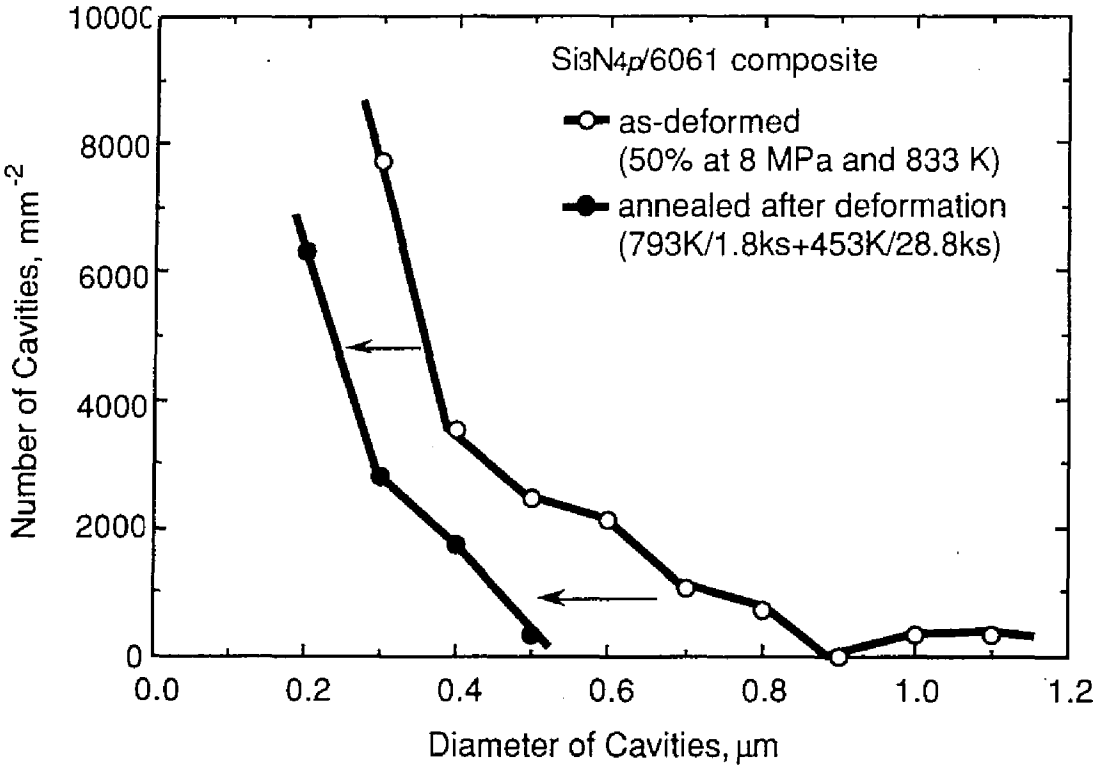

Fig. 8.11 Effect of static annealing on cavity size distributions.

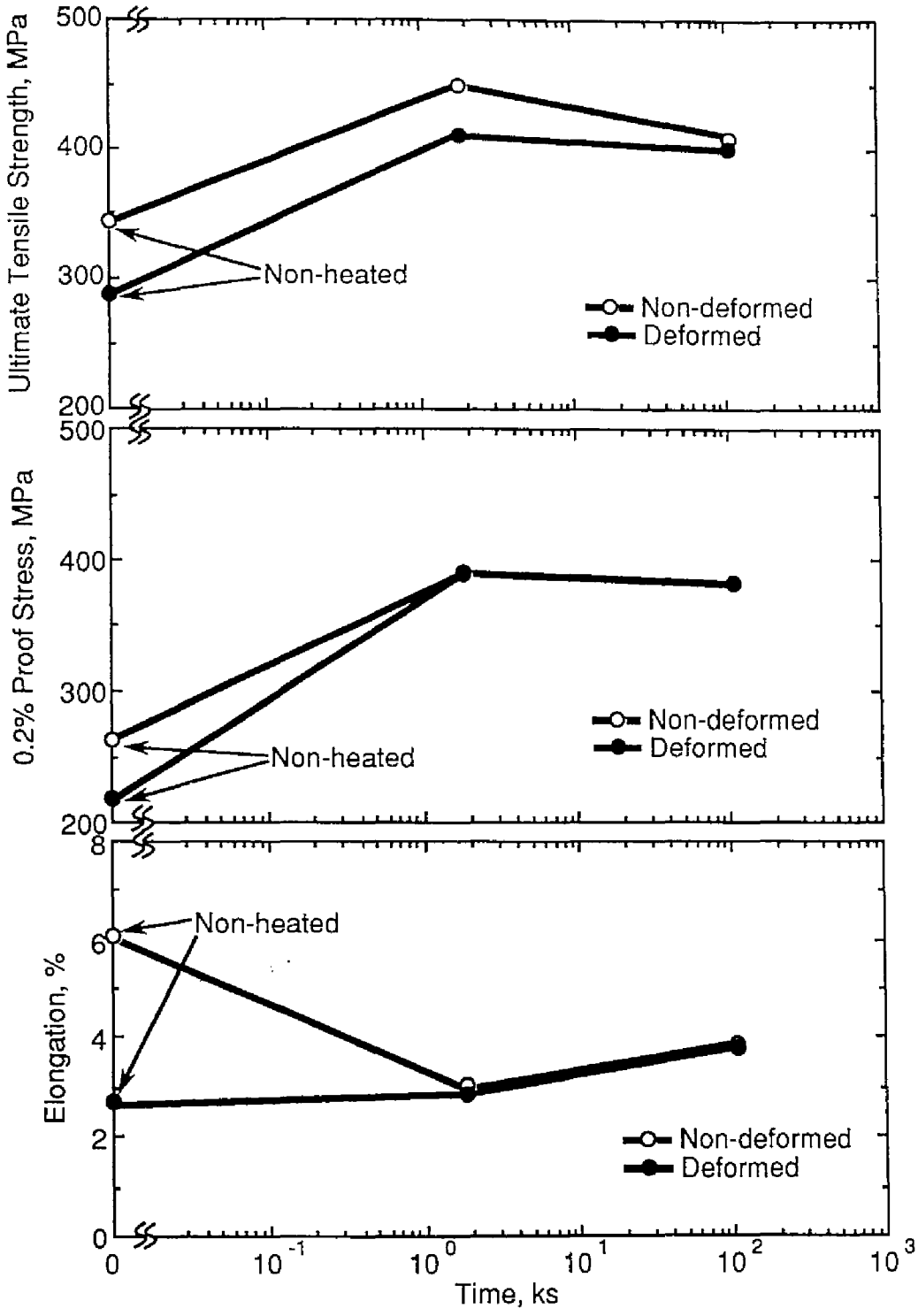

Fig. 8.12 Post-deformation tensile properties at room temperature as a function of annealing time at 793K for the non-deformed and the deformed (50% at 8 MPa and 833 K) Si3N4*p*/Al-Mg-Si composite, where annealing at 793 K are followed by heat-treatment at 453 K for 28.8 ks.

Fig. 8.12 that the decreases in post-deformation tensile properties were sufficiently recovered by the static annealing after superplastic deformation. In particular, it should be noted that even short-time annealing of 1.8×10^3 s gave rise to sufficient recovery of the post-deformation tensile properties. The recovery of the tensile properties is attributed to shrinkage and enclosure of cavities by static annealing. It is likely that static annealing after superplastic deformation is one of effective ways to reduce cavitation and thereby to recover post-deformation tensile properties for metal matrix composites exhibiting high strain rate superplasticity.

8.4 Conclusions

(1) The matrix/reinforcement interfaces were the sites for cavities to nucleate. Many cavities were nucleated during very short straining of $\varepsilon < 0.2$, however, excessive strain-induced cavity nucleation was not caused during superplastic straining at the optimum testing temperature, which is slightly above the onset temperature for partial melting.

(2) A theoretical analysis showed that when the stress concentrations are caused due to the presence of reinforcements, the cavity growth rate is very high in particular in a small cavity size range and the critical cavity size is very small, however, the growth rates are significantly decreased and the critical cavity size is increased by relaxation of the stress concentrations.

(3) The experimental values of the critical cavity size and the growth rate were in agreement with the values predicted in the case of relaxation of the stress concentrations. This supports the accommodation helper mechanism by a liquid phase.

(4) Cavities occurring during superplastic deformation were reduced by static annealing at 793 K for a relatively short time of 1.8×10^3 s without

superimposed pressure, and consequently the post-deformation tensile properties were sufficiently recovered.

References

1. H.Iwasaki, M.Takeuchi, T.Mori, M.Mabuchi and K.Higashi, Scripta Metall. Mater., **31**, 255 (1994).
2. H.Iwasaki, M.Mabuchi, K.Higashi and T.G.Langdon, Mater. Sci. Eng., **A208**, 116 (1996).
3. R.D.Schelleng and G.H.Reynolds, Metall. Trans., **4**, 2199 (1973).
4. C.C.Bampton and J.W.Edington, J. Eng. Mater. Tech., **105**, 55 (1983).
5. N.Ridley, D.W.Livesey and A.K.Mukherjee, Metall. Trans. A, **15A**, 1443 (1984).
6. D.S.McDarmaid, Mater. Sci. Eng., **70**, 123 (1985).
7. M.T.Cope, D.R.Evetts and N.Ridley, Mater. Sci. Tech., **3**, 455 (1987).
8. T.Eto, M.Hirano, M.Hino and Y.Miyagi, in *Superplasticity in Aerospace*, edited by H.C.Heikkenen and T.R.McNelley, (The Metallurgical Society, Warrendale, PA, 1988), p.199.
9. C.C.Bampton and R.Raj, Acta Metall., **30**, 2043 (1982).
10. J.Pilling and N.Ridley, Acta Metall., **34**, 669 (1986).
11. A.Varloteaux, J.J.Blandin and M.Suéry, Mater. Sci. Tech., **5**, 1109 (1989).
12. H.Iwasaki, Y.Irie, S.Hayami, K.Higashi and T.Ito, J. Japan Inst. Light Met., **39**, 791 (1989).
13. H.Iwasaki, M.Mabuchi and K.Higashi, Mater. Sci. Tech., in press (1996).
14. *Aluminum Handbook*, (Japan Institute of Light Metals, Tokyo, 1990), p. 9.
15. .Pilling and N.Ridley, in *Superplasticity in Crystalline Solid*, (The Institute of Metals, London, 1989).
16. D.Hull and D.Rimmer, Philos. Mag., **4**, 673 (1959).
17. M.V.Speight and W.Beere, Metal Sci., **9**, 190 (1975).
18. A.H.Chokshi and T.G.Langdon, Acta Metall., **35**, 1089 (1987).
19. J.W.Hancock, Metal Sci., **10**, 319 (1976).
20. A.C.F.Cocks and M.F.Ashby, Metal Sci., **16**, 465 (1982).

21. D.W.Livesey and N.Ridley, Metall. Trans. A, **13A**, 1619 (1982).

22. A.H.Chokshi and T.G.Langdon, J. Mater. Sci., **24**, 143 (1989).

Appendix

The cavity size-spacing parameter α is given by [18]

$$\alpha = \frac{1}{4\,ln(a/2r) - [1-(2r/a)^2]\,\{3-(2r/a)^2\}} \tag{A1}$$

where a is the cavity spacing and r is the cavity radius. For the composite in the present investigation, $a \approx 5 \times 10^{-6}$ m and $r \approx 5 \times 10^{-7}$ m, respectively. Therefore α is calculated to be approximately 1/4.

CHAPTER 9

SUMMARY

Superplasticity has been extensively investigated since the original study in the Pb-Sn and Bi-Sn eutectic alloys by Pearson in 1934 [1], and superplasticity has been utilized in industrial applications because complex shaped components can be produced readily by superplastic forming. Recently, there were two remarkable advances on superplasticity research: (i) superplasticity of materials with poor workability such as ceramics, intermetallics and metal matrix composites and (ii) high strain rate superplasticity. These discoveries are expected to lead to new fields of superplasticity research and a lot of opportunities for commercial applications. In particular, high strain rate superplasticity is very attractive for commercial applications because one of the current drawbacks in superplastic forming technology is a slow forming rate. It is important to understand microstructural control for high strain rate superplasticity and deformation characteristics in order to utilize high strain rate superplasticity.

The present thesis described microstructural control and deformation characteristics in the aluminum matrix composites and the magnesium matrix composites exhibiting high strain rate superplasticity. High stain rate superplasticity for materials containing a second hard phase such as metal matrix composites is very attractive not only for scientific aspects but also for industrial applications because the materials containing a second hard phase generally show poor workability.

The results in the present investigation revealed that a liquid phase plays an important role in high strain rate superplasticity. From this view, a new concept of the accommodation mechanism by a liquid phase for superplastic flow was proposed. The following is a brief summary of the present study.

Following Chapter 1, backgrounds and review on superplasticity, Chapter 2 described experimental procedure: materials preparation, tensile testing methods and cavitation study methods.

Chapter 3 described processing of the high strain rate superplastic composites. Microstructural requirements for high strain rate superplasticity in the composites are (i) uniform distribution of reinforcements and (ii) a very small grain size. These requirements were attained by hot extrusion without special thermo-mechanical treatments for the aluminum alloy matrix composites. The grain refinement results from an interaction of recrystallization and dynamic precipitation during hot extrusion.

In Chapter 4, the deformation characteristics of high strain rate superplasticity for the aluminum matrix composites were investigated by constant strain rate tensile tests. An analysis of the experimental data through the threshold stress concept showed that the activation energy for superplastic flow was drastically changed by the presence of a liquid phase. It was suggested that the dominant deformation process in a temperature range below the onset temperature for partial melting is grain boundary sliding accommodated by dislocation movement controlled by lattice diffusion of a matrix material. In the temperature range, the strengthening due to the presence of reinforcements was retained and the mechanical properties of superplastic flow were affected by the reinforcements.

In Chapter 5, the similar investigation was made on the magnesium matrix composites. In a solid state including no liquid, the relationship between the diffusion- and grain size-compensated strain rate and the modulus-

and threshold stress-compensated stress for the magnesium matrix composites was roughly in agreement with that for magnesium alloys, taking into consideration a threshold stress and an increase in the shear modulus due to the presence of the reinforcements. It is suggested that the deformation characteristics of superplasticity for the composites are intrinsically the same as those for metals without reinforcements, at least in a state including no liquid phase.

In Chapter 6, partial melting at matrix/reinforcement interfaces and grain boundaries at elevated temperatures was evidenced by *in situ* TEM observation and DSC measurements. The partial melting is likely attributed to segregation of solute atoms such as magnesium and silicon.

Chapter 7 described the origins of high strain rate superplasticity. It is required not only to attain a very small grain size, but also to accommodate the sliding process, that is, to relax the stress concentrations around the reinforcements in order to attain high strain rate superplasticity for metal matrix composites because stress concentrations cause excessive cavity formation. Many experimental results revealed that the optimum superplastic temperature was very close to the onset temperature for partial melting. On the basis of the results, a new concept of the accommodation mechanisms by a liquid phase for superplastic deformation was proposed.

In Chapter 8, cavitation characteristics in a state including a liquid phase were investigated. It is shown that the development of cavities was limited by the presence of a liquid phase. In addition, cavities occurring during superplastic deformation were reduced by static annealing without superimposed pressure, and consequently the post-deformation tensile properties were sufficiently recovered.

High strain rate superplasticity is a new research field and there are few examples of applications of high strain rate superplasticity. In near future,

however, high strain rate superplasticity will be extensively utilized in industrial applications because complex shaped components can be produced readily and *quickly* by high strain rate superplastic forming.

The author would be very happy if this thesis is of some contribution to superplasticity research and its applications.

References

1. C.E.Pearson, J. Inst. Met., **54**, 111 (1934).

LIST OF PUBLICATIONS

The publications related to this thesis are listed in the following :

Chapter 3. Microstructural control and mechanism of grain refinement

1. M.Mabuchi, T.Imai and K.Higashi, "*Production of superplastic aluminum composites reinforced with Si_3N_4 by powder metallurgy*", J. Mater. Sci., **28**, (1993), 6582-6586.
2. M.Mabuchi and K.Higashi, "*Processing of high-strain-rate superplastic Si_3N_{4w}/Al-Mg-Si composites*", J. Mater. Res., **10,** (1995), 2494-2502.

Chapter 4. Deformation characteristics in high strain rate superplastic aluminum matrix composites

3. M.Mabuchi, K.Higashi and T.G.Langdon, "*An investigation of the role of a liquid phase in Al-Cu-Mg metal matrix composites exhibiting high strain rate superplasticity*", Acta Metall. Mater., **42**, (1994), 1739-1745.
4. M.Mabuchi and K.Higashi, "*Constitutive equation of a superplastic Al-Zn-Mg composite reinforced with Si_3N_4 whisker*", Mater. Trans. JIM, **36**, (1995), 420-425.
5. M.Mabuchi and K.Higashi, "*Activation energy for superplastic flow in aluminum matrix composites exhibiting high-strain-rate superplasticity*", Scripta Mater., **34**, (1996), 1893-1897.

Chapter 5. Deformation characteristics in high strain rate superplastic magnesium matrix composites

6. M.Mabuchi, K.Kubota and K.Higashi, "*High strength and high strain rate superplasticity in a Mg-Mg_2Si composite*", Scripta Metall. Mater., **33**, (1995), 331-335.
7. M.Mabuchi and K.Higashi, "*High-strain-rate superplasticity in magnesium matrix composites containing Mg_2Si*", Philos. Mag. A, **74**, (1996), 887-905.

Chapter 6. Partial melting at interfaces and grain boundaries

8. M.Mabuchi and K.Higashi, "*Thermal Stability in a superplastic Si_3N_4/Al-Mg composite*", Mater. Sci. Eng., **A179/A180**, (1994), 625-627.
9. M.Mabuchi and K.Higashi, "*Thermal Stability and superplastic characteristics in Si_3N_4/Al-Mg-Si composites*", Mater. Trans. JIM, **35**, (1994), 399-405.

Chapter 7. Deformation mechanisms of high strain rate superplasticity

10. M.Mabuchi and K.Higashi, "*Superplastic deformation mechanism accommodated by the liquid phase in metal matrix composites*", Philos. Mag. Lett., **70**, (1994), 1-6.

Chapter 8. Cavitation and cavitation control

11. K.Higashi and M.Mabuchi, "*Experimental investigation of cavitation and fracture at very high strain rates in superplastic aluminum alloy matrix composites*", Mater. Sci. Eng., **A176**, (1994), 461-470.